

Copyright

by

Peyman Pourafshary

2007

**The Dissertation Committee for Peyman Pourafshary Certifies that this is the
approved version of the following dissertation:**

**A COUPLED WELLBORE/RESERVOIR SIMULATOR TO MODEL
MULTIPHASE FLOW AND TEMPERATURE DISTRIBUTION**

Committee:

Kamy Sepehrnoori, Co-Supervisor

Augusto L. Podio, Co-Supervisor

Roger T. Bonnecaze

Choongyong Han

Quoc P. Nguyen

**A COUPLED WELLBORE/RESERVOIR SIMULATOR TO MODEL
MULTIPHASE FLOW AND TEMPERATURE DISTRIBUTION**

by

Peyman Pourafshary, B.S., M.S.

Dissertation

Presented to the Faculty of the Graduate School of

The University of Texas at Austin

in Partial Fulfillment

of the Requirements

for the Degree of

Doctor of Philosophy

The University of Texas at Austin

December 2007

Dedication

To my wife, Bahar

Acknowledgements

I would like to take this opportunity to thank my supervising professors, Dr. Kamy Sepehrnoori and Dr. Augusto Podio, for their guidance and support throughout the course of this work, and also for the opportunity to learn from and work with them. I would also like to thank the other members of the supervising committee, Dr. Bonnecaze, Dr. Han, and Dr. Nguyen, for their time and comments.

I would like to express my sincere appreciation to the members of the GPAS team, past and present, for their contributions to the project. I would especially like to express my gratitude to Mr. Jalil Varavei and Mr. Farhad Tarahom for their assistance with my research. I am also truly indebted to my professors, fellow students, and administrative personnel in the Center for Petroleum and Geosystems Engineering, and express my sincere thanks to one and all.

I gratefully acknowledge the financial support of the Iran Ministry of Science, Research and Technology, and the University of Tehran for my Ph.D. education.

Finally, I would like to express gratitude to my wife, Bahar, for her love, support, and understanding, without which this work would not have been accomplished.

A Coupled Wellbore/Reservoir Simulator to Model Multiphase Flow and Temperature Distribution

Publication No. _____

Peyman Pourafshary, PhD.

The University of Texas at Austin, 2007

Supervisors: Kamy Sepehrnoori and Augusto L. Podio

Hydrocarbon reserves are generally produced through wells drilled into reservoir pay zones. During production, gas liberation from the oil phase occurs due to pressure decline in the wellbore. Thus, we expect multiphase flow in some sections of the wellbore. As a multi-phase/multi-component gas-oil mixture flows from the reservoir to the surface, pressure, temperature, composition, and liquid holdup distributions are interrelated. Modeling these multiphase flow parameters is important to design production strategies such as artificial lift procedures. A wellbore fluid flow model can also be used for pressure transient test analysis and interpretation. Considering heat exchange in the wellbore is important to compute fluid flow parameters accurately. Modeling multiphase fluid flow in the wellbore becomes more complicated due to heat transfer between the wellbore fluids and the surrounding formations.

Due to mass, momentum, and energy exchange between the wellbore and the reservoir, the wellbore model should be coupled with a numerical reservoir model to simulate fluid flow accurately. This model should be non-isothermal to consider the effect of temperature. Our research shows that, in some cases, ignoring compositional effects may lead to errors in pressure profile prediction for the wellbore. Nearly all multiphase wellbore simulations are currently performed using the “black oil” approach.

The primary objective of this study was to develop a non-isothermal wellbore simulator to model transient fluid flow and temperature and couple the model to a reservoir simulator called General Purpose Adaptive Simulator (GPAS). The coupled wellbore/reservoir simulator can be applied to steady state problems, such as production from, or injection to a reservoir as well as during transient phenomena such as well tests to accurately model wellbore effects. Fluid flow in the wellbore may be modeled either using the blackoil approach or the compositional approach, as required by the complexity of the fluids.

The simulation results of the new model were compared with field data for pressure gradients and temperature distribution obtained from wireline conveyed pressure recorder and acoustic fluid level measurements for a gas/oil producer well during a buildup test. The model results are in good agreement with the field data.

Our simulator gave us further insights into the wellbore dynamics that occur during transient problems such as phase segregation and counter-current multiphase flow. We show that neglecting these multiphase flow dynamics would lead to unreliable results in well testing analysis.

Table of Contents

List of Figures	xiii
List of Tables	xxv
CHAPTER 1: INTRODUCTION AND LITERATURE SURVEY	1
1.1 Introduction.....	1
1.2 Literature Survey	6
1.2.1 Multiphase Flow Modeling.....	6
1.2.2 Well Testing.....	10
1.2.3 Transient Coupled Wellbore/Reservoir Simulators.....	14
1.3 Problem Statement	18
CHAPTER 2. MULTIPHASE FLUID FLOW AND	
TEMPERATURE MODEL	20
2.1 Introduction.....	20
2.2 Multiphase-Flow Basic Parameters	21
2.2.1 Flow Patterns	22
2.2.2 Superficial Velocities.....	23
2.2.3 Volume Fraction, Mass Fraction.....	23
2.3 Pressure Gradient Calculation in the Wellbore.....	26
2.3.1 Methods for Calculating Pressure Drop.....	26
2.3.2 Comparison of Existing Multiphase Flow Models	29
2.3.3 Pressure Gradient Model used in this Research.....	31
2.4 Temperature Distribution.....	39
2.4.1 Calculation of Temperature Profile in Wellbore	40
2.4.2 The Overall Heat Transfer Coefficient	47
2.5 Solution Procedure.....	50
2.6 Results.....	51
2.6.1 Case Study 1: Oil/Gas Producer Well.....	51

2.6.2	Case Study 2: Water/Oil/Gas Producer Well.....	52
2.7	Effect of Production Parameters on Temperature Distribution in Wellbores	53
2.7.1	Base Case Study.....	53
2.7.2	Effect of Tubing Diameter	54
2.7.3	Effect of Gas Liquid Ratio (GLR)	55
2.7.4	Effect of Water Oil Ratio (WOR).....	56
2.7.5	Effect of Formation Thermal Conductivity	56
CHAPTER 3: COMPOSITIONAL WELLBORE/RESERVOIR		
STEADY STATE FLOW MODEL.....		73
3.1	Introduction.....	73
3.2	Phase behavior of hydrocarbon fluids.....	76
3.3	Governing Equations	77
3.3.1	Continuity Equations	78
3.3.2	Momentum Equations.....	79
3.3.3	Energy Equation	81
3.4	Solution Procedure.....	81
3.5	Effect of Slip velocity	82
3.6	The Need for Compositional Modeling	84
3.6.1	Case 1: Oil production.....	85
3.6.2	Case 2: Volatile Oil Production.....	87
3.6.3	Case 3: Gas Condensate Production.....	88
3.7	Results.....	90
3.7.1	Case 1: Three Phase Flow Production.....	90
3.7.2	Case 2: Wellbore/Reservoir Simulation	92
CHAPTER 4: TRANSIENT COUPLED WELLBORE/RESERVOIR MODEL		113
4.1	Introduction.....	113
4.2	Governing Equations	115
4.3	Solving Procedure.....	122
4.4	Results.....	123

4.4.1	Case 1: Comparison with field data	124
4.4.2	Case 2: Stand-alone wellbore simulator	126
4.4.3	Case 3: Coupled wellbore/reservoir transient problem.....	129
CHAPTER 5: APPLICATIONS.....		160
5.1	The Effect of Pressure Sensor Position on Well Testing Analysis....	160
5.1.1	Introduction	160
5.1.2	Analysis of a Buildup Test	161
5.1.3	Problem Statement.....	164
5.1.4	Comparison with Method 1 (Pressure Recording at Different Depths).....	167
5.1.5	Comparison with Method 2 (Liquid Level Measurement)....	171
5.2	Estimation of Accumulated Liquid Phase in a Gas Well.....	173
5.2.1	Modeling Procedure	173
5.2.2	Results.....	178
CHAPTER 6: SUMMARY, CONCLUSIONS AND RECOMMENDATIONS		200
6.1	Summary and Conclusions	200
6.2	Recommendations.....	204
Appendix A: Correlations Used in Blackoil Modeling.....		206
A.1	Blackoil Fluid Correlations.....	206
A.2	Thermal Parameters Calculation.....	208
Appendix B: Well Model.....		211
B.1	Introduction.....	211
B.2	Constant Flowing Bottomhole Pressure Injector	213
B.3	Constant Molar Rate Injector.....	215
B.4	Constant Volume Rate Injector.....	216
B.5	Constant Molar Rate Production Wells	217
B.6	Constant Flowing Bottomhole Pressure Producer	218
B.7	Constant Volume Oil Rate Producer.....	218

Appendix C: Discretized Governing Equations for Blackoil Fluid-flow in the Wellbore.....	220
Appendix D: Brief Description of a General Purpose Reservoir Simulator (GPAS).....	222
D.1 Governing Equations	222
D.2 Assumptions Used in GPAS	225
D.3 Physical property models.....	226
D.4 GPAS Solution Procedure.....	227
Appendix E: PETSc Linear Solvers.....	229
Appendix F: Phase Behavior and Equilibrium Calculations	231
F.1 Phase Stability Analysis.....	231
F.2 Flash Calculation	232
F.2.1 Equality of the Component Fugacity.....	233
F.2.2 Composition Constraint.....	233
F.2.3 Rachford-Rice Equation.....	233
F.3 Equation of State.....	234
F.4 Phase Identification and Tracking	237
Appendix G: Input Data Description and Examples.....	238
G.1 Wellbore/Reservoir Input Data Description	238
G.1.1 GPAS General Input Flags.....	238
G.1.2 GPAS General Data Variables.....	239
G.1.3 GPAS General Input Flags for Well Description	241
G.1.4 GPAS General Data Variables for Well Description.....	241
G.2 Sample Input Files	243
G.2.1 Transient Wellbore/Reservoir Case.....	243
G.2.2 Gas Injection Case	247
G.2.3 Stand-alone Steady-State Wellbore Simulation.....	251
G.2.4 Makefile.....	253

Glossary	272
References.....	276
Vita	285

List of Figures

Figure 2.1	Schematic representation of a production system.....	58
Figure 2.2	Schematic flow patterns in a vertical wellbore	58
Figure 2.3	Schematic of liquid and gas fraction definition in a control volume	59
Figure 2.4	Schematic two-phase flow patterns in a vertical tube.....	59
Figure 2.5	Comparison between accuracy of different multiphase flow models used to simulate U of Tulsa well data (1381 wells)	60
Figure 2.6	Comparison between accuracy of different multiphase flow models used to simulate U of Tulsa vertical well data (755 wells)	60
Figure 2.7	Errors between field data and simulated results by Ansari model for calculation bottomhole pressure in different producing wells.	61
Figure 2.8	Schematic of two sections of slug flow (Taylor bubbles and liquid slugs).....	61
Figure 2.9	Typical map to define two-phase flow pattern based on superficial liquid and gas velocity in a vertical tubing.	62
Figure 2.10	Error between field data and bottomhole pressure calculated by two different methods (Ansari et al. model and homogeneous model)	62
Figure 2.11	Resistances to heat flow between wellbore fluid and surrounding formation (Wang, 1996).....	63
Figure 2.12	Pressure distribution from modeling and field data (Case 1: A 5151 ft vertical well produces 23 °API dry oil at flow rate equal to 1140 STB/D through a 2.99-in ID tubing. The gas/oil ratio is 450 scf/STB, and the gas gravity is 0.80).....	64
Figure 2.13	Simulated holdup and flow regimes in the wellbore (Case 1: A 5151 ft vertical well produces 23 °API dry oil at flow rate equal to 1140 STB/D through a 2.99-in ID tubing. The gas/oil ratio is 450 scf/STB, and the gas gravity is 0.80).....	64

Figure 2.14	Simulated phase velocities distribution in the wellbore (Case 1: A 5151 ft vertical well produces 23 °API dry oil at flow rate equal to 1140 STB/D through a 2.99-in ID tubing. The gas/oil ratio is 450 scf/STB, and the gas gravity is 0.80).....	65
Figure 2.15	Simulated temperature distribution in the wellbore (Case 1: A 5151 ft vertical well produces 23 °API dry oil at flow rate equal to 1140 STB/D through a 2.99-in ID tubing. The gas/oil ratio is 450 scf/STB, and the gas gravity is 0.80).....	65
Figure 2.16	Computed and measured wellbore fluid temperature profiles (Case 2: A 5355 ft vertical well produces 59 STB/D oil, 41 Mscf/D gas and 542 STB/D water. Fluid enters the wellbore at 108 °F. The oil gravity is 34.3 °API, the gas gravity is 1.04)	66
Figure 2.17	Computed pressure profile in the wellbore (Case 2: A 5355 ft vertical well produces 59 STB/D oil, 41 Mscf/D gas and 542 STB/D water. Fluid enters the wellbore at 108 °F. The oil gravity is 34.3 °API, and the gas gravity is 1.04)	66
Figure 2.18	Simulated liquid holdup profile and flow regime in the wellbore (Case 2: A 5355 ft vertical well produces 59 STB/D oil, 41 Mscf/D gas and 542 STB/D water. Fluid enters the wellbore at 108 °F. The oil gravity is 34.3 °API, the gas gravity is 1.04)	67
Figure 2.19	Simulated phase velocity profile in the wellbore (Case 2: A 5355 ft vertical well produces 59 STB/D oil, 41 Mscf/D gas and 542 STB/D water. Fluid enters the wellbore at 108 °F. The oil gravity is 34.3 °API, and the gas gravity is 1.04).....	67
Figure 2.20	Pressure, liquid holdup and gas velocity differences between assuming constant temperature and simulating temperature profile.....	68
Figure 2.21	Pressure, liquid holdup and gas velocity differences if we assume that the fluid temperature profile is same as formation temperature or if we simulate fluid temperature profile.....	68
Figure 2.22	Effect of tubing diameter on temperature profile in the wellbore (A 5355 ft vertical well produces 59 STB/D oil, 41 Mscf/D gas and 542 STB/D water.....	69
Figure 2.23	Effect of gas liquid rate ratio (GLR) on temperature profile in the wellbore (A 5355 ft vertical well produces 59 STB/D oil and 542 STB/D water, the gas flow rate was changed to vary the GLR values).....	69

Figure 2.24	Effect of water oil ratio (WOR) on temperature profile in the wellbore (A 5355 ft vertical well produces 59 STB/D oil and 41 Mscf/D gas, the water flow rate was changed to vary the WOR values).....	70
Figure 2.25	Effect of earth thermal conductivity on temperature profile in the wellbore (A 5355 ft vertical well produces 59 STB/D oil, 41 Mscf/D gas and 542 STB/D water when diameter is 2 7/8. Earth thermal conductivity unit is Btu/hr-ft-°F.)	70
Figure 2.26	Thermal coefficient $\frac{r_{io}T_D}{k_e}$ as a function of formation heat conductivity.....	71
Figure 3.1	The phase behavior diagram for a hypothetical hydrocarbon fluid in a binary gas/oil system (Ahmed 1990)	94
Figure 3.2	Oil/gas composition changing during an isothermal pressure depletion process when temperature is below the critical point	94
Figure 3.3	Oil/gas composition changing during an isothermal pressure depletion process when temperature is above the critical point	95
Figure 3.4	Procedure to model pressure and temperature distribution.....	95
Figure 3.5	Schematic of thermodynamics equilibrium between moving phases in a block, when there is a slip velocity between phases.	97
Figure 3.6	Phase behavior diagram for a system of oil/gas hydrocarbon composition which is categorized as a blackoil.....	97
Figure 3.7	Pressure profiles calculated by blackoil and compositional approaches during production of 1000 lbm.mole/D oil/gas mixture from a 5100 ft tubing with 0.125 ft diameter	98
Figure 3.8	Oil/gas composition changing during pressure and temperature depletion in the hydrocarbon production	98
Figure 3.9	Phase behavior diagram for a system of oil/gas hydrocarbon composition which is categorized as volatile crude oil	99
Figure 3.10	Pressure profiles in a wellbore producing volatile oil calculated by blackoil and compositional approaches (1500 lbm.mole/D oil/gas mixture is produced from a 8000 ft tubing with 0.125 ft diameter, the oil gravity at the surface is 50 °API)	99

Figure 3.11	Oil/gas composition changing during pressure and temperature depletion in the volatile oil production	100
Figure 3.12	Phase behavior diagram for a system of oil/gas hydrocarbon composition which is categorized as retrograde oil and gas system.....	100
Figure 3.13	Pressure profiles in a wellbore producing retrograde oil calculated by blackoil and compositional approaches	101
Figure 3.14	Oil/gas composition changing during pressure and temperature depletion in the retrograde oil production	101
Figure 3.15	Simulated pressure profile in the wellbore during three phase flow production from 10000 ft tubing with 0.125 ft diameter.....	102
Figure 3.16	Simulated holdup profile in the wellbore during three phase flow production from 10000 ft tubing with 0.125 ft diameter	102
Figure 3.17	Simulated liquid velocity profile in the wellbore during three phase flow production from 10000 ft tubing with 0.125 ft diameter.....	103
Figure 3.18	Simulated gas velocity profile in the wellbore during three phase flow production from 10000 ft tubing with 0.125 ft diameter	103
Figure 3.19	Simulated temperature distribution profile in the wellbore during three phase flow production from 10000 ft tubing with 0.125 ft diameter.	104
Figure 3.20	Simulated liquid composition fractions in the wellbore sandface and surface sides during three phase flow production from 10000 ft tubing with 0.125 ft diameter	104
Figure 3.21	Simulated gas composition fractions in the wellbore sandface and surface sides during three phase flow production from 10000 ft tubing with 0.125 ft diameter (The production consists of 2500 lbm mole/day of hydrocarbon and 5800 lbm mole/day of water at the surface).....	105
Figure 3.22	Schematic gridding of reservoir/wellbore system (The reservoir dimensions are $560 \times 560 \times 100$ ft, and the producer wellbore depth is 5000 ft. the reservoir is divided to $8 \times 8 \times 3$ grid blocks and wellbore is divided into 20 gridblocks in z direction).....	105
Figure 3.23	Well hydrocarbhone production profile from a reservoir with initial pressure equal to 1500 psi (initial reservoir composition consist of 0.5 C1, 0.03 C3, 0.07 C6, 0.2 C10, 0.15 C15 and 0.05 C20)	106

Figure 3.24	Simulated transient pressure profiles in the wellbore during production from a reservoir with initial pressure equal to 1500 psi	106
Figure 3.25	Simulated producer pressure history at 4500 ft depth during production from a reservoir with initial pressure equal to 1500 psi	107
Figure 3.26	Simulated producer pressure history at 2500 ft depth during production from a reservoir with initial pressure equal to 1500 psi.....	107
Figure 3.27	Simulated producer pressure history at wellbore surface during production from a reservoir with initial pressure equal to 1500 psi	108
Figure 3.28	Simulated oil production history for a injector/producer case..	108
Figure 3.29	Simulated gas production history for a injector/producer case.....	109
Figure 3.30	Comparison of oil production and reservoir pressure at the producer perforated zone for hydrocarbon production from a injector/producer system.....	109
Figure 4.1	Schematic of wellbore/reservoir grid blocks used in transient simulator.....	133
Figure 4.2	Schematic of notation used in wellbore gridblock in the coupled simulator.....	133
Figure 4.3	Flowchart for one time step to solve transient problems by the coupled wellbore/reservoir simulator	134
Figure 4.4	Schematic of a liquid loaded gas well where the acoustic field level measurements were undertaken	135
Figure 4.5	Pressure- depth traverses. Field data BHP recorded by a quartz pressure sensor. Fluid level recorded acoustically before and after shutting in a liquid loaded gas well	135
Figure 4.6.a	Simulated pressure-depth traverses for a liquid loaded gas well before shut in. (The well is completed with 2-7/8 tubing and was producing gas at the time of test at an average rate of about 172 MSCF/D.)	136
Figure 4.6.b	Simulated pressure-depth traverse (solid line) and field data (dots) 4.5 min after shut in for a liquid loaded gas well with 2-7/8 tubing (Solid line is simulated data and dots are field data)	136

Figure 4.6.c	Simulated pressure-depth traverse(solid line) and field data (dots) 12.8 min after shut in for a liquid loaded gas well with 2-7/8 tubing (Solid line is simulated data and dots are field data).....	137
Figure 4.6.d	Simulated pressure-depth traverse (solid line) and field data (dots) 14.7 min after shut in for a liquid loaded gas well with 2-7/8 tubing (Solid line is simulated data and dots are field data).....	137
Figure 4.6.e	Simulated pressure-depth traverse (solid line) and field data (dots)19.7 min after shut in for a liquid loaded gas well with 2-7/8 tubing (Solid line is simulated data and dots are field data).....	138
Figure 4.6.f	Simulated pressure-depth traverse(solid line) and field data (dots) 30.7 min after shut in for a liquid loaded gas well with 2-7/8 tubing (Solid line is simulated data and dots are field data).....	138
Figure 4.6.g	Simulated pressure-depth traverse (solid line) and field data (dots) 35.3 min after shut in for a liquid loaded gas well with 2-7/8 tubing (Solid line is simulated data and dots are field data).....	139
Figure 4.6.h	Simulated pressure-depth traverse (solid line) and field data (dots)89.4 min after shut in for a liquid loaded gas well with 2-7/8 tubing (Solid line is simulated data and dots are field data).....	139
Figure 4.7	Simulated bottomhole pressure buildup during shut in test for a liquid loaded gas well (The well is completed with 2-7/8 tubing and was producing gas at an average rate of about 172 MSCF/D before shut in)....	140
Figure 4.8	Simulated transient pressure at different locations in the wellbore during shut in test for a liquid loaded gas well (The well is completed with 2-7/8 tubing and was producing gas at an average rate of about 172 MSCF/D before shut in).....	140
Figure 4.9	Simulated transient holdup profiles during shut in for a liquid loaded gas well (The well is completed with 2-7/8 tubing and was producing gas at an average rate of about 172 MSCF/D before shut in).....	141
Figure 4.10	Simulated transient holdup profiles at the upper sections of the wellbore during shut in for a liquid loaded gas well (The well is completed with 2-7/8 tubing and was producing gas at an average rate of about 172 MSCF/D before shut in).....	141

Figure 4.11	Simulated transient holdup profiles at the lower sections of the wellbore during shut in for a liquid loaded gas well (The well is completed with 2-7/8 tubing and was producing gas at an average rate of about 172 MSCF/D before shut in).....	142
Figure 4.12	Simulated transient superficial velocity profiles in the wellbore during a shut in test for a liquid loaded gas well (The well is completed with 2-7/8 tubing and was producing gas at an average rate of about 172 MSCF/D before shut in).....	142
Figure 4.13	Simulated transient superficial velocity at different sections of the wellbore during shut in for a liquid loaded gas well (The well is completed with 2-7/8 tubing and was producing gas at an average rate of about 172 MSCF/D before shut in).....	143
Figure 4.14	Simulated transient liquid backflow from the wellbore to reservoir during a shut in test for a liquid loaded gas well (The well is completed with 2-7/8 tubing and was producing gas at an average rate of about 172 MSCF/D before shut in).....	143
Figure 4.15	Simulated transient gas superficial velocity profiles in the wellbore during a shut in test for a liquid loaded gas well (The well is completed with 2-7/8 tubing and was producing gas at an average rate of about 172 MSCF/D before shut in).....	144
Figure 4.16	Transient gas superficial velocity at different sections of the well during shut in for a liquid loaded gas well (The well is completed with 2-7/8 tubing and was producing gas at an average rate of about 172 MSCF/D before shut in)	144
Figure 4.17	Simulated transient gas backflow during a shut in test for a liquid loaded gas well (The well is completed with 2-7/8 tubing and was producing gas at an average rate of about 172 MSCF/D before shut in).....	145
Figure 4.18	Simulated transient liquid holdup in the wellbore during a shut in test for a 5151 ft well with 0.125 ft tubing diameter which was producing 1140 STB/D oil and 513 Mscf/D gas before shut in.....	145
Figure 4.19	Simulated transient liquid holdup at different well depth during a shut in test for a 5151 ft well with 0.125 ft tubing diameter which was producing 1140 STB/D oil and 513 Mscf/D gas before shut in	146

Figure 4.20	Simulated transient simulated pressure profiles during a shut in test for a 5151 ft well with 0.125 ft tubing diameter which was producing 1140 STB/D oil and 513 Mscf/D gas before shut in.....	146
Figure 4.21	Simulated transient pressure history profiles in different well depth during a shut in test for a 5151 ft well with 0.125 ft tubing diameter which was producing 1140 STB/D oil and 513 Mscf/D gas before shut in.....	147
Figure 4.22	Simulated transient bottomhole pressure during a shut in test for a 5151 ft well with 0.125 ft tubing diameter which was producing 1140 STB/D oil and 513 Mscf/D gas before shut in.....	147
Figure 4.23	Simulated transient liquid superficial velocity profiles in wellbore during a shut in test for a 5151 ft well with 0.125 ft tubing diameter which was producing 1140 STB/D oil and 513 Mscf/D gas before shut in.....	148
Figure 4.24	Simulated transient gas superficial velocity profiles in wellbore during a shut in test for a 5151 ft well with 0.125 ft tubing diameter which was producing 1140 STB/D oil and 513 Mscf/D gas before shut in.....	148
Figure 4.25	Simulated transient superficial liquid velocity history profiles in different well depth during a shut in test for a 5151 ft well with 0.125 ft tubing diameter which was producing 1140 STB/D oil and 513 Mscf/D gas before shut in.....	149
Figure 4.26	Simulated transient liquid afterflow history profile between reservoir and wellbore during a shut in test for a 5151 ft well with 0.125 ft tubing diameter which was producing 1140 STB/D oil and 513 Mscf/D gas before shut in.....	149
Figure 4.27	Simulated transient gas superficial velocity history profile at different well depth during a synthetic shut in test for a 5151 ft well with 0.125 ft tubing diameter which was producing 1140 STB/D oil and 513 Mscf/D gas before shut in.....	150
Figure 4.28	Simulated transient gas afterflow history profile between reservoir and wellbore during a shut in test for a 5151 ft well with 0.125 ft tubing diameter which was producing 1140 STB/D oil and 513 Mscf/D gas before shut in.....	150

Figure 4.29	Simulated transient temperature distribution profiles during a shut in test for a 5151 ft well with 0.125 ft tubing diameter which was producing 1140 STB/D oil and 513 Mscf/D gas before shut in. The surface temperature is 76 °F and reservoir temperature is 120 °F	151
Figure 4.30	Simulated transient temperature distribution in different well depth during a shut in test for a 5151 ft well with 0.125 ft tubing diameter which was producing 1140 STB/D oil and 513 Mscf/D gas before shut in, the surface temperature is 76 °F and reservoir temperature is 120 °F	151
Figure 4.31	Schematic of a wellbore/reservoir system nodes, wellbore consists of 20 nodes in the vertical direction and 560×560×100 hydrocarbon reservoir has 7 by 7 by 3 nodes	152
Figure 4.32	Schematic of pressure definition for wellbore and reservoir nodes to use in well model	152
Figure 4.33	Simulation of the effect of shutting in the well at the top of the wellbore on reservoir pressure, the initial reservoir pressure is 2200 psi, and initial produced hydrocarbon composition is 0.57 C1, 0.09 C3, 0.01 C6, 0.01 C10, 0.21 C15 and 0.11 C20.....	153
Figure 4.34	Simulated reservoir pressure near the wellbore during buildup test, the initial reservoir pressure is 2200 psi, and initial produced hydrocarbon composition before shut in consists of 0.57 C1, 0.09 C3, 0.01 C6, 0.01 C10, 0.21 C15 and 0.11 C20	153
Figure 4.35	Simulated reservoir pressure and wellbore bottomhole pressure during buildup test for a 5300 ft wellbore with 0.165 ft tubing diameter, the initial pressure is 2200 psi.....	154
Figure 4.36	Simulated liquid volume rate exchanged between reservoir and wellbore after shut in for a 5300 ft wellbore with 0.165 ft tubing diameter, the initial reservoir pressure is 2200 psi	154
Figure 4.37	Simulated cumulative liquid volume exchanged between reservoir and wellbore after shut in for a 5300 ft wellbore with 0.165 ft tubing diameter, the initial reservoir pressure is 2200 psi.....	155
Figure 4.38	Simulated gas volume rate exchanged between reservoir and wellbore after shut in for a 5300 ft wellbore with 0.165 ft tubing diameter, the initial reservoir pressure is 2200 psi	155

Figure 4.39	Simulated gas volume exchanged between reservoir and wellbore after shut in for a 5300 ft wellbore with 0.165 ft tubing diameter, the initial reservoir pressure is 2200 psi.....	156
Figure 4.40	Simulated initial and final holdup profiles in the wellbore during shut in for a 5300 ft wellbore with 0.165 ft tubing diameter	156
Figure 4.41	Simulated final pressure and holdup profiles in the wellbore during shut in for a 5300 ft wellbore with 0.165 ft tubing diameter.....	157
Figure 5.1.	A typical log-log plot for a buildup test.....	180
Figure 5.2.	A typical semilog plot for buildup test	180
Figure 5.3.	An example of bottomhole pressure response during a buildup test which is affected by phase redistribution (Qasem et al., 2001)	181
Figure 5.4.	An example of an acoustic response of multiphase flow in a wellbore during a buildup test.....	181
Figure 5.5.	Schematic of liquid level in a wellbore containing more than one phase when the well is shut in at the surface	182
Figure 5.6.	A schematic of pressure recording during a well test in a wellbore when pressure recorder sensor is located in front of the perforation zone (Case 1).....	182
Figure 5.7.	A schematic of pressure recording during a well test in a wellbore when pressure recorder sensor is located at the wellhead (Case 2).....	183
Figure 5.8.	A schematic of pressure recording during a well test in a wellbore when pressure recorder sensor is located at a depth higher than the perforation zone (Case 3).....	183
Figure 5.9.	A schematic of pressure recording during a well test in a wellbore when pressure recorder sensor is lowering from the surface to the perforation zone (Case 4).....	184
Figure 5.10.	Schematic of wellbore/reservoir system used in buildup simulation	184
Figure 5.11.	Simulated transient liquid fraction profiles during buildup test (Wellbore depth is 7200 ft and the tubing diameter is 0.125 ft. The well is shut in at the surface).....	185

Figure 5.12.	Simulated transient liquid fraction profiles at different sections of the wellbore during a buildup test	185
Figure 5.13.	Simulated wellbore bottomhole Pressure history profile during buildup test.....	186
Figure 5.14.	Simulated diagnostic pressure and pressure derivative plots during buildup test	186
Figure 5.15.	Semilog line used to analyze simulated buildup test and calculate reservoir properties	187
Figure 5.16.	Calculated bottomhole pressure profile from measured pressure when recorder sensor is located at the wellhead.....	187
Figure 5.17.	Semilog plot used to analyze buildup test when bottomhole pressure profile is calculated from recorded pressure at the wellhead	188
Figure 5.18.	Simulated transient pressure gradient profiles in the wellbore during a buildup test.....	188
Figure 5.19.	Simulated pressure gradient profile at T= 3 hr during a buildup test (The S area is used to calculate bottomhole pressure from the recorded surface pressure).....	189
Figure 5.20.	Calculated bottomhole pressure profile from measured pressure when recorder sensor is located at the depth equal to 5400 ft in the wellbore.....	189
Figure 5.21.	Semilog plot used to analyze buildup test when bottomhole pressure profile is calculated from recorded pressure at the depth equal to 5400 ft in the wellbore.....	190
Figure 5.22.	Transient pressure sensor position when pressure recorder is lowered into the wellbore from the surface to the sandface	190
Figure 5.23.	Calculated bottomhole pressure profile from measured pressure when recorder sensor is lowered from the wellbore surface to the perforation zone.....	191
Figure 5.24.	Semilog plot used to analyze buildup test when bottomhole pressure profile is calculated from recorded pressure by a moving sensor.....	191

Figure 5.25.	Simulated liquid fraction profile when well flows at steady rate before shut in (Wellbore depth is 7200 ft and the tubing diameter is 0.125 ft. Well produces 1500 lbm. mole/D hydrocarbon, the composition consists of 0.57 C1, 0.09 C3, 0.09 C6, 0.11 C10, 0.12 C15 and 0.02 C20)	192
Figure 5.26.	Simulated liquid level history profile in the wellbore during buildup test (Wellbore depth is 7200 ft and the tubing diameter is 0.125 ft. Well produces 1500 lbm.mole/D hydrocarbon before shut in.....	192
Figure 5.27.	Simulated bottomhole pressure profile during a buildup test obtained from liquid level method.....	193
Figure 5.28.	The schematic effect of gas velocity on liquid accumulation at the bottom section of a gas well (Type 1- left: High gas velocity, Type 2- middle: Medium gas velocity, Type 3- right: Low gas velocity)	193
Figure 5.29.	Schematic of liquid accumulation in a gridblock (a. Gas and liquid phases move with same velocity, b. Liquid phase velocity is zero, c. Gas moves faster that the liquid phase, the liquid velocity is not zero).....	194
Figure 5.30.	Simulated gas velocity at the surface versus pressure difference between reservoir and wellbore	194
Figure 5.31.	Simulated liquid velocity at the surface versus pressure difference between reservoir and wellbore.....	195
Figure 5.32.	Simulated slip velocity at the surface versus pressure difference between reservoir and wellbore	195
Figure 5.33.	Simulated holdup and accumulated liquid fraction profiles versus surface gas velocity.....	196
Figure 5.34.	Accumulated fraction of liquid phase at the bottom of the wellbore versus surface gas velocity in a liquid loaded gas well	196
Figure 5.35.	Accumulated fraction of liquid phase at the bottom of the wellbore versus pressure difference between wellbore and reservoir in a liquid loaded gas well.....	197

List of Tables

Table 2.1.	Comparison between bottomhole pressure measured at field and calculated by our multiphase flow model used.....	72
Table 2.2.	Input parameters for the base case	72
Table 3.1.	General parameters for wellbore modeling.....	110
Table 3.2.	Blackoil composition	110
Table 3.3.	A typical composition for a volatile crude oil	110
Table 3.4.	Composition for a typical gas-condensate system.....	110
Table 3.5.	Production parameters for three phase flow case	111
Table 3.6.	Reservoir parameters for Case 2	112
Table 3.7.	Producer wellbore parameters for Case 2	112
Table 4.1.	Wellbore parameters for transient Case 1	158
Table 4.2.	Wellbore parameters for transient Case 2.....	158
Table 4.3.	Reservoir input parameters for transient Case 3	159
Table 4.4.	Wellbore input parameters for transient Case 3.....	159
Table 5.1.	Reservoir initial parameters	198
Table 5.2.	Producer wellbore and solution parameters.....	198
Table 5.3.	Accumulated fraction of liquid phase and drawdown pressure at different simulations	199

CHAPTER 1: INTRODUCTION AND LITERATURE SURVEY

1.1 INTRODUCTION

A large fraction of the energy consumed in the world comes from hydrocarbon reserves in the earth. These reserves are finite and should be produced efficiently. The hydrocarbon mixture is generally produced through wells drilled into the reservoir pay zones. During production, pressure declines in the reservoir due to fluid withdrawal. Pressure also decreases in the wellbore when fluid moves from the bottomhole to the wellhead. Typically, gas liberates from the oil phase if the pressure becomes less than the bubble point in the reservoir or wellbore. Water is often produced with the hydrocarbon mixture. Hence, we expect multiphase flow in some sections of the wellbore.

Multiphase flow pressure profiles are important in well design. For example, if the pressure in the reservoir is not high enough for the fluid to flow to the surface, then, artificial lift procedures are designed and utilized. Multiphase flow properties should also be known in order to design production facilities. A comprehensive wellbore/reservoir simulator developed to model the fluid flow from the reservoir through the wellbore to the surface would be a useful tool for design and analysis of hydrocarbon production systems.

Modeling multiphase flow in the wellbore becomes more complicated due to heat transfer between wellbore fluid and the surrounding formations. As the temperature of

the fluid produced from the reservoir differs from the surrounding formations temperature, heat exchange occurs and since fluid properties are temperature sensitive, it is important to model temperature distribution in the wellbore for more accurate multiphase flow simulation.

Most of the available wellbore simulators use the simplified blackoil approach that considers only three distinct phases: oil, water and gas with the oil and gas composition values assumed to remain constant along the wellbore. In the blackoil model, the gas phase is considered to be dissolved in the oil phase. Phase properties such as density, viscosity and specific volume are computed using experimental correlations as functions of temperature, pressure and specific gravity. Hence, the effect of composition changes along the flow path is neglected. Since the flowing liquid and gas are mixtures of several components, the validity of the blackoil approach is questionable when there are significant variations in pressure and temperature. A comprehensive compositional wellbore/reservoir simulator can improve the accuracy of fluid flow modeling in the wellbore. The term ‘compositional’ implies that the in-situ fluid composition may vary point by point in the wellbore as a function of pressure, temperature and slip between the phases. Using the compositional approach is essential when the mixture phase behavior is complex, as in gas condensate production.

Successful oil field development requires reliable information about reservoir conditions such as reservoir permeability, near wellbore damage, reservoir pressure, drainage area, reservoir faults and boundaries. Many of these parameters are obtained through geological studies, core examination, well logs and pressure transient tests.

During a pressure transient test, fluid flow rate is changed and the pressure response due to the flow rate change is measured at the same well or at neighboring wells. The recorded data are then analyzed to estimate reservoir properties and completion efficiency. Pressure transient tests are performed in a variety of forms. One major type is a drawdown test, which is performed by measurement and analysis of the wellbore bottomhole pressure decline during production, using a semilog method or type-curve matching techniques. After the well has been produced for a period of time at a constant rate, a pressure buildup test can be conducted by recording the bottomhole wellbore pressure responses when the well is closed at the surface or sandface. The measured data can be analyzed using different methods, such as Horner analysis or type-curve matching.

One major complication involved in well test interpretation is the wellbore storage effect. The main purpose of well test analysis is to measure and understand the exact responses of the reservoir, but well test responses are generally given and measured through the wellbore and not exactly inside the reservoir. The wellbore related effects may be easily misunderstood as reservoir effects, causing distortion of reservoir transients. Wellbore related phenomena have been addressed in the literature but considering only wellbore storage and phase redistribution. (Mattar et al., 1992)

When a well with a high gas/oil ratio is shut in, anomalous pressure buildup behavior may occur due to phase segregation. Bottomhole pressure may temporarily build up to a value greater than reservoir pressure and cause backflow to the reservoir before leveling off to the average reservoir pressure. This phase segregation takes place due to the difference between gas and oil densities. The gas phase moves upward while

the oil phase moves to the lower section of the well due to gravity. This segregation affects the interpretation of the well testing analysis and the reliability of the measured data in the wellbore.

During a pressure transient test, the temperature also changes as a function of time. For example, when a well is shut in at the surface, the warm fluid in the wellbore loses heat to the colder formation; thus, fluid temperature declines which affects the fluid properties.

All the well test calculations are based on the sandface pressure. Due to operational and completion difficulties, it is generally impossible to record pressure data opposite the perforation zone. Hence, in many cases, pressure data are recorded at a depth above the sandface and then converted to the pressure at the point of interest. When more than one phase flows in the wellbore, the conversion requires knowledge of the gradient of the fluid between the pressure recorder and the formation. Using the wrong or an approximate gradient makes the well test results useless. A comprehensive wellbore simulator can be used for accurate computation of bottomhole pressure when the recorder is located above perforation zones.

In the case of many gas wells, the higher density liquid phase may be transported to the surface by the gas phase. Liquid can come from condensation of hydrocarbon gas or from interstitial water in the reservoir matrix (Turner et al., 1969). If the gas phase does not maintain sufficient velocity to lift the liquid to the surface, the liquid phase will accumulate at the bottom sections of the well. The production capacity of the well is reduced by the backpressure due to the liquid accumulation. A wellbore simulator can be

used to compute the accumulated liquid as a function of the pressure difference between the wellbore and reservoir and also the gas velocity. It can also be used as a tool to design tubing size for the production from gas wells.

The primary objective of this study is to develop a wellbore simulator to model transient fluid flow and temperature and which is coupled to a reservoir numerical simulator called GPAS (Wang et al., 1997; 1999, Han et al., 2007). The reservoir simulator is a parallel, 3D, fully implicit, equation of state compositional model that uses numerical algorithms for solving very large, sparse linear systems (Naimi-Tajdar, 2005). The coupled wellbore/reservoir simulator can be applied to steady state problems, such as production from or injection to a reservoir as well as during transient phenomena such as well tests to accurately model wellbore effects. Fluid flow in the wellbore may be modeled either using the blackoil approach, or the compositional approach as required by the complexity of the fluids.

The dissertation is organized in keeping with the objectives stated above. In the first chapter, we discuss available literature on fluid flow and energy transport in wellbores. In Chapter 2, we present different parameters important in multiphase flow pattern prediction and modeling. A blackoil model is also presented to model steady state pressure, phase fraction, phase velocity and temperature profiles in wellbores during production or injection. In Chapter 3, we discuss the compositional approach to model fluid flow in the wellbore. We show the importance of the compositional approach to explore the validity of the blackoil approximation for multiphase flow modeling in wellbores. Case studies are presented to show the benefits of using a coupled

wellbore/reservoir compositional simulator. In Chapter 4, a transient wellbore/reservoir model is presented. We discuss the mass, momentum and energy governing equations for the wellbore and reservoir. We also present the numerical procedure used for solving the coupled wellbore/reservoir equations. Different case studies are discussed and compared to field data to show the validity of our model and the ability of the simulator to model various wellbore related phenomena such as backflow and phase segregation during transient problems. In Chapter 5, different applications of our simulator are presented to discuss the effect of wellbore dynamics and the effect of pressure gauge position on the validity of the well test analysis. The simulator is also used as a tool to predict the accumulated liquid fraction in liquid-loaded gas wells. In Chapter 6, conclusions and recommendations for future work are presented.

1.2 LITERATURE SURVEY

1.2.1 Multiphase Flow Modeling

Multiphase flow is commonly encountered during oil production, and has a strong impact on the performance of reservoir and surface facilities. The frequent occurrence of multiphase flow in petroleum industry emphasizes the challenge of analyzing and modeling multiphase systems to optimize the performance of wells or reservoirs coupled to surface facilities.

Parameters, such as pressure, temperature, velocities and phase fractions, must be modeled in production operations. When co-current flows of multiple phases occur, the interface between phases can take on a variety of configurations, known as flow patterns

(Chen, 2001). The particular flow pattern depends on the conditions of pressure, flow, and channel geometry and is a very important feature of two-phase flow (Hasan et al., 1988). The hydrodynamics of the flow and the flow mechanisms change significantly from one flow pattern to another. To accurately estimate the pressure drop and phase fraction, it is necessary to know the flow pattern for any flow conditions. These patterns include bubble, slug, churn and annular flow for vertical multiphase flow (flow regimes will be discussed in the next chapter).

Due to the complexity of multiphase flow, empirical correlations are widely used to solve such problems. Empirical correlations are based on experimental results obtained from special cases, so they cannot be used with confidence for a wide range of problems. The empirical correlations can be either specific for each flow regime or can be independent from flow regimes. The Hagedorn and Brown correlation (Hagedorn et al., 1965) is one of the correlations used in oil wells, and the Orkiszewski correlation (Orkiszewski, 1967) is the first correlation developed for gas wells with gas/liquid ratio above 50000 scf/bbl. Duns et al. (1963), Beggs et al. (1973), and Mukherjee et al. (1983) developed different experimental correlations for multiphase flow in vertical and inclined pipes. Another approach to model multiphase flow is the use of homogeneous models. A homogeneous model assumes that the fluid properties can be represented by mixture properties, so single-phase flow can be applied to the mixture. These models can also consider the velocity difference between moving phases (slip velocity). Empirical parameters are required to calculate slip velocity. Homogeneous models with slip are called drift-flux models. (Shi et al., 2005)

Mechanistic models are based on fundamental laws and detailed description of the physics of each of the flow patterns. Mechanistic models improve our ability to predict pressure and phase fraction profiles in pipes, especially for those cases that cannot be easily modeled in a laboratory, or when reliable empirical correlations are not available (Petalas et al., 2000). The procedure of this modeling approach consists of determining the flow regimes and then using separate models for each flow regime to predict flow characteristics like holdup and pressure drop. Taitel et al. (1976, 1980) presented the pioneering work in mechanistic modeling by describing the physical mechanism controlling the transition between different flow patterns. Following the work of Taitel et al., different mechanistic models are presented in the literature. Ozon et al. (1987), Hasan and Kabir (1988), and Ansari et al. (1994) published studies on comprehensive mechanistic modeling of two-phase flow in vertical pipes. Xiao et al. (1990) and Kaya et al. (2001) presented other models limited in applicability to only some pipe inclinations. Petalas et al. (2000), and Gomez et al. (2000) published more general studies on comprehensive mechanistic modeling of multiphase flow in wellbores.

Most wellbore multiphase-flow models assume isothermal conditions. Hydrocarbon production or injection of fluids into the wellbore involves heat exchange between the fluid and surrounding formations. As heat exchange takes place, temperature may change in the wellbore, which affects fluid parameters and also the dynamics of fluid flow, which makes the problem more complicated. An accurate multiphase fluid-flow model requires that the energy equation be solved simultaneously with the other governing equations to model temperature distribution.

During oil production, the sandface temperature is often the same as the formation temperature. When very large drawdown occurs at the bottomhole, temperature increases for the oil phase and decreases for the gas phase due to the Joule-Thompson effect (Hasan et al., 2002). As the fluid rises to the surface, its temperature changes due to heat exchange with the surrounding formation.

Many papers have been published on various aspects of heat transfer between a wellbore fluid and the formation. Ramey (1962) was the first to present a theoretical model for estimating fluid temperature in the wellbore as a function of well depth and producing time. However, due to neglecting the effects of kinetic energy and friction and consideration of single-phase flow, his method has a few limitations. He presented a general expression for the overall heat transfer coefficient for wellbores based on the various resistances to heat transfer to the formation. Ramey also suggested that the well radius be considered to be vanishingly small, that is it acts as a line-source. Satter et al. (1965) extended Ramey's model to include multiphase flow. They accounted for kinetic energy effects and Joule-Thompson expansion. Alves et al. (1992) presented a unified model to predict temperature distribution in the wellbore for the entire range of inclination angles. Hasan et al. (1994) presented a general method to model wellbore heat loss and flowing fluid temperature. They showed that the assumption of a line-source well could be removed for the general case of steady-state wellbore two-phase flow.

1.2.2 Well Testing

A transient pressure test is a fluid-flow test conducted on wells to obtain reservoir and well completion data. During the test, the well's flow rate is changed and the well's pressure response as a function of time is measured at the same well or at other neighboring wells. The pressure response is a function of reservoir rock properties, fluid properties completion efficiency and flow geometry. Based on the well type (injector or producer) and flow rate (producing or shut in) several kinds of tests may be designed.

The most common well test type is the pressure buildup test. This test is conducted on a well which has been producing at a constant rate and is then shut in at the surface or sandface. A pressure recorder is lowered into the well to record the pressure in the wellbore for several hours, depending on the anticipated formation permeability. The pressure may be measured opposite the producing zone near the formation or at other parts of the wellbore. If the recorder is located far from the perforation zones, the measured pressure should be converted to sandface pressure, which is then analyzed to estimate formation permeability, skin factor, average reservoir pressure, distance to a fault if present, fracture length and fracture conductivity.

It is important to be certain that the measured data are not affected by the wellbore dynamics due to wellbore storage and phase redistribution when more than one phase is flowing simultaneously in the wellbore.

Most well tests are performed by changing the flow rate at the surface, rather than at the bottomhole in order to minimize costs. For example, during a buildup test, the well

is shut in at the surface not at the bottomhole, hence, fluid influx from the reservoir is allowed to flow into the wellbore after shut in. This phenomenon, whereby the change in sandface flow rate lags behind the surface flow rate change, has been called wellbore storage, which dominates the initial pressure response. To use this period in well testing interpretation, it is necessary to detect the presence and duration of wellbore storage in early transient pressure data.

One of the early papers addressing this issue was written by van Everdingen et al. (1949), who presented a solution for infinite-acting radial flow in the reservoir, including wellbore storage effects. They used the Laplace transform method to couple the solution of infinite-acting radial flow in the reservoir with flow in the wellbore. Agarwal et al. (1970) extended their solution to include skin damage effects. Gringarten et al. (1979) developed a more convenient type-curve matching method to analyze wellbore storage.

In the effort to quantify and evaluate the wellbore related effects, the concept of wellbore storage is followed by the concept of phase redistribution phenomena (Qasem et al., 2001).

Wellbore phase redistribution occurs in a shut-in well with gas and liquid flowing simultaneously in the tubing. In such wells, the gravity effects cause the liquid to fall to the bottom and the gas to rise to the top of the tubing. Due to the relative incompressibility of the liquid and the inability of the gas to expand in a closed system, phase segregation yields a net increase in the wellbore pressure (Qasem et al., 2002). The increased pressure in the wellbore is then relieved to the formation and equilibrium occurs between the wellbore and the adjacent formation. During the early time, pressure

increase above the formation pressure may cause an anomaly in the buildup pressure response, typically a “hump”.

Stegemeier and Matthews (1958) were the first to observe anomalous pressure responses in a number of buildup tests in an oil field in South Texas. They observed the predominance of the phase redistribution phenomenon in wells with large positive skin and in reservoirs with moderate permeability.

Different models have been developed to distinguish phase redistribution during a well testing. Stegemeier et al. (1958) and Pitzer et al. (1959) documented the relation of phase redistribution to the pressure buildup hump and its size. Later, Thompson et al. (1986) and Olarewaju (1990) illustrated that phase redistribution is not always associated with the pressure hump on the analysis plot. Hence, the absence of the hump may lead the well test analyst to make serious errors. Olarewaju and Lee (1989) used pressure derivative type curves to detect the presence of phase segregation distortion. They stated that a V-shaped curvature of pressure derivative curve is evidence for the presence of phase segregation. Mattar and Zaoral (1992) proposed the use of Primary Pressure Derivative (PPD) which is defined as $dP_{ws}/d\Delta t$ to differentiate between the wellbore dominated phenomena and the reservoir fluid flow responses. They showed that PPD curve has an increasing trend during the phase redistribution dominated period. Recently, Qasem et al. (2002) used the SLPD curve, which is defined as $d \log(PPD)/d \log \Delta t$ as an indicator for this period. The SLPD data does not deviate from a horizontal line when the pressure responses are not affected by wellbore effects.

Different methods are used to analyze phase redistribution during a buildup test. Fair (1981), Thompson et al. (1986) and Hageman et al. (1991) proposed different mathematical models for phase redistribution. In their models dimensionless pressure solutions were presented for type-curve matching to analyze pressure buildup tests influenced by this phenomenon. Fair (1981) used a simple exponential function to describe the pressure change resulting from the oil and gas segregation. Hageman et al. (1991) modified Fair's method by using an error function to represent the pressure change when Fair's model did not give a good fit of field data influenced by wellbore phase redistribution. Several authors, such as Winterfeld (1989), Almehaideb et al. (1989), Hasan et al. (1992) and Xiao et al. (1996) developed numerical simulators to model multiphase flow during phase redistribution.

Although wellbore storage and phase redistribution are well discussed and modeled in literature, there are few papers published on other wellbore related phenomena during well testing. For example, one of the important wellbore effects is related to pressure gauge placement and data measurement.

All the theories in well testing are based on analyzing the reservoir pressure and not the recorded pressure. Hence, the reservoir pressure should be measured at the producing zone. Downhole completion hardware or physical restrictions, such as plugs formed by hydrates, paraffins, or asphaltenes, often prevent running a gauge all the way to the desired point at the perforation zone (Kabir et al., 1996). The problem that arises is the difference between the recorded pressure and the sandface true pressure due to the wellbore effects. Hence, the way we record the data and the method we use to convert

them to the sandface pressure should be considered carefully. Very few papers have discussed issues related to pressure sensors positions and their effect on well testing accuracy. Kabir et al. (1996) discussed the interpretation problems caused by wellbore thermal effects due to the sensor position. Mattar et al. (1992) also showed several examples of tests that have been affected by wellbore dynamics, which could have been misinterpreted as reservoir phenomena instead of wellbore effects. For example, they showed how the sensor position could make well testing results invalid. They suggested the examination and pre-processing of the raw test data and conducting validity checks of all the data before using conventional methods such as the semilog method to analyze the data.

It is important to identify any of the non-reservoir effects. These effects can either be filtered out, corrected or ignored, but must not be interpreted as reservoir effects (Qasem et al., 2001). A coupled wellbore/reservoir simulator can be used to recognize the influence of these wellbore related effects. We can use a comprehensive simulator to model and discuss the effects that are less noticed and discussed in the literature, such as pressure gauge position.

1.2.3 Transient Coupled Wellbore/Reservoir Simulators

Exchange of mass, momentum and energy occurs in the wellbore and reservoir systems during well testing, drilling or normal production operations. Generally, the oil/gas fluid moves from the reservoir to the wellbore bottomhole and then to the wellhead through a tubing string. In many cases, these transport processes may be

transient and may influence each other. Any perturbation in a wellbore/reservoir fluid-flow system may cause transient flow of mass, momentum and energy. The perturbation may occur by changing volumetric flow rates. For example, in most buildup and drawdown tests fluid-flow rates change in the surface. Hence, transient modeling of multiphase flow in the wellbore is useful for a better understanding of different physical behaviors of phases such as phase redistribution during well tests. A fully transient wellbore/reservoir simulator is also useful for different production applications, such as computing dynamic productivity, transient nodal analysis and temperature logs. Transient simulations can also be used to design flow lines, production equipment and facilities. (Hasan et al., 2002) Pressure profile, phase fraction profiles and temperature distribution in the wellbore are the main parameters that affect the wellbore and reservoir relation. Due to the limitations of analytical modeling, numerical approaches are widely used to describe the transient temperature and pressure behavior in a coupled wellbore/reservoir system when flow rate or pressure is changed in the wellbore. Few simulators have been reported in literature that deals with transient problems with coupled simulators.

Miller (1980) developed one of the earliest wellbore transient simulators. She developed a numerical model of transient two-phase flow in the wellbore with heat and mass transfer. She used the model to investigate the early-time interaction of the well flow and reservoir flow during a well test in geothermal wells. She also studied the long-time effect of temperature changes on the well test analysis. In her model, mass and momentum equations are combined with a simple energy equation and solved semi

implicitly. The energy equation did not consider convective heat exchange in the wellbore. Miller also assumed that there is no slip between the phases in the wellbore.

Another isothermal model was presented by Winterfeld (1989) to simulate a multiphase pressure buildup test. The model solves the transient wellbore equation simultaneously with the reservoir equations. An empirical relationship was used for phase to phase and phase to wall friction terms to use in gas and liquid wellbore momentum equations. He used a “two-fluid” flow model to solve physical cases in which gas and liquid phases flow in different directions, as may happen during a buildup test.

Almehaideb et al. (1989) presented a fully-implicit isothermal wellbore model, which is coupled to a blackoil reservoir model. They performed a mass balance on the oil, water and gas components using the standard blackoil approach. They suggested two options for momentum equations: using a two-fluid model, or using a mixture momentum equation. However, they noted that the mixture momentum equation couldn't be used to model countercurrent two-phase flow. Almehaideb et al. (1989) used steady state empirical correlation to evaluate the in-situ liquid volume fraction at each section of the wellbore under transient conditions. In their model, oil and water are lumped into one liquid phase and slip is neglected. They used the model to simulate phase segregation during a buildup test.

Stone et al. (1989) presented a fully-implicit, thermal wellbore/reservoir simulator. In this model, the energy equation is solved with the mass and momentum equations for a gas/liquid system.

Hasan et al. (1996, 1997, and 1998) reported the blackoil hybrid modeling approach for simulating flow of single-phase gas, single-phase oil and two-phase oil/gas in wellbores. They numerically modeled two-phase flow in the wellbore, but for simplicity, they applied an analytical single-phase model for the reservoir fluid flow. In their model, material balances for each phase, one momentum balance equation for the mixture and an energy balance are used to generate the constitutive equations in the wellbore. These equations are solved numerically to obtain pressure, velocity, temperature and fluid density in the wellbore. When the well is shut in at the surface, they used a different approach; while other researchers considered mechanistic models or empirical models to compute liquid fraction (holdup) at each section of the wellbore, Hasan et al. (1998) adopted an approach to track the migration of gas bubbles throughout the wellbore to compute phase fractions at each section of the wellbore.

Fan et al. (2000) developed a semi analytical wellbore/reservoir simulator for describing general wellbore effects, especially the thermal effect, on a high-temperature gas well pressure buildup test. Mass, momentum and energy balances for single-phase gas are used as wellbore flow governing equations. As a boundary condition, a simple analytical reservoir model was connected to the wellbore model at the bottomhole using Duhamel's principle. They simulated and predicted pressure, temperature, velocity and gas properties inside the wellbore during a buildup test.

Fairuzov et al. (2002) developed and numerically solved a blackoil isothermal lumped-parameter model of transient two-phase gas/liquid flow in the wellbore. They assumed thermal equilibrium between the phases. Their model is based on the

assumption that the flow process is essentially one-dimensional in a wellbore so that an area's average properties can be represented as a function of one space variable and time. Mass balance equation and an approximate Navier-Stokes equation of momentum are used as governing equations in the wellbore, while the Darcy type flow is assumed in the reservoir model. Reservoir model and wellbore model are solved separately to avoid an increase in the computation time. The model was used to determine the behavior of the wellbore flow during a pressure buildup test.

Izgec et al. (2006) presented a single-phase transient wellbore simulator coupled with a semi analytic temperature model. In their model, finite difference forms of mass and momentum equations are coupled with a semi analytic heat-transfer model, to represent heat exchange in a wellbore/formation system in both vertical and radial directions.

A correct description of multiphase flow in the wellbore needs a model that incorporates separate equations of continuity for each phase, two-fluid model momentum, and energy balance. The wellbore model should be coupled to a multiphase numerical reservoir model to simulate mass, momentum and energy exchanges between reservoir and wellbore accurately.

1.3 PROBLEM STATEMENT

The primary objectives of this study are:

1.a. To develop a blackoil wellbore simulator to model pressure, temperature, phase fractions and phase velocities in wellbores

- 1.b. To verify and validate the developed model against field data
- 1.c. To investigate the effects of production parameters and wellbore geometry on temperature distribution in wellbores
- 2.a. To develop a compositional wellbore/reservoir coupled simulator to model pressure, temperature, phase compositions, phase fractions and phase velocities in wellbores
- 2.b. To compare the developed compositional model against a blackoil model to investigate the importance of simulating wellbores by compositional approach
- 3.a. To develop a transient wellbore simulator coupled to a reservoir simulator called GPAS, developed in the University of Texas at Austin
- 3.b. To apply the new simulator to transient problems to model pressure, temperature, phase velocities and holdup transient profiles in wellbores
- 3.c. To compare simulated results with field data to validate our model
- 3.d. To use our simulator to model wellbore related effects during well testing problems

CHAPTER 2. MULTIPHASE FLUID FLOW AND TEMPERATURE MODEL

2.1 INTRODUCTION

Multiphase flow is a general name for the simultaneous movement of more than one fluid in a piping system. The most common multiphase flow is the flow of gas and liquid, such as water and air or oil and natural gas. Multiphase flow phenomena occur in different industries such as oil, nuclear power, geothermal electricity generation, and chemical processing. Because of diverse applications of multiphase-flow, much research has been done in this area to understand and describe the physics of this type of fluid flow.

Most petroleum wells produce both liquid, such as oil and water, and gas, so we expect multiphase flow to occur in different sections of the wellbore. In the wellbore, the liquid phase can change to the gas phase due to variation of temperature or pressure, and it is also possible for the gas phase to dissolve in the liquid phase when pressure is increased by pumping. Multiphase flow may also exist during the advancement of fluid from the wellhead to the separator. Schematic figure of a system that can produce both oil and gas is shown in Figure 2.1. In the steam injection for oil recovery, we also expect the movement of two-phase flow in some parts of the wellbore.

In this section, we focus on the multiphase-flow regimes and various methods for modeling the fluid flow in the wellbore.

2.2 MULTIPHASE-FLOW BASIC PARAMETERS

Multiphase flow is complicated because at each section of the wellbore multiple phases are simultaneously competing for the available cross-sectional area. Computing each phase fraction is very important for determining the pressure gradient in multiphase-flow. The basic governing equation used to calculate the pressure drop in a steady state condition is the momentum equation:

$$\frac{dP}{dz} = -(\rho_m v_m \frac{dv_m}{dz} + \rho_m g \sin\theta + \frac{2\rho_m f_m v_m^2}{d}) \quad (2.1)$$

where P is the pressure in the wellbore and v_m , ρ_m and f_m represent mixture properties for velocity, density, and friction factor. On the right side of Equation 2.1, the first

term, $\rho_m v_m \frac{dv_m}{dz}$, shows the momentum flux. The second term, $\rho_m g \sin\theta$, is the body

force due to gravity. The last term, $\frac{2\rho_m f_m v_m^2}{d}$, represents the momentum losses due to

friction. Hence, we can rewrite the steady state pressure gradient as a combination of

kinetic energy, $(\frac{dP}{dz})_A$, static head, $(\frac{dP}{dz})_H$, and friction gradient, $(\frac{dP}{dz})_F$

$$\frac{dP}{dz} = (\frac{dP}{dz})_A + (\frac{dP}{dz})_H + (\frac{dP}{dz})_F \quad (2.2)$$

Equation 2.1 shows that we need mixture parameters, such as mixture density, to calculate pressure change in wellbores. Mixture parameters depend directly on in-situ volume fractions of the phases. For example, in a two-phase gas and oil system, the

mixture density and viscosity are related to the in-situ liquid volume fraction (holdup), H , as follows:

$$\rho_m = \rho_l H + \rho_g (1 - H) \quad (2.3-a)$$

$$\mu_m = \mu_l H + \mu_g (1 - H) \quad (2.3-b)$$

The in-situ fraction of a phase is generally different from its input fraction. The main reason for this is the differences between gas and liquid velocities caused by their density differences. Thus, a major effort in modeling multiphase-flow is the correct estimation of in-situ phase volume fraction. In this section we discuss some definitions that are used in multiphase flow. In the next section we present different models to compute phase fractions in the wellbore.

2.2.1 Flow Patterns

Because of many parameters such as phase velocity, geometry, wellbore orientation and fluid densities, the flowing phases take up a number of distinct configurations, called flow patterns or flow regimes. For example, when the fraction of liquid is very high, it acts as a continuous phase, and the gas phase appears as bubbles distributed in this continuous phase. When the velocity and fraction of the gas phase in a vertical channel are high, gas behaves as a continuous phase and moves fast in the middle of pipe while transporting finely divided liquid drops. These examples are two types of flow regimes in the multiphase flow but the physics of these flow regimes is totally

different. A schematic of different flow regimes that could exist in a vertical wellbore is shown in Figure 2.2. We discuss these patterns in more detail later.

2.2.2 Superficial Velocities

Superficial velocity of any phase is its velocity if we assume that it occupies 100% of the cross section of the pipe. Thus, the superficial velocity for liquid phase, v_{sl} , is given in terms of the in-situ volumetric flow rate of liquid phase, q_l and the cross-sectional area, A by Equation 2.4

$$v_{sl} = \frac{q_l}{A} \quad (2.4)$$

A similar equation is valid for the gas phase, so its superficial velocity is a function of cross sectional area and the in-situ gas flow rate, q_g as

$$v_{sg} = \frac{q_g}{A} \quad (2.5)$$

Since during two-phase flow none of the phases occupies the entire cross-sectional area, the available area for each phase is less than A , and the actual velocity of each phase is higher than the superficial velocity.

2.2.3 Volume Fraction, Mass Fraction

Since multiphase flow contains more than one phase we need to know the relative amount of each phase in each section of the wellbore. We can express this value either as

a volume fraction or as a mass fraction. The liquid volume fraction, c_l , is the fraction of volumetric flow rate of liquid divided by the total flow rate of the mixture.

$$c_l = \frac{q_l}{q_t} = \frac{q_l}{q_l + q_g} = \frac{v_{sl}}{v_{sl} + v_{sg}} \quad (2.6)$$

Similarly, the gas volume fraction is the volumetric flow rate of gas divided by the total flow rate of the mixture.

$$c_g = \frac{q_g}{q_t} = \frac{q_g}{q_l + q_g} = \frac{v_{sg}}{v_{sl} + v_{sg}} \quad (2.7)$$

The flowing gas mass fraction or quality, γ_g , is defined in terms of the mass flow rates of the liquid phase (w_l) and gas phase (w_g) as

$$\gamma_g = \frac{w_g}{w_t} = \frac{w_g}{w_g + w_l} = \frac{v_{sg}\rho_g}{v_{sg}\rho_g + v_{sl}\rho_l} \quad (2.8)$$

Similarly, the flowing liquid mass fraction, γ_l , is defined as

$$\gamma_l = \frac{w_l}{w_t} = \frac{w_l}{w_g + w_l} = \frac{v_{sl}\rho_l}{v_{sg}\rho_g + v_{sl}\rho_l} \quad (2.9)$$

From Equations 2.8 and 2.9

$$\gamma_g + \gamma_l = 1 \quad (2.10)$$

The void fraction of gas in the mixture (in-situ gas volume fraction) f_g is defined as the ratio of the total cross sectional area through which the gas flows, A_g and the total cross sectional area A .

$$f_g = \frac{A_g}{A} \quad (2.11)$$

Since gas flows only through A_g , the actual velocity of gas phase is expressed as $\frac{q_g}{A_g}$. From Equation 2.5 the actual velocity of the gas phase can be written as

$$v_g = \frac{v_{sg}}{f_g} \quad (2.12)$$

Similarly, we can define the in-situ fraction of liquid in the mixture, f_l , which is also called holdup, H . Normally, the liquid flows more slowly than the gas and accumulates in the pipe section.

$$H = f_l = \frac{A_l}{A} = 1 - f_g \quad (2.13)$$

where A and A_l are the total cross sectional area and the available area for liquid movement respectively. Figure 2.3 shows a schematic of liquid and gas fraction definition. Similar to Equation 2.12, the actual liquid velocity is defined as

$$v_l = \frac{v_{sl}}{f_l} \quad (2.14)$$

The total velocity of the mixture, v_m , is defined as

$$v_m = v_{sg} + v_{sl} \quad (2.15)$$

Combining Equations 2.12 through 2.15 the mixture velocity can be rewritten as

$$v_m = H v_l + (1 - H) v_g \quad (2.16)$$

The velocities of phases depend on fluid gravity, so in a vertical wellbore the lighter phase moves faster than the heavier phase. The difference between the velocities is denoted as slip velocity, v_s

$$v_s = v_g - v_l = \frac{v_{sg}}{1-H} - \frac{v_{sl}}{H} \quad (2.17)$$

2.3 PRESSURE GRADIENT CALCULATION IN THE WELLBORE

Computing correct values of mixture properties is essential to modeling the wellbore pressure profile accurately. A major effort in modeling mixture properties is directed toward accurately estimating the in-situ volume fractions occupied by each phase. In this section, we discuss the methods used to estimate in-situ phase fractions, and present the methods for gas-liquid two-phase flow. In the case of three-phase gas/oil/water flow, treating the two liquid phases as one effectively reduces the system to a two-phase flow situation and has been generally found to yield acceptable predictive accuracy (Wang, 1996).

2.3.1 Methods for Calculating Pressure Drop

Different approaches are widely used to calculate phase fractions and pressure distribution in multiphase-flow systems. The simplest approach is considering the multiphase flow as a pseudo single phase flow, which is called a homogeneous model. This method assumes that all phases are well mixed and move with the same velocity, so

there is no slip between the phases. With this assumption, the in-situ phase fraction becomes the same as the input volume fraction, hence

$$H = c_l \quad (2.18)$$

Using this method, fluid properties' values are computed as an average of the constituent phases. The calculations for this method are very simple and are independent of flow regimes. Although this method is very fast and simple, the results are unrealistic in some cases, such as vertical or near vertical gas/liquid mixture flow. In vertical flow, the lighter phase, gas, tends to channel through the center of the conduit and moves faster than the liquid. This velocity difference makes the homogenous assumption invalid.

In contrast, another method considers a separated flow approach that assumes that the phases may move with unequal velocity in the same or in different directions. Computing the flow parameters in this method sometimes requires the use of empirical correlations. Since the correlations are based on experimental data, the equations will not give accurate values for a wide range of conditions outside the range of correlation parameters. These correlations have generally performed better than the homogenous model. The experimental separated flow models take into account differences in flow patterns by some correlations. The main attempt is to develop a number of correlations and maps to recognize flow regime at each section of wellbores and then predict pressure drop for each regime consistent with the observed physical phenomena. Generally, in this method there are totally different fluid flow governing equations and parameters for each flow regime based on experimental results. To summarize, a separated method based on correlations is an accurate method to predict multiphase flow parameters in comparing

with homogeneous models. But we are not sure that we can extrapolate the method to all situations different from the database in which they are developed.

Another approach for modeling separated flow is based on using mechanistic models. These models consist of describing the flow mechanics using fundamental governing equations and also including correlations to describe some fluid distribution. This method is based on recognizing the hydrodynamic conditions that lead to the various patterns of flow and then proposing individual models for each flow regime to estimate holdup and pressure loss. Four major flow patterns are recognized in vertical and near-vertical systems: bubbly flow, slug flow, churn flow and annular flow. These flow patterns are clearly distinguishable and are generally recognized by all researchers. A schematic of different flow regimes in a vertical wellbore is shown in Figure 2.4, showing bubbly, slug, churn and annular flow from left to right.

- **Bubbly flow:** At low gas velocity, the liquid phase is the continuous phase and gas or vapor phase flows as bubbles in it. When the gas velocity is low, especially in vertical flow, the bubbles are uniformly distributed.
- **Slug flow:** As gas velocity increases, the bubbles coalesce and make larger bubbles, known as Taylor bubbles. These large bubbles sometimes have almost the same diameter as the wellbore. Hence, as shown in Figure 2.4, the slug flow consists of two parts: large bubbles (Taylor bubbles) and continuous liquid phase containing small bubbles.
- **Churn flow:** This flow regime forms by the breakdown of slug flow Taylor bubbles because of high mixture velocity. The gas phase flows in a chaotic

manner through the liquid phase and it is relatively unstable, hence the multiphase flow parameters such as holdup vary with time at each section when churn flow exists in the tubing.

- **Annular flow:** As the flow rate and fraction of the gas phase increases, this phase starts to flow through the center of the wellbore as a continuous core with some liquid droplets. The liquid phase forms a layer along the pipe wall and flows as an annulus.

In the next section we present a comparison of different two-phase flow models and then describe the method which is used in this work in detail.

2.3.2 Comparison of Existing Multiphase Flow Models

To select between existing homogeneous, empirical separated and mechanistic separated models, a comparison between the field data and model results is needed. As described by Ansari et al. (1994), the evaluation was carried out by comparing the pressure drop calculated by different methods with the measured data collected in the University of Tulsa well data bank. A criterion for this comparison was developed, based on average error and standard deviation. The minimum and maximum possible values for this criterion are 0 and 6. The smaller the value, the more accurate is the model. The following methods are compared:

- 1) Homogeneous method: Hagedorn and Brown model (1965)

2) Separated empirical models: Duns and Ros correlation (1963), Beggs and Brill correlation (1973), Orkiszewski correlation (1967), and Mukherjee and Brill correlation (1983)

3) Separated mechanistic models: Ansari et al. mechanistic model (1994), Hasan and Kabir mechanistic model (1988), and Petalas and Aziz mechanistic model (2000)

The relative performance factors calculated from several field data sets are shown in Figures 2.5 and 2.6. As shown in these two figures, the Ansari et al. mechanistic model appears to be the most accurate with the lowest score.

To show the magnitude of the error in some examples, we modeled the field data available in Orkiszewski's paper (1967) using the Ansari's method. For each case, we know the well geometry, the surface flow rates and surface pressure. The bottomhole pressure is simulated and the result is compared with the field data. Some of the results are presented in Table 2.1 and Figure 2.7. Our calculation shows that the average error between the model and the actual data is less than 10 percent in all cases, which means a good agreement.

Based on these results, we decided to use Ansari's model, with some corrections based on Hasan and Kabir's work (2005), in our research to model blackoil steady state multiphase flow in the wellbore. This method is described in the next section in more detail.

2.3.3 Pressure Gradient Model used in this Research

The first step to calculate pressure gradient in two-phase flow is the determination of the type of flow and flow regime. Based on primary variables such as phase velocity and phase density, different conditions may occur. There are two general methods to define these conditions: flow-regimes map and individual transition criteria. By using the map method, a two-dimensional graph is presented where the coordinates are either superficial velocities or dimensionless parameters containing velocities. Based on these parameters, it is possible to determine the flow regime using the maps that are generated by experiments. In the second approach, the efforts are directed to modeling the transition mechanism between the regimes; hence equations are developed to define the regime based on these criteria. This method is more reliable than experimental maps. As the two-phase flow pattern maps are generated in special experimental conditions, the extrapolation of the results to other cases may not be very accurate. On the other hand, the second method is based on the modeling of transition criteria and is less case dependent and more accurate. In the following, we discuss these transition criteria between different flow regimes.

Bubble/Slug flow transition: When the gas velocity is low, the liquid phase is the continuous phase and the gas phase moves in the terms of bubbles through the continuous phase. As gas velocity increases, the transition from bubble flow to slug flow occurs because of an agglomeration of small bubbles to make larger bubbles. These large Taylor bubbles may occupy almost the entire pipe cross-section area. This transition was

experimentally found to occur at a gas fraction of approximately 0.25, so H should be less than 0.75 (Taitel et al., 1980). From Equation 2.17:

$$v_s < \frac{v_{sg}}{0.25} - \frac{v_{sl}}{0.75}$$

Hence, we can express the transition in terms of superficial and slip velocities:

$$v_{sg} > 0.25v_s + 0.333v_{sl} \quad (2.19)$$

The slip velocity (bubble-rise velocity) can be defined based on the Harmathy (1960) correlation as

$$v_s = 1.53 \left\{ \frac{g\sigma_s(\rho_l - \rho_g)}{\rho_l^2} \right\}^{1/4} \quad (2.20)$$

where σ_s is the surface tension. Pipe diameter also has influences on the transition criteria. Shoham et al. (1982) maintains that in narrow pipes the bubbly flow is unstable and slug flow occurs at much lower gas velocities.

At high-liquid rates, turbulent forces break large gas bubbles down into small ones. Hence, even for a gas fraction greater than 0.25, bubble flow exists. This type of bubble flow is known as dispersed bubbly flow. The following equation yields the transition from the bubble flow to dispersed bubble flow (Barnea, 1987). When the mixture velocity makes the left hand side of Equation 2.21 greater than the right hand side, bubbly flow persists up to a void fraction of 0.52.

$$2 \left(\frac{0.4\sigma_s}{(\rho_l - \rho_g)g} \right)^{0.5} \left(\frac{\rho_l}{\sigma_s} \right)^{0.6} \left(\frac{f}{2d} \right)^{0.4} (v_{sl} + v_{sg})^{1.2} > 0.725 + 4.15 \left(\frac{v_{sg}}{v_{sl} + v_{sg}} \right)^{0.5} \quad (2.21)$$

It should be noted that Taitel et al. (1980) showed that the gas fraction could not be more than 0.52 at most. At a higher gas fraction, the transition to the slug flow occurs even though the mixture velocity ($v_{sl} + v_{sg}$) is more than the value calculated in Equation 2.21.

Slug/Churn flow transition: Slug flow consists of two parts: large bubbles, named Taylor bubbles and liquid slugs. Small bubbles are dispersed axially in liquid slugs which are separated by the Taylor bubbles. (Figure 2.8)

As the gas flow rate increases, the interaction between the falling film and the rising Taylor bubble also increases. This interaction causes the bubbles to break up and churn flow appears. For the transition to churn flow, Barnea (1987) showed that the mixture velocity must be higher than one calculated by Equation 2.21, and the gas velocity must be high enough to break the bubbles. Ansari et al., recommended Equation 2.22 to compute gas velocity transition criterion from slug to churn flow:

$$f_g > 0.76 \rightarrow \frac{v_{sg}}{v_{sg} + v_{sl}} > 0.76 \rightarrow v_{sg} > 3.17v_{sl} \quad (2.22)$$

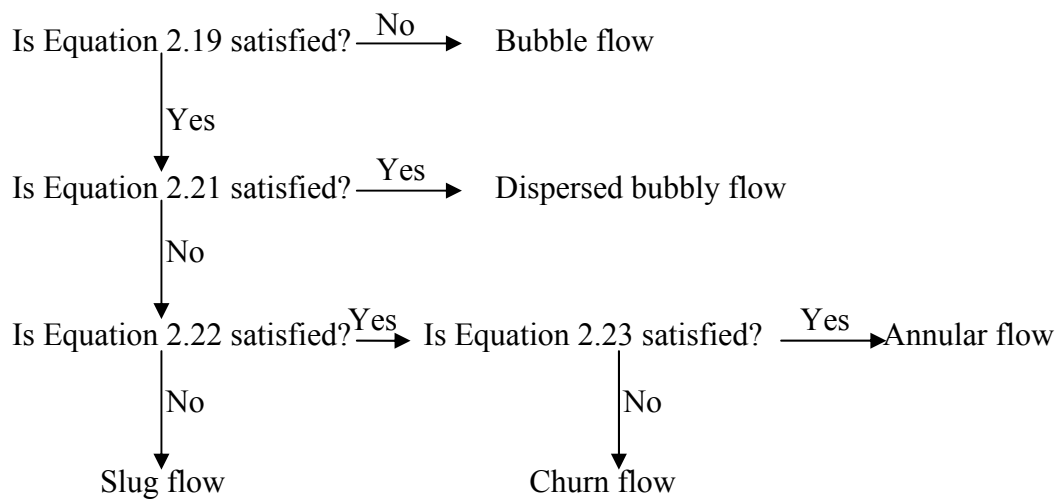
Many of the researchers believe that the churn flow is really some kind of slug flow, for example, experiments by Hasan and Kabir (2002) show that the churn flow can be treated much like slug flow for oil field applications.

Churn/Annular flow transition: In the annular flow, the liquid flows upward along the tube wall, while the gas core flows through the center of the pipe. Annular flow occurs when the gas velocity is high enough to prevent the entrained liquid droplets from falling

back into the gas stream. The criterion for this transition is based on work by Taitel et al. (1980) as

$$v_{sg} > 3.1 \left\{ \frac{g \sigma_s (\rho_l - \rho_g)}{\rho_g^2} \right\}^{1/4} \quad (2.23)$$

Based on these equations, the flow pattern can be defined by the following procedure:



The typical flow patterns map obtained from Equations 2.19 through 2.23 is plotted as Figure 2.9. Hence, with these equations, it is possible to define the flow regime at each section of the wellbore. Now we present a brief description of the physical methods that are used to calculate flow parameters in each flow regime. These equations are for bubble, slug/churn and annular flow.

Bubble flow model: For bubble flow, we assume that the bubbles are uniformly distributed in the liquid phase, so this regime can be approximated as a pseudo-single phase. The in-situ gas velocity is influenced by the tendency of bubbles to move through

the central portion of the conduit. In turbulent flow, the center velocity is 1.2 times the cross-sectional average mixture velocity. Also, there is a slippage between the gas phase and the liquid phase because of the difference in densities. Hence, the gas velocity is a combination of both center velocity and slip velocity and can be expressed as

$$v_g = 1.2v_m + v_s \quad (2.24)$$

Using Equations 2.12 and 2.20, Equation 2.24 is rewritten as an implicit equation, which can be solved numerically to obtain liquid holdup in bubble flow.

$$1.53 \left\{ \frac{g \sigma_s (\rho_l - \rho_g)}{\rho_l^2} \right\}^{1/4} H^{0.5} = \frac{v_{sg}}{1-H} - 1.2v_m \quad (2.25)$$

Hence, the following procedure is used to calculate the pressure gradient in a bubble flow system:

- 1) Holdup is calculated from Equation 2.25 using Newton's method.
- 2) Equations 2.3-a and 2.3-b are used to calculate mixture properties:

$$\rho_m = \rho_l H + \rho_g (1-H) \quad (2.3-a)$$

$$\mu_m = \mu_l H + \mu_g (1-H) \quad (2.3-b)$$

- 3) As previously discussed, the two-phase pressure gradient is made up of three components which are due to elevation, acceleration, and friction. The total pressure gradient is computed from Equation 2.1:

$$\frac{dP}{dz} = -(\rho_m v_m \frac{dv_m}{dz} + \rho_m g \sin\theta + \frac{2\rho_m f_m v_m^2}{d}) \quad (2.1)$$

In Equation 2.1, the friction factor, f_m , is obtained from a Moody diagram for a Reynolds

number which is defined as $\frac{\rho_m v_m d}{\mu_m}$

Slug/Churn flow: Each slug unit in the Slug flow consists of two parts: 1) Taylor bubbles and 2) liquid slugs as shown in Figure 2.8. The main parameter that we want to

calculate is β , the ratio of the Taylor bubble size to the slug unit, which is defined as $\frac{L_{TB}}{L_{SU}}$

Modeling this kind of regime is based on material balance for these two sections. The overall gas and liquid mass balance give:

$$v_{sg} = \beta v_{gTB} (1 - H_{TB}) + (1 - \beta) v_{gLS} (1 - H_{LS}) \quad (2.26-a)$$

$$v_{sl} = -\beta v_{lTB} H_{TB} + (1 - \beta) v_{lLS} H_{LS} \quad (2.26-b)$$

In these equations, subscript TB represents the Taylor bubble, and subscript LS represents the liquid slug section in a slug unit.

The mass balances for liquid and gas from liquid slug to Taylor bubble give

$$(v_{TB} - v_{lLS}) H_{LS} = (v_{TB} - (-v_{lTB})) H_{TB} \quad (2.27-a)$$

$$(v_{TB} - v_{gLS})(1 - H_{LS}) = (v_{TB} - v_{gTB})(1 - H_{TB}) \quad (2.27-b)$$

where v_{TB} is the Taylor bubble-rise velocity, and is equal to the summation of centerline velocity in the Taylor bubble section, and the rise velocity in a stagnant liquid column.

Hence,

$$v_{TB} = 1.2v_m + 0.35 \sqrt{\frac{gd(\rho_l - \rho_g)}{\rho_l}} \quad (2.28)$$

Similarly, in the liquid slug the velocity of the gas bubbles is calculated from Equation 2.29.

$$v_{gLS} = 1.2v_m + 1.534\sqrt{\frac{g\sigma_l(\rho_l - \rho_g)}{\rho_l^2} H_{LS}^2} \quad (2.29)$$

where the second term in this equation, $1.534\sqrt{\frac{g\sigma_l(\rho_l - \rho_g)}{\rho_l^2} H_{LS}^2}$, represents the bubble-rise velocity, as defined in Equation 2.25. the velocity of the falling film can be expressed in terms of Taylor bubble void fraction as

$$v_{ITB} = 9.916\sqrt{gd(1 - \sqrt{1 - H_{TB}})} \quad (2.30)$$

The liquid slug void fraction can be obtained by Sylvester's equation (Sylvester, 1987) as

$$H_{LS} = 1 - \frac{v_{sg}}{0.425 + 2.65v_m} \quad (2.31)$$

The mass balance equations are solved to calculate liquid and gas fraction and pressure gradients in the slug and bubble zones. The following procedure is used to calculate the pressure gradient in a slug flow system.

- 1) Values for Taylor bubble velocity, gas velocity in the liquid slug, liquid velocity in the falling film, and liquid fraction in the liquid slug section are calculated from Equations 2.28 through 2.31, respectively.
- 2) Equations 2.26-a, 2.26-b, 2.27-a, and 2.27-b are solved iteratively to obtain the following four unknowns: β , H_{TB} , V_{ILS} , and V_{gTB} .

3) The total pressure gradient is computed from Equation 2.32:

$$\frac{dP}{dz} = -(\rho_m v_m \frac{dv_m}{dz} + ((1-\beta)\rho_{LS} + \beta\rho_g)g \sin\theta + \frac{2\rho_{LS}f_{LS}v_m^2(1-\beta)}{d}) \quad (2.32)$$

where $\rho_{LS} = \rho_l H_{LS} + \rho_g (1 - H_{LS})$

The friction factor, f_{LS} , is obtained from a Moody diagram for a Reynolds number defined

as $\frac{\rho_{LS} v_m d}{\mu_{LS}}$.

For more details of the slug model, see Ansari et al. (1994) and Mukherjee et al. (1983).

Annular flow: This model is based on the Hasan and Kabir research (2005). They showed that a homogeneous modeling approach for annular flow shows accuracy comparable to existing mechanistic models. Figure 2.10 shows errors in calculation pressure loss in well bank data. The maximum error is about 26 psi, with both models tracking each other well. Hence, we use the homogenous method to model annular flow because of its accuracy and simplicity. The following procedure is used to calculate the pressure gradient in an annular flow system:

1) Liquid volume fraction is calculated from Equation 2.6:

$$c_l = \frac{v_{sl}}{v_{sl} + v_{sg}} \quad (2.6)$$

2) Equations 2.33-a and 2.33-b are used to calculate mixture properties:

$$\rho_m = \rho_l c_l + \rho_g (1 - c_l) \quad (2.33-a)$$

$$\mu_m = \mu_l c_l + \mu_g (1 - c_l) \quad (2.33-b)$$

3) As previously discussed, the two-phase pressure gradient is made up of three components, which are due to elevation, acceleration, and friction. The total pressure gradient is computed from Equation 2.1:

$$\frac{dP}{dz} = -(\rho_m v_m \frac{dv_m}{dz} + \rho_m g \sin\theta + \frac{2\rho_m f_m v_m^2}{d}) \quad (2.1)$$

where the friction factor, f_m , is obtained from a Moody diagram for a Reynolds number,

defined as $\frac{\rho_m v_m d}{\mu_m}$.

Note that the method discussed here can be used for all vertical and near vertical wellbores. Based on the comparison done by Ansari et al. (1994) the overall performance of this model is superior to all other available mechanistic and empirical models, although this model does not give satisfactory results for deviated wells. The discussed model performed significantly better than all other methods for slug, churn, and annular flow modeling. The Hasan and Kabir model (Hasan et al., 1988) performed better than Ansari's model when over 75% of the well length was predicted to be in bubble flow regime.

2.4 TEMPERATURE DISTRIBUTION

During oil or gas production, the temperature of the produced fluid is different from the temperature of the surrounding formations, so heat exchange happens between the fluid and formations. This heat exchange causes temperature variation in the wellbore, which is very important for fluid properties calculation. As fluid properties,

such as density depend on temperature, accurate estimation of temperature profiles in wellbores becomes essential. In addition, accelerated corrosion potential at certain temperature ranges makes this estimation important for choosing the materials for the facilities and for equipment design (Wang, 1996).

The energy balance equation in wellbores can be written as

$$\frac{d}{dz} \left\{ h_m + \frac{v_m^2}{2} + gz \sin \theta \right\} + Q = 0 \quad (2.34)$$

In Equation 2.34 the first section, $\frac{d}{dz} \left\{ h_m + \frac{v_m^2}{2} + gz \sin \theta \right\}$, is the energy convection in the wellbore which consists of energy convection because of enthalpy difference, kinetic energy and potential energy. The last term, Q , represents heat transfer between the formation and the wellbore. In this equation, h_m is the mixture enthalpy in the wellbore and Q shows the heat exchange between the fluid flow and the formation.

2.4.1 Calculation of Temperature Profile in Wellbore

The second term in Equation 2.34 is the heat flux between the formation and the wellbore. As we mentioned before, hydrocarbon production or fluid injection involves significant heat exchange between the wellbore fluid and its surroundings. For example during production, the hot produced fluid loses heat to the increasingly cooler surrounding formation as it ascends the borehole, or the cooler gas due to Joule-Thompson effect gains heat from the formation. Hence, during production, the wellbore

fluid acts like a thermal source or sink term of the heat for the formation. Figure 2.11 shows the various thermal resistances that exist in the wellbore. In this research we follow the work performed by Hasan and Kabir (1994) to model temperature profiles. We assume that the steady-state heat flow from the tubing fluid to the wellbore/formation interface equals the heat flow from the interface to the formation. First, we need to model the temperature profile in the formation. We assume that there is no heat diffusion in the vertical direction in the earth around the wellbore; hence we expect one-dimensional radial diffusion. The general heat diffusion equation is

$$\frac{\partial^2 T_e}{\partial r^2} + \frac{1}{r} \frac{\partial T_e}{\partial r} = \frac{c_{pe} \rho_e}{k_e} \frac{\partial T_e}{\partial t} \quad (2.35)$$

In Equation 2.35, T_e is the formation temperature at any arbitrary depth at time t , and r is the radial distance measured from the center of the wellbore. In the right hand side c_{pe}, ρ_e, k_e are heat capacity, density and thermal conductivity for the formation, respectively. Initial formation temperature is known; in this work we assume that at $t = 0$, the formation temperature profile is linear based on the local geothermal gradient. We also assume that at the outer boundary of the formation, temperature does not change. At the wellbore/formation interface, constant heat conduction is assumed. The solution of Equation 2.35 is analogous to that used for pressure diffusion. Using the Laplace transformation, we can present an equation for the temperature distribution as a function of distance and time. The general solution is a combination of Bessel functions, which can be found in the literature (Dake, 1978). Hasan and Kabir (1994) presented an

approximation for the analytical solution to calculate the solution quite accurately as follows:

$$T_D = \left[0.4063 + 0.5 \ln t_D\right] \left(1 + \frac{0.6}{t_D}\right) \quad \text{If } t_D > 1.5 \quad (2.36)$$

$$T_D = 1.128\sqrt{t_D} (1 - 0.3\sqrt{t_D}) \quad \text{If } t_D < 1.5 \quad (2.37)$$

In Equations 2.36 and 2.37, T_D, t_D are the dimensionless temperature and time respectively.

$$T_D = \frac{2\pi k_e}{Q} (T_{wb} - T_e) \quad (2.38)$$

$$t_D = \frac{k_e t}{\rho_e c_{Pe} r_{wb}^2} \quad (2.39)$$

The above equations show the heat transfer between the earth and the wellbore/formation interface. In these equations, T_{wb} and T_e are wellbore/formation interface temperature and earth temperature, respectively. We need to know the rate of heat flow from the wellbore to the interface. Figure 2.11 shows a schematic for a general wellbore configuration. As shown in this figure, different elements are involved in transferring heat to wellbore fluid. There are conductive heat transfers through cement, casing, annulus, installation and tubing. There is also a natural convective heat transfer in the annulus because of the temperature gradient. The general heat transfer between the wellbore fluid and the surroundings is expressed in the terms of an overall heat transfer coefficient. The rate of heat flow through the wellbore per unit length of the well can be written as

$$Q = 2\pi r_{to} U_{to} (T_f - T_{wb}) \quad (2.40)$$

where T_f is the temperature of the flowing fluid and U_{to} is the overall heat transfer coefficient based on the outside tubing area.

The general equation of the overall heat transfer coefficient is

$$\frac{1}{U_{to}} = \frac{r_{to}}{r_{ti} h_{to}} + \frac{r_{to} \ln(r_{to}/r_{ti})}{k_t} + \frac{r_{to} \ln(r_{ins}/r_o)}{k_{ins}} + \frac{r_{to}}{r_{ins} (h_c + h_r)} + \frac{r_{to} \ln(r_{co}/r_{ci})}{k_{cas}} + \frac{r_{to} \ln(r_{wb}/r_{co})}{k_{cem}} \quad (2.41)$$

This equation shows different resistances that exist in heat transmission between the fluid

and the interface. $\frac{r_{to}}{r_{ti} h_{to}}$ shows the convection inside the tubing.

$\frac{r_{to} \ln(r_{to}/r_{ti})}{k_t}$, $\frac{r_{to} \ln(r_{ins}/r_o)}{k_{ins}}$ are conduction heat transfer through the tubing thickness and

the insulation around the tubing. $\frac{r_{to}}{r_{ins} (h_c + h_r)}$, $\frac{r_{to} \ln(r_{co}/r_{ci})}{k_{cas}}$, $\frac{r_{to} \ln(r_{wb}/r_{co})}{k_{cem}}$ are terms for

convective heat transfer inside the tubing, conduction through the casing and conduction

through the thickness of cement, respectively. More details in computing the heat transfer

coefficient are presented in next section. The heat transfer to the formation can be

determined by definition of the overall heat transfer coefficient. Combining Equations

2.38 and 2.40

$$T_f - T_{ei} = (T_f - T_{wb}) + (T_{wb} - T_e) = \frac{Q}{2\pi r_{to} U_{to}} + \frac{QT_D}{2\pi k_e} = \frac{Q}{2\pi} \left\{ \frac{1}{r_{to} U_{to}} + \frac{T_D}{k_e} \right\}$$

Hence, we obtain the expression for heat transfer between the formation and the fluid

$$Q = 2\pi \left\{ \frac{r_{io} U_{io} k_e}{r_{io} U_{io} T_D + k_e} \right\} (T_f - T_e) \quad (2.42)$$

Hence, the overall heat transfer is

$$Q = 2\pi r_{io} U (T_f - T_e) \quad (2.43)$$

where U is the overall heat transfer coefficient between the flowing fluid and the

formation and is defined as $\frac{U_{io} k_e}{r_{io} U_{io} T_D + k_e}$.

Equation 2.43 can be used as the second term in the general energy balance Equation (2.34). We assume that the formation temperature varies linearly with depth.

Thus,

$$T_e = T_{ebh} - g_T z \quad (2.44)$$

where T_{ebh} is the bottomhole temperature and g_T shows the temperature gradient in the earth. To compute the temperature profile in the wellbore it is clear from Equation 2.34 that we need a correct calculation of enthalpy variation. The enthalpy gradient can be written in terms of the temperature and pressure gradient as

$$\frac{dh_m}{dz} = c_P \frac{dT_f}{dz} - \eta c_P \frac{dP}{dz} \quad (2.45)$$

where η is the Joule-Thompson coefficient. Inserting Equations 2.45 and 2.43 in the general energy balance equation (Equation 2.34) results

$$\frac{d}{dz} \left\{ h_m + \frac{v_m^2}{2} + gz \sin \theta \right\} + \frac{q \pi d}{w} = 0$$

Hence,

$$\frac{dh_m}{dz} + v_m \frac{dv_m}{dz} + g \sin \theta + \left\{ \frac{2\pi r_{to} U}{w} \right\} (T_f - T_{ei}) = 0$$

Simplifying the above equations results

$$c_p \frac{dT_f}{dz} - \eta c_p \frac{dP}{dz} + v_m \frac{dv_m}{dz} + g \sin \theta + \left\{ \frac{2\pi r_{to} U}{w} \right\} T_f - \left\{ \frac{2\pi r_{to} U}{w} \right\} (T_{ebh} - g_T z) = 0$$

Finally we arrive to the following equation:

$$\begin{aligned} \frac{dT_f}{dz} + \frac{2\pi r_{to} U}{w c_p} T_f &= \frac{2\pi r_{to} U}{w c_p} (T_{ebh} - g_T z) \\ &+ \frac{1}{c_p} (\eta c_p \frac{dP}{dz} - g \sin \theta - v_m \frac{dv_m}{dz}) \end{aligned} \quad (2.46)$$

We assume that at depth L , the temperature is T_i (Boundary condition). Solving

Equation 2.46 with this boundary condition:

$$\begin{aligned} T_f &= (T_{ebh} - g_T z) + (T_i - T_{ebh}) \exp\left(\frac{-L}{A}\right) + \\ &g_T A \left[1 - \exp\left(\frac{-L}{A}\right) \right] + \frac{1}{\rho c_p} \frac{dP}{dL} \phi A \left[1 - \exp\left(\frac{-L}{A}\right) \right] \end{aligned} \quad (2.47)$$

In Equation 2.47, A is thermal relaxation distance and defined as

$$A = \frac{w c_p}{2\pi r_{to} U} \quad (2.48)$$

Also,

$$\phi = (\rho \eta c_p \frac{dP}{dL} - \rho g \sin \theta - \rho v \frac{dv}{dL}) / (\frac{dP}{dL}) \quad (2.49)$$

c_p represents the average heat capacity for the multiphase flow in the wellbore, which can be calculated from equation 2.50. Heat capacity for gas and oil is computed with blackoil correlations presented in Appendix A.

$$c_p = c_{pg} (1-H) \frac{\rho_g}{\rho_m} + c_{pL} H \frac{\rho_L}{\rho_m} \quad (2.50)$$

The change in enthalpy per unit change in pressure is expressed by the Joule-Thompson effect. In a multiphase system, it is possible to use the empirical correlation presented by Sagar et al. (1991), or the theoretical approach developed by Alves et al. (1992) to estimate the Joule-Thompson coefficient. Alves et al. (1992) showed that temperature profiles calculated by using their approach are more accurate. Hence, we use Alves's equation which is defined by Equation 2.51

$$\eta = \frac{1}{c_p \rho_m} \left\{ (1-H) \left(\frac{-T}{Z} \right) \left(\frac{dZ}{dT} \right)_P + H \right\} \quad (2.51)$$

Real gas and incompressible liquid conditions are assumed to perform calculations by Equation 2.51.

The following procedure is used to calculate the steady state temperature distribution in the wellbore:

- 1) First, we define the temperature distribution in the formation. Based on the formation type, the temperature gradient in the earth is known.
- 2) From Equations 2.50 and 2.51, we calculate the heat capacity and Joule-Thompson coefficient of the flowing mixture based on the holdup profile which is computed from pressure loss calculations described in section 2.3.

3) We compute the overall heat transfer coefficient from Equation 2.43, which is discussed in more detail in the next section.

4) Equation 2.47 gives the temperature distribution in the wellbore.

2.4.2 The Overall Heat Transfer Coefficient

One of the most important parts of energy equation is the heat transfer between the formation and the wellbore fluid. To calculate this part we recall the heat transfer equation

$$\frac{1}{U_{to}} = \frac{r_{to}}{r_{ti} h_{to}} + \frac{r_{to} \ln(r_{to} / r_{ti})}{k_t} + \frac{r_{to} \ln(r_{ins} / r_o)}{k_{ins}} + \frac{r_{to}}{r_{ins} (h_c + h_r)} + \frac{r_{to} \ln(r_{co} / r_{ci})}{k_{cas}} + \frac{r_{to} \ln(r_{wb} / r_{co})}{k_{cem}} \quad (2.41)$$

Equation 2.41 includes all the possible heat transfer mechanisms through each of the wellbore elements. Some of the terms in Equation 2.41 are negligible as the resistance of some parts of well configuration is small. In most wells we can consider the following assumptions:

1) Tubing insulation is absent.

2) Due to the small value of the tubing diameter, we can assume that the fluid temperature is equal to the temperature at the inner side of the tubing. So $T_f = T_{ti}$

3) Both the tubing and casing are made of metals like steel with high conductivity, so we can neglect the temperature distribution in them. Hence, $T_{ti} = T_{to}$ and $T_{ci} = T_{co}$.

4) The radiation term in the annulus is negligible.

Based on these assumptions for a typical well, the overall heat transfer is

$$\frac{1}{U_{to}} = \frac{r_{to}}{r_{ins} h_c} + \frac{r_{to} \ln(r_{wb} / r_{co})}{k_{cem}} \quad (2.52)$$

The fluid in the annulus is in contact with the annulus surface, which is at a different temperature. In this situation, heat transfer takes place not only because of conduction but also because of natural convection. This phenomenon arises because of the density difference of the fluids in the annulus. There is temperature difference between the bulk fluid and fluid close to the pipe surface. Hence, densities of these two parts are different, and this causes fluid circulation (natural convection), which enhances heat transfer.

The heat transfer coefficient for natural convection in the annulus can be approximated by calculating this coefficient for fluid between two vertical plates.

Dropkin and Sommerscales (1965) presented the following correlation

$$h_c = \frac{0.049(Gr Pr)^{0.333} Pr^{0.074} k_a}{r_{ins} \ln\left(\frac{r_{ci}}{r_{ins}}\right)} \quad (2.53)$$

where the Grashof number, Gr , in Equation 2.53 defined as

$$Gr = (r_{ci} - r_{ins})^3 g \rho_a^2 \beta (T_{ins} - T_{ci}) / \mu_a^2 \quad (2.54)$$

The Grashof number reflects the extent of motion of the annular fluid owing to natural convection. Also, the Prandtl number (Pr) is $\frac{c_p \mu_a}{k_a}$ which is a measurement of the interaction between the hydrodynamic boundary layer and the thermal boundary layer.

Computing h_c from Equation 2.53 requires an iterative method because we need the temperature distribution to calculate the Grashof number. We use the following procedure for this purpose:

- 1) Estimate a typical value for natural heat transfer coefficient (h_c).
- 2) Compute the overall heat transfer in the wellbore from Equation 2.52.
- 3) Compute the thermal relaxation distance in the wellbore/formation system

from Equation 2.55

$$A = \frac{w c_p}{2 \pi r_{io}} \left(\frac{k_e + r_{io} U_{io} T_D}{U_{io} k_e} \right) \quad (2.55)$$

- 4) Use Equation 2.47 to compute the wellbore fluid temperature distribution.
- 5) Calculate $T_{ins} - T_{ci}$ to find the Grashof number. Based on the assumptions

we made (assumptions 1 through 3), it is obvious that

$$T_{ins} - T_{ci} = T_f - T_{cem} \quad (2.56)$$

On the other hand, from basic principles of heat transfer

$$T_f - T_{cem} = \frac{U}{h_c} (T_f - T_{ei}) \quad (2.57)$$

Hence, we can calculate the Grashof number.

6) Calculate h_c from Equation 2.53. If the difference between the estimated value and new value is larger than a specific tolerance, start from step 1 with this new natural convection factor.

2.5 SOLUTION PROCEDURE

When multiphase flow movement in the wellbore is not a function of time, the steady state condition exists. We assume that pressure, temperature and phase fraction profiles do not change with time. During the steady state period, pressure, phase velocities, phase fractions and temperature are only functions of depth. To compute these variables we can solve Equations 2.1 and 2.34 simultaneously. We can consider different boundary conditions to solve these equations, for example:

- 1) Pressure and the flow rate are constant at the surface.
- 2) Bottomhole pressure is known.
- 3) Flow rate between the reservoir and the wellbore is constant.

This wellbore simulator can be used as a stand-alone tool or it can be coupled to a reservoir simulator. In a coupled simulator, it is necessary to relate the fluid flow and the pressure in the reservoir and wellbore segments. A well model is used to connect the wellbore to the reservoir that is described in Appendix B.

The wellbore is divided into segments and continuity, momentum balance equation, and energy balance equation are solved in each segment as the following procedure:

- 1) For each segment we solve Equation 2.1 by a pressure loss model to compute pressure, flow rate and phase fraction.
- 2) We solve Equation 2.34 and calculate the temperature distribution in the wellbore.
- 3) With simulated temperature we can update the flow properties such as density and viscosity and update Equation 2.1 solutions (pressure, flow rate and fractions). If the difference between updated results and old results is greater than a specific tolerance steps 2 and 3 will be redone.

2.6 RESULTS

2.6.1 Case Study 1: Oil/Gas Producer Well

The first case that we modeled with this simulator is based on the measurements presented by Hasan and Kabir (2002). A 5151 ft vertical well produces 23 °API dry oil at a flow rate equal to 1140 STB/D through a 2.99-in ID tubing. The gas/oil ratio is 450 scf/STB, and the gas gravity is 0.80. Graphs 2.12 through 2.15 show pressure, temperature, phase fraction and phase velocity in the wellbore. It can be seen from Figure 2.12 that the pressure is increasing along the wellbore. The simulated results are very close to the measured data. Figure 2.13 shows the liquid holdup in the wellbore. As depth increases because of the pressure increasing, more gas remains in solution in the oil phase, so the gas fraction declines. It can also be observed that the flow regime is changing around a depth of 2000 ft. we can observe the effect of the regimes in the velocity figure (Figure 2.14). When the flow regime switches from the slug flow to

bubbly flow, the slopes of the gas velocity and liquid velocity profiles change which is a problem because of the discontinuity between pressure equations for bubble flow and slug flow (AB in Figure 2.14).

2.6.2 Case Study 2: Water/Oil/Gas Producer Well

The second case that we discussed is based on the data reported by Sagar et al. (1991) from a vertical flowing well. The well produced oil, water and gas. The well parameters are given in more detail in Appendix G.2.3 for the input file, which is used in this simulator. In this case, field data are only available for the temperature distribution in the wellbore. Two other researchers also presented model results for this data set: Sagar et al. (1991) and Hasan and Kabir (2002). Their results and our model are shown for temperature distribution in Figure 2.16. It can be seen that our model and the Hasan et al. model show a good agreement with the field data. The Sagar et al. model differs from the actual data mainly because it ignores natural convection in the annulus. At each section of the wellbore we calculated the heat capacity for gas, water and oil, so we do not assume a constant value for heat capacity in the wellbore. Also, computations are done in segments to allow variable natural convective factor with well depth. These calculations make our results different from the Hasan et al. method in which it is assumed that the annulus is filled with liquid up to the wellhead (so that the natural convection factor is constant). Figures 2.17 through 2.19 show pressure profile, liquid holdup and phase velocities in the wellbore for this case. The hydrostatic pressure gradient is the dominant part, so the pressure profile is near linear. We can also see the two-phase flow regime

change in the wellbore. In this case, the discontinuity in velocity profiles due to pattern is less severe. For depths greater than 4500 ft, there is no gas in the wellbore; hence the gas velocity is zero.

Some simulators assume a constant temperature in the wellbore (mean of surface and bottomhole temperature) or formation temperature. These assumptions cause the pressure, velocity or phase fraction profiles to be different from the profiles computed with simulated temperature. Figures 2.20 and 2.21 show these differences. As can be seen, an almost 2% difference may result when ignoring the temperature distribution.

The results shown for fluid flow parameters profile and temperature profile in these two cases indicate a good agreement between our simulator and field data. These results also show the importance of temperature simulation in the wellbore.

2.7 EFFECT OF PRODUCTION PARAMETERS ON TEMPERATURE DISTRIBUTION IN WELLBORES

2.7.1 Base Case Study

The energy equation in the wellbore was presented by Equation 2.34. In this equation, the last term on the right hand side considers the exchange of heat between the fluid and the surrounding formation, due to temperature difference, which causes cooling of the fluid during production.

Changing of the fluid enthalpy causes temperature variation. Different parameters involved in the heat exchange rate can affect enthalpy derivation in the wellbore. For

example, the size of the wellbore, the earth temperature gradient, gas, oil and water fraction in multiphase flow and fluid thermal properties all influence enthalpy variation. The enthalpy gradient can be written in terms of temperature and pressure gradient as

Equation 2.45, where
$$\frac{dh_m}{dz} = c_p \frac{dT_f}{dz} - \eta c_p \frac{dP}{dz}$$

This equation shows that the higher heat-flow rate from the wellbore fluid to the formation causes the higher value for the temperature gradient in the wellbore.

In the following section we discuss the sensitivity of the temperature distribution in the wellbore to each parameter given in Table 2.1, and observe its influence on temperature distribution.

2.7.2 Effect of Tubing Diameter

In this section, we change the wellbore geometry by changing the tubing, annulus and casing diameters. We assume that the velocity of each phase does not change. In the base case the tubing diameter is 2 7/8". For example, when we change the diameter to 2" we decrease the flow rate to keep the phase velocity unchanged. Figure 2.22 shows the effect of tubing diameter on the temperature distribution, and that the temperature gradient is lower in larger tubing.

As the tubing size increases, the amount of mass flowing in the wellbore is larger for the same velocity. From Equation 2.52 it can be concluded that the value of $U_{io}r_{io}$ does not change noticeably as we vary the size of the wellbore. We can assume that the heat flow rate from the hot wellbore fluid into the formation is not a strong function of

the radial geometry of the wellbore. Hence, by increasing flowing mass in the wellbore and considering the same heat flow rate, Equation 2.34 shows that $\frac{dh}{dz}$ declines. From Equation 2.45 we expect a lower temperature value in the wellbore.

2.7.3 Effect of Gas Liquid Ratio (GLR)

The GLR value is obtained from Equation 2.58. In this case, we changed the GLR from the value of 6.1 scf/bbl to 120 and 300 scf/bbl, respectively.

$$GLR = \frac{q_g}{q_o + q_g} \quad (2.58)$$

The higher values for GLR cause higher-temperature changes in the wellbore. Hence, assuming constant temperature for the flowing fluid from the reservoir, the surface temperature will be lower in a higher GLR case. Figure 2.23 shows this effect for three different cases. The heat capacity value for gas is less than that for liquid at each temperature and pressure. Hence, increasing the fraction of gas in produced fluid results in lower overall heat capacity. Equation 2.52 shows that the exchanged heat between wellbore fluid and the reservoir is a function of well geometry and its thermal properties. Hence, changing GLR does not have significant effect on Q . With a constant heat loss from the wellbore fluid, decreasing heat capacity results in higher changes in the temperature. Hence, higher GLR leads to a higher value for the temperature at each point.

2.7.4 Effect of Water Oil Ratio (WOR)

The produced fluid in a typical well can consist of both oil and water in a liquid state. Changing the fraction of water and oil in the produced liquid may influence the temperature profile in the wellbore. In this section we model the profile for three different values of WOR: 1, 5, and 10, respectively. Figure 2.24 shows that for a higher value of WOR, variation of temperature with respect to wellbore depth is lower. The main reason for this behavior is the heat capacity. We know that water has a higher heat capacity value than oil, with specific gravity of about 34. Hence, by increasing the fraction of water in liquid, the overall heat capacity increases. With the same heat exchange between the fluid and formation, cooling down a system with high-heat capacity is more difficult; hence a high value of WOR causes lower $\frac{dT}{dz}$, which is shown in Figure 2.24.

2.7.5 Effect of Formation Thermal Conductivity

Earth thermal properties influence the temperature distribution due to their effect on the heat flow rate from the wellbore fluid to the formation. Equation 2.52 combines all the mechanisms that govern this heat exchange. Changing the formation conductivity results in the variation of the overall heat transfer coefficient. In this section, we change thermal conductivity from the base case, 1.4 Btu/hr-ft-°F, to 1 Btu/hr-ft-°F and 2 Btu/hr-ft-°F, respectively. It should be noted that the heat conductivity of quartzite, limestone and shale are about 2, 1.4 and 1 Btu/hr-ft-°F, respectively (Encyclopedia Britannica website). Figure 2.25 shows different temperature profiles in the wellbore. It can be

observed that for higher-thermal conductivity the slope of temperature distribution is steeper. From Equations 2.42 and 2.43:

$$U = \frac{U_{io}k_e}{k_e + r_{io}U_{io}T_D} \rightarrow \frac{1}{U} = \frac{1}{U_{io}} + \frac{r_{io}T_D}{k_e} \quad (2.59)$$

In this equation the second term in the right hand side is a function of $\frac{r_{io}T_D}{k_e}$.

Figure 2.34 shows the variation of $\frac{r_{io}T_D}{k_e}$ as a function of k_e . It is clear that this curve is a monotonically decreasing function. Hence, from Equation 2.59 we can conclude that U is an ascending function of k_e . This means that at higher-heat-thermal conductivity, the thermal resistance between the surrounding formation and fluid flow is also higher. Hence, lower heat loss occurs from the wellbore fluid to the surrounding formation. This results in a lower-temperature gradient in the wellbore, which is in agreement with Figure 2.25.

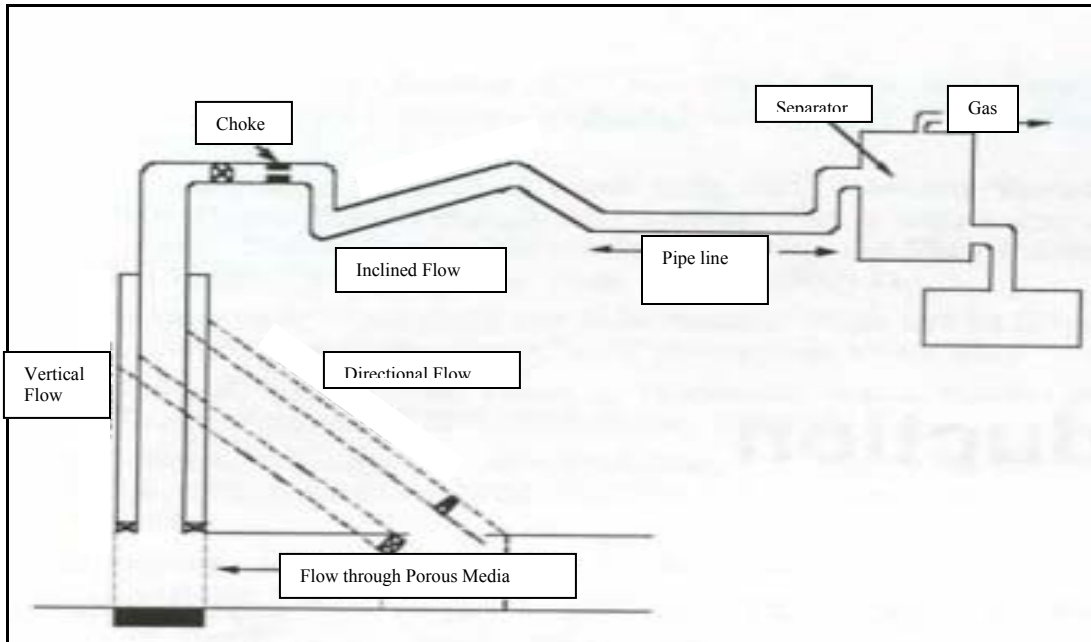


Figure 2.1 Schematic representation of a production system (Brown, 1984)

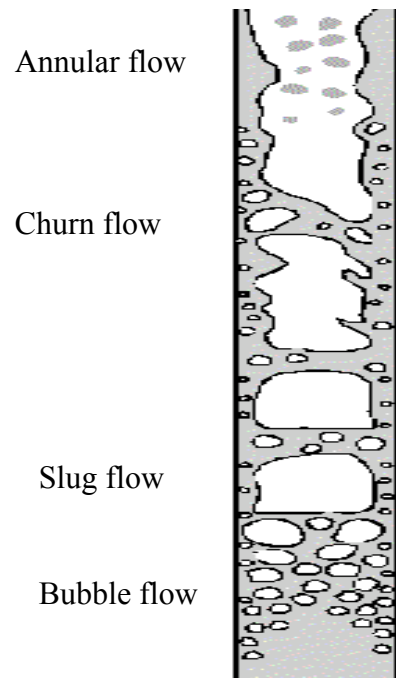


Figure 2.2 Schematic flow patterns in a vertical wellbore

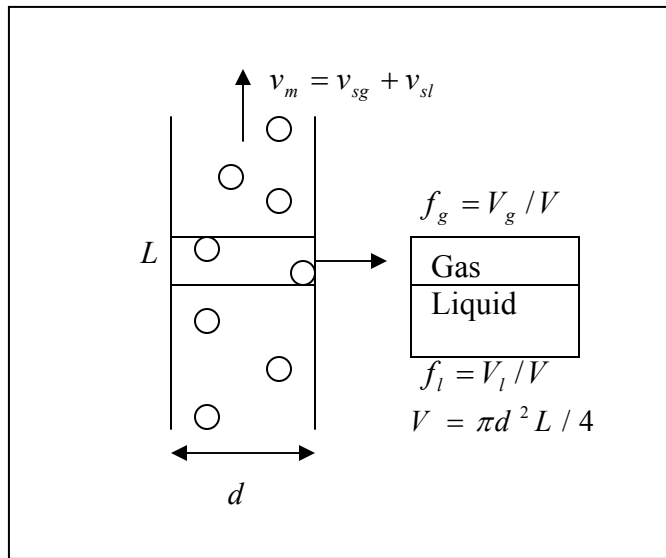


Figure 2.3 Schematic of liquid and gas fraction definition in a control volume

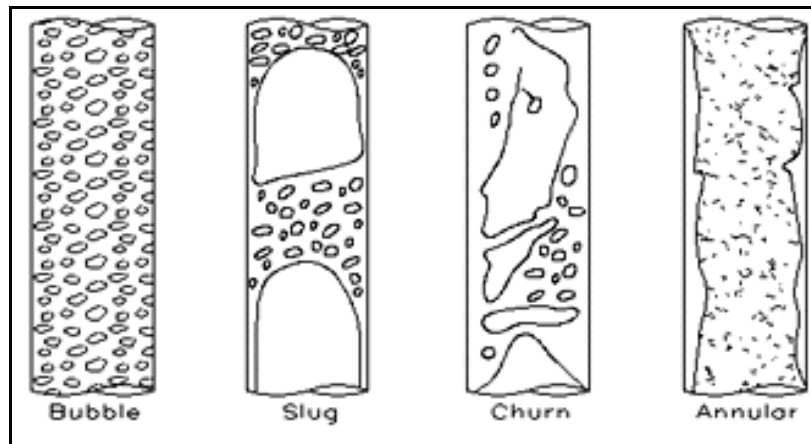


Figure 2.4 Schematic two-phase flow patterns in a vertical tube (From left to right: bubble flow, slug flow, churn flow and annular flow)

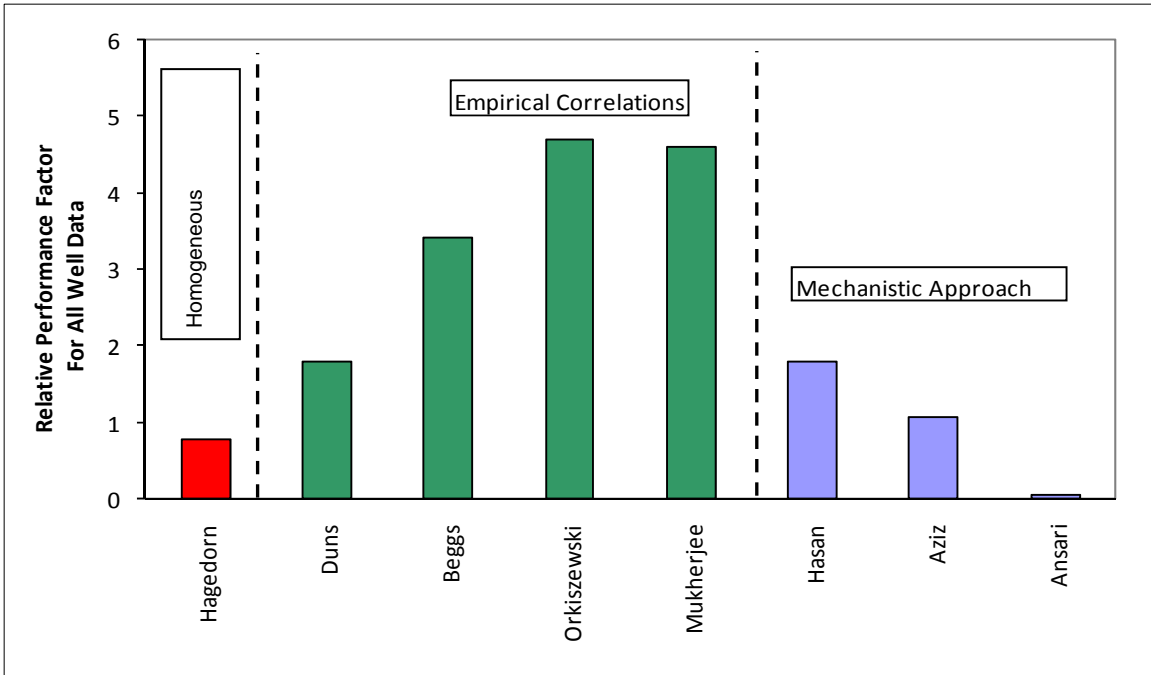


Figure 2.5 Comparison between accuracy of different multiphase flow models used to simulate U of Tulsa well data (1381 wells). (The smaller the relative performance factor, the more accurate is the model)

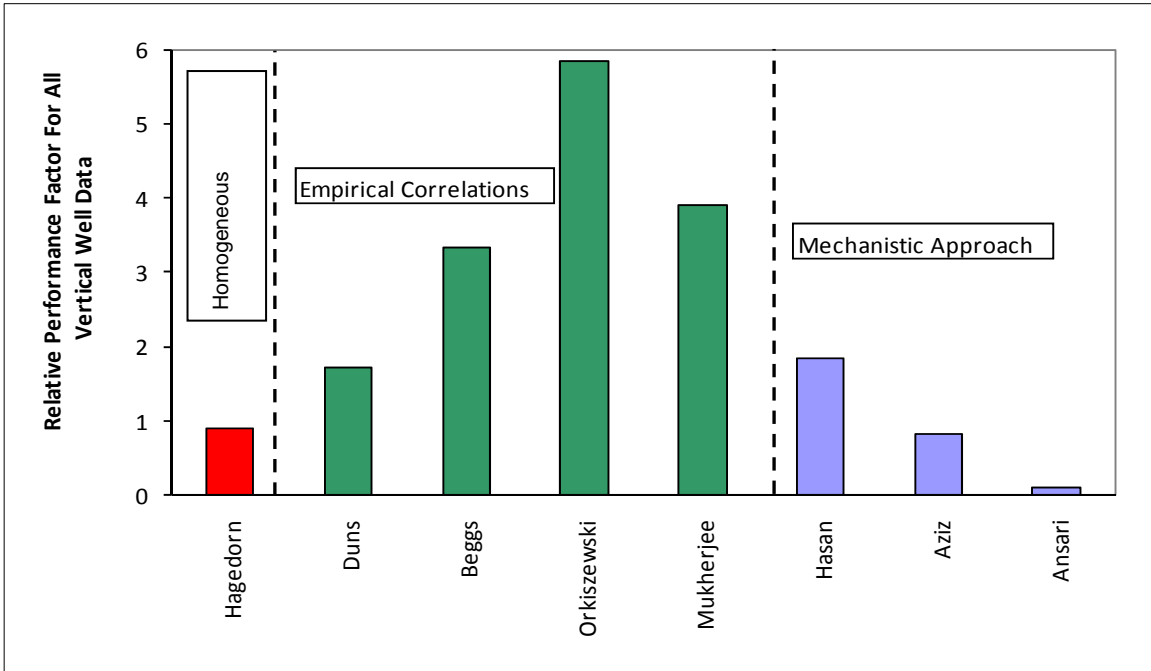


Figure 2.6 Comparison between accuracy of different multiphase flow models used to simulate U of Tulsa vertical well data (755 wells). (The smaller the relative performance factor, the more accurate is the model)

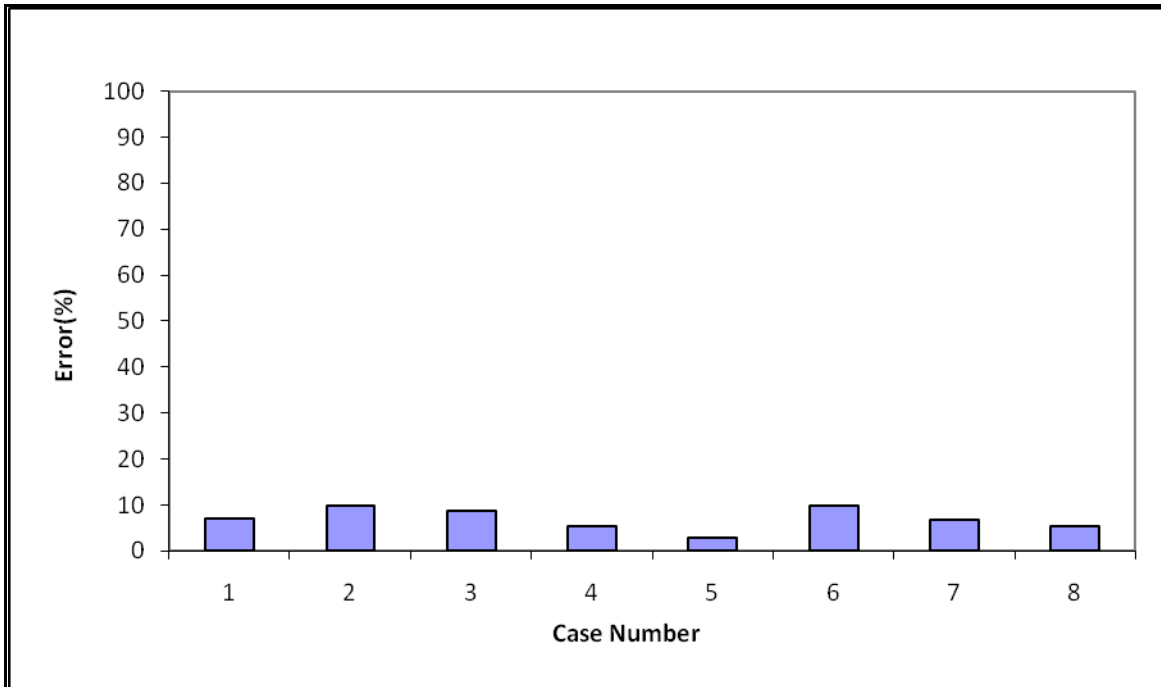


Figure 2.7 Errors between field data and simulated results by Ansari model for calculation bottomhole pressure in different producing wells

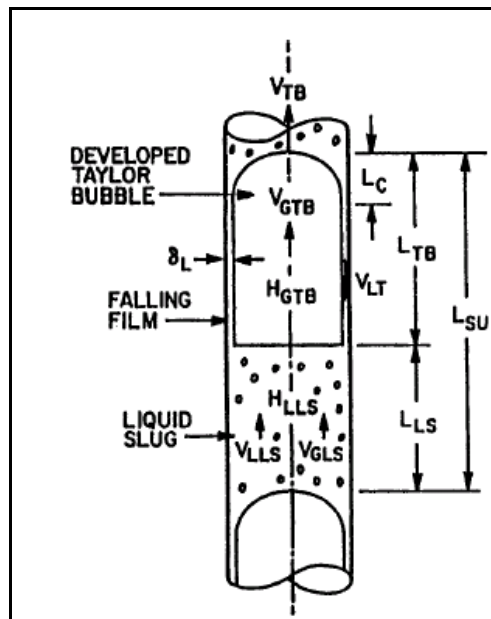


Figure 2.8 Schematic of two sections of slug flow (Taylor bubbles and liquid slugs) (Ansari et al., 1994)

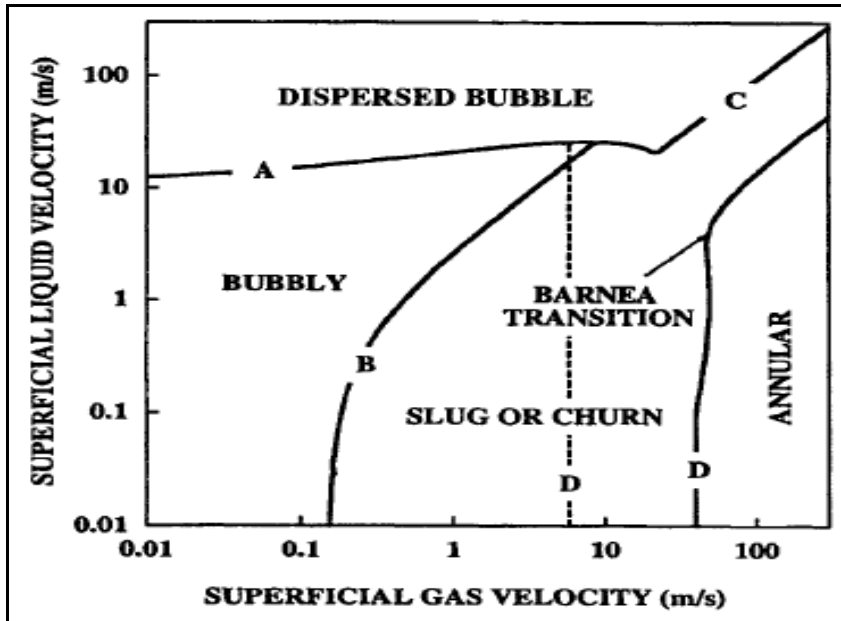


Figure 2.9 Typical map to define two-phase flow pattern based on superficial liquid and gas velocity in a vertical tubing. (Ansari et al., 1994)

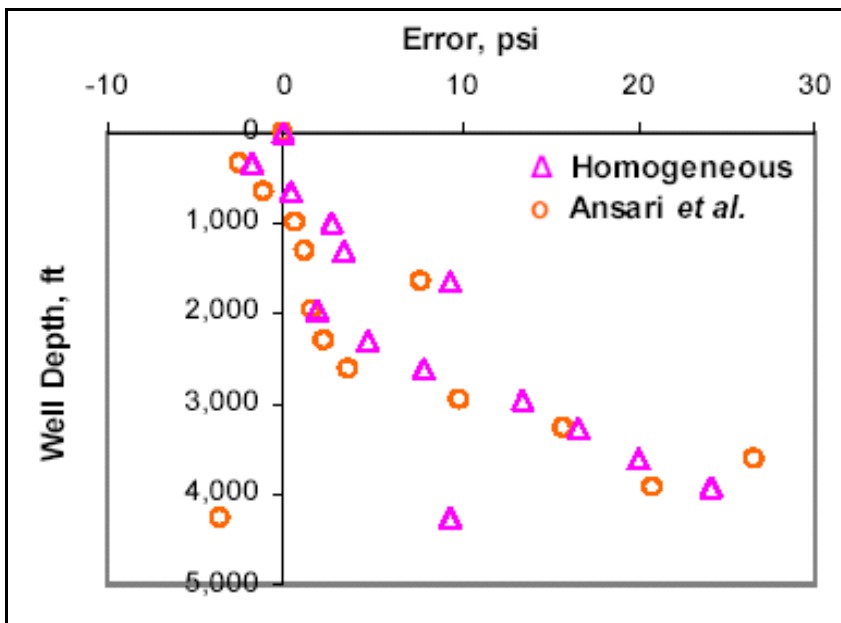


Figure 2.10 Error between field data and bottomhole pressure calculated by two different methods (Ansari et al. model and homogeneous model); dataset encompass a wide range of flowing bottomhole pressure, liquid content (1.2-256 STB/MMsf), and flow rate (0.5-30 MMscf/D) (Hasan and Kabir, 2005)

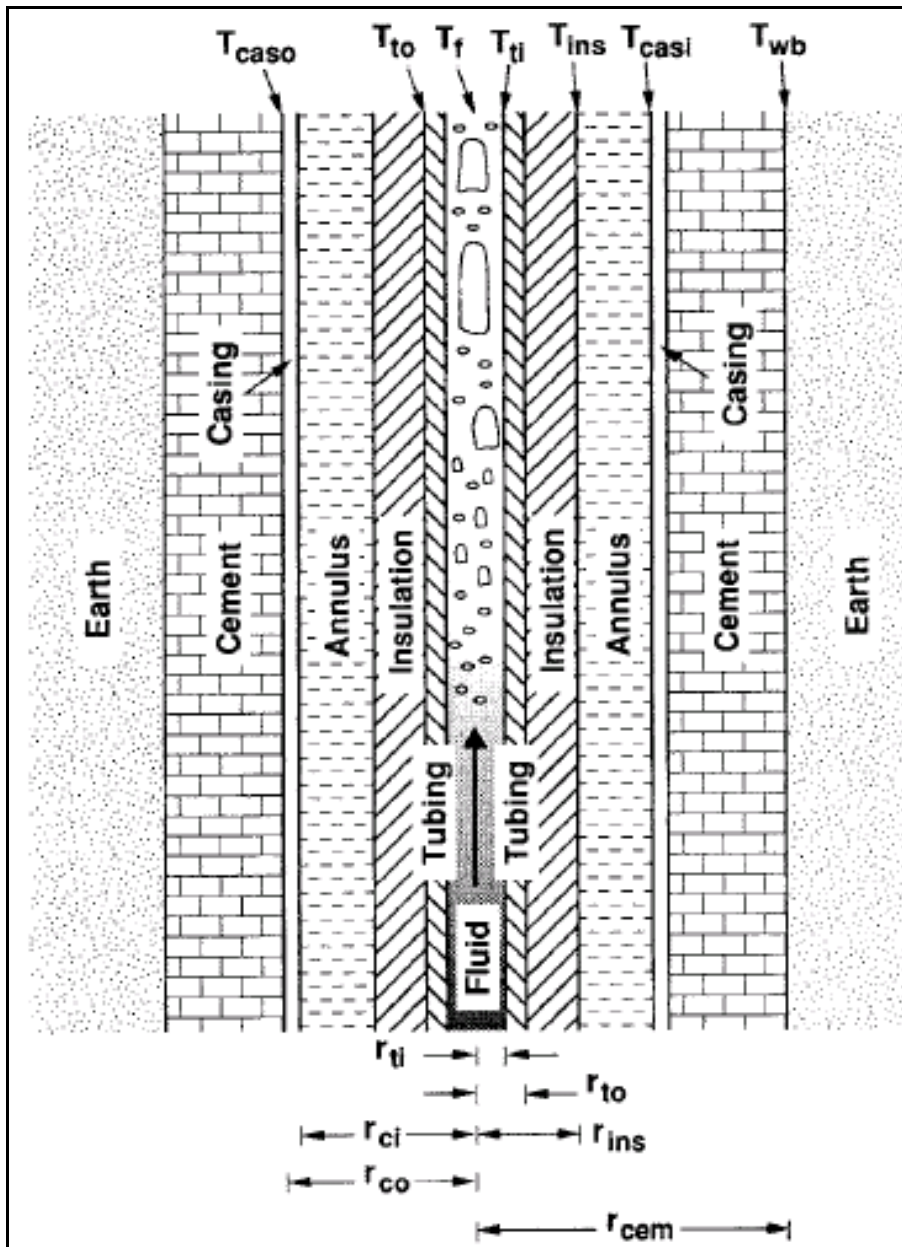


Figure 2.11 Resistances to heat flow between wellbore fluid and surrounding formation (Wang, 1996)

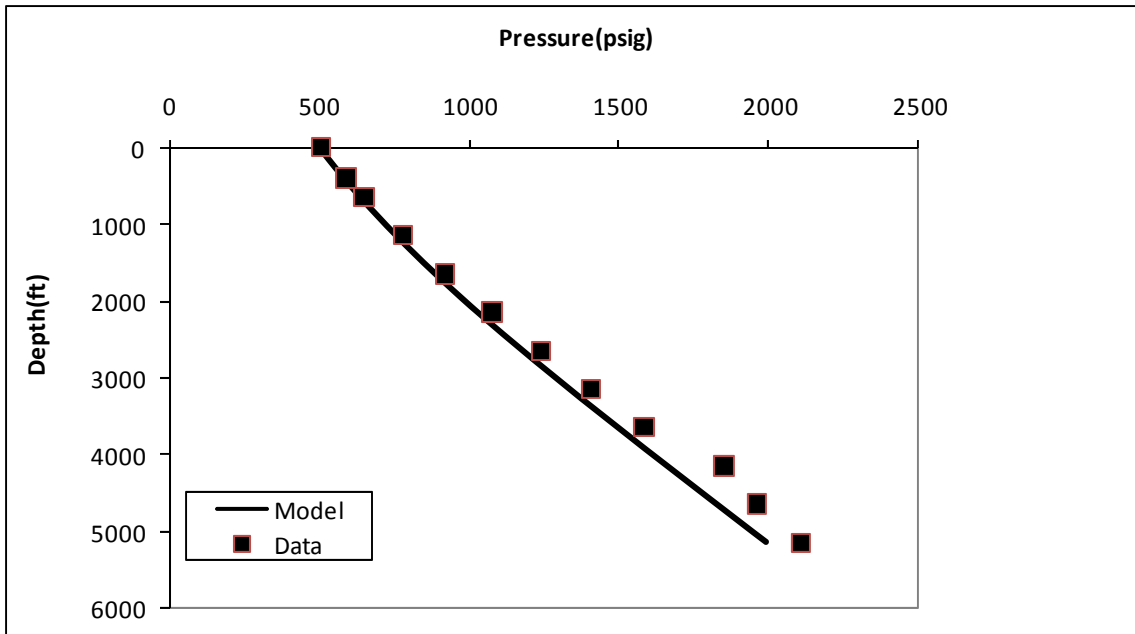


Figure 2.12 Pressure distribution from modeling and field data (Case 1: A 5151 ft vertical well produces 23 °API dry oil at flow rate equal to 1140 STB/D through a 2.99-in ID tubing. The gas/oil ratio is 450 scf/STB, and the gas gravity is 0.80)

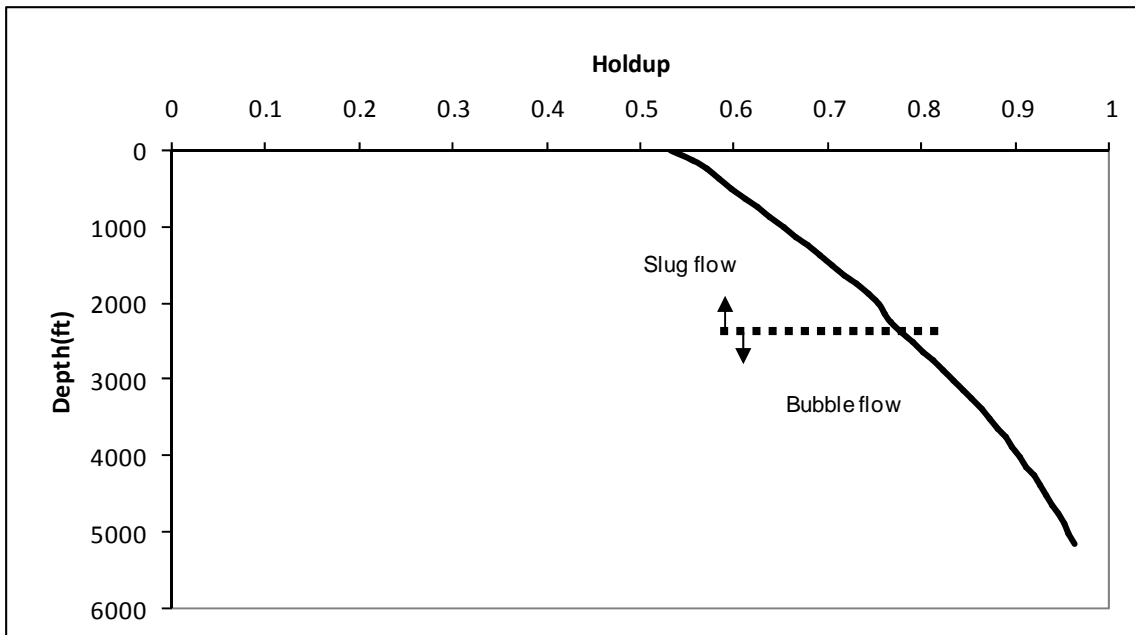


Figure 2.13 Simulated holdup and flow regimes in the wellbore (Case 1: A 5151 ft vertical well produces 23 °API dry oil at flow rate equal to 1140 STB/D through a 2.99-in ID tubing. The gas/oil ratio is 450 scf/STB, and the gas gravity is 0.80)

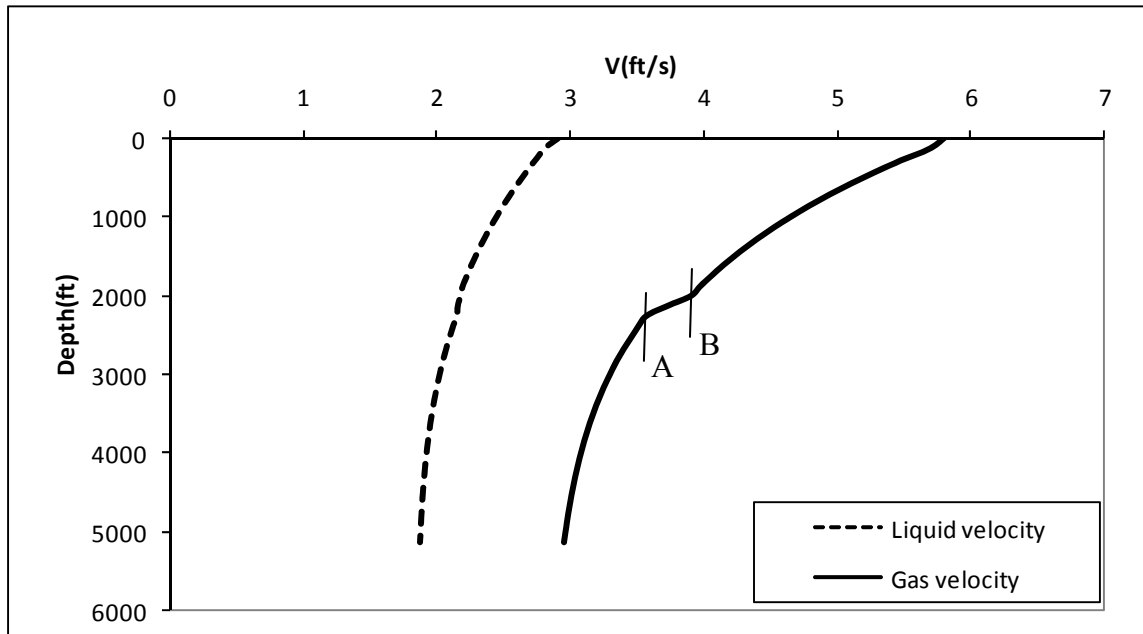


Figure 2.14 Simulated phase velocities distribution in the wellbore (Case 1: A 5151 ft vertical well produces 23 °API dry oil at flow rate equal to 1140 STB/D through a 2.99-in ID tubing. The gas/oil ratio is 450 scf/STB, and the gas gravity is 0.80)

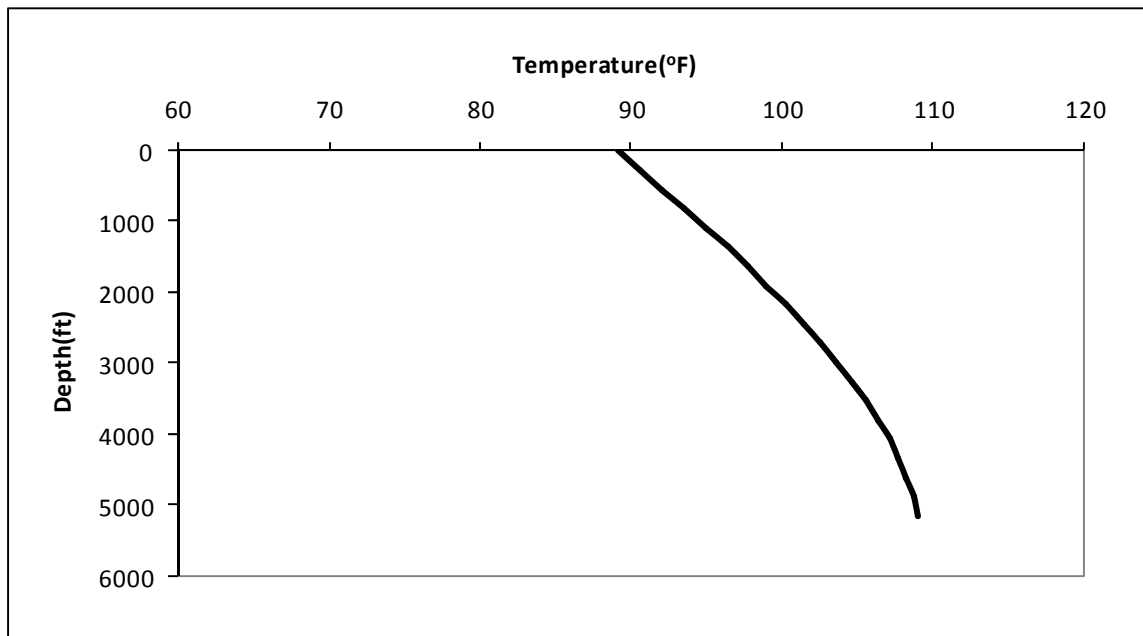


Figure 2.15 Simulated temperature distribution in the wellbore (Case 1: A 5151 ft vertical well produces 23 °API dry oil at flow rate equal to 1140 STB/D through a 2.99-in ID tubing. The gas/oil ratio is 450 scf/STB, and the gas gravity is 0.80)

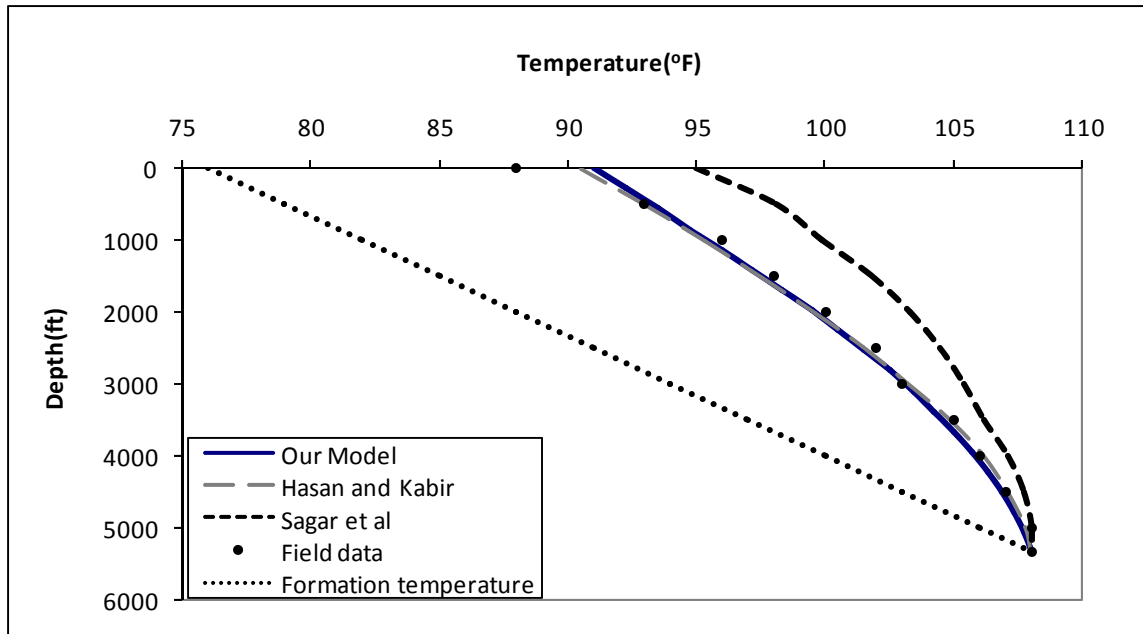


Figure 2.16 Computed and measured wellbore fluid temperature profiles (Case 2: A 5355 ft vertical well produces 59 STB/D oil, 41 Mscf/D gas and 542 STB/D water. Fluid enters the wellbore at 108 °F. The oil gravity is 34.3 °API, the gas gravity is 1.04)

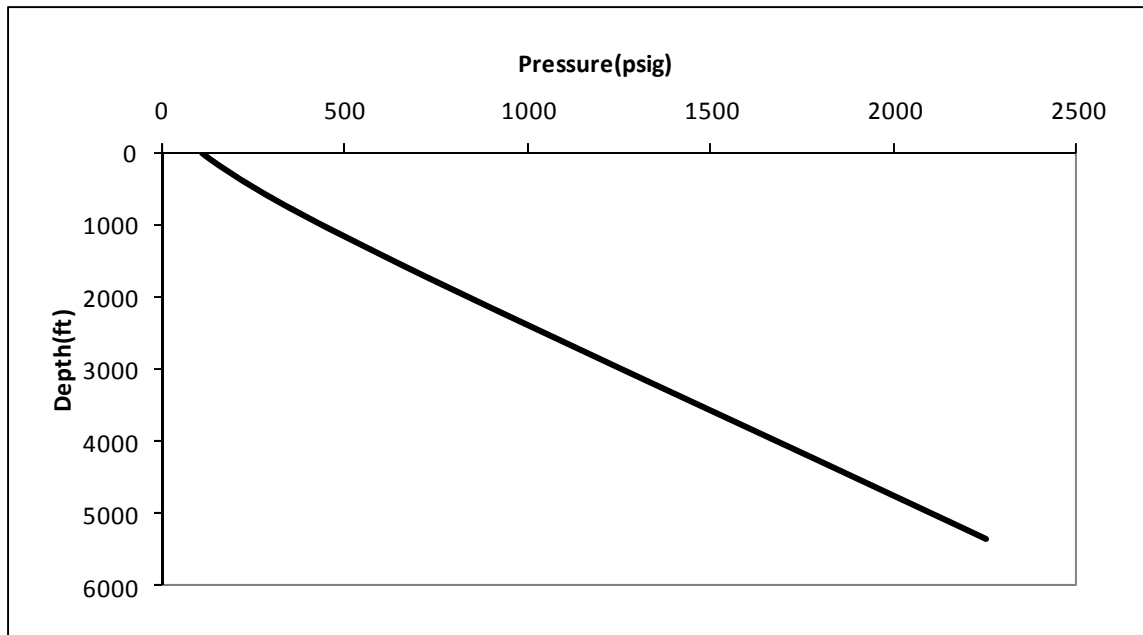


Figure 2.17 Computed pressure profile in the wellbore (Case 2: A 5355 ft vertical well produces 59 STB/D oil, 41 Mscf/D gas and 542 STB/D water. Fluid enters the wellbore at 108 °F. The oil gravity is 34.3 °API, and the gas gravity is 1.04)

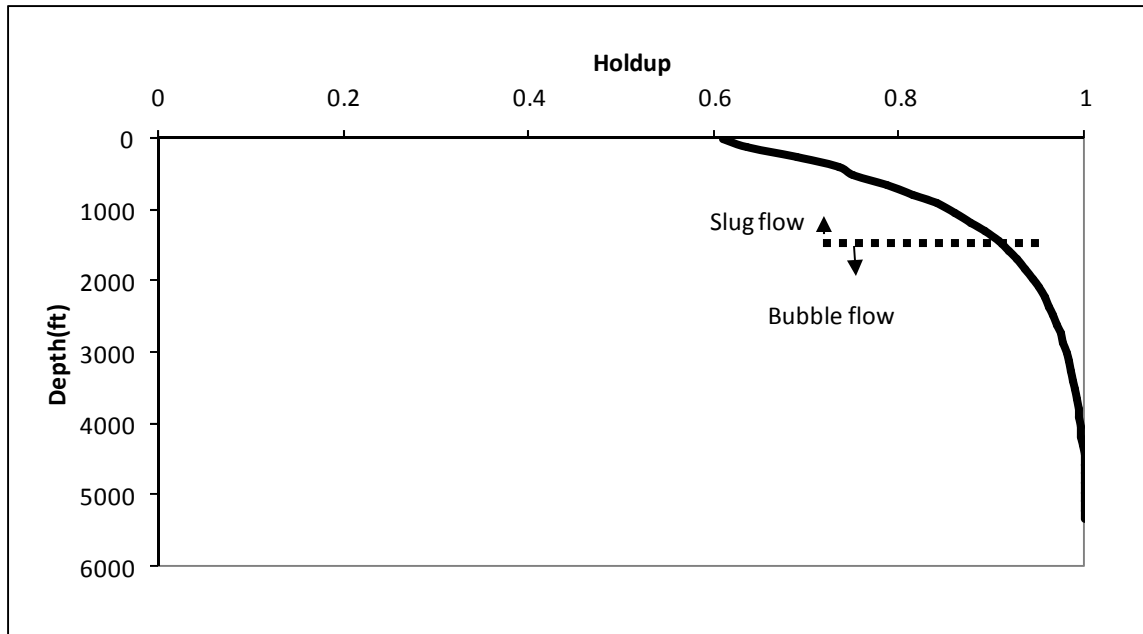


Figure 2.18 Simulated liquid holdup profile and flow regime in the wellbore (Case 2: A 5355 ft vertical well produces 59 STB/D oil, 41 Mscf/D gas and 542 STB/D water. Fluid enters the wellbore at 108 °F. The oil gravity is 34.3 °API, the gas gravity is 1.04)

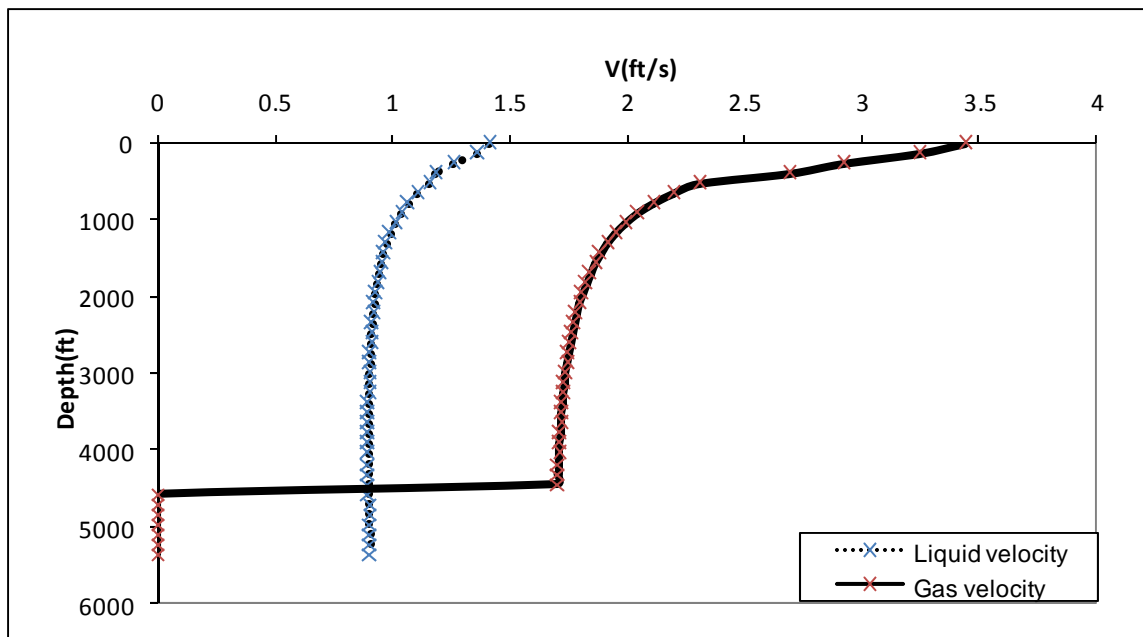


Figure 2.19 Simulated phase velocity profile in the wellbore (Case 2: A 5355 ft vertical well produces 59 STB/D oil, 41 Mscf/D gas and 542 STB/D water. Fluid enters the wellbore at 108 °F. The oil gravity is 34.3 °API, and the gas gravity is 1.04)

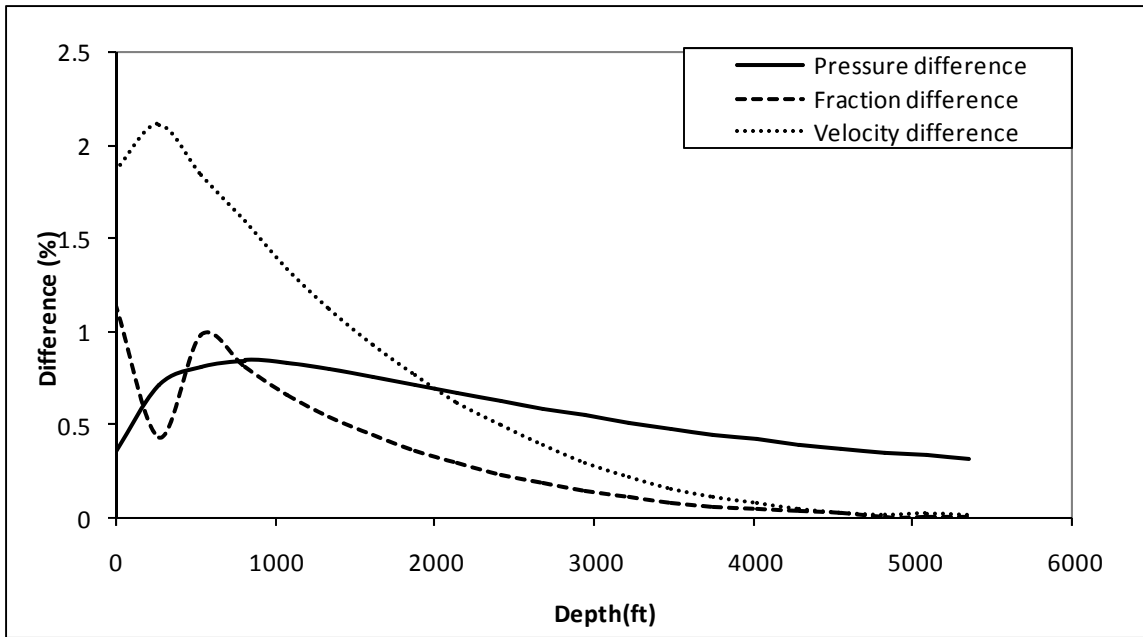


Figure 2.20 Pressure, liquid holdup and gas velocity differences between assuming constant temperature and simulating temperature profile

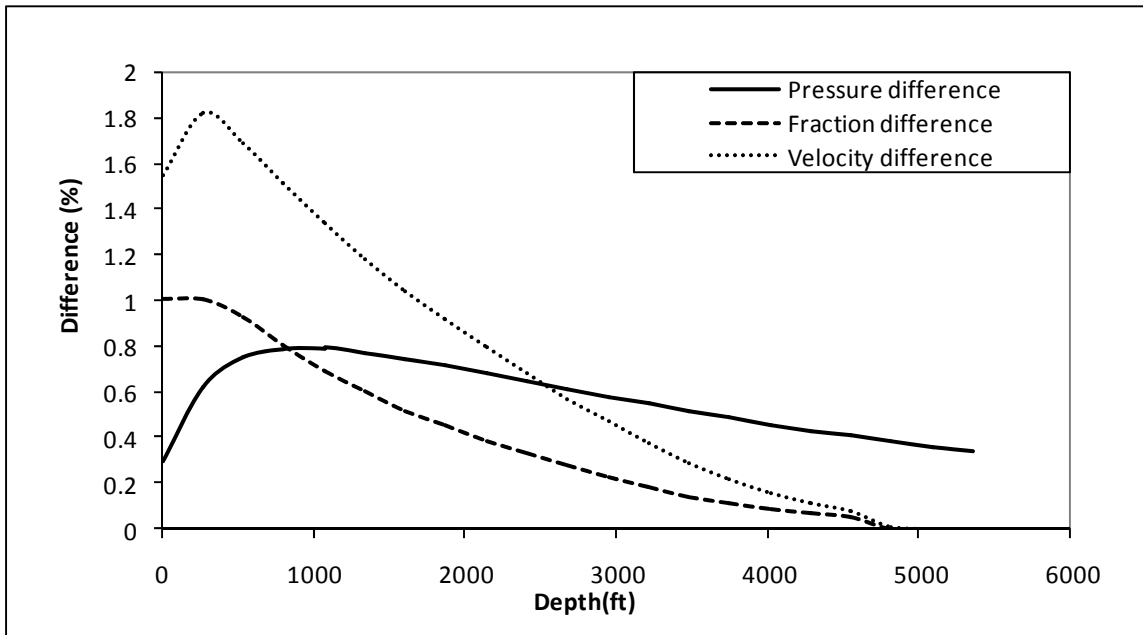


Figure 2.21 Pressure, liquid holdup and gas velocity differences if we assume that the fluid temperature profile is same as formation temperature or if we simulate fluid temperature profile

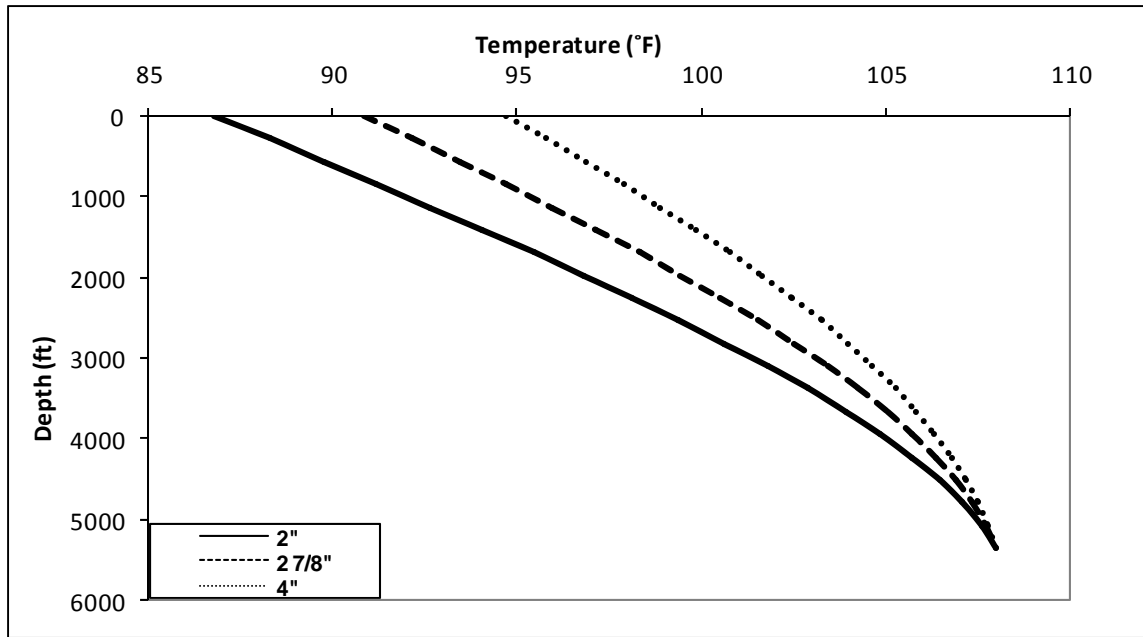


Figure 2.22 Effect of tubing diameter on temperature profile in the wellbore (A 5355 ft vertical well produces 59 STB/D oil, 41 Mscf/D gas and 542 STB/D water; flow rates change to keep velocity constant for different tubing diameters)

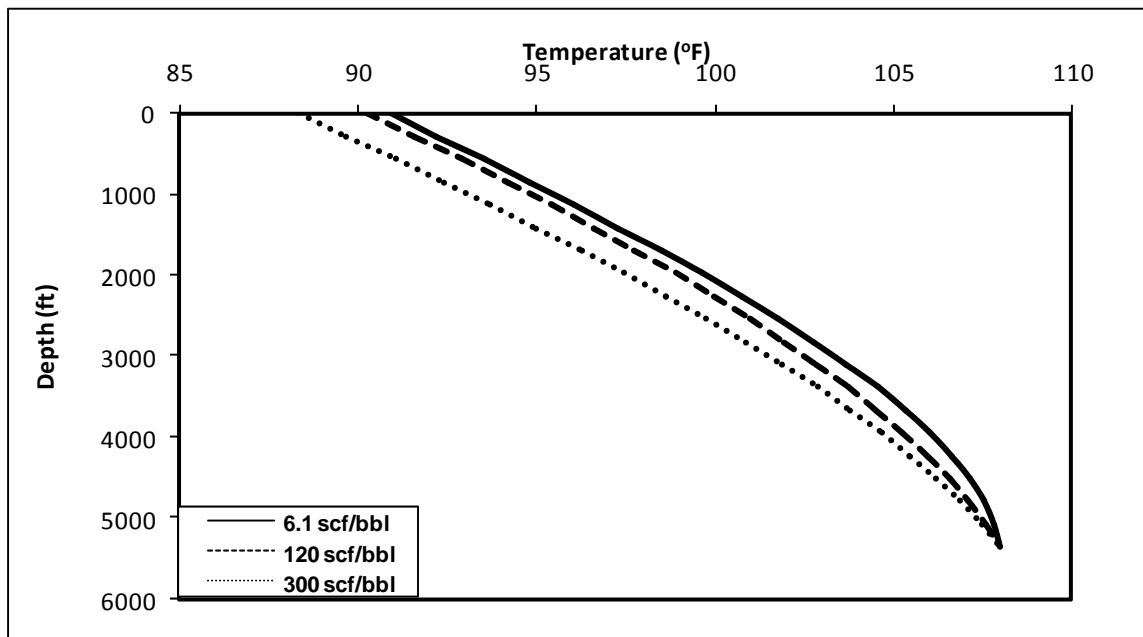


Figure 2.23 Effect of gas liquid rate ratio (GLR) on temperature profile in the wellbore (A 5355 ft vertical well produces 59 STB/D oil and 542 STB/D water, the gas flow rate was changed to vary the GLR values, the GLR unit is scf/bbl)

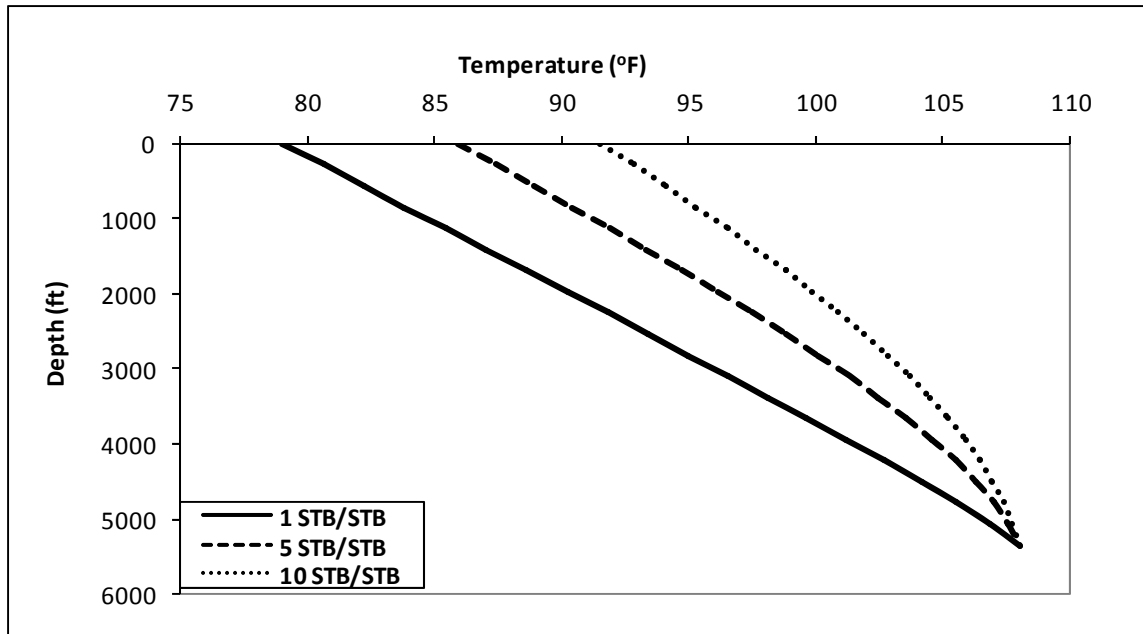


Figure 2.24 Effect of water oil ratio (WOR) on temperature profile in the wellbore (A 5355 ft vertical well produces 59 STB/D oil and 41 Mscf/D gas, the water flow rate was changed to vary the WOR values.

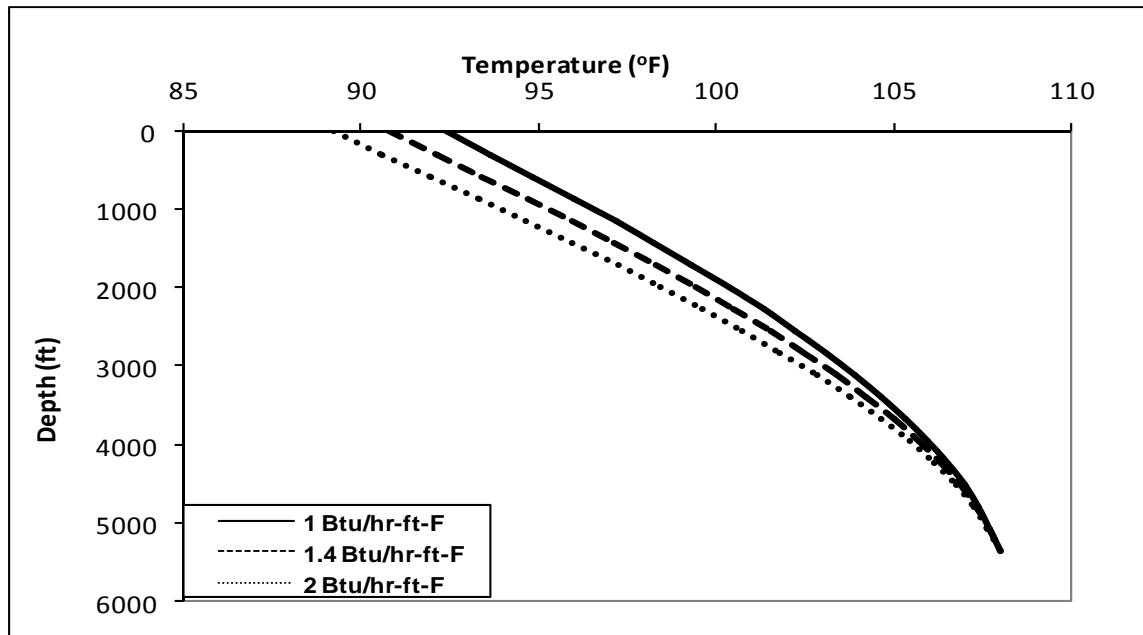


Figure 2.25 Effect of earth thermal conductivity on temperature profile in the wellbore (A 5355 ft vertical well produces 59 STB/D oil, 41 Mscf/D gas and 542 STB/D water when diameter is 2 7/8)

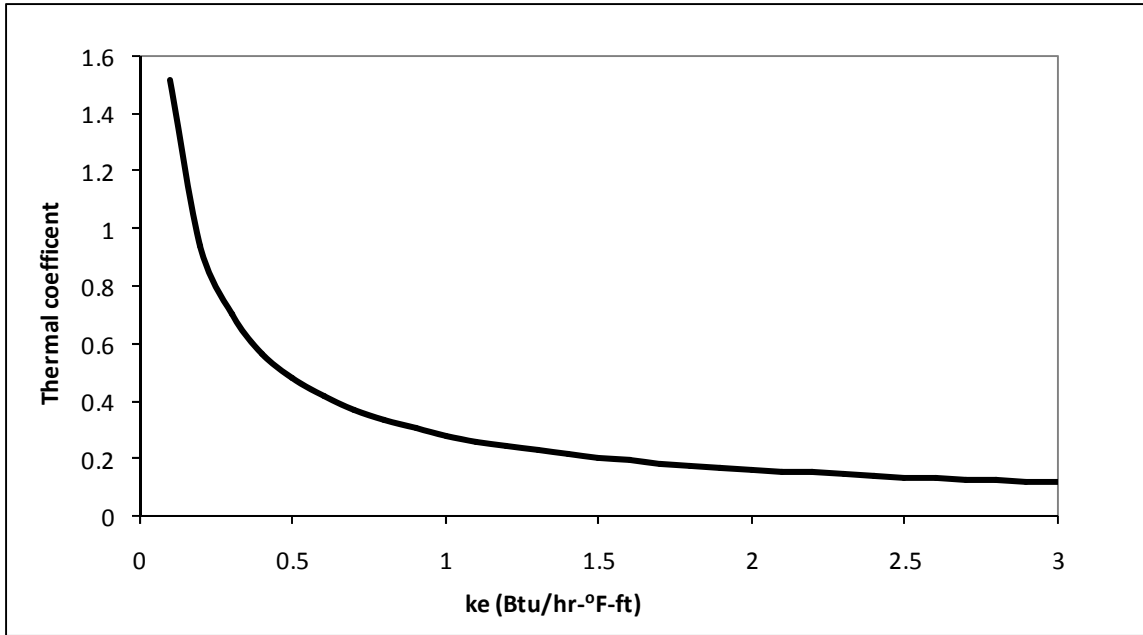


Figure 2.26 Thermal coefficient $\frac{r_{io}T_D}{k_e}$ as a function of formation heat conductivity

	Oil Rate	GOR	Gas rate	Oil Gravity	Depth	P_wellhead	BHP (Field Data)	BHP (Our model)	Error
Case	B/D	(scf/bbl)	(Mscf/D)	API	ft	psi	psi	psi	%
1	1965	232	455.88	14.4	3720	300	1200	1285.1	7.09
2	2700	267	720.9	15.6	4175	300	1500	1354.5	9.7
3	855	185	158.175	12.9	4355	250	1700	1554.5	8.56
4	1040	472	490.88	18.6	4400	400	1350	1420.6	5.23
5	1310	335	438.85	13.6	3705	500	1450	1492.7	2.94
6	788	222	174.936	16	4210	350	1750	1578.3	9.81
7	967	193	186.631	13.3	4766	250	1550	1652.4	6.61
8	1850	575	1063.75	18.7	3924	700	1500	1580.1	5.34

Table 2.1. Comparison between bottomhole pressure measured at field and calculated by our multiphase flow model used

Table 2.2- Input Parameters for the Base Case	
Total depth of the well, ft	5355
Tubing inner radius, in	1.45
Tubing outer radius, in	1.5
Wellbore radius, in	4.5
Casing inner radius, in	3.2
Casing outer radius, in	3.5
Wellbore friction factor	0.0006
Oil production rate, STB/D	59
Water production rate, STB/D	542
Gas production rate, MScf/D	41
Oil specific gravity, °API	34.3
Water gravity	1.01
Gas specific gravity (air=1)	1.04
Surface formation temperature, °F	76
Geothermal gradient, °F/ft	0.006
Bottomhole temperature, °F	108
Thermal conductivity of the earth, Btu/hr-ft-°F	1.4
Formation density, lbm/ft ³	144
Heat capacity of earth, Btu/lbm-°F	0.22
Thermal conductivity of the cement, Btu/hr-ft-°F	4.021
Number of Grids	40

Table 2.2. Input parameters for the base case

CHAPTER 3: COMPOSITIONAL WELLBORE/RESERVOIR STEADY STATE FLOW MODEL

3.1 INTRODUCTION

As hydrocarbon is produced from a wellbore, pressure drop occurs due to gravity, friction and acceleration. Correct estimation of pressure drop is essential in artificial lift design calculations and well productivity computations. Produced gas and oil phases consist of different components such as methane, ethane, propane and other hydrocarbons. However, in most of available pressure loss models, pressure calculations are performed based on the simplified blackoil equations. The basic assumption in the blackoil approach is to consider three distinct phases: gas, oil and water. Oil and gas phases are recognized with oil specific gravity and gas specific gravity, respectively, which are assumed to remain constant in the wellbore. In the blackoil model, the gas is considered to be dissolved in the oil phase. A blackoil model usually treats PVT properties of hydrocarbon phases as single functions of pressure and temperature. Hence, oil and gas properties such as density, viscosity and specific volume are computed by experimental correlations at each pressure and temperature. Empirical correlations are applied to calculate dissolved gas in the oil phase. In the blackoil approach, the effect of composition changing on pressure and temperature distribution modeling is neglected.

Changes in the compositions of phases influence flow characteristics and multiphase flow patterns in the wellbore. The main question when using the blackoil

approximation is its validity because when the flowing liquid and gas include more than one component, several complex problems and questions arise:

- 1) What is the composition of the phases generated from the flowing mixture along the wellbore?
- 2) What is the effect of temperature and pressure profiles on the composition of moving fluid?
- 3) What is the effect of compositions on pressure and temperature predictions in the wellbore?
- 4) What is the effect of composition on fluid properties such as density?

One approach is to use a compositional model instead of the blackoil model. The term “compositional” implies that the in-situ fluid composition may vary point by point in the wellbore as functions of pressure, temperature and slip between the phases. If the actual compositions are known, fluid-flow properties are obtained from phase behavior calculations. A compositional wellbore simulator is needed to model pressure profile, phase velocity profile and temperature distribution in the wellbore. To the best of our knowledge, the importance of compositional modeling of multiphase/multicomponent fluid flow in vertical wellbores has not been presented in the literature.

In a compositional approach, the composition changes at each temperature and pressure. Two limiting models can be applied to compute composition of a moving multi-component fluid in the wellbore. The first assumes equilibrium between vapor and liquid phases at all positions in the wellbore. With this assumption, it is possible to apply a flash calculation at each section of the wellbore to calculate compositions. On the other hand,

differential vaporization may be considered based on the assumption of no mass transfer of vapor components back into the liquid due to the slip of the gas phase relative to the liquid phase. We believe that the actual flow condition in the wellbore falls somewhere between the two extremes of equilibrium and differential mechanisms.

Choice between these two models is dependent on the method that we use to compute pressure and temperature profiles in the wellbore. For example if we use a homogeneous model to predict the pressure profile in the wellbore, the liquid phase and vapor phase flow at the same average velocity. This no-slip behavior of the phases in the wellbore justifies the assumption of equilibrium between liquid and gas. Hence, physical properties of the mixture are an average of the liquid and vapor properties. On the other hand, if we use the mechanistic models based on actual flow conditions, there is a slip velocity between phases. The gas phase moves faster than the liquid phase in each section. Because of this significant difference in relative velocities, it would appear that the phases are not in equilibrium. This case is more complex and modifications should be made to the flash calculations, to include the effect of the slip velocity. The same problem occurs in fluid flow modeling in a pipeline. Anis et al. (1974) showed that in a pipeline by assuming equilibrium, the model always results in more pressure drop than when using the differential model. They also showed that the differential model predicts a lower vapor velocity than the equilibrium model. In our simulator, a flash calculation equilibrium assumption is made at each section of the wellbore and results are modified by considering the effect of slip velocity on the composition. We present the phase behavior and effect of slip in more detail in the following section.

In this chapter, we present a compositional simulator to model pressure profile, phase velocity profile and temperature distribution in the wellbore. This wellbore simulator is also coupled to a compositional reservoir simulator to accurately compute fluid flow between the wellbore and reservoir. First we present the method, equations and procedure used for this purpose. Different cases are then modeled with these coupled simulators to study when the compositional approach is important and when the blackoil approximation is accurate enough to predict pressure and temperature profiles in the wellbore. In the last section, some case studies are analyzed with our simulator.

3.2 PHASE BEHAVIOR OF HYDROCARBON FLUIDS

For a binary gas/oil system, two phases can exist in equilibrium at various pressures at a given temperature. In these systems, the thermodynamic and physical properties of the phases depend on pressure, temperature and compositions. For any composition, a pressure-temperature phase behavior diagram is available to estimate phase fraction at a specified pressure and temperature. The phase behavior diagram for a hypothetical hydrocarbon fluid is given in Figure 3.1. A phase envelope, like curve ACB in Figure 3.1, delineates the two-phase region of the mixture. The dashed lines within the phase envelope, called the quality lines, describe the pressure and temperature conditions for equal volumes of liquid. Point C is called the critical point of the mixture. At this point, all distinctions between the liquid and the vapor phases disappear and all properties of the gas phase are identical to the liquid phase. Curve AC which corresponds to a 100%

liquid fraction line, is called the bubble-point curve. Similarly, the 0% liquid fraction curve is called the dew-point curve.

In the reservoir, as pressure depletes, Figures 3.2 and 3.3 show two possible paths at constant temperature. Figure 3.2 shows the isothermal expansion at temperatures below the critical point. In this case, the pressure declines to the bubble point and vapor appears; more reduction in pressure increases the percentage of vapor in the mixture until the dew point is reached. As pressure becomes less than the dew point pressure, the fluid becomes a single vapor phase. The solid line in the figure shows the path of pressure decline.

Figure 3.3 shows the retrograde condensation phenomena. In this case, expansion occurs at a temperature above the critical temperature. Liquid forms when the dew point line is encountered. As the pressure is reduced, the liquid content first increases and then decreases as it revaporizes, until reaching the second dew point at the lower pressure.

3.3 GOVERNING EQUATIONS

As discussed in Chapter 2, the mass, momentum and energy balance equations govern fluid flow in the wellbore. The same equations are considered for the compositional approach. A flash calculation method and an equation of state are used to calculate compositions and phase properties. The equation of state is discussed in Appendix F in detail. The wellbore is divided into segments in the z direction, and governing equations are solved at each grid block. Boundary and initial conditions are defined based on the physics of the problem. For example, when the surface fluid and

flow parameters are known, the governing equations are solved from the wellhead to the bottom of the wellbore in order to calculate pressure, temperature, phase fractions, phase velocity and compositions for each block.

3.3.1 Continuity Equations

In a three phase gas/oil/water system, three continuity equations are written at each gridblock. Generally, at each block for each phase, the output moles to the neighboring wellbore blocks or reservoir blocks are equal to the input moles from neighboring blocks or reservoir. We assume that all components in each phase are moving with the same velocity. Continuity equation is written for each component within a phase. For example, for component i in the liquid phase:

$$i = 1, nc$$

$$A \frac{\partial}{\partial t} \{\rho_{i1} x_i\} + A \frac{\partial}{\partial z} \{\rho_{i1} x_i v_1\} + m'_{i1} = 0 \quad (3.1)$$

In this equation, nc shows the number of components, ρ_{i1} is the molar density of i th component in phase 1 (liquid) and x_i is the fraction of i th component in the liquid phase. For the whole liquid phase, we can add all the component equations as

$$\sum_{i=1}^{nc} (A \frac{\partial}{\partial t} \{\rho_{i1} x_i\} + A \frac{\partial}{\partial z} \{\rho_{i1} x_i v_1\} + m'_{i1}) = 0$$

$$\rightarrow \sum_{i=1}^{nc} A \frac{\partial}{\partial t} \{\rho_{i1} x_i\} + \sum_{i=1}^{nc} A \frac{\partial}{\partial z} \{\rho_{i1} x_i v_1\} + \sum_{i=1}^{nc} m'_{i1} = 0$$

$$\rightarrow A \frac{\partial}{\partial t} \sum_{i=1}^{nc} \{\rho_{i1} x_i\} + A \frac{\partial}{\partial z} v_1 \sum_{i=1}^{nc} \{\rho_{i1} x_i\} + \sum_{i=1}^{nc} m'_{i1} = 0$$

Hence, the oil phase continuity equation can be rewritten as

$$A \frac{\partial}{\partial t} \sum_{i=1}^{nc} \{\rho_{i1} x_i\} + A \frac{\partial}{\partial z} v_1 \sum_{i=1}^{nc} \{\rho_{i1} x_i\} + \sum_{i=1}^{nc} m'_{i1} = 0 \quad (3.2)$$

The same procedure can be used for the gas continuity equation. If y_i shows the component fraction in the gas phase and ρ_{i2} shows the molar density of i th component in the gas phase, then for component i :

$$i = 1, nc$$

$$A \frac{\partial}{\partial t} \{\rho_{i2} y_i\} + A \frac{\partial}{\partial z} \{\rho_{i2} y_i v_2\} + m'_{i2} = 0 \quad (3.3)$$

Hence, for the gas phase

$$\sum_{i=1}^{nc} A \frac{\partial}{\partial t} \{\rho_{i2} y_i\} + A \frac{\partial}{\partial z} \{\rho_{i2} y_i v_2\} + m'_{i2} = 0$$

$$\rightarrow \sum_{i=1}^{nc} A \frac{\partial}{\partial t} \{\rho_{i2} y_i\} + \sum_{i=1}^{nc} A \frac{\partial}{\partial z} \{\rho_{i2} y_i v_2\} + \sum_{i=1}^{nc} m'_{i2} = 0$$

Hence, the overall continuity equation for the gas phase can be written as

$$A \frac{\partial}{\partial t} \sum_{i=1}^{nc} \{\rho_{i2} y_{i2}\} + A \frac{\partial}{\partial z} v_2 \sum_{i=1}^{nc} \{\rho_{i2} y_{i2}\} + \sum_{i=1}^{nc} m'_{i2} = 0 \quad (3.4)$$

3.3.2 Momentum Equations

Pressure losses in the wellbore are due to gravity, friction and acceleration effects. In a compositional approach we consider these mechanisms in separate momentum equations for the gas and liquid phases. The liquid momentum equation can be written as

$$\begin{aligned} \frac{\partial}{\partial t} v_1 \sum_{i=1}^{nc} (\rho_{i1} x_i) + \frac{\partial}{\partial z} v_1^2 \sum_{i=1}^{nc} (\rho_{i1} x_i) + g \sin \theta \sum_{i=1}^{nc} x_i \rho_{i1} + \\ \frac{\partial P}{\partial z} \alpha_1 + \left(\frac{\partial P}{\partial z}\right)_{Wall,1} + \left(\frac{\partial P}{\partial z}\right)_{int\ erphase} = 0 \end{aligned} \quad (3.5)$$

In this equation the first term, $\frac{\partial}{\partial t} v_1 \sum_{i=1}^{nc} (\rho_{i1} x_i)$ is the transient part of pressure loss which is zero for a steady state case. $\frac{\partial}{\partial z} v_1^2 \sum_{i=1}^{nc} (\rho_{i1} x_i)$, $g \sin \theta \sum_{i=1}^{nc} x_i \rho_{i1}$, $\left(\frac{\partial P}{\partial z}\right)_{Wall,1}$ and $\left(\frac{\partial P}{\partial z}\right)_{int\ erphase}$ are pressure loss due to acceleration, gravity, wall friction and friction between phases, respectively. Hence, this equation accounts for the part of pressure drop due to the liquid, which is shown as $\frac{\partial P}{\partial z} \alpha_1$. (α_1 is the liquid mole fraction in the mixture.)

Similar mechanisms are involved in pressure drop for the gas phase. The gas momentum equation includes all of the same terms as

$$\begin{aligned} \frac{\partial}{\partial t} u_2 \sum_{i=1}^{nc} (\rho_{i2} y_i) + \frac{\partial}{\partial z} u_2^2 \sum_{i=1}^{nc} (\rho_{i2} y_i) + g \sin \theta \sum_{i=1}^{nc} y_i \rho_{i2} + \\ \frac{\partial P}{\partial z} \alpha_2 + \left(\frac{\partial P}{\partial z}\right)_{Wall,2} - \left(\frac{\partial P}{\partial z}\right)_{int\ erphase} = 0 \end{aligned} \quad (3.6)$$

Adding Equation 3.6 to 3.5, a mixture momentum equation is obtained. We use Equation 3.7 to calculate the steady state pressure distribution in the wellbore.

$$\begin{aligned} \frac{\partial P}{\partial z} = \frac{\partial}{\partial z} u_1^2 \sum_{i=1}^{nc} (\rho_{i1} x_i) + \frac{\partial}{\partial z} u_2^2 \sum_{i=1}^{nc} (\rho_{i2} y_i) \\ + g \sin \theta \sum_{i=1}^{nc} (x_i \rho_{i1} + y_i \rho_{i2}) + \left(\frac{\partial P}{\partial z}\right)_{Wall} \end{aligned} \quad (3.7)$$

3.3.3 Energy Equation

As discussed in Chapter 2, the general energy equation is expressed for the mixture as follows.

$$\begin{aligned} & \sum_{j=1}^{np} \sum_{i=1}^{nc} \left(h_{ij} - \frac{P}{\rho_{ij}} \right) \frac{\partial \rho_{ij}}{\partial t} + \sum_{j=1}^{np} \sum_{i=1}^{nc} \rho_{ij} c_{p,ij} \frac{\partial T}{\partial t} + \sum_{j=1}^{np} \sum_{i=1}^{nc} \rho_{ij} \eta_{ij} c_{p,ij} \frac{\partial P}{\partial t} \\ & - \sum_{j=1}^{np} \sum_{i=1}^{nc} \rho_{ij} \frac{\partial (P/\rho_{ij})}{\partial t} = q + \sum_{j=1}^{np} \sum_{i=1}^{nc} \rho_{ij} v_{ij} \frac{d}{dz} \left(h_{ij} + \frac{v_{ij}^2}{2} + gz \sin \theta \right) \end{aligned} \quad (3.8)$$

In this equation, the left hand side is the transient energy term which is equal to zero in a steady state case. In the right hand side, q is the heat flux from the surrounding formation to the wellbore fluid and the last term, $\sum_{j=1}^{np} \sum_{i=1}^{nc} \rho_{ij} v_{ij} \frac{d}{dz} \left(h_{ij} + \frac{v_{ij}^2}{2} + gz \sin \theta \right)$ is the energy convection in the z direction due to enthalpy, acceleration and gravity changes. For steady state the energy equation can be rewritten as

$$q + \sum_{j=1}^{np} \sum_{i=1}^{nc} \rho_{ij} v_{ij} \frac{d}{dz} \left(h_{ij} + \frac{v_{ij}^2}{2} + gz \sin \theta \right) = 0 \quad (3.9)$$

3.4 SOLUTION PROCEDURE

Consider a case where we know surface pressure and surface temperature. The molar flow rate at the surface is also known. The goal is to calculate the pressure and temperature distribution in the wellbore. Starting from the surface gridblock, the

procedure shown in Figure 3.4 is applied. The effect of slip velocity on the composition is discussed in the next section.

3.5 EFFECT OF SLIP VELOCITY

The general method for calculating component fractions in each phase is by using equilibrium flash calculation. In this method we assume that the liquid and gas phases are in equilibrium, but this is not quite correct when the phases are moving at different velocities. To account for the slip velocity effect on phase compositions we assume that at each block in the wellbore the gas phase is in equilibrium with *only a portion* of the liquid phase. Hence, the liquid phase is divided into two parts as shown in Figure 3.5: L_e which is in equilibrium with the gas phase and L_{ne} , which appears because of slip velocity and is not in equilibrium with the gas phase.

By performing flash calculations for each temperature and pressure, G and L_e , are computed. Only these two portions are in equilibrium, and $G+L_e=I$. From the mole balance, we know that $z_{ii} = y_i G + x_i L_e$.

Consider a block as shown in Figure 3.5. The holdup value, which is defined as the volume fraction of liquid, calculated by the following equations.

In a block, liquid volume is

$$V_{liquid} = \frac{Z_l n_l RT}{P} \quad (3.10)$$

where Z_l is the liquid compressibility factor and n_l is liquid moles. Similarly, for gas volume, we can write

$$V_{Gas} = \frac{Z_g n_g RT}{P} \quad (3.11)$$

Hence,

$$Holdup = \frac{V_{liquid}}{V_{liquid} + V_{Gas}} = \frac{Z_l n_l}{Z_l n_l + Z_g n_g} \quad (3.12)$$

We assume that both L_e and L_{ne} sections in Figure 3.5 have same composition and the same compressibility factor. By dividing Equation 3.12 into total moles in the block,

$$H = Holdup = \frac{Z_l \frac{n_l}{n_{total}}}{Z_l \frac{n_l}{n_{total}} + Z_g \frac{n_g}{n_{total}}} = \frac{Z_l (L_e + L_{ne})}{Z_l (L_e + L_{ne}) + Z_g G} \quad (3.13)$$

Hence,

$$L_e + L_{ne} = \frac{Z_g HG}{Z_l (1 - H)} \quad (3.14)$$

Equation 3.14 updates the phase fractions in the gridblock. The in-situ overall fraction of i th component, z_{2i} , is then computed by

$$\begin{aligned} z_{2i} &= y_i \frac{G}{G + L_e + L_{ne}} + x_i \frac{L_e}{G + L_e + L_{ne}} + x_i \frac{L_{ne}}{G + L_e + L_{ne}} \\ &= \frac{(y_i G + x_i L_e) + x_i L_{ne}}{1 + L_{ne}} = \frac{z_{1i} + x_i L_{ne}}{1 + L_{ne}} \end{aligned} \quad (3.15)$$

where, x_i shows the fraction of i th component in liquid phase.

y_i shows the fraction of i th component in gas phase

z_{li} shows the overall fraction of i th component measured at equilibrium.

Equation 3.15 shows the new overall component fractions, so the total in-situ composition in the wellbore will vary point-by-point. It is clear that the holdup calculation is strongly dependent on the composition of the mixture, so an iterative method should be used to update composition and holdup accurately.

3.6 THE NEED FOR COMPOSITIONAL MODELING

We developed a compositional model to simulate wellbore fluid flow and calculate pressure loss and temperature distribution in the wellbore. Using a compositional approach requires more data than using blackoil estimation, and it also involves more computations. The main question is the need for using this more complicated approach instead of the simpler blackoil procedure. In this section, we compare the results obtained from both approaches and discuss the difference by comparing three different test cases. In the first case, a well is producing oil, in the second case the well is producing volatile oil and in the third case we assume that condensate gas is produced from the reservoir. The general parameters used in these simulations are detailed in Table 3.1.

3.6.1 Case 1: Oil production

The gravity for the oil with the composition shown in Table 3.2 is 38 °API. This oil consists of six components and the °API value shows that this oil can be classified as a blackoil.

Based on this composition, the phase behavior of the oil is calculated as shown in Figure 3.6.

The need to use the compositional approach is discussed by comparing the pressure profile obtained from the blackoil and the compositional procedures. The compositions are lumped into two phases and their properties are computed by the following procedure.

- 1) We use the equilibrium flash calculation for the overall composition of Table 3.2 to calculate each phase composition at standard conditions.
- 2) The density of liquid phase and gas phase are calculated at standard condition by Equations 3.16 and 3.17.

$$\rho_g = \frac{P_S \sum_{i=1}^{nc} y_i M_i}{RZ_y T_S} \quad (3.16)$$

$$\rho_o = \frac{P_S \sum_{i=1}^{nc} x_i M_i}{RZ_x T_S} \quad (3.17)$$

In these Equations, M_i is the molecular weight for component i . x_i and y_i are the mole fractions of component i in liquid phase and gas phase respectively. Z_x and Z_y are

the compressibility for oil and gas phase obtained from the flash calculation. ρ_o , ρ_g are oil density and gas density in lbm/ft³.

3) The main parameters for a blackoil approach are oil specific gravity (γ_{API}) and gas gravity (γ_g). These parameters are calculated with Equations 3.18 and 3.20.

$$\gamma_g = \frac{\sum_{i=1}^{nc} y_i M_i}{29 Z_y} \quad (3.18)$$

$$\gamma_o = \frac{\rho_o}{62.37} \quad (3.19)$$

$$\gamma_{API} = \frac{141.5}{\rho_o / 62.37} - 131.5 \quad (3.20)$$

4) In the compositional approach, the production is given by the molar production rate, n_t . This value is converted to oil flow rate and gas flow rate by Equations 3.21 and 3.22. In these Equations V_l is the liquid mole fraction in the mixture.

$$q_o = \frac{n_t V_l R Z_x T_S}{P_S} \quad (3.21)$$

$$q_g = \frac{n_t (1 - V_l) R Z_y T_S}{P_S} \quad (3.22)$$

Knowing the phase flow rates and phase specific densities, it is possible to run the simulation in blackoil mode and compare the results with those obtained from the compositional procedure. Figure 3.7 shows the pressure distribution for both cases.

The difference in calculated pressure is less than 1%, so this shows that using blackoil approximation is a reasonable approximation for this kind of oil production. The

corresponding pressure and temperature changes are shown on the phase equilibrium curve in Figure 3.8.

3.6.2 Case 2: Volatile Oil Production

The same procedure is applied for a high-shrinkage oil (volatile oil). The phase diagram of this kind of crude oil is given in Figure 3.9.

It should be noted that the quality lines are close together near the bubble point and at lower pressures they are more widely spaced. During pressure decrease, in this kind of oil, a high liquid shrinkage occurs immediately below the bubble point corresponding to the rapid decrease in the quality. Table 3.3 shows the composition for an oil with gravity equal to 50 °API, which can be classified as volatile oil.

With the same wellbore configuration we simulate the fluid flow when the pressure at the surface is 1000 psi, and the wellbore is producing 1500 lbm.mole/day of the hydrocarbon mixture. Figure 3.10 shows the pressure profiles for both blackoil and compositional approaches.

The average difference between the two curves is about 2%, but it should be noted that at the bottomhole, the estimated pressure by compositional approach is 70 psi less than the computed value with blackoil approach, which is a noticeable difference in bottomhole pressure calculation. It seems that in simulating volatile oil flow, using the compositional approach improves pressure estimation.

The corresponding pressure-temperature change along the flow path is shown in Figure 3.11 on the phase behavior diagram. At the bottomhole only liquid is produced.

As the pressure declines, gas comes out of the liquid phase. In high-shrinkage oil, quality lines are close together near the bubble point and more widely spaced at lower pressure. Hence, a high-liquid shrinkage occurs immediately below the bubble point because of a rapid decrease in the quality.

3.6.3 Case 3: Gas Condensate Production

In this case we model gas condensate production. The wellbore fluid temperature lies between the critical temperature and cricondenthem of the produced fluid. This reservoir is classified as a retrograde gas condensate reservoir. The composition is described in Table 3.4 and yields a gas condensate system with gravity equal to 60 °API.

Figure 3.12 shows a typical pressure-temperature diagram for a gas condensate wellbore/reservoir system.

Similar to the previous two cases, we model pressure and temperature distribution in the wellbore with both compositional and blackoil approaches. In this case, we assume that the surface pressure is 1500 psi and that the well is producing 1500 lbm mole/D of hydrocarbon mixture. Figure 3.13 shows the pressure profiles in the wellbore.

Figure 3.13 shows that the bottomhole pressure calculated from the compositional approach differs by 360 psi or about 11% from the result obtained from blackoil approach, which is a considerable value. The simulation shows that due to the more complex phase behavior of the gas condensate system, using blackoil approximation may cause noticeable errors in the pressure prediction.

Figure 3.14 shows the corresponding pressure-temperature trajectory along the wellbore. Since the reservoir pressure is above the upper dew-point line, the hydrocarbon system exists as a single vapor phase. This means that the sandface flow consists of only one phase. As the pressure declines in the wellbore from the sandface to the surface, liquid begins to condense. As the pressure is further decreased, instead of expanding the gas or vaporizing the liquid phase as might be expected, the hydrocarbon mixture tends to condense. This condensation process continues until a maximum of liquid drop-out. As the pressure decreases further the vaporization resumes. In the wellbore, where the pressure drop is high, enough liquid drop-out occurs to yield two-phase flow of gas and retrograde liquid.

From these simulations it can be concluded that using the blackoil approximation instead of modeling the flow with the compositional approach gives good accuracy in most cases. But, in condensate gas because of the unique phase behavior, there is a noticeable difference between the two approaches. We recommend using the compositional simulator in the gas condensate system when high accuracy is needed. In volatile oil production, blackoil approximation estimated the bottomhole pressure as about 2% different from the compositional approach, which can be important in some cases. These conclusions are similar to the results obtained from the simulations done for pipeline flow of gas by Anis et al. (1974) and Gregory et al. (1973).

3.7 RESULTS

In this section, we present two cases to show the simulator ability to model pressure profile, temperature distribution, phase velocity and phase fraction in wellbores.

3.7.1 Case 1: Three Phase Flow Production

In this case we consider a three-phase oil/water/gas fluid flow from a wellbore. Table 3.5 shows the well parameters that we used. The production consists of 2500 lbm mole/day of hydrocarbon at the surface. At the surface hydrocarbon gas, hydrocarbon liquid and water are produced, but based on the pressure and temperature changes in the wellbore we expect only liquid flowing in some parts. In this case, we know the surface pressure and mass rates.

Figure 3.15 shows the pressure profile in the wellbore. It can be seen that in the deeper sections, the gradient of pressure profile increases. This is because of the greater fluid density in deep sections.

Figure 3.16 shows the liquid fraction or holdup in the wellbore. At each section, the liquid phase consists of water and oil. The amount of oil is calculated by flash calculation which is modified by slip effects as discussed before.

At the lower portion of the wellbore there is no gas because of high pressure and temperature, the liquid volume does not change significantly. We can see a near constant holdup below 9000 ft depth. Figure 3.17 and Figure 3.18 show the actual velocity profiles for liquid and gas, respectively. Gas velocity is higher near the surface;

this is because of the expansion near the surface due to lower pressure. As holdup decreases, less liquid exists near the surface; hence, liquid velocity should also be higher to satisfy continuity. As discussed before, we conclude that assuming phase equilibrium at each point of the wellbore is not a correct assumption. Gas and liquid velocity profiles are good evidence for our conclusion. It can be seen that the gas velocity is much higher than the liquid velocity at each section, hence there is not sufficient time to reach equilibrium, and this effect of slip velocity should be considered. Figure 3.19 shows the temperature profile in the wellbore. This figure shows that temperature changes significantly in the wellbore, hence it is important to consider the effect of temperature on composition.

Another advantage of using the compositional simulator is the ability to calculate the composition change of each phase during production. The oil phase and gas phase that enter the wellbore from the reservoir have compositions different from the produced fluid. Figures 3.20 and 3.21 compare the composition of liquid phase and gas phases at the sandface, surface and standard condition. These two figures show that at low pressure and temperature the heavier components concentrations in the liquid phase are larger and lighter components do not appear in high concentration. But at higher pressure, lighter components also are present in the liquid phase causing significant effects on liquid properties. The same behavior can be noticed for the gas phase, at high pressure only very light components remain in the gas phase.

3.7.2 Case 2: Wellbore/Reservoir Simulation

Our simulator is coupled to a compositional reservoir model. The method for coupling is discussed in detail in Appendix B. In this case we model hydrocarbon production in a reservoir/wellbore system. The system consists of two wells, one injector and one producer. Figure 3.22 shows a schematic of the system, and Tables 3.6 and 3.7 present the reservoir characteristics and the production parameters.

During production, the composition of the fluid entering the producer varies because of the composition of the injected gas. Because of the injection, the recovery increases, so more hydrocarbon enters the wellbore from the reservoir. Figure 3.23 shows the total production molar rate from the reservoir.

From Figure 3.23, we can see that the production is increasing, so the flow rate in the wellbore is higher and we expect higher pressure because of higher phase velocity. Figure 3.24 shows the pressure profile at different times in the wellbore.

The decrease in the pressure in the wellbore can be seen from Figure 3.24. Figures 3.25 through 3.27 show pressure history at different depths in the wellbore. Hence, our coupled simulator has this ability to model pressure versus time in any position in the wellbore.

We can compare pressure profile with production history. Figures 3.28 and 3.29 show oil and gas production. Before breakthrough, the production decreases because of the pressure reduction in the reservoir, but when the injected fluid reaches the producer, pressure starts to build up again so that the production increases. Figure 3.30 shows both

bottomhole pressure and oil production in the same graph. As pressure starts to stabilize again, it enhances the oil production.

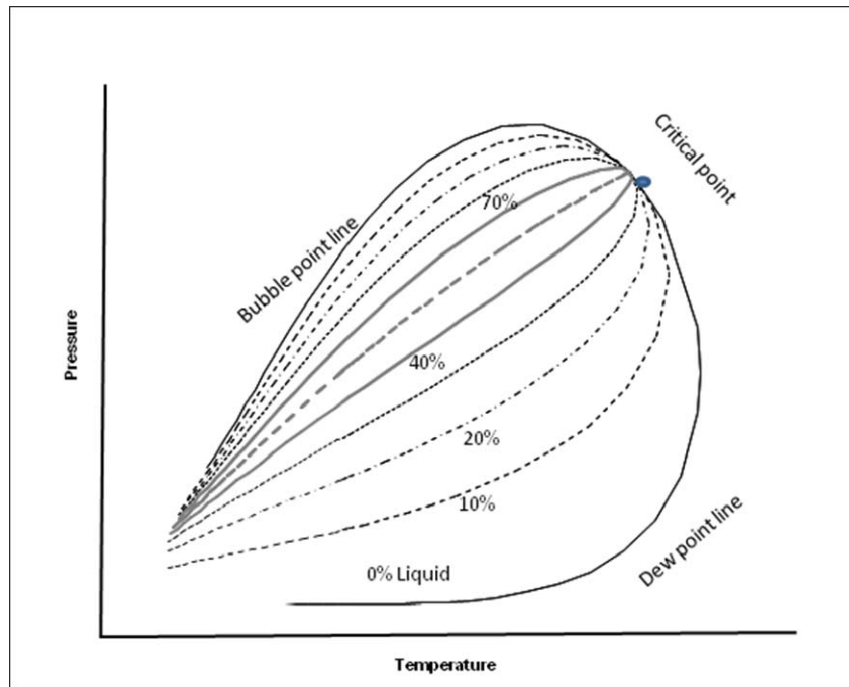


Figure 3.1 The phase behavior diagram for a hypothetical hydrocarbon fluid in a binary gas/oil system

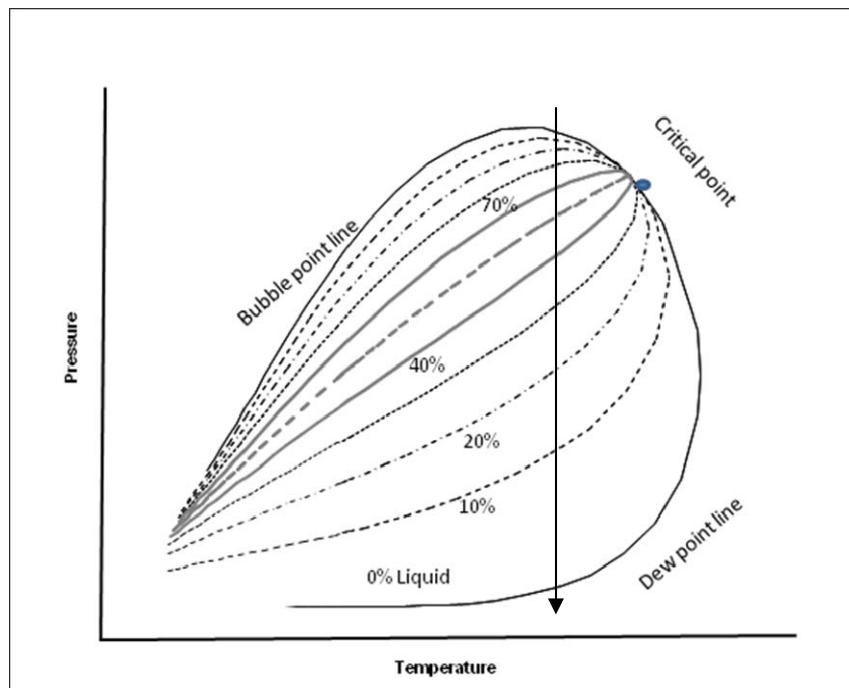


Figure 3.2 Oil/gas composition changing during an isothermal pressure depletion process when temperature is below the critical point (The arrow shows the direction of depletion)

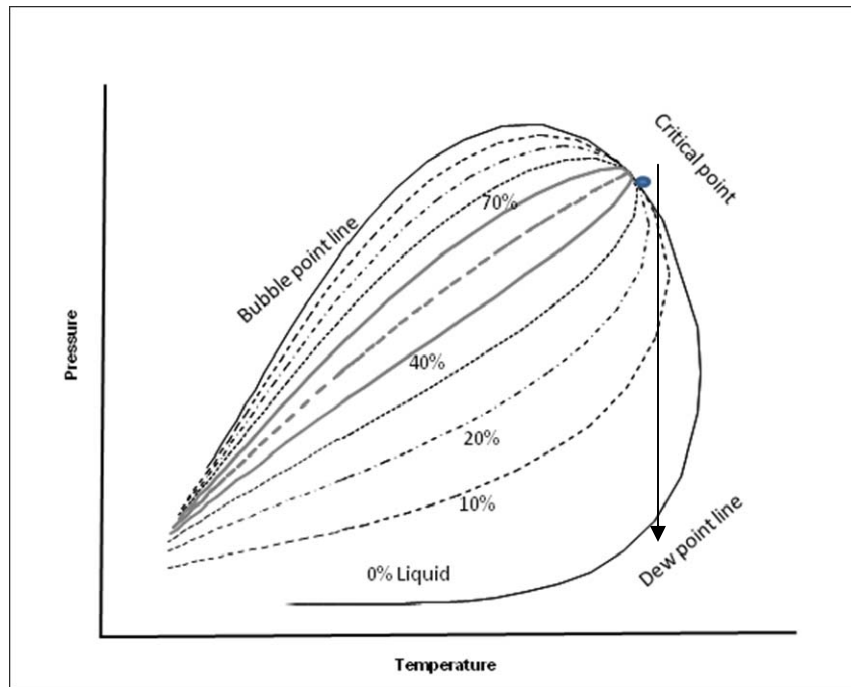


Figure 3.3 Oil/gas composition changing during an isothermal pressure depletion process when temperature is above the critical point (The arrow shows the direction of depletion)

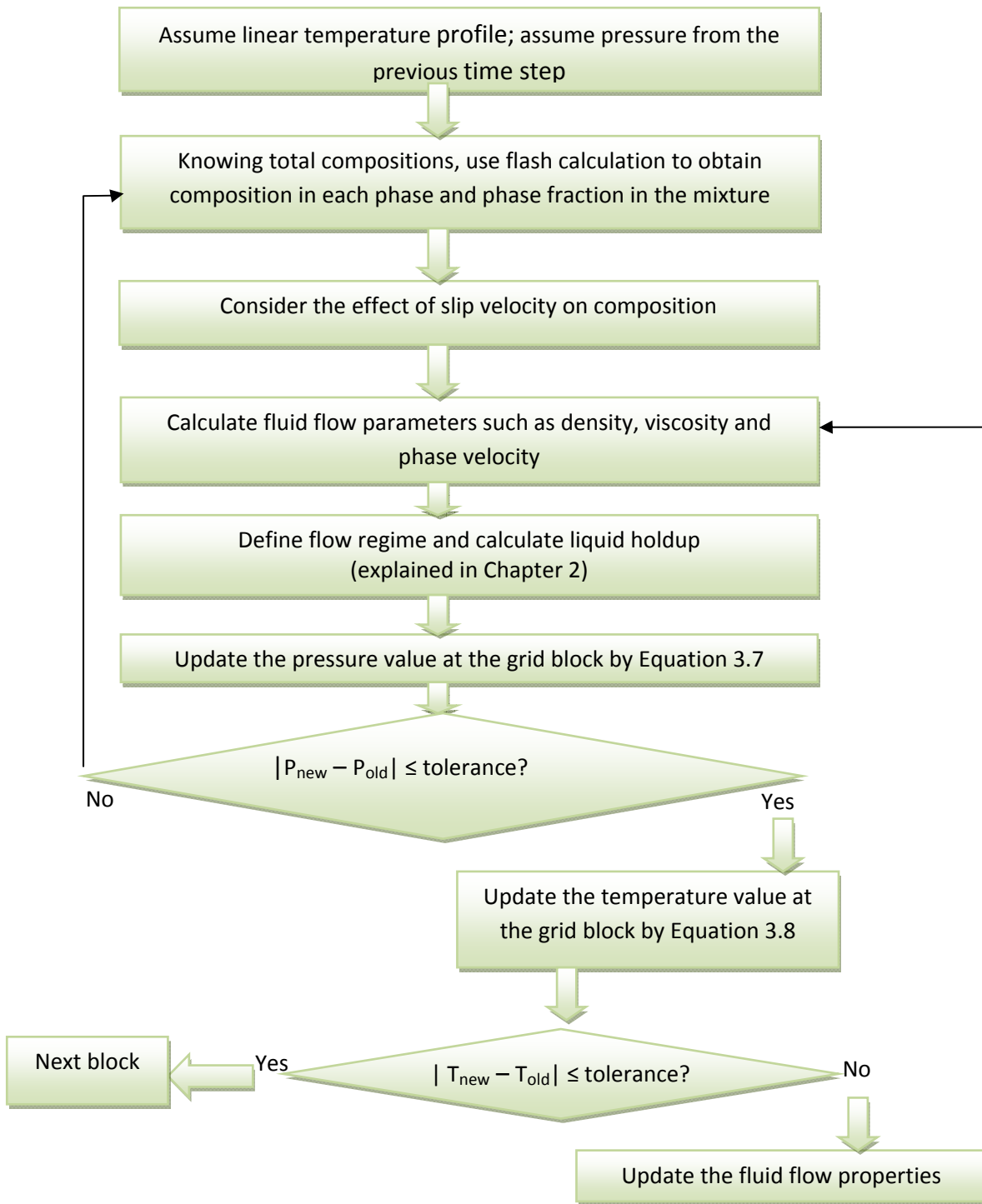


Figure 3.4 Procedure to model pressure and temperature distribution in wellbores

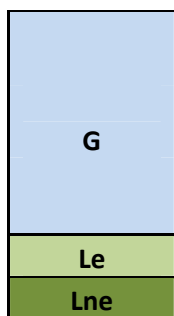


Figure 3.5 Schematic of thermodynamics equilibrium between moving phases in a block, when there is a slip velocity between phases. (G shows the gas fraction, L_e is the liquid portion which is in equilibrium with gas and L_{ne} is a fraction of liquid which is not in equilibrium due to slip)

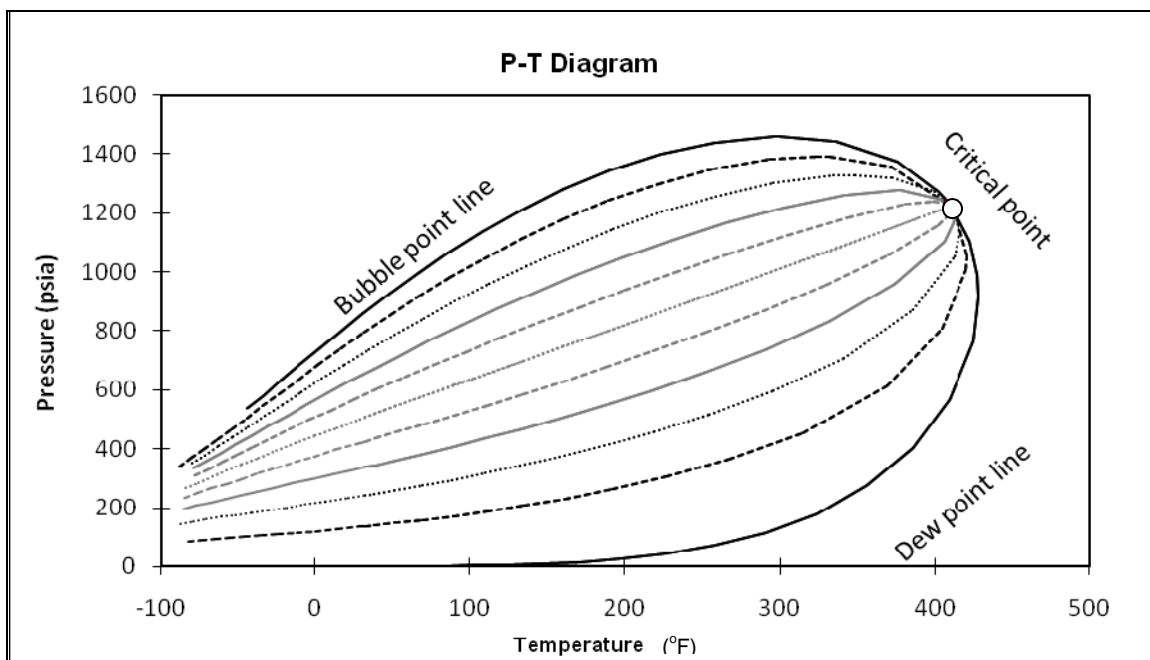


Figure 3.6 Phase behavior diagram for a system of oil/gas hydrocarbon composition which is categorized as a blackoil

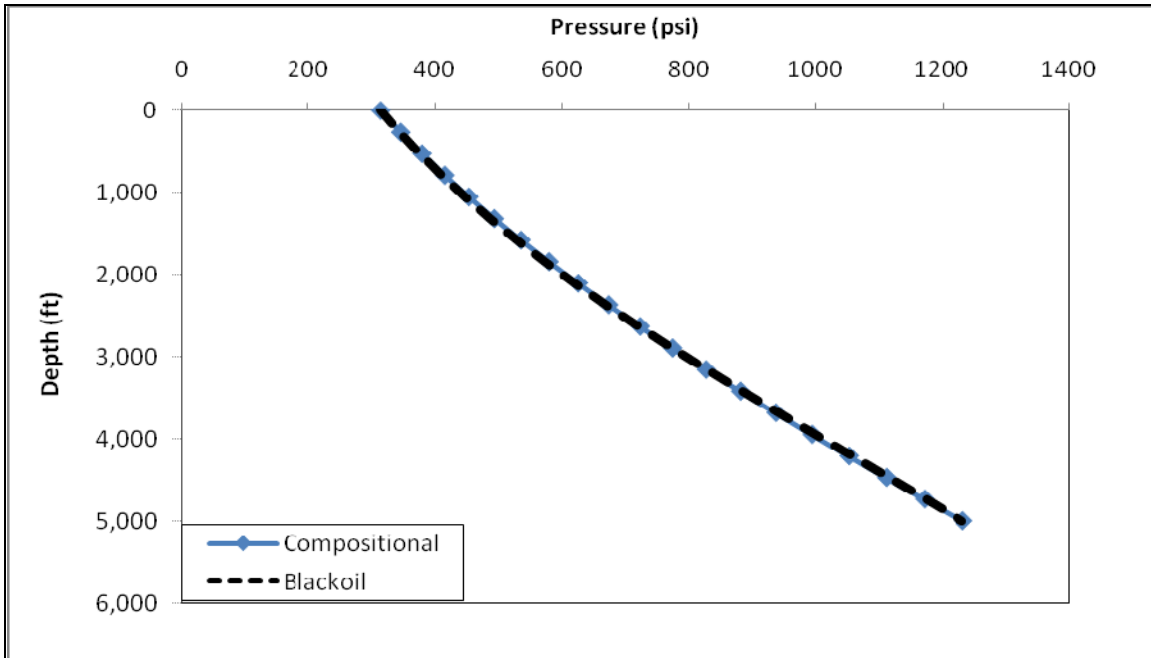


Figure 3.7 Pressure profiles calculated by blackoil and compositional approaches during production of 1000 lbm.mole/D oil/gas mixture from a 5100 ft tubing with 0.125 ft diameter (The oil gravity at the surface is 38 °API)

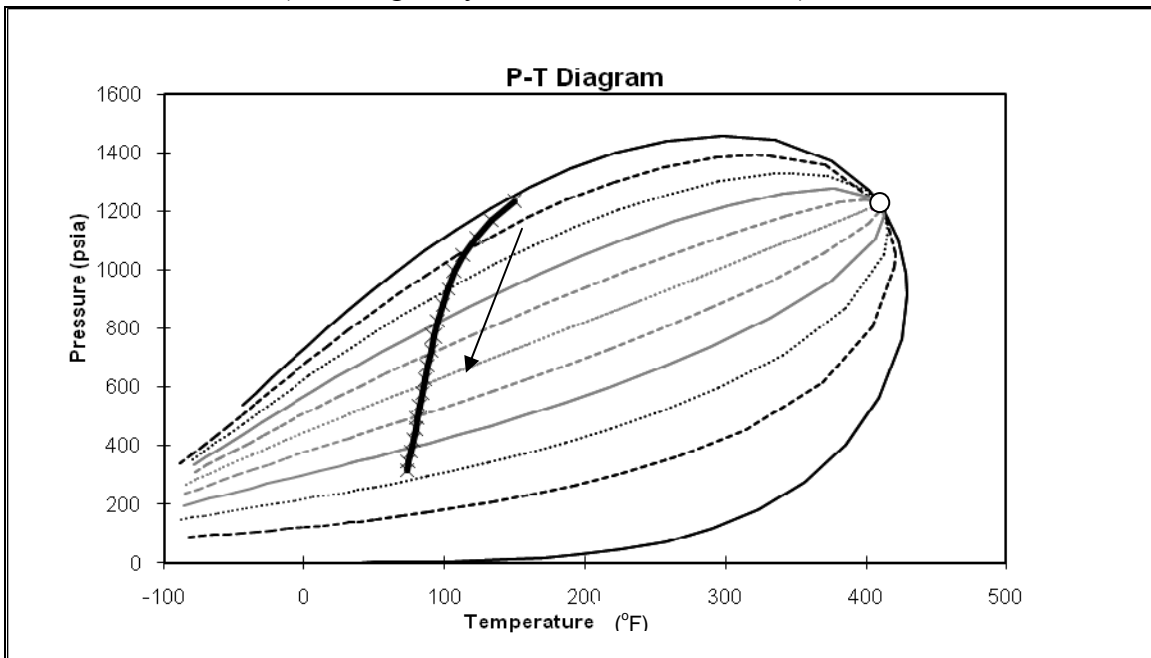


Figure 3.8 Oil/gas composition changing during pressure and temperature depletion in the hydrocarbon production (The arrow shows the direction of depletion from the sandface to the surface and the solid line on the phase diagram curves shows pressure/temperature values at different depths in the wellbore)

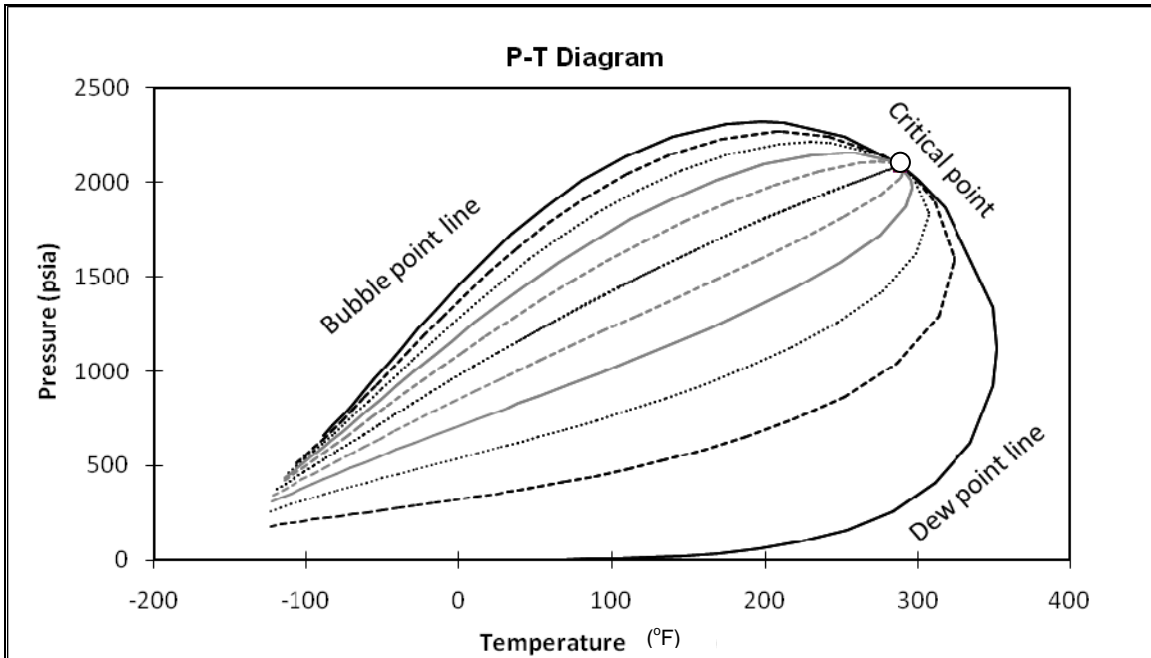


Figure 3.9 Phase behavior diagram for a system of oil/gas hydrocarbon composition which is categorized as volatile crude oil

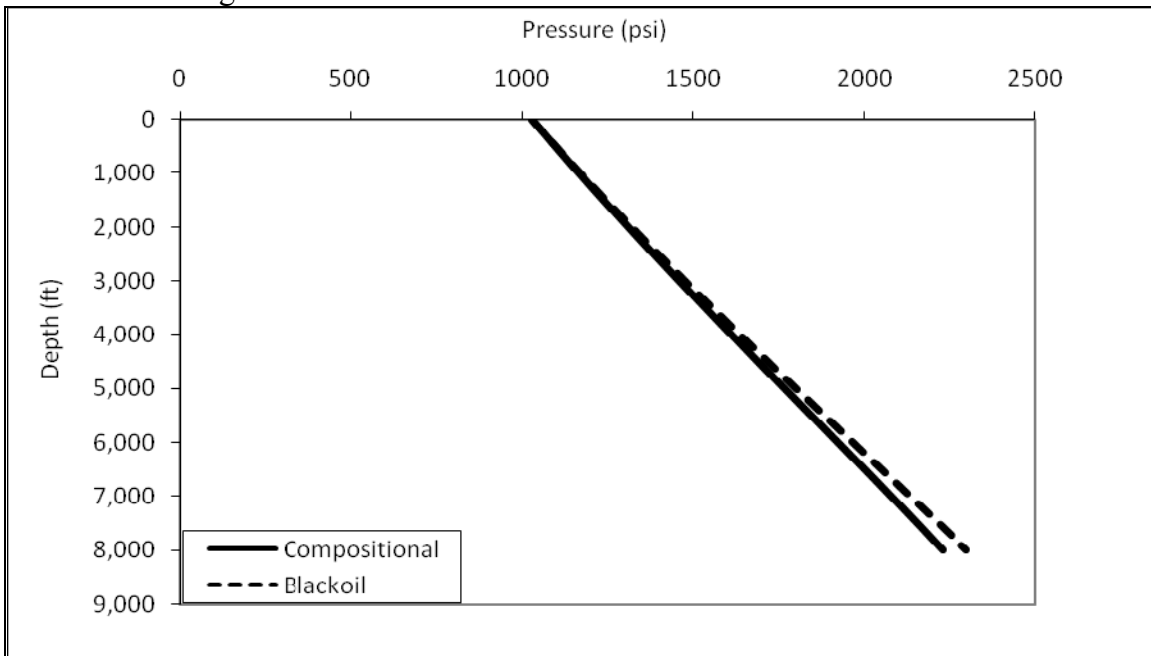


Figure 3.10 Pressure profiles in a wellbore producing volatile oil calculated by blackoil and compositional approaches (1500 lbm.mole/D oil/gas mixture is produced from a 8000 ft tubing with 0.125 ft diameter, the oil gravity at the surface is 50 °API)

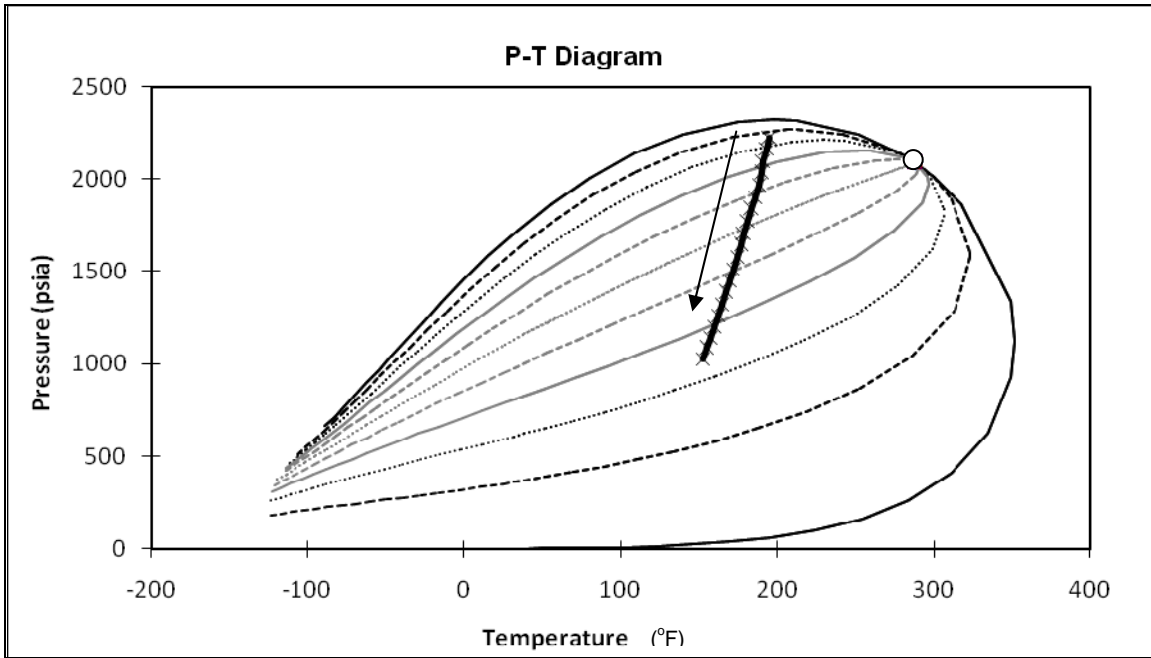


Figure 3.11 Oil/gas composition changing during pressure and temperature depletion in the volatile oil production (The arrow shows the direction of depletion from the sandface to the surface and the solid line on the phase diagram curves shows pressure/temperature values at different depths in the wellbore)

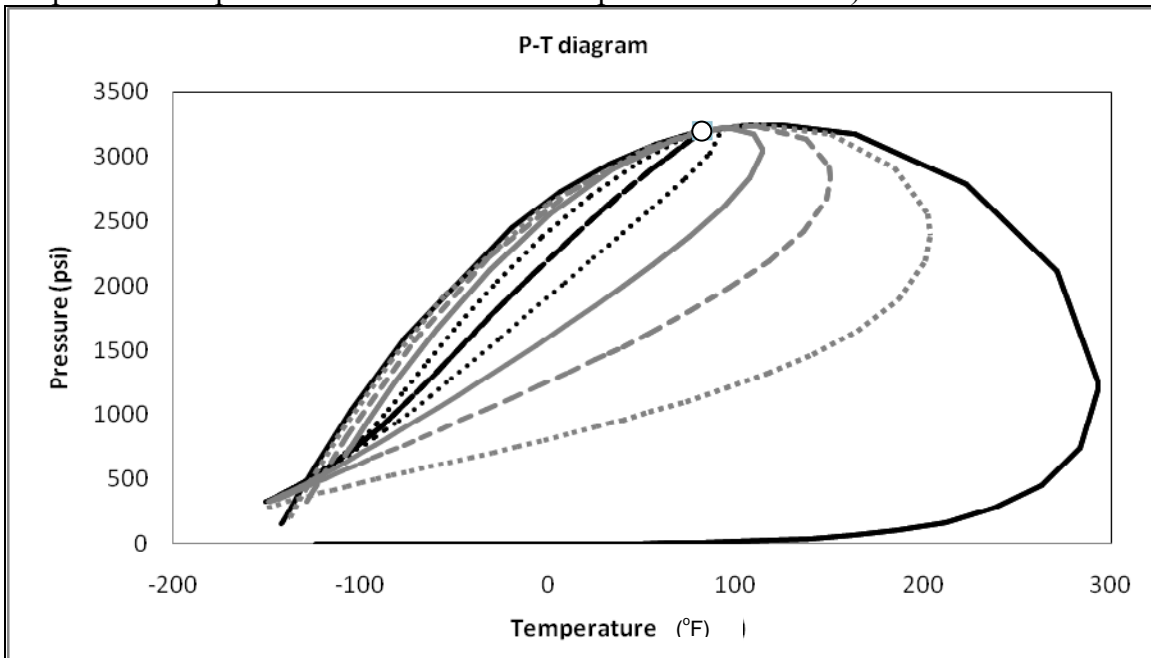


Figure 3.12 Phase behavior diagram for a system of oil/gas hydrocarbon composition which is categorized as retrograde oil and gas system

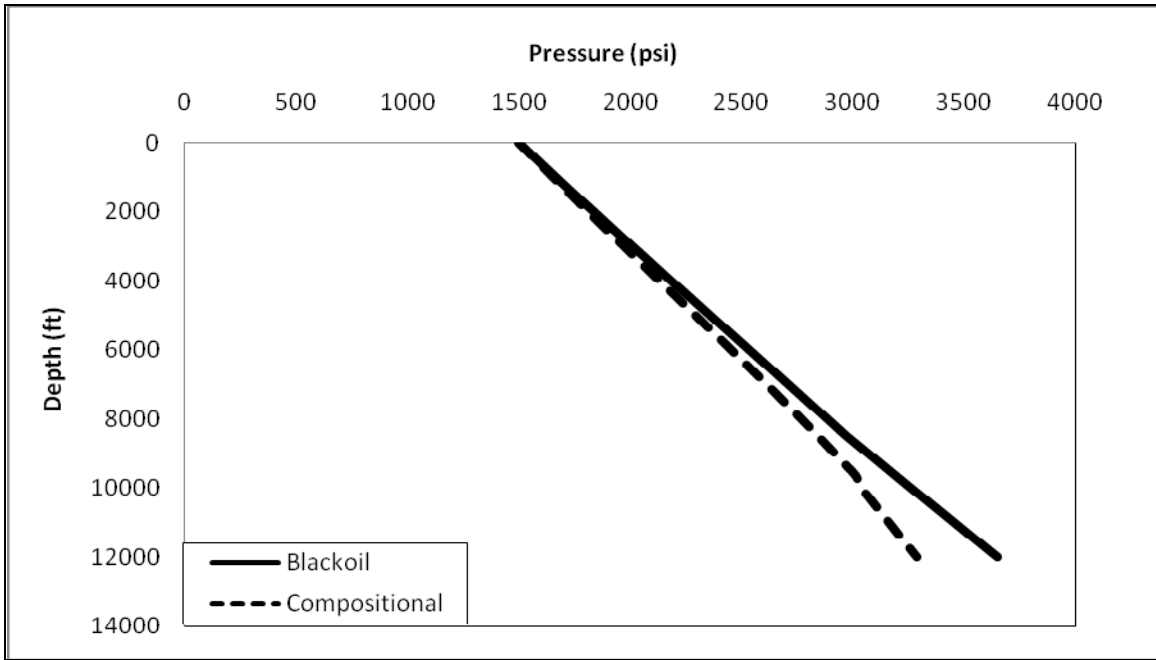


Figure 3.13 Pressure profiles in a wellbore producing retrograde oil calculated by blackoil and compositional approaches (1500 lbm.mole/D oil/gas mixture is produced from a 12000 ft tubing with 0.125 ft diameter, the oil gravity is 60 °API)

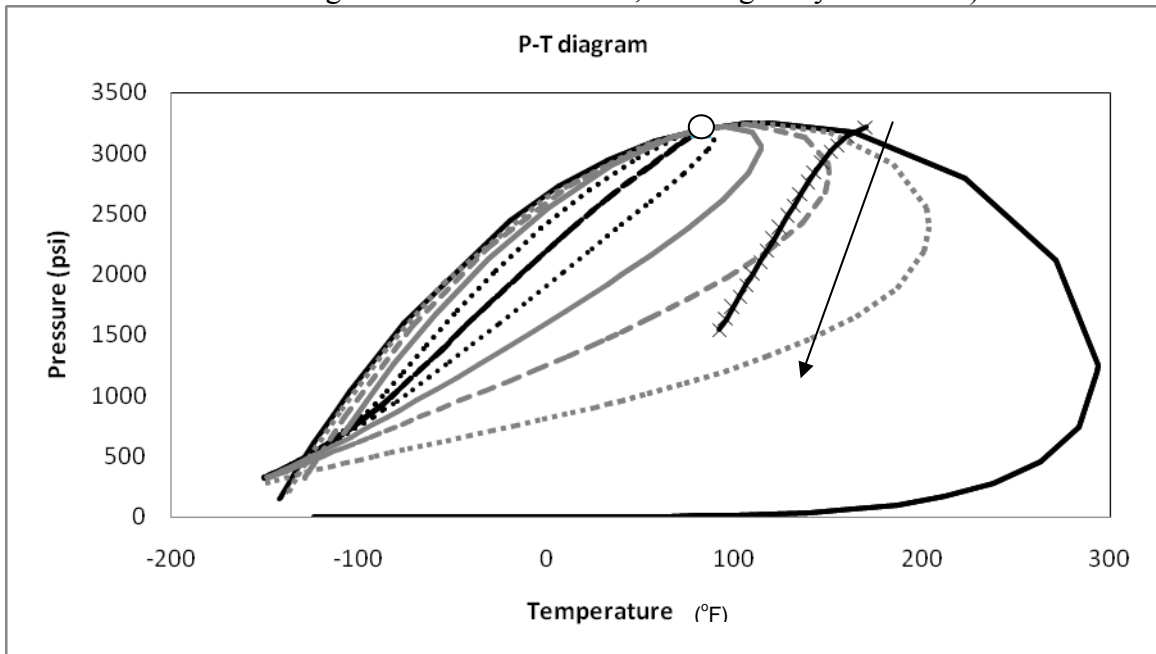


Figure 3.14 Oil/gas composition changing during pressure and temperature depletion in the retrograde oil production (The arrow shows the direction of depletion from the sandface to the surface and the solid line on the phase diagram curves shows pressure/temperature values at different depths in the wellbore)

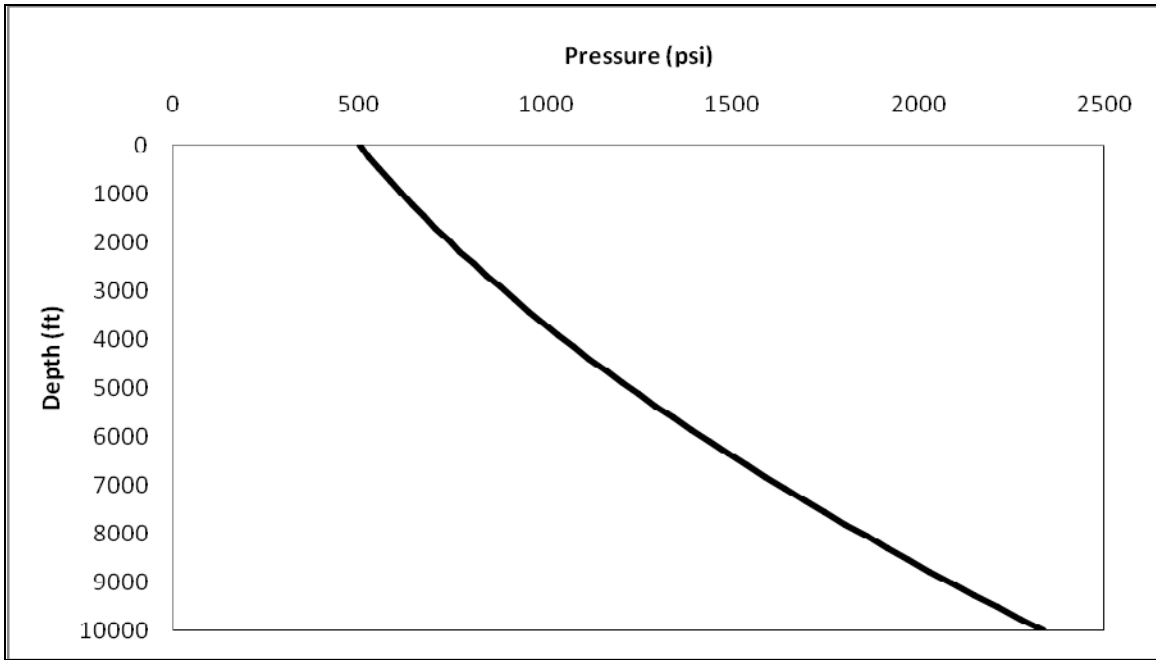


Figure 3.15 Simulated pressure profile in the wellbore during three phase flow production from 10000 ft tubing with 0.125 ft diameter (The production consists of 2500 lbm mole/day of hydrocarbon and 5800 lbm mole/day of water at the surface)

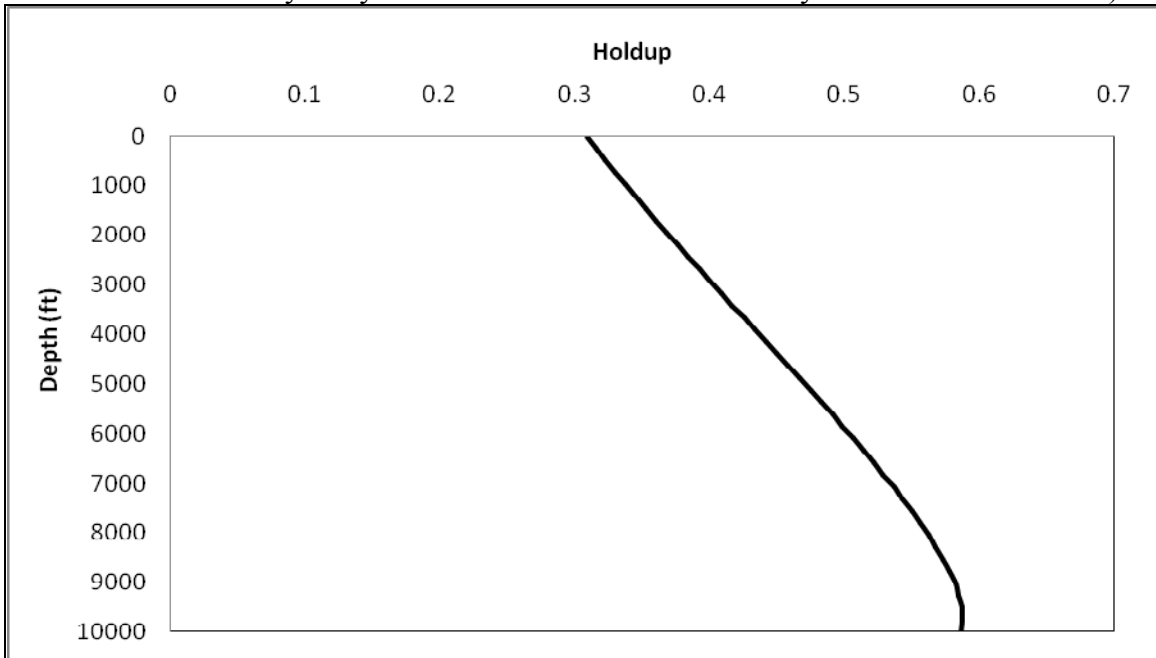


Figure 3.16 Simulated holdup profile in the wellbore during three phase flow production from 10000 ft tubing with 0.125 ft diameter (The production consists of 2500 lbm mole/day of hydrocarbon and 5800 lbm mole/day of water at the surface)

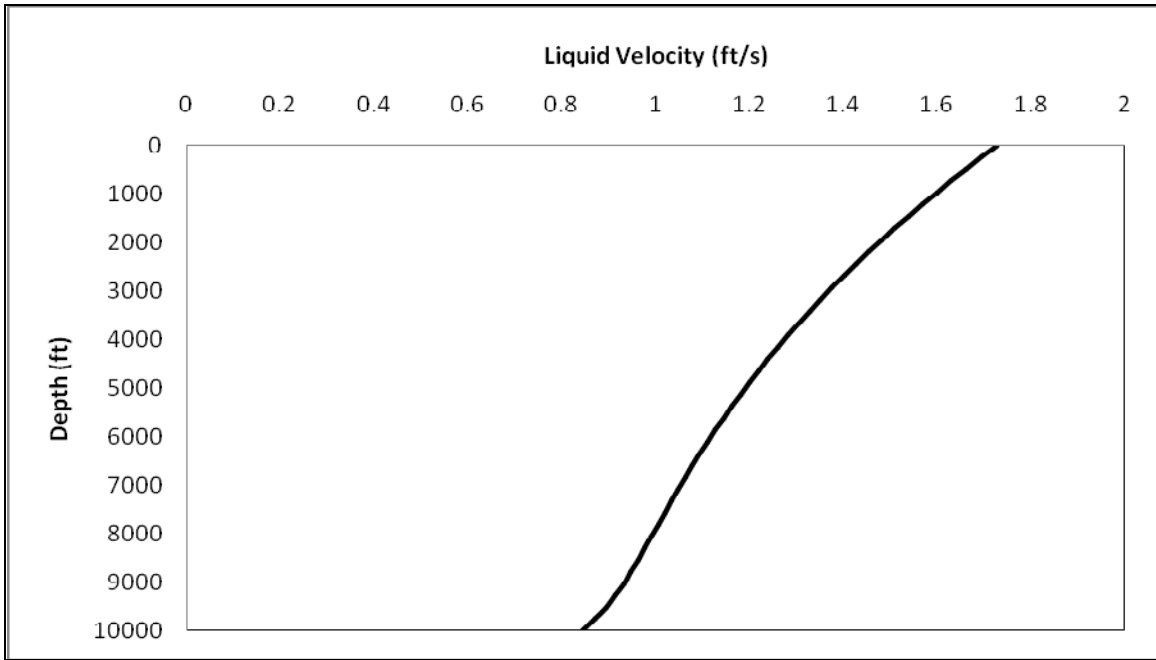


Figure 3.17 Simulated liquid velocity profile in the wellbore during three phase flow production from 10000 ft tubing with 0.125 ft diameter (The production consists of 2500 lbm mole/day of hydrocarbon and 5800 lbm mole/day of water at the surface)

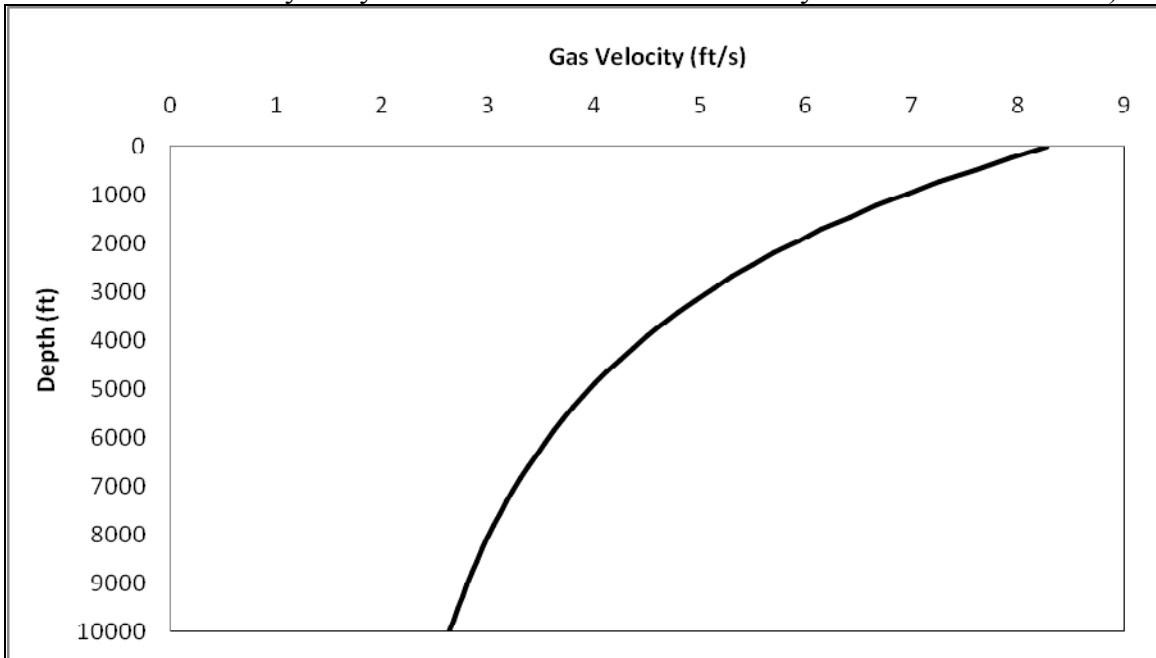


Figure 3.18 Simulated gas velocity profile in the wellbore during three phase flow production from 10000 ft tubing with 0.125 ft diameter (The production consists of 2500 lbm mole/day of hydrocarbon and 5800 lbm mole/day of water at the surface)

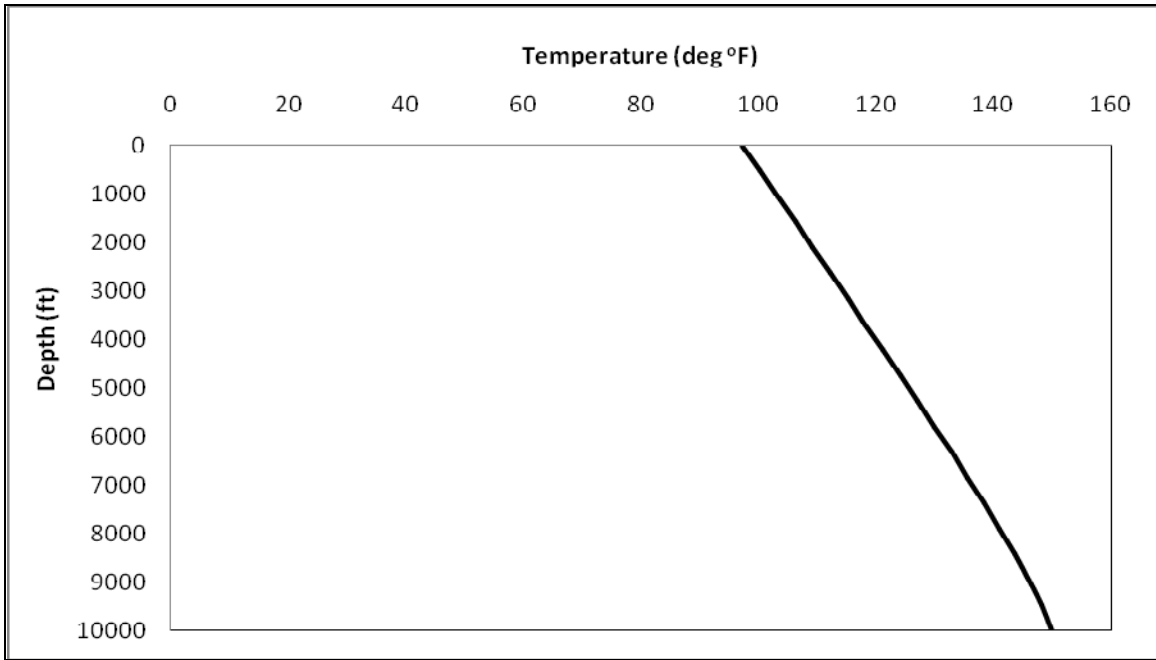


Figure 3.19 Simulated temperature distribution profile in the wellbore during three phase flow production from 10000 ft tubing with 0.125 ft diameter (The production consists of 2500 lbm mole/day of hydrocarbon and 5800 lbm mole/day of water at the surface. The surface temperature is 90 °F and the reservoir temperature is 150 °F)

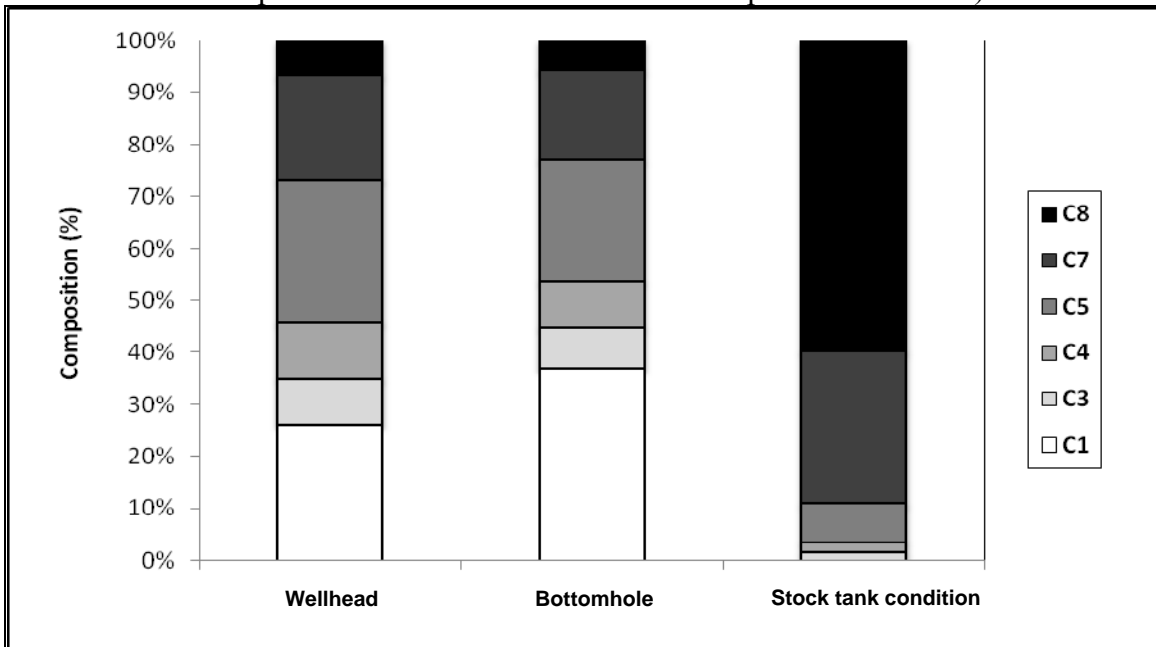


Figure 3.20 Simulated liquid composition fractions in the wellbore sandface and surface sides during three phase flow production from 10000 ft tubing with 0.125 ft diameter (The production consists of 2500 lbm mole/day of hydrocarbon and 5800 lbm mole/day of water at the surface)

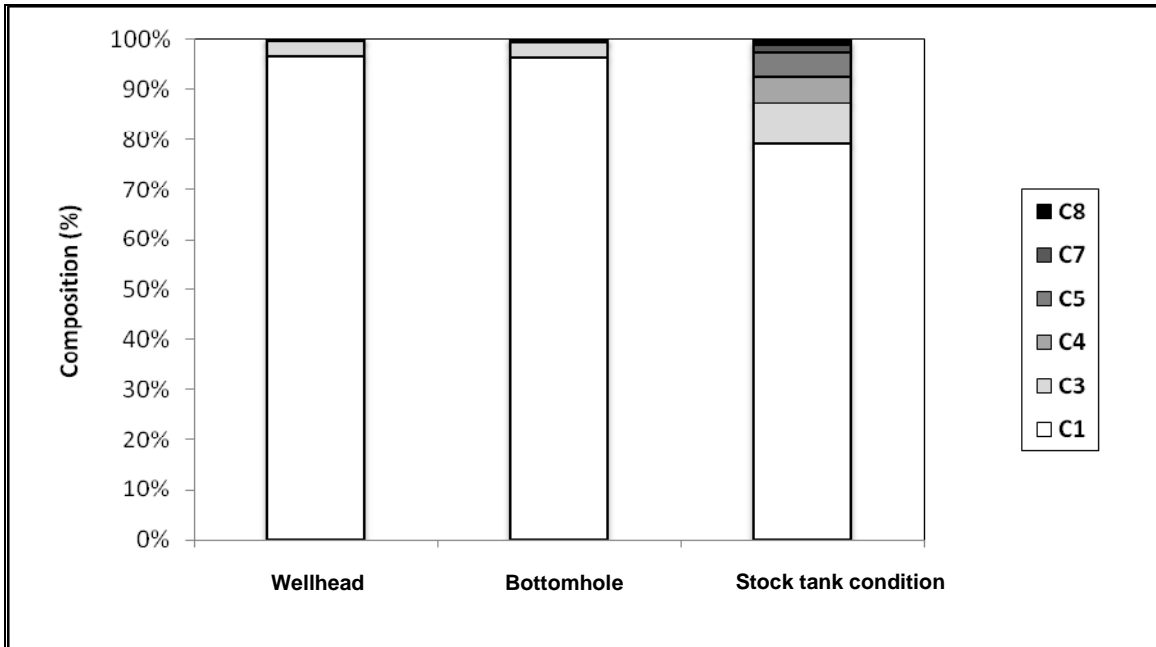


Figure 3.21 Simulated gas composition fractions in the wellbore sandface and surface sides during three phase flow production from 10000 ft tubing with 0.125 ft diameter (The production consists of 2500 lbm mole/day of hydrocarbon and 5800 lbm mole/day of water at the surface)

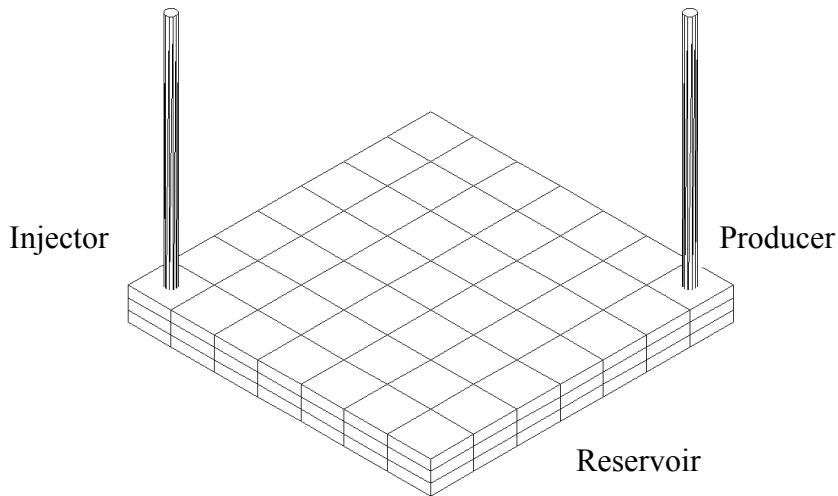


Figure 3.22 Schematic gridding of reservoir/wellbore system (The reservoir dimensions are $560 \times 560 \times 100$ ft, and the producer wellbore depth is 5000 ft. the reservoir is divided to $8 \times 8 \times 3$ grid blocks and wellbore is divided into 20 gridblocks in z direction)

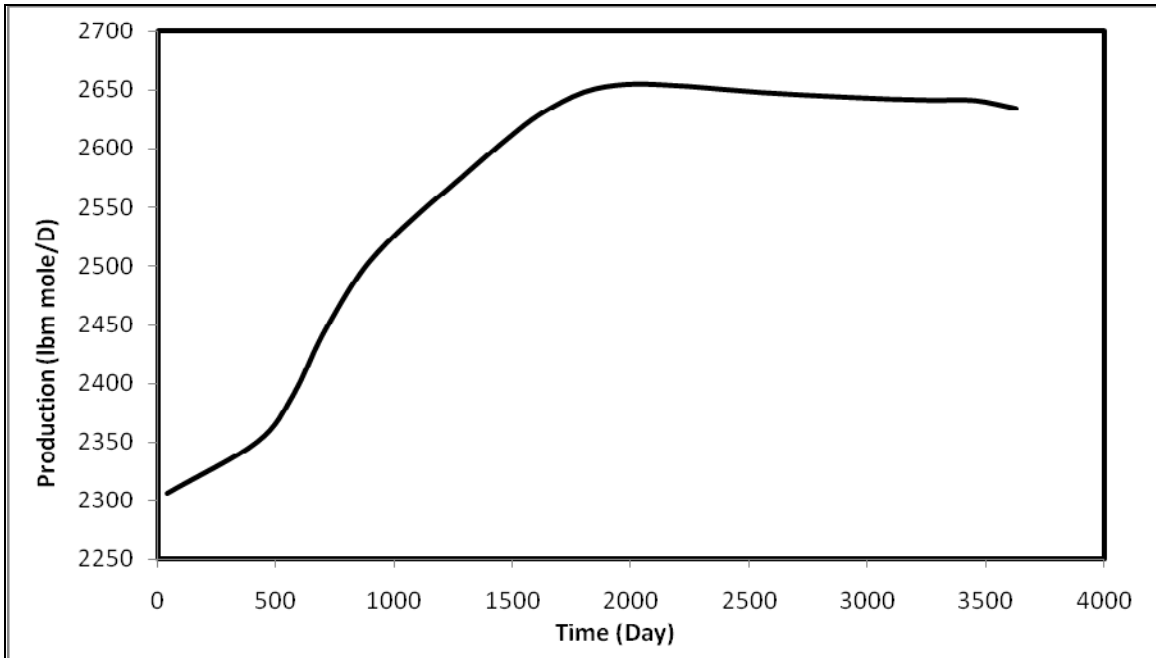


Figure 3.23 Well hydrocarbon production profile from a reservoir with initial pressure equal to 1500 psi (initial reservoir composition consist of 0.5 C1, 0.03 C3, 0.07 C6, 0.2 C10, 0.15 C15 and 0.05 C20)

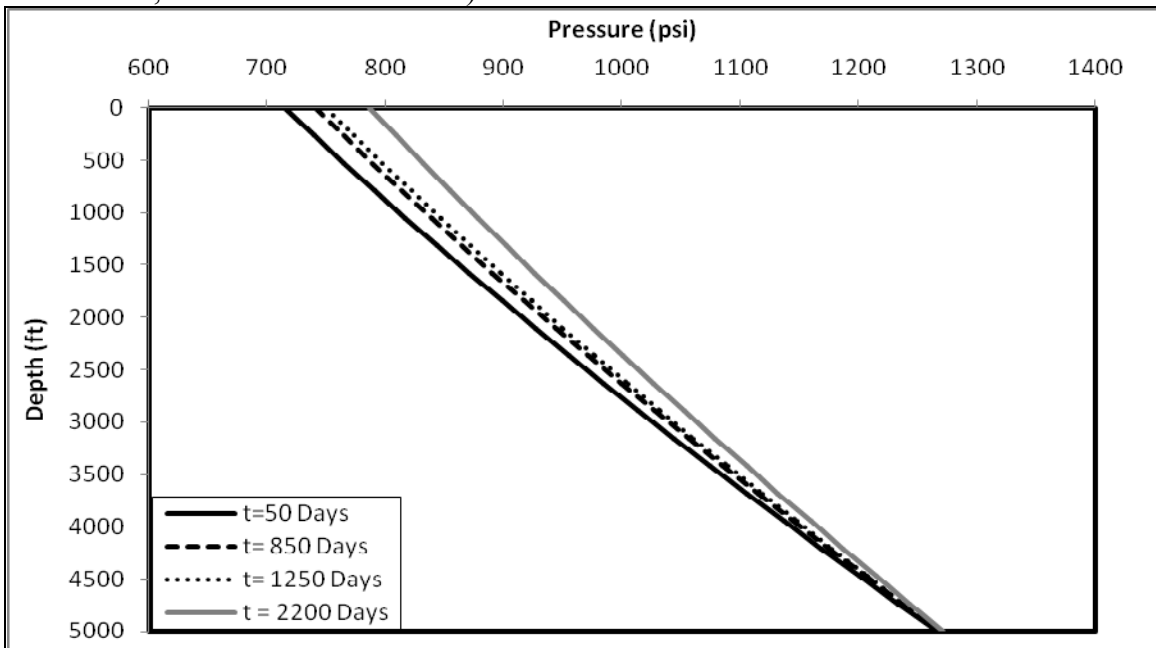


Figure 3.24 Simulated transient pressure profiles in the wellbore during production from a reservoir with initial pressure equal to 1500 psi (initial reservoir composition consist of 0.5 C1, 0.03 C3, 0.07 C6, 0.2 C10, 0.15 C15 and 0.05 C20, the tubing depth is 5000 ft and the tubing diameter is 0.25 ft)

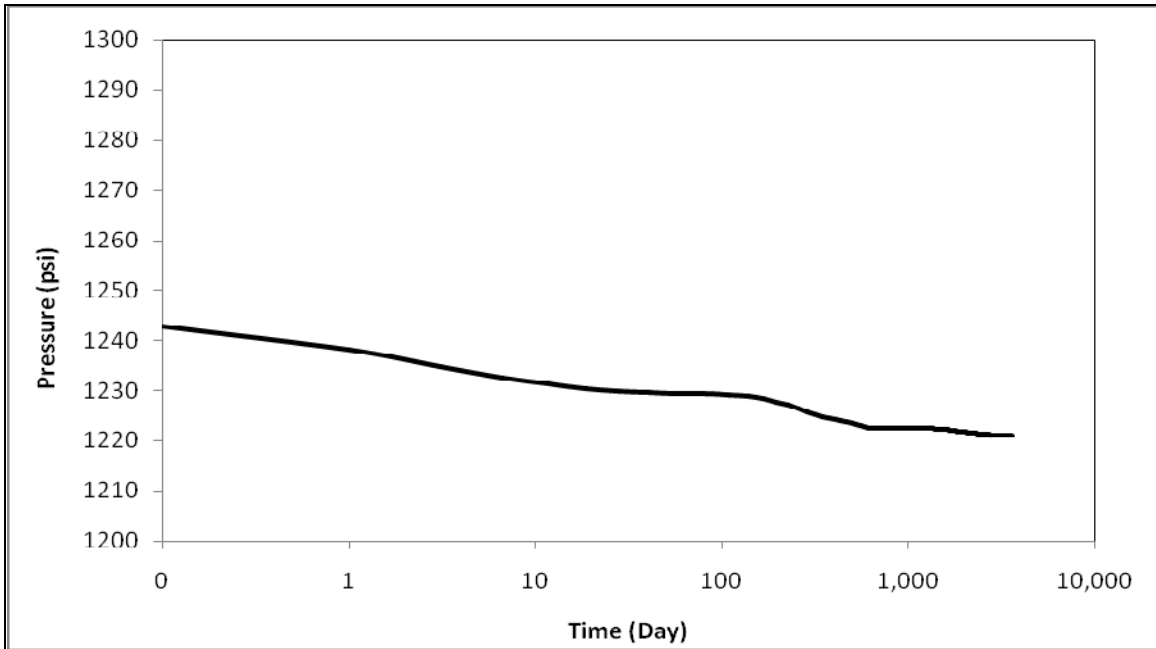


Figure 3.25 Simulated producer pressure history at 4500 ft depth during production from a reservoir with initial pressure equal to 1500 psi (Initial reservoir composition consist of 0.5 C1, 0.03 C3, 0.07 C6, 0.2 C10, 0.15 C15 and 0.05 C20, the tubing depth is 5000 ft and the tubing diameter is 0.25 ft)

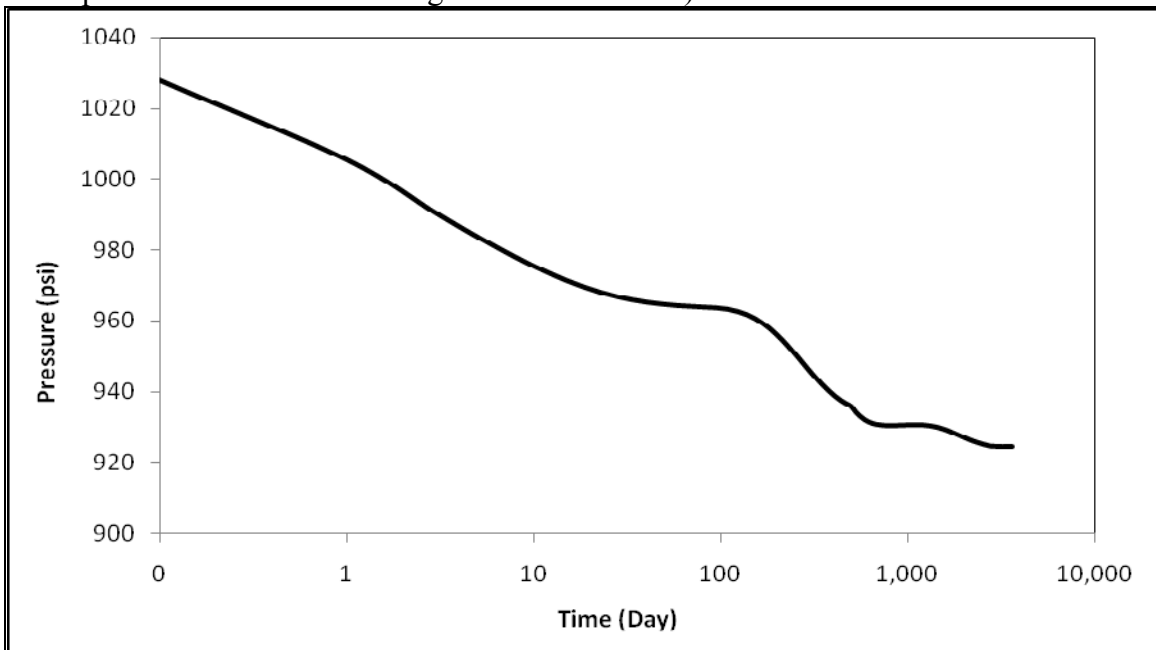


Figure 3.26 Simulated producer pressure history at 2500 ft depth (middle of the wellbore) during production from a reservoir with initial pressure equal to 1500 psi (Initial reservoir composition consist of 0.5 C1, 0.03 C3, 0.07 C6, 0.2 C10, 0.15 C15 and 0.05 C20, the tubing depth is 5000 ft and the tubing diameter is 0.25 ft)

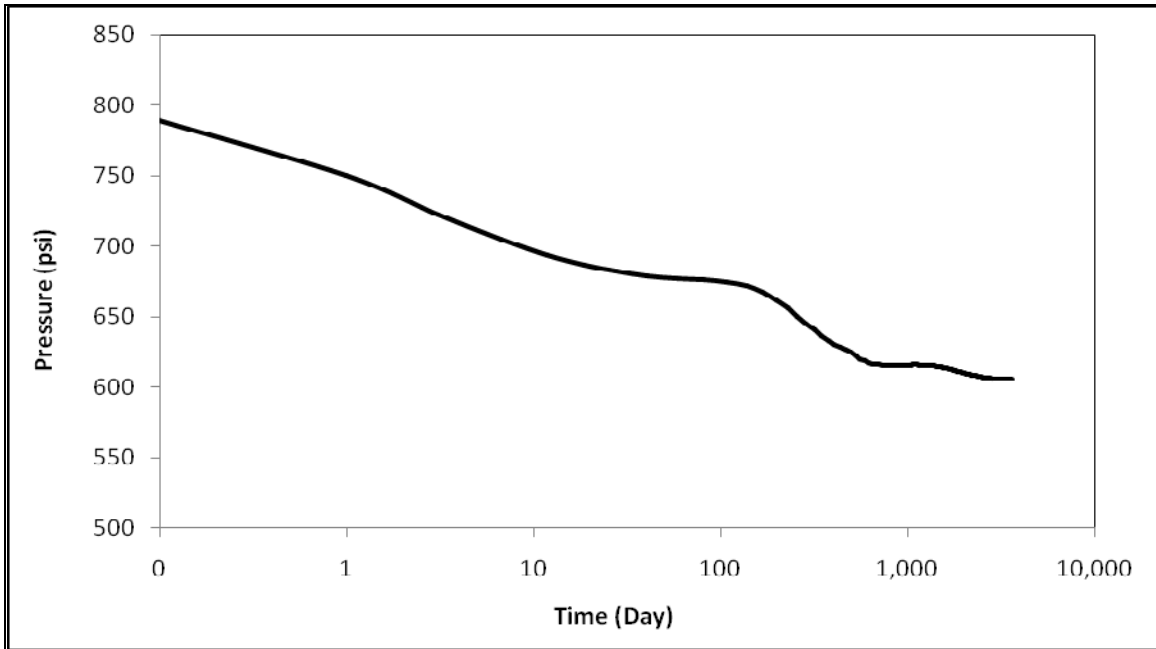


Figure 3.27 Simulated producer pressure history at wellbore surface during production from a reservoir with initial pressure equal to 1500 psi (Initial reservoir composition consist of 0.5 C1, 0.03 C3, 0.07 C6, 0.2 C10, 0.15 C15 and 0.05 C20, the tubing depth is 5000 ft and the tubing diameter is 0.25 ft)

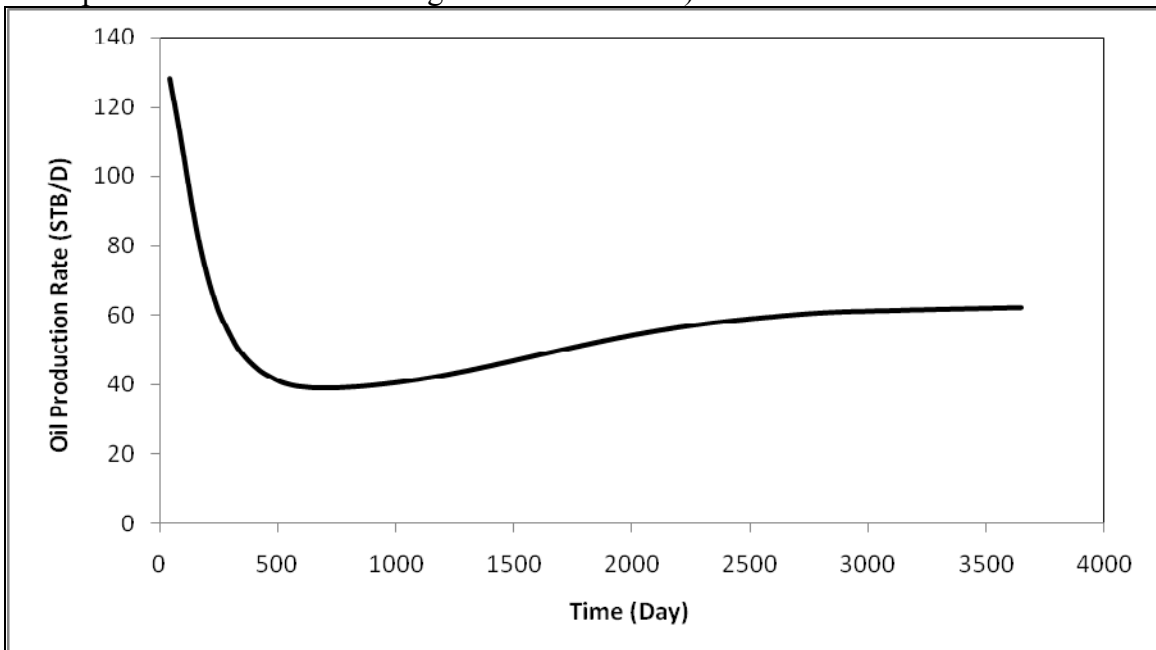


Figure 3.28 Simulated oil production history for an injector/producer case (Initial pressure equal to 1500 psi, initial reservoir composition consist of 0.5 C1, 0.03 C3, 0.07 C6, 0.2 C10, 0.15 C15 and 0.05 C20, the tubing depth is 5000 ft and the tubing diameter is 0.25 ft)

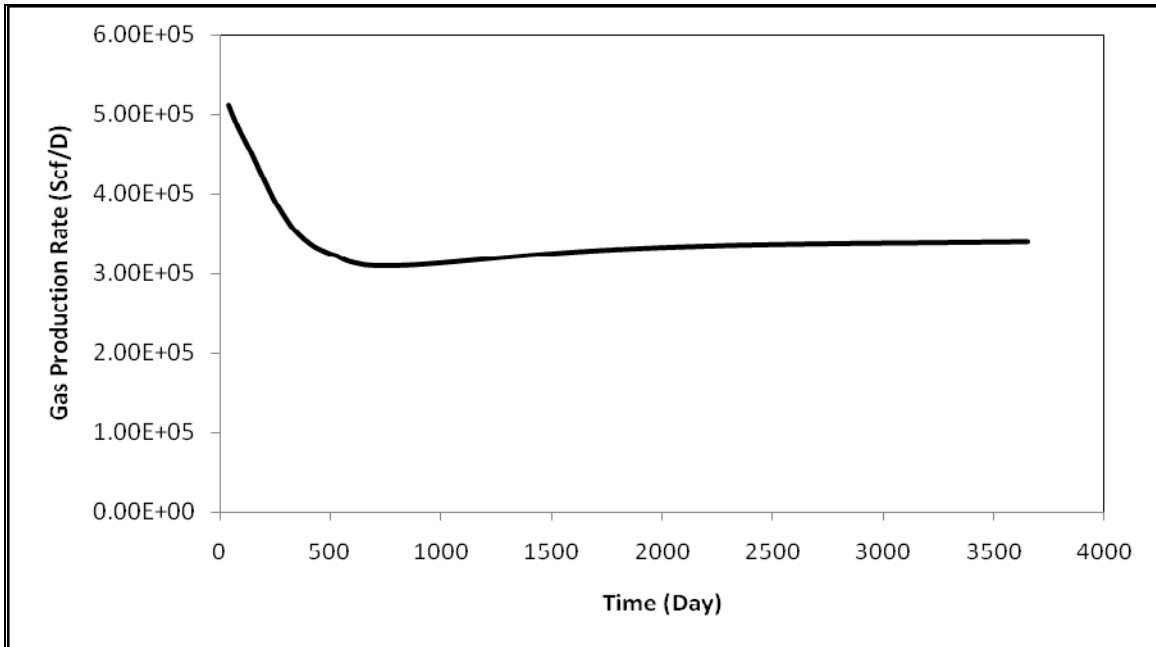


Figure 3.29 Simulated gas production history for a injector/producer case (Initial pressure equal to 1500 psi, initial reservoir composition consist of 0.5 C1, 0.03 C3, 0.07 C6, 0.2 C10, 0.15 C15 and 0.05 C20, the tubing depth is 5000 ft and the tubing diameter is 0.25 ft)

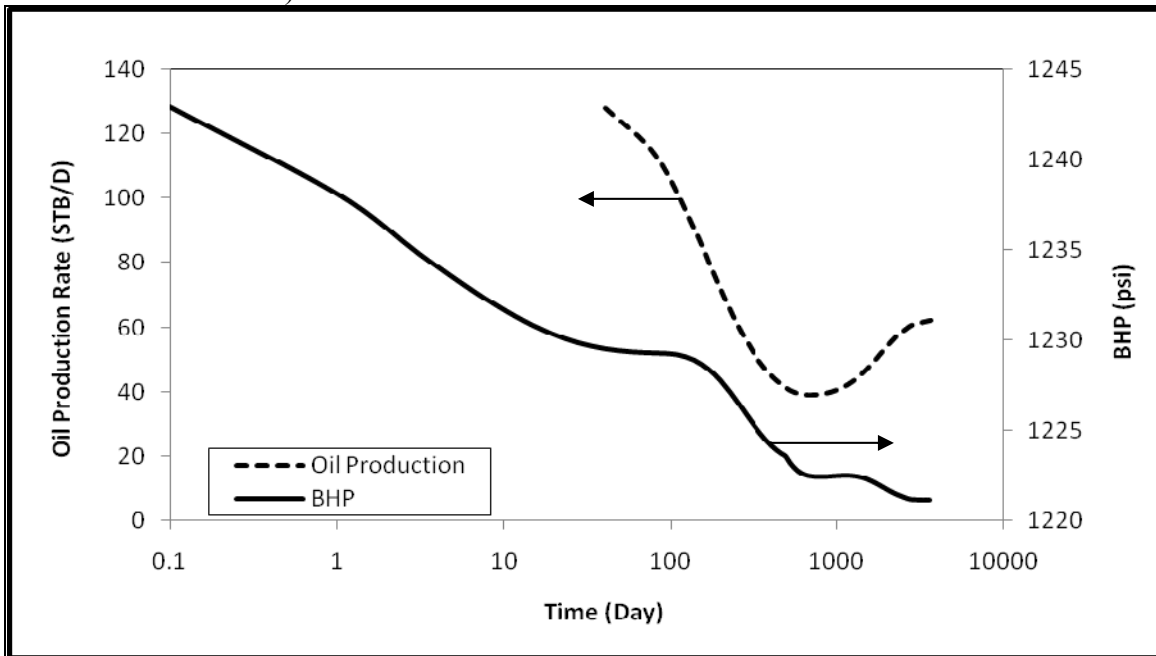


Figure 3.30 Comparison of oil production and reservoir pressure at the producer perforated zone for hydrocarbon production form a injector/producer system (Initial reservoir composition consist of 0.5 C1, 0.03 C3, 0.07 C6, 0.2 C10, 0.15 C15 and 0.05 C20, the tubing depth is 5000 ft and the tubing diameter is 0.25 ft)

Inner tubing radius (ft)	0.124583
Outer tubing radius (ft)	0.129
Wellbore radius (ft)	0.425
Inner casing radius (ft)	0.2843
Outer casing radius (ft)	0.3154
Tubing friction coefficient	0.0006
Formation heat conductivity (Btu/(hr-ft-°F))	1.4
Formation density (lbm/ft ³)	144
Formation heat capacity (Btu/(lbm-°F))	0.22
Cementing heat conductivity (Btu/(hr-ft-°F))	4.021

Table 3.1. General parameters for wellbore modeling

C1	0.3
C3	0.12
C4	0.12
C5	0.12
C7	0.17
C8	0.17

Table 3.2. Blackoil composition

C1	0.55
C3	0.1
C4	0.1
C5	0.1
C7	0.075
C8	0.075

Table 3.3. A typical composition for a volatile crude oil

C1	0.8
C3	0.04
C4	0.04
C5	0.04
C7	0.04
C8	0.04

Table 3.4. Composition for a typical gas-condensate system

Depth (ft)	10000
Inner tubing radius (ft)	0.125
Outer tubing radius (ft)	0.129
Wellbore radius (ft)	0.525
Inner casing radius (ft)	0.28
Outer casing radius (ft)	0.315
Tubing friction coefficient	0.0006
Water molar flow rate (lbm mole/D)	5800
Water gravity	1
Total hydrocarbon molar rate (lbm mole/D)	2500
Surface formation temperature (°F)	90
Formation temperature gradient (°F/ft)	0.006
Formation heat conductivity (Btu/(hr-ft-°F))	1.4
Formation density (lbm/ft ³)	144
Formation heat capacity (Btu/(lbm-°F))	0.22
Cementing heat conductivity (Btu/(hr-ft-°F))	4.02
Annulus brine salinity (ppm)	35000
Bottomhole wellbore temperature (°F)	150
Surface pressure (psi)	500
Number of nodes	40
Number of phases	3
Number of components	6
Total mole fraction (c1,c3,c4,c5,c7,c8)	0.78,0.08,0.05,0.05,0.02,0.02

Table 3.5. Production parameters for three phase flow case

Dimensions	560 X 560 X 100
Grid Blocks	8 X 8 X 3
Initial P	1500 Psi
Initial Water Saturation	0.17
Initial Oil Saturation	0.612
Initial Gas Saturation	0.218
Initial Composition:C1,C3,C6,C10,C15,C20	0.5,0.03,0.07,0.2,0.15,0.05

Table 3.6. Reservoir parameters for Case 2

Constant BHP	1300 psi
Depth	5000 ft
Grid Blocks	20 X 1
Diameter	3"

Table 3.7. Producer wellbore parameters for Case 2

CHAPTER 4: TRANSIENT COUPLED WELLBORE/RESERVOIR MODEL

4.1 INTRODUCTION

In most oil wells, multiphase fluids are produced through the wellbore to the surface. Different fluids flow from the reservoir into and through the wellbore with different velocities; so at each section of the wellbore, we expect different phase fractions. Whenever the flow in a section of the wellbore/reservoir system is perturbed, transient transfer of mass, momentum and energy occur in the wellbore. Since heat exchange occurs during this transient period, the flow condition becomes more complex. During well testing, in which the reservoir properties are estimated from the pressure response of the well, this transient period cannot be ignored or serious errors will be introduced into the results. Ordinary well testing consists of two main categories: buildup tests and drawdown tests. In buildup tests, a producing well is generally shut in at the surface or infrequently at the bottom of the tubing, then the bottomhole pressure response is measured directly or inferred from surface measurements. During a drawdown test a previously shut-in well is produced at a constant rate and the transient response of bottomhole pressure is measured and analyzed to obtain information about reservoir characteristics.

A fully transient wellbore simulator can be used to perform analysis of well test data more accurately. In some cases it is difficult and expensive to measure bottomhole pressure directly during the test time period; hence, with this simulator it is possible to model and estimate pressure and temperature profiles during well testing based on surface measurements. It can also be used as a tool to design well testing programs. It should be noted that the complicated wellbore dynamics during the early-time transient response may lead to reservoir model misdiagnosis, so it is crucial to develop a simulator for the wellbore to model transient effects.

During production of fluids at high or moderate temperature from an oil well, considerable heat exchange takes place between the fluid in the wellbore and the surrounding formation. Hence, temperature distribution in the wellbore will change and this influences fluid properties such as density and viscosity. A comprehensive transient wellbore model should handle these temperature effects. A few simulators have been presented in the literature to study transient flow in the wellbore; most of them consider an isothermal wellbore. In this model we solve the energy equation in addition to other governing equations in the wellbore to compute the temperature distribution in the wellbore from the sandface to the surface.

This simulator models the flow of each phase from the reservoir and in the wellbore during any transient period, including computing backflow and reverse flow from the wellbore to the reservoir as required by the pressure conditions. Each phase property, such as velocity and volume fraction, is modeled based on the multiphase flow regime in the wellbore. Due to the ability of this simulator to model the temperature

distribution, it can be also used in injection modeling to calculate the injected fluid temperature at the bottomhole.

Recognizing the limitations of analytic wellbore models, numerical models were advanced to simulate the general transient behavior of multiphase fluid flow. This chapter presents a transient wellbore/reservoir simulator. In this efficient model, flow and temperature distribution in the wellbore are modeled numerically while this simulator is fully coupled to a reservoir numerical simulator. In this research, a reservoir simulator called GPAS is used for this purpose (Wang et al., 1997; 1999; Han et al., 2007). GPAS is developed in the University of Texas at Austin. A brief description of GPAS is presented in Appendix D.

This chapter presents the governing equations for the wellbore/reservoir transient system and the solving procedure is followed by a case study and the comparison of simulated results with field data.

4.2 GOVERNING EQUATIONS

We consider multiphase flow inside the wellbore with flow occurring only in the z direction. The wellbore communicates with the reservoir through one or more perforated zones. A schematic of the wellbore/reservoir system is shown in Figure 4.1. Mathematical description of multiphase flow during injection or production involves coupling the wellbore flow equations with the reservoir performance governing equations. In our model, we assume that a wellbore system exists that consists of three phases: oil, water and gas. Mass transfer can take place between the oil phase and the gas

phase. We also assume that there is no slip between oil and water, so that the water and oil phases are moving at the same velocity. Governing equations consist of conservation of mass for each phase, conservation of momentum for liquid and gas and conservation of energy. These equations are coupled to the reservoir equations.

The wellbore is divided into a set of control volumes and the governing equations are discretized for each gridblock using finite difference techniques. A schematic of one grid block in the wellbore is shown in Figure 4.2. These equations are connected to the reservoir equations to model mass, momentum and energy exchange between reservoir and wellbore. The system of nonlinear partial differential equations governing the fluid-flow in the wellbore is arranged and solved using finite-difference method. The wellbore governing equations are:

Mass Balance:

Equation 4.1 shows the mass balance for each phase in the wellbore.

$$\frac{\partial}{\partial t} \{ \rho_i H_i \} + \frac{\partial}{\partial z} \{ \rho_i v_i H_i \} + \frac{M_i'}{V} = 0 \quad i = o, w, g \quad (4.1)$$

In this equation,

ρ_i = Phase density (lbm/ft³)

H_i = Phase fraction

v_i = Phase velocity (ft/s)

M_i' = Mass rate from the reservoir (lbm/s)

V = Control volume (ft³)

The change of mass for each phase in the control volume per unit time is equal to the mass rate of fluid leaving the system minus that entering from other control volumes or from the reservoir. In Equation 4.1 the first term, $\frac{\partial}{\partial t}\{\rho_i H_i\}$, is the accumulation of phase i in the control volume, the second term, $\frac{\partial}{\partial z}\{\rho_i v_i H_i\}$, is the convection of each phase between control volumes and the last term, $\frac{M'_i}{V}$, is mass exchange with the reservoir.

Momentum Balance:

A “two-fluid” model is used to express the conservation of momentum in the system. The equations for the gas phase and the liquid phase are shown in Equations 4.2 and 4.3.

$$\frac{\partial}{\partial t}(\rho_l H_l v_l) + \frac{\partial}{\partial z}(\rho_l H_l v_l^2) + H_l \rho_l g \sin \theta + H_l \frac{\partial P}{\partial z} + \left(\frac{\partial P}{\partial z}\right)_{fl} + \left(\frac{\partial P}{\partial z}\right)_{gl} = 0 \quad (4.2)$$

$$\begin{aligned} \frac{\partial}{\partial t}(\rho_g (1-H_l) v_g) + \frac{\partial}{\partial z}(\rho_g (1-H_l) v_g^2) + (1-H_l) \rho_g g \sin \theta + \\ (1-H_l) \frac{\partial P}{\partial z} + \left(\frac{\partial P}{\partial z}\right)_{fl} - \left(\frac{\partial P}{\partial z}\right)_{gl} = 0 \end{aligned} \quad (4.3)$$

In these equations, subscript l is for liquid and g is for gas. Also,

ρ_i = Phase density (lbm/ft³)

H_i = Phase fraction

v_i = Phase velocity (ft/s)

P = Control volume pressure in wellbore (psi)

In the liquid momentum equation, the first term, $\frac{\partial}{\partial t}(\rho_l H_l u_l)$, is the accumulation term. The second one, $\frac{\partial}{\partial z}(\rho_l H_l u_l^2)$, is the convection term, and the third term, $H_l \rho_l g \sin \theta$, is the hydrostatic pressure. Term $H_l \frac{\partial P}{\partial z}$ shows the pressure gradient in the wellbore due to the liquid phase. The term $(\frac{\partial P}{\partial z})_{fl}$ represents the pressure gradient due to the wall friction between the liquid phase and the tubing. $(\frac{\partial P}{\partial z})_{gl}$, the last term in the momentum equations, expresses the pressure gradient caused by the friction between phases. Similar terms appear in the gas momentum equation. The wall friction can be computed as

$$(\frac{\partial P}{\partial z})_{fl} = -\frac{f}{2D} \rho_l v_l |v_l| \quad (4.4)$$

where f , the friction coefficient, can be expressed as

$$f = \frac{64}{\text{Re}} \quad \text{for laminar flow and}$$

$$\frac{1}{f} = 114 - 2 \log\left(\frac{e}{D} + \frac{2125}{\text{Re}^{0.9}}\right) \quad \text{for turbulent flow.}$$

In these equations Re denotes the Reynolds number which is defined as usual as $\text{Re} = \frac{D v_l \rho_l}{\mu_l}$. D is the tubing diameter and e is the absolute surface roughness.

Another friction term is caused by the drag between liquid and gas phase. In our work, the approach presented by Winterfeld (1989) is used to model this phase-to-phase

friction term, which occurs because of the relative motion between phases and is a function of interfacial area and relative velocity. In laminar flow, the phase-to-phase friction is inversely proportional to relative velocity, but in turbulent flow the drag often tends to be less sensitive to changes in relative velocity (Perry, 1963). It should be noted that the interfacial area is dependent on phase holdup. A simple functional representation of phase/phase viscous force term for liquid and gas is (Winterfeld, 1989):

$$\left(\frac{\partial P}{\partial z}\right)_{gl} = C_{gl} (H^{w_l})(1-H)^{w_g} (v_l - v_g) |v_l - v_g|^{w_u} \quad (4.5)$$

where,

C_{gl} = Drag coefficient between gas and liquid phase

H = Liquid holdup

w_l, w_g, w_u = Parameters between zero and one

Energy Balance:

During production or injection, heat is exchanged between the surrounding formation and the wellbore system. Thus, the energy balance includes the convective heat exchange with the formation, as well as the convective energy transport into and out of a control volume. This convective term involves change in enthalpy, kinetic energy and potential energy for the fluid system. The sum of the convective and conductive terms equals the accumulation of the energy in the system which causes a change in the temperature of the wellbore fluid and the tubing/casing/cement material. The energy equation can be written as

$$Q = \frac{d(m_m E_m + m_{icc} E_{icc})}{dt} + \frac{d}{dz} w \left(h_m + \frac{v_m^2}{2} + gz \sin \theta \right) \quad (4.6)$$

The heat exchange, Q , is equal to the summation of fluid internal energy change,

$\frac{d(m_m E_m)}{dt}$, the wellbore system internal energy change, $\frac{d(m_{icc} E_{icc})}{dt}$ and the convection

term.

We can express the fluid internal energy gradient as a function of enthalpy, pressure and temperature. We obtain:

$$\begin{aligned} \frac{d(m_m E_m)}{dt} &= A \frac{d(\rho_m E_m)}{dt} = A \frac{d\{\rho_m (h_m - P / \rho_m)\}}{dt} \\ &= A \rho_m \frac{dh_m}{dt} - A \rho_m \frac{d(P / \rho_m)}{dt} + A (h_m - P / \rho_m) \frac{d\rho_m}{dt} \\ &= A \rho_m \frac{dh_m}{dP} \left(\frac{dP}{dt} \right)_T + A \rho_m \frac{dh_m}{dT} \left(\frac{dT}{dt} \right)_P - A \rho_m \frac{d(P / \rho_m)}{dt} + A (h_m - P / \rho_m) \frac{d\rho_m}{dt} \\ &= -A \rho_m c_{pm} \eta_m \frac{dP}{dt} + A \rho_m c_{pm} \frac{dT}{dt} - A \rho_m \frac{d(P / \rho_m)}{dt} + A (h_m - P / \rho_m) \frac{d\rho_m}{dt} \end{aligned} \quad (4.7)$$

Equation 4.6 can be rewritten as

$$\begin{aligned} q &= -\rho_m c_{pm} \eta_m \frac{dP}{dt} + \rho_m c_{pm} \frac{dT}{dt} - \rho_m \frac{d(P / \rho_m)}{dt} + (h_m - P / \rho_m) \frac{d\rho_m}{dt} \\ &+ \rho_{icc} c_{pcc} \frac{dT}{dt} + \frac{d}{Adz} w \left(h_m + \frac{v_m^2}{2} + gz \sin \theta \right) \end{aligned}$$

Hence,

$$\begin{aligned} q &= \left(h_m - \frac{P}{\rho_m} \right) \frac{\partial \rho_m}{\partial t} + \rho_m c_{pm} \frac{\partial T}{\partial t} + \rho_{icc} c_{pcc} \frac{dT}{dt} - \rho_m \eta_m c_{pm} \frac{\partial P}{\partial t} - \rho_m \frac{\partial \left(\frac{P}{\rho_m} \right)}{\partial t} + \\ &\frac{d}{Adz} w \left(h_m + \frac{v_m^2}{2} + gz \sin \theta \right) \end{aligned} \quad (4.8)$$

where,

H_m = Mixture enthalpy (Btu/lbm)

P = Pressure (psi)

ρ_m = Mixture density (lbm/ft³)

ρ_{tcc} = tubing/casing/cementing average density (lbm/ft³)

c_{pm} = Heat capacity of mixture (Btu/lbm-°F)

c_{ptcc} =Weighted average heat capacity of wellbore system (Btu/lbm-°F)

η_m = Joule-Thompson coefficient (°F/psi)

v_m = Mixture velocity (ft/s)

T = Temperature (°F)

In this derivation we assume that,

- 1) The density does not change in a control volume
- 2) The temperature of the wellbore system is same as the fluid temperature

The method used to compute mixture heat capacity and mixture Joule-Thompson effect is discussed in Chapter 2. Wellbore system heat capacity is calculated as the weighted average between cement, casing and tubing heat capacities as

$$c_{ptcc} = \frac{m_{tubing}}{m_{total}} c_{p,tubing} + \frac{m_{casing}}{m_{total}} c_{p,casing} + \frac{m_{Cement}}{m_{total}} c_{p,cement} \quad (4.9)$$

where $m_{total} = m_{tubing} + m_{casing} + m_{Cement}$, and m is the weight of casing, cement and tubing in a control volume section.

Heat exchange between the wellbore fluids and formation, q , can be calculated from Equation 2.35, described in Chapter 2.

The control volumes shown in Figure 4.2 are for the momentum equations. The control volume for energy and mass is staggered one half-block distance from the control volume for the momentum balance. So the values for liquid and gas velocities are defined at the edges of the control volumes. Values for pressure, density, temperature and phase fractions are computed at the control volume center nodes. Values of phase fractions and density at the edges are calculated by an upwind method.

4.3 SOLVING PROCEDURE

The governing equations are discretized at each block as shown in Appendix C. For this simulation, the wellbore continuity Equations C.1 through C.3, momentum Equations C.4, C.5 and energy Equation C.6 form a set of consistent equations whose primary variables are liquid and gas velocities, phase fractions, pressure and temperature. Due to the fully implicit treatment, these equations are coupled with a reservoir model. The wellbore is connected to the reservoir by applying a well model relating the sandface flow rate to the pressure difference between wellbore and reservoir.

The non-linear set of equations is solved by Newton's method applied simultaneously to the wellbore and reservoir equations using commercially available software named Petsc. Additional details about the solver are presented in Appendix E.

For a fully implicit treatment, momentum and continuity equations are solved first and the energy equation is then solved to update the temperature. With the new value for temperature the model updates values for pressure, phase fractions and phase velocities.

When the hydrocarbon flow rate changes in a wellbore/reservoir system, the transient period starts. For example, consider a buildup test. Usually, in this kind of well testing the gas and liquid flow stop at the wellhead. To model this test with our coupled simulator, boundary and initial conditions should be defined. We have developed a steady-state compositional wellbore/reservoir simulator which is fully described in Chapter 3. We used this steady state simulator to make the initial condition before perturbation. Hence, pressure, temperature and phase fraction profiles are modeled at steady state condition to be the initial condition for the transient simulator. The wellbore boundary condition depends on the particular problem that is modeled; for example, in a shut in well, this boundary condition is zero phase velocity at the wellhead. The schematic flowchart of the solution method is shown in Figure 4.3.

4.4 RESULTS

In this section, we describe the application of the simulator to a field example that provides considerable information about the mechanics of transient flow in the wellbore. First, a two-phase flow field example is presented to show the validity of our model, then we present stand-alone wellbore simulator's results. Finally, results obtained from a coupled wellbore/reservoir simulator are presented.

4.4.1 Case 1: Comparison with field data

This case is based on the results of a unique field test in a liquid loaded gas well, where the acoustic field level measurements were undertaken simultaneously with a wireline survey of flowing, and static pressure was recorded every second by means of a 0.01 psi resolution quartz pressure sensor. (Rowlan et al., 2006) The well is completed with 2-7/8 tubing as a monobore completion. At the time of test, the well was producing gas at an average rate of about 172 MSCF/D. It was also producing oil with a low rate. (Figure 4.4) The set of data for flowing pressure gradient and transient pressure profile during shut in are presented in Figure 4.5. Figure 4.5 shows the pressure traverses during shut in for this case, based on the field data showing how the pressure at the tubing head is increasing, and the gas/liquid interface is moving down, and the gradient of the gaseous liquid column is increasing. The last measured data shows that a 700 ft column of mostly liquid has accumulated at the bottom of the tubing and the pressure at bottomhole has stabilized at 404 psi.

In Figure 4.5, the four first plots (Flowing 1 through Flowing 4) correspond to measured data when the gas was flowing at the surface and the acoustic measuring tool was being lowered into the well; consequently there is no data for the pressure at 7150 feet. These four lines correspond to the pressure in the gas column above the gas/liquid interface. The first shut-in shot corresponds closely to the condition that existed in the well when gas was flowing. It may be considered that the pressure distribution corresponds to the average flowing condition.

We simulated this case with our simulator. Table 4.1 shows the parameters used in this simulation. Figures 4.6 through 4.17 represent different results obtained from this simulation.

Figure 4.6.a through 4.6.h show the simulated values and measured pressure data at different times after shut in. The solid line shows our simulation results and the dots are field data. It can be observed from Figure 4.6 that the simulated results are in good agreement with the field data. It should be noted that, in the measurement, the acoustic tool might affect the flow pattern of the gaseous liquid column. During shut in, the graphs show the phase segregation. It is obvious that there are two sections in the well: one gaseous column with lower pressure gradient at the top and one liquid column with higher pressure gradient at the bottom. After the well is shut in and during the early time period the flow regime in the tubing is disturbed and liquid falls back toward the bottom of the tubing. Our simulation shows this phenomenon in detail. Figures 4.7 and 4.8 present pressure vs. time at different sections of the well. These graphs show how the pressure builds up during shut in.

Figures 4.8 through 4.11 show the transient liquid holdup in the wellbore. Phase segregation can be clearly observed in these graphs. In the top section of the well the liquid fraction decreases and liquid falls down. In the bottom section, gas fraction decreases and liquid accumulates. When the system reaches steady state, two different sections, a gas column and a liquid column, are formed.

Figures 4.12 through 4.14 show the transient superficial velocity for liquid. We can observe three different periods; at early time, liquid continues to flow to the wellbore

from the reservoir. As wellbore pressure increases in the middle time period, flow rate from the reservoir decreases and liquid falls down to the bottom section of the well. We can distinguish this period by negative velocity, which means flow to the bottom. As pressure builds further, it may overcome reservoir pressure and back flow may occur, as shown in Figure 4.14. As this backflow takes place, the pressure in the wellbore decreases and reaches in equilibrium with reservoir, and the liquid flow stops.

Figures 4.15 through 4.17 are the results of transient superficial gas velocity simulation. It can be seen that when we shut the well in, gas velocity starts to decrease to zero. Superficial gas velocity in the lower sections of the well is lower than at the wellhead because of lower gas fraction at the bottom. After nearly 2000 seconds, the gas flow stops in the wellbore.

4.4.2 Case 2: Stand-alone wellbore simulator

A pressure-buildup test was simulated considering multiphase flow. The system was producing at a constant gas flow rate and a constant oil flow rate and then shut in. We modeled the transient behavior of fluid-flow and temperature in the wellbore with our blackoil simulator. Table 4.2 presents the data used for this case.

We divided the wellbore into 20 nodes and we model pressure, temperature, phase velocity and phase fractions in each segment. The steady state model discussed in Chapter 2, was used to obtain the initial conditions. For the boundary condition we used the following.

- 1) Phase velocity at the surface is zero because we shut the well in

2) At the bottomhole, the wellbore equations are coupled with a reservoir analytical model.

3) Bottomhole temperature is known and is constant during the buildup test

We also assume that formation temperature does not change during the transient test. With these conditions, the buildup test is simulated. Figures 4.18 through 4.30 present the results. Figure 4.18 shows liquid holdup. As discussed earlier, liquid holdup is one of the most important two-phase flow parameters, which represents the phase fraction in each part of the wellbore. When we shut in a flowing well, the gas phase continues to move upward and the denser phase, liquid, tends to move downwards due to gravity, causing phase segregation in the wellbore. This is an important phenomenon in well testing because it can influence the early pressure buildup results. In this study case, the simulated data show phase segregation clearly. As can be seen from Figure 4.18, as time increases the liquid fraction in the bottom of the wellbore starts to increase while decreasing at the wellhead. When the system reaches steady state we distinguish three different sections including one section from the wellhead up to a depth of 700 ft that is full of gas with no liquid. Between this point and 1800 ft, we observe a transition zone with a decreasing gas fraction and the denser phase occupies most of the wellbore. Below 1800 ft there is only liquid. Figure 4.19 shows this segregation effect in more detail, showing how the liquid fraction decreases with time in the upper sections and increases in the lower sections.

During a buildup test, as the gas phase migrates to the upper section because of the relative incompressibility of the liquid and the inability of the gas to expand in a

closed system, a net increase in the wellbore pressure occurs (Fair, 1981). When this phenomenon occurs, the increased pressure in the wellbore is relieved through the formation, and equilibrium between wellbore fluid and reservoir fluid will be attained. At early times, the pressure may increase above the formation pressure. The simulated pressure at different times is shown as Figure 4.20. From this figure it can be seen how the pressure is built up in the wellbore. At the late time two different slopes occur in the pressure profiles because of phase segregation. The smaller slope is for the gas section and the larger one is for the liquid part. Figure 4.21 shows this pressure change in more detail. We can observe a transient period in which pressure increases in the wellbore; after that pressure stabilizes and reaches the steady state period again. Figure 4.22 shows the bottomhole pressure vs. time that is important to define the boundary condition for the reservoir simulators.

At shut in, the velocity for both liquid and gas phases changes to zero at the surface, so the superficial velocity in the wellbore for both phases starts to decrease during the buildup test. The liquid phase moves downward because of gravity and we can observe backflow to the reservoir. Figures 4.23 and 4.24 show the transient superficial velocities. This back flow is more obvious in Figures 4.25 and 4.26 for liquid. At early times after shut in, fluid continues to flow from the reservoir to the wellbore. As the pressure increases, and because of gravity, liquid flows back into the reservoir, so that at middle times we can observe a negative velocity in these figures because the pressure in the wellbore is larger than that of the reservoir. As the back flow takes place, the pressure in the wellbore starts to decrease until equilibrium is reached. Figures 4.27 and 4.28

show the gas superficial velocity. Since the concentration of gas in the bottom sections of the wellbore is very small, we expect low values for gas superficial velocities near the reservoir. But we can still observe the backflow to the reservoir.

Another parameter that we can model with this simulator is temperature. Initial temperature is calculated with the steady state simulator described in Chapter 2. When we shut in the well, during the early time period, hot fluid continues to flow into the wellbore from the reservoir. Because of the inability of this fluid to exit, the temperature initially increases but later, because of the lower formation temperature, the wellbore fluids start to cool down until reaching thermal equilibrium with formation. Figures 4.29 and 4.30 show this temperature distribution in the wellbore. Notice the small increase at the early time and then the cooling because of heat loss to the formation.

4.4.3 Case 3: Coupled wellbore/reservoir transient problem

In this case the pressure transient test is modeled in a coupled wellbore/reservoir system. Figure 4.31 shows the schematic of the system. One producer wellbore is assumed at the middle of a $560 \times 560 \times 100$ ft³ hydrocarbon reservoir. The reservoir is divided into 7×7 gridblocks in the horizontal surface. The 100 ft thickness of the reservoir is divided into 3 gridblocks; we assume that all these vertical blocks are perforated at the wellbore connection. Hence, gas and oil flow to the wellbore from all the blocks adjoined to the reservoir. The wellbore is divided into 20 gridblocks in the z direction. The geometry of the reservoir and the wellbore and their parameters is presented in Tables 4.3 and 4.4. We ran our steady state compositional wellbore/reservoir

simulator to model the pressure and temperature profiles in the wellbore and reservoir before shut in. The compositional steady state simulator is discussed in detail in Chapter 3. When the buildup test starts, we deal with a transient problem for both wellbore and reservoir. Wellbore and reservoir governing equations are solved simultaneously, as discussed earlier. In this case, the time step was selected to be 4 sec.

We are interested in modeling the pressure profile in the wellbore, especially bottomhole pressure. Also, the pressure differences between the wellbore and the reservoir at perforation zones is crucial due to fluid exchange between the wellbore and reservoir. Figure 4.32 shows a schematic of wellbore/reservoir system gridblocks. Reservoir nodes around the wellbore are in communication with wellbore gridblocks through perforations. It is possible to model transient pressure in the reservoir at different positions. In this case, our purpose from the reservoir pressure is pressure at the deepest reservoir node connected to the wellbore. Before the shut in and during production, reservoir pressure depletes with time. When we shut the well in, hydrocarbon fluids continue to flow into the wellbore through perforation zones. This afterflow causes more depletion for the reservoir. As the wellbore pressure increases due to expansion of gas in a closed system, the flow rate from the reservoir to the wellbore decreases. This flow rate is a function of pressure difference between the reservoir and wellbore in perforation zones (If reservoir node pressure is greater than wellbore bottomhole pressure then the flow is from reservoir to the wellbore). It is possible that the wellbore bottomhole pressure overcomes the reservoir pressure; then we expect the backflow from the wellbore to the reservoir. Backflow will compensate the pressure depletion in the

reservoir. As the reservoir pressure becomes equal to the wellbore pressure, fluid flow stops and a steady state condition is reached. Figures 4.33 through 4.35 show this discussion more accurately. Figure 4.33 shows how shutting in the wellbore affects the pressure history in the reservoir. Instead of normal depletion, reservoir pressure may increase due to backflow. Figure 4.34 presents reservoir pressure in a different scale. Figure 4.35 shows the pressure difference between the reservoir and the wellbore. We can notice three periods, up to about 0.1 hr, fluid flows into the wellbore due to higher reservoir pressure. Between 0.1 hr and 0.5 hr, the wellbore bottomhole pressure becomes greater than the reservoir pressure so backflow occurs to the reservoir. After $t=0.5$ hr, the reservoir pressure and wellbore bottomhole pressure become close to each other, so the flow rate declines. After about 1 hr of the test, fluid flow ceases in the system.

Figures 4.36 through 4.39 present the phase flow exchange between the wellbore and reservoir after the shut in. Figure 4.36 shows the liquid volume rate that comes into the wellbore. Again, three different periods are clearly distinguished; after flow, backflow and steady state periods. Figure 4.37 shows the cumulative liquid volume that enters the wellbore after shut in. Most of the liquid that entered the wellbore returns to the reservoir during the backflow period. The same physics takes place for the gas phase. At the early times, gas flows into the wellbore from the reservoir. As pressure increase in the wellbore bottomhole, all the gas solves in the liquid phase so backflow consists of liquid only. Hence, gas flow stops sooner. Figures 4.38 and 4.39 show the afterflow for the gas phase.

If we focus on the wellbore in this case, we again observe the phase segregation in the wellbore. After shutting the well, liquid moves downward and accumulates at the bottom section of the wellbore, while gas travels to the upper part. Figure 4.40 shows the final holdup profile in the wellbore; we can distinguish three sections in the wellbore. The upper 2500 ft is full of only gas, while below 3500 ft only liquid exists. Between 2500 and 3500 ft, a transition zone is formed at which a mixture of gas and liquid coexists. Figure 4.41 shows the pressure profile after end of the test; we can see two different pressure gradients in the wellbore which are exactly in agreement with the liquid fraction profiles. The lower gradient is for the gas region and the larger gradient occurs in the liquid section.

Our tests show that we can use this simulator as a stand-alone tool or in a comprehensive coupled wellbore/reservoir simulator to model multiphase flow in the wellbore. It is also possible to simulate fluid flow exchange between the wellbore and reservoir in different transient problems.

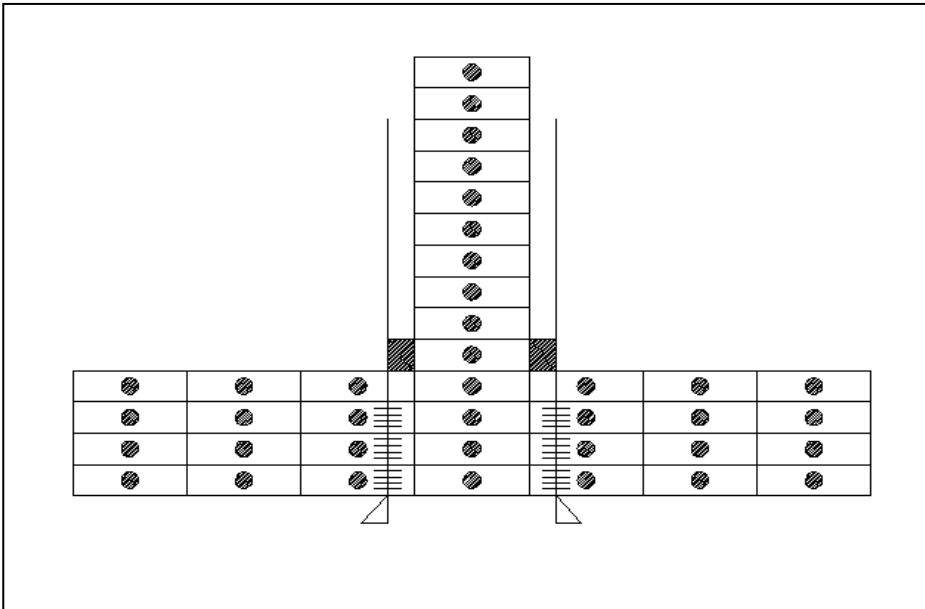


Figure 4.1 Schematic of wellbore/reservoir gridblocks used in transient simulator

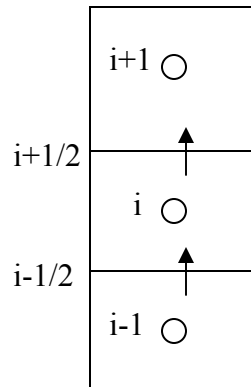


Figure 4.2 Schematic of notation used in wellbore gridblock in the coupled simulator

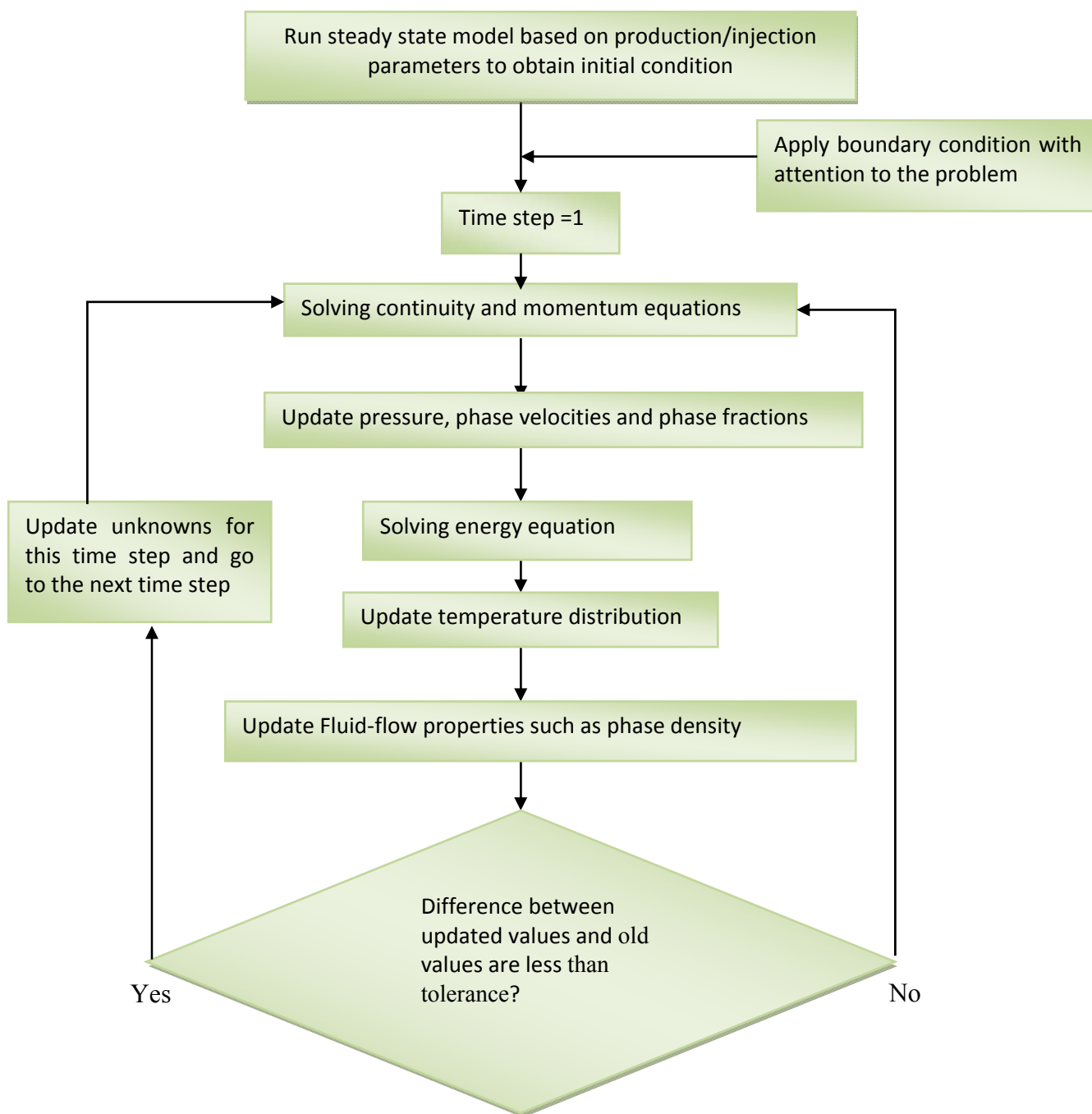


Figure 4.3 Flowchart for one time step to solve transient problems by the coupled wellbore/reservoir simulator

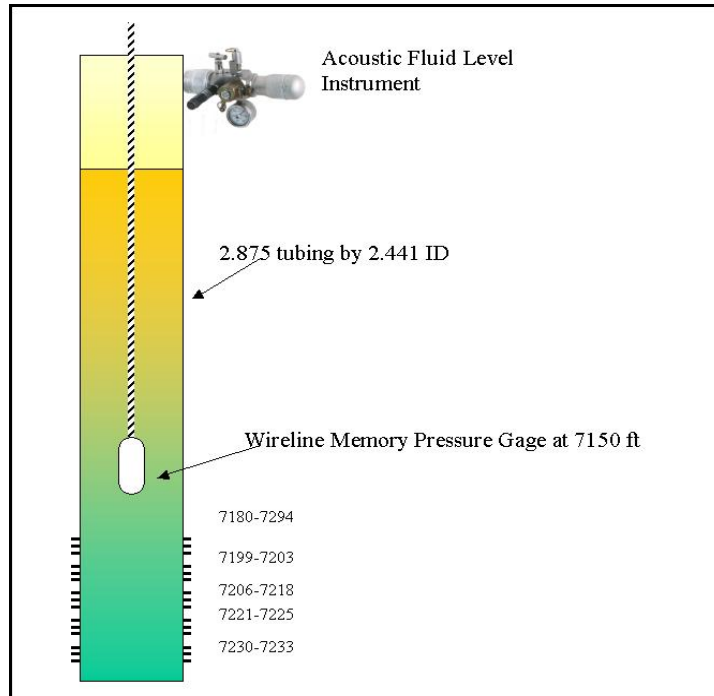


Figure 4.4 Schematic of a liquid loaded gas well where the acoustic field level measurements were undertaken (Rowaln et al., 2006)

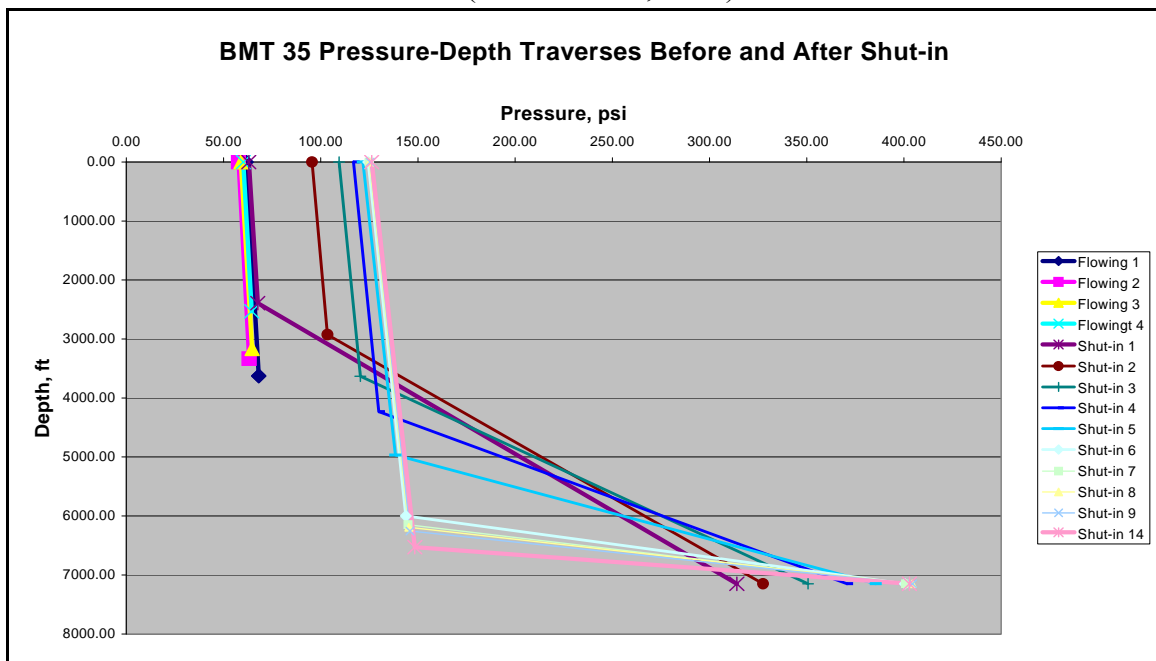


Figure 4.5 Pressure- depth traverses. Field data BHP recorded by a quartz pressure sensor. Fluid level recorded acoustically before and after shutting in a liquid loaded gas well (Rowlan et al., 2006)

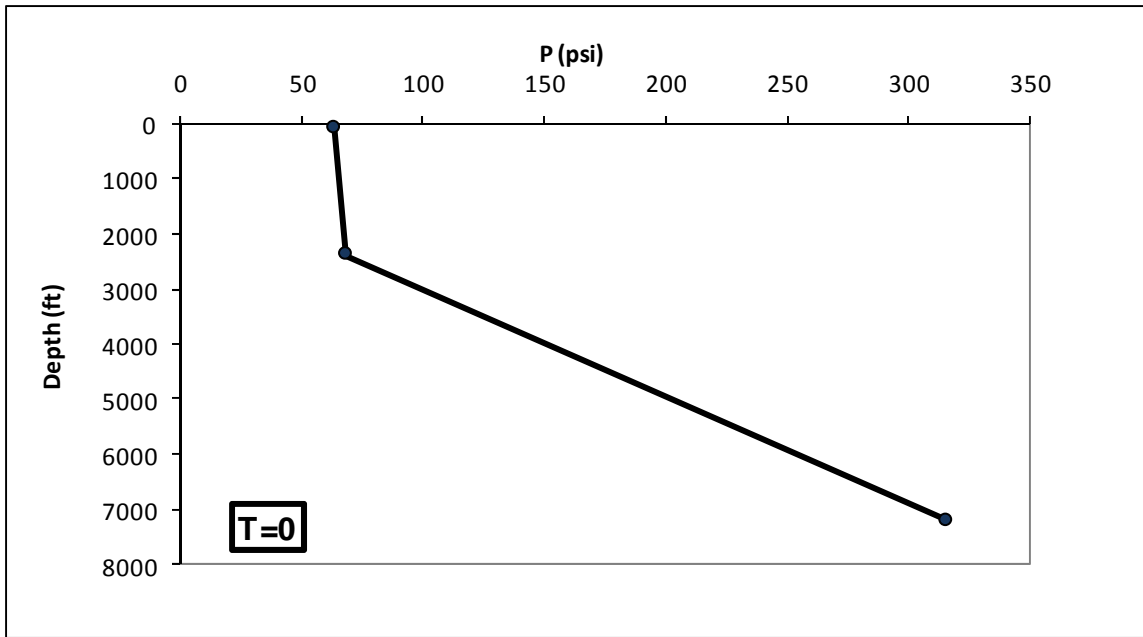


Figure 4.6.a Simulated pressure-depth traverses for a liquid loaded gas well before shut in. (The well is completed with 2-7/8 tubing and was producing gas at the time of test at an average rate of about 172 MSCF/D, (Solid line is simulated data and dots are field data)

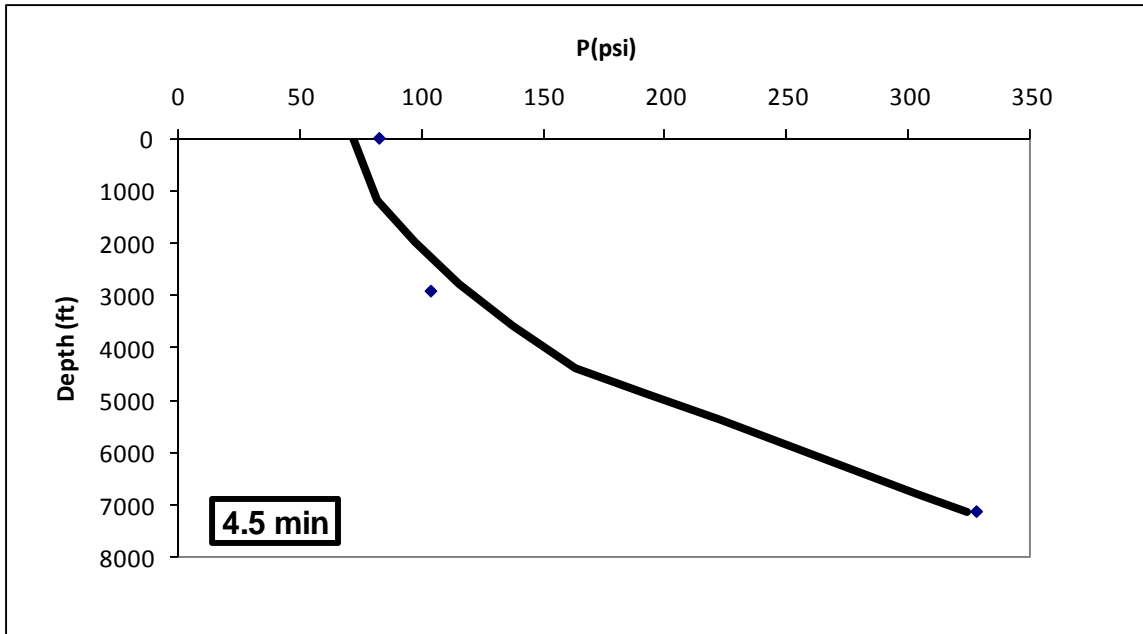


Figure 4.6.b Simulated pressure-depth traverse (solid line) and field data (dots) 4.5 min after shut in for a liquid loaded gas well with 2-7/8 tubing (Solid line is simulated data and dots are field data)

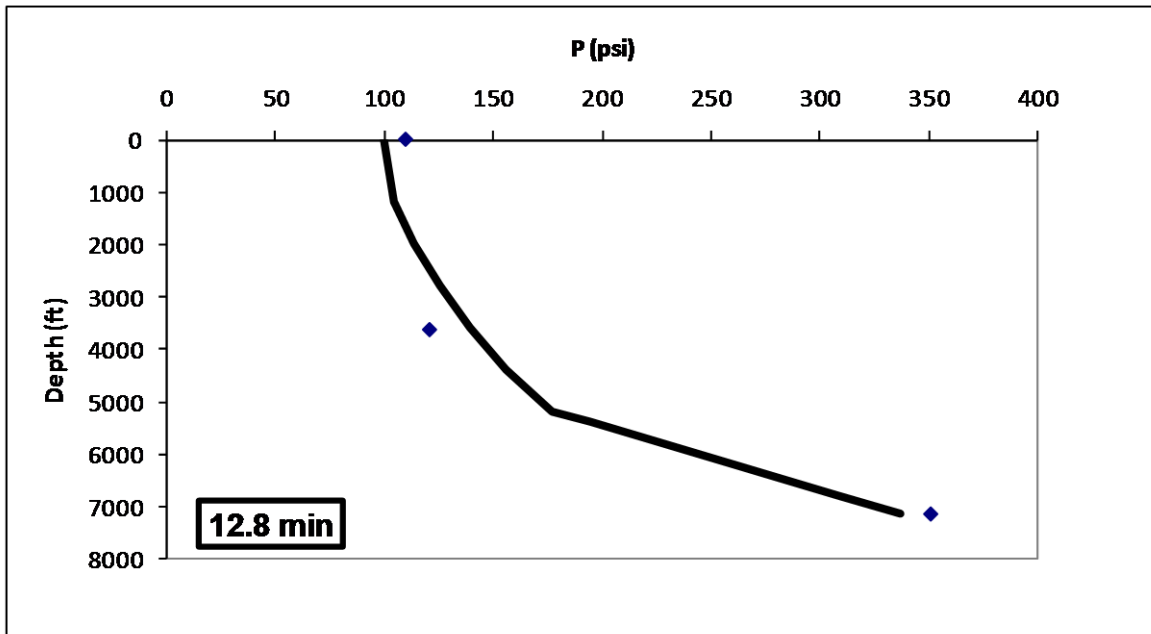


Figure 4.6.c Simulated pressure-depth traverse(solid line) and field data (dots) 12.8 min after shut in for a liquid loaded gas well with 2-7/8 tubing (Solid line is simulated data and dots are field data)

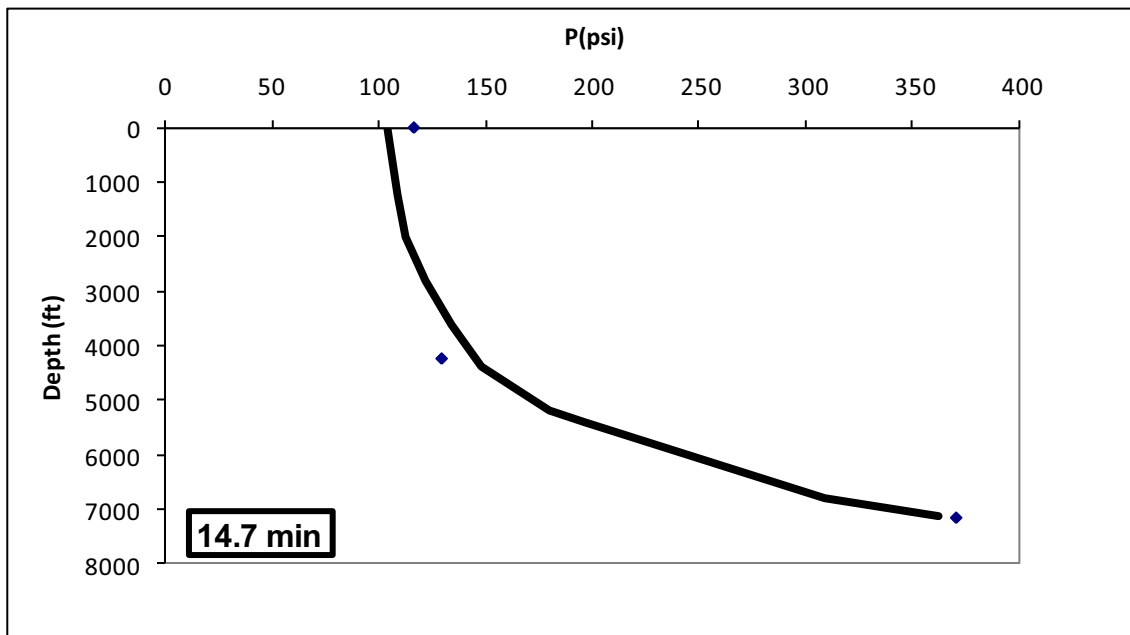


Figure 4.6.d Simulated pressure-depth traverse (solid line) and field data (dots) 14.7 min after shut in for a liquid loaded gas well with 2-7/8 tubing (Solid line is simulated data and dots are field data)

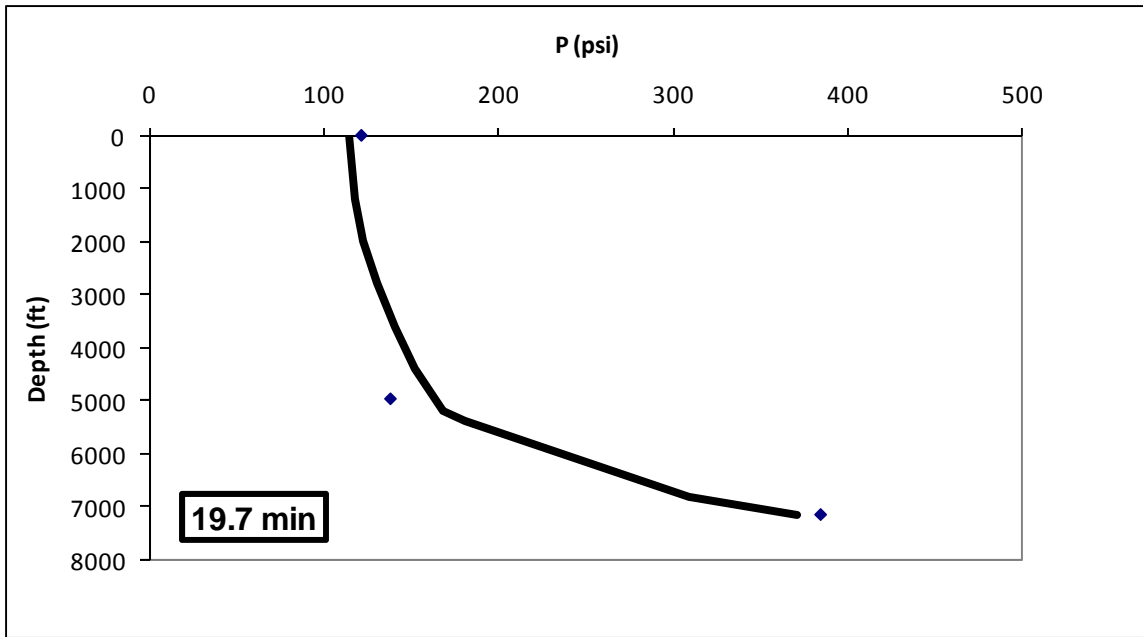


Figure 4.6.e Simulated pressure-depth traverse (solid line) and field data (dots) 19.7 min after shut in for a liquid loaded gas well with 2-7/8 tubing (Solid line is simulated data and dots are field data)

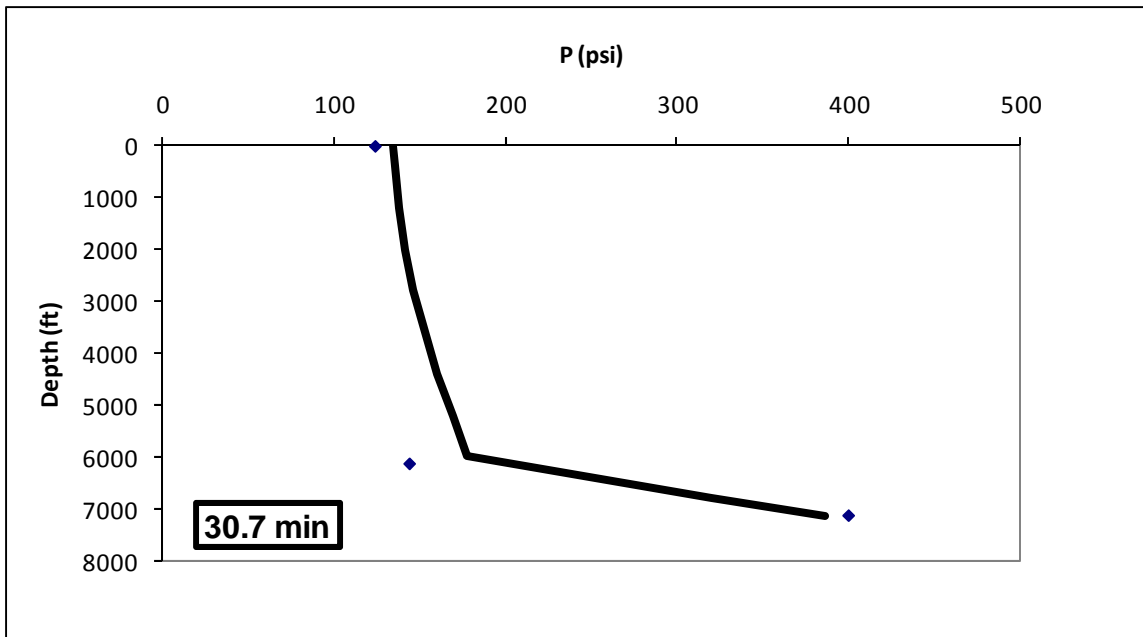


Figure 4.6.f Simulated pressure-depth traverse (solid line) and field data (dots) 30.7 min after shut in for a liquid loaded gas well with 2-7/8 tubing (Solid line is simulated data and dots are field data)

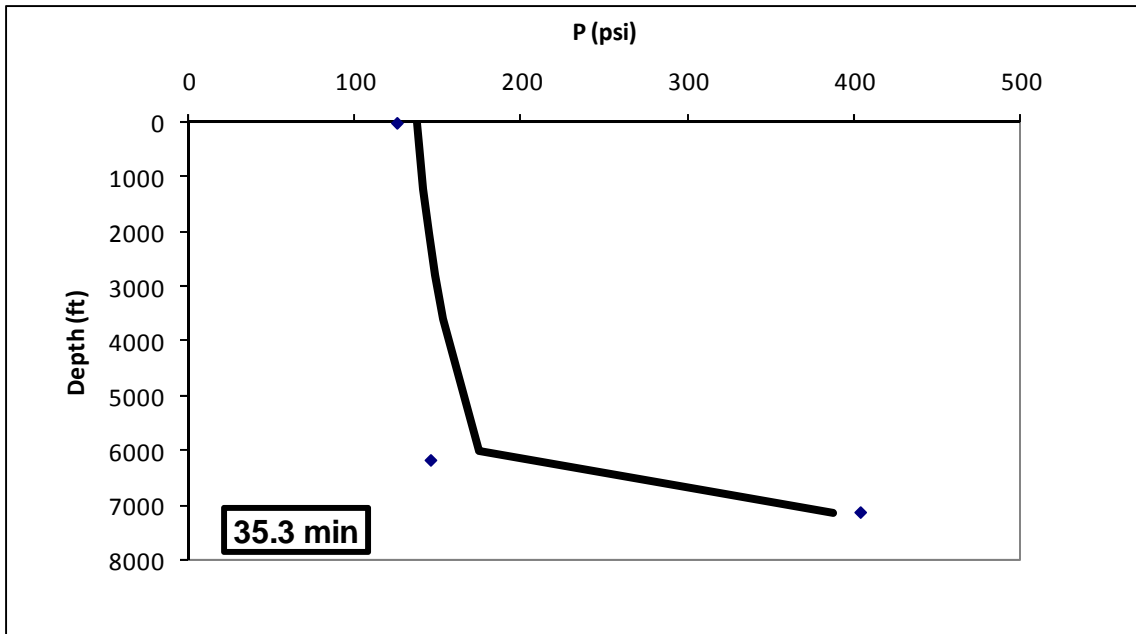


Figure 4.6.g Simulated pressure-depth traverse (solid line) and field data (dots) 35.3 min after shut in for a liquid loaded gas well with 2-7/8 tubing (Solid line is simulated data and dots are field data)

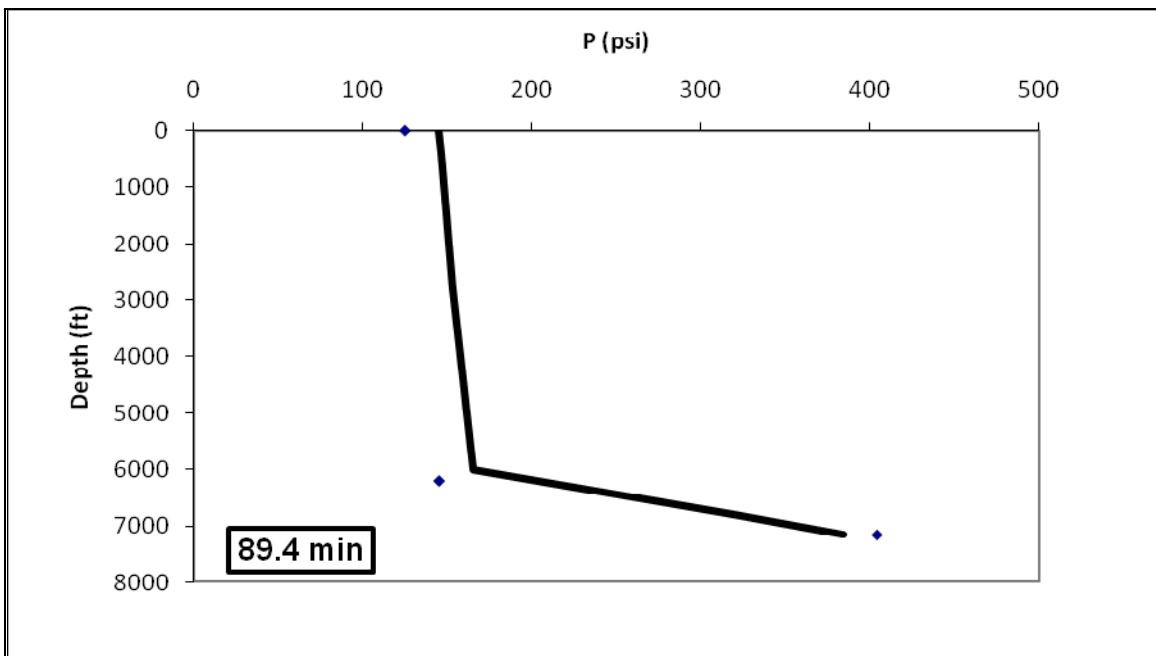


Figure 4.6.h Simulated pressure-depth traverse (solid line) and field data (dots) 89.4 min after shut in for a liquid loaded gas well with 2-7/8 tubing (Solid line is simulated data and dots are field data)

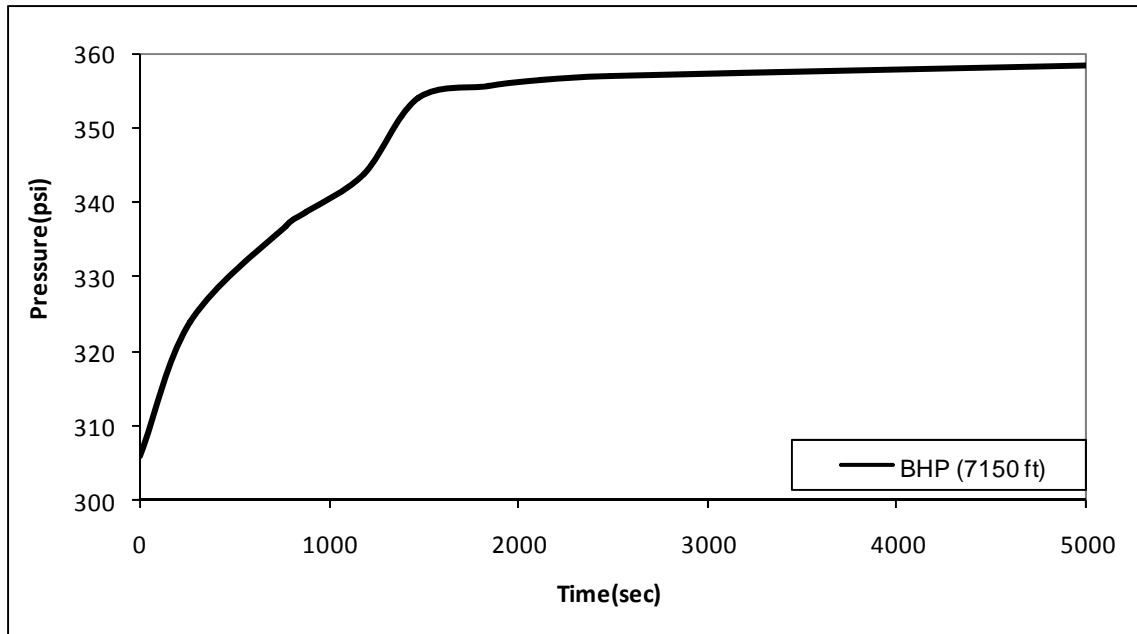


Figure 4.7 Simulated bottomhole pressure buildup during shut in test for a liquid loaded gas well (The well is completed with 2-7/8 tubing and was producing gas at an average rate of about 172 MSCF/D before shut in)

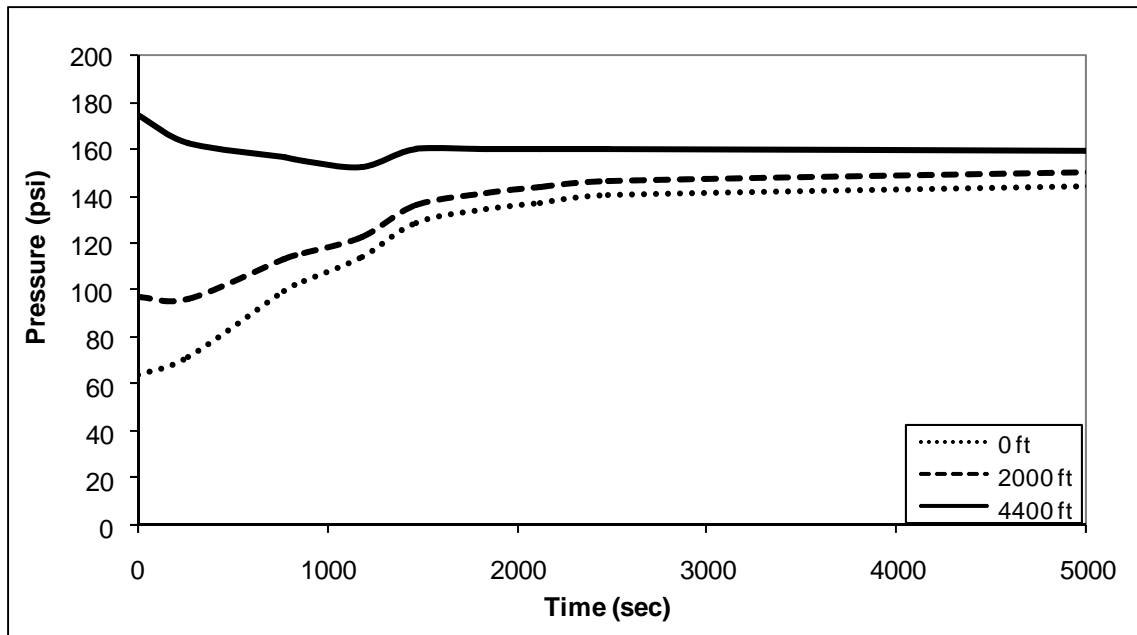


Figure 4.8 Simulated transient pressure at different locations in the wellbore during shut in test for a liquid loaded gas well (The well is completed with 2-7/8 tubing and was producing gas at an average rate of about 172 MSCF/D before shut in)

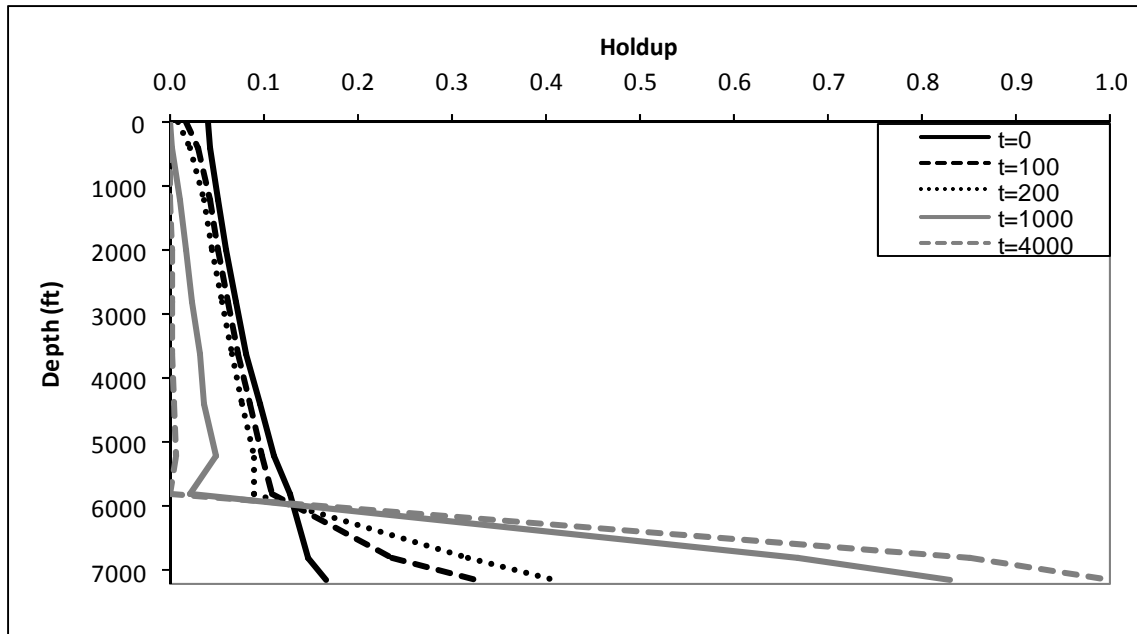


Figure 4.9 Simulated transient holdup profiles during shut in for a liquid loaded gas well (The well is completed with 2-7/8 tubing and was producing gas at an average rate of about 172 MSCF/D before shut in)

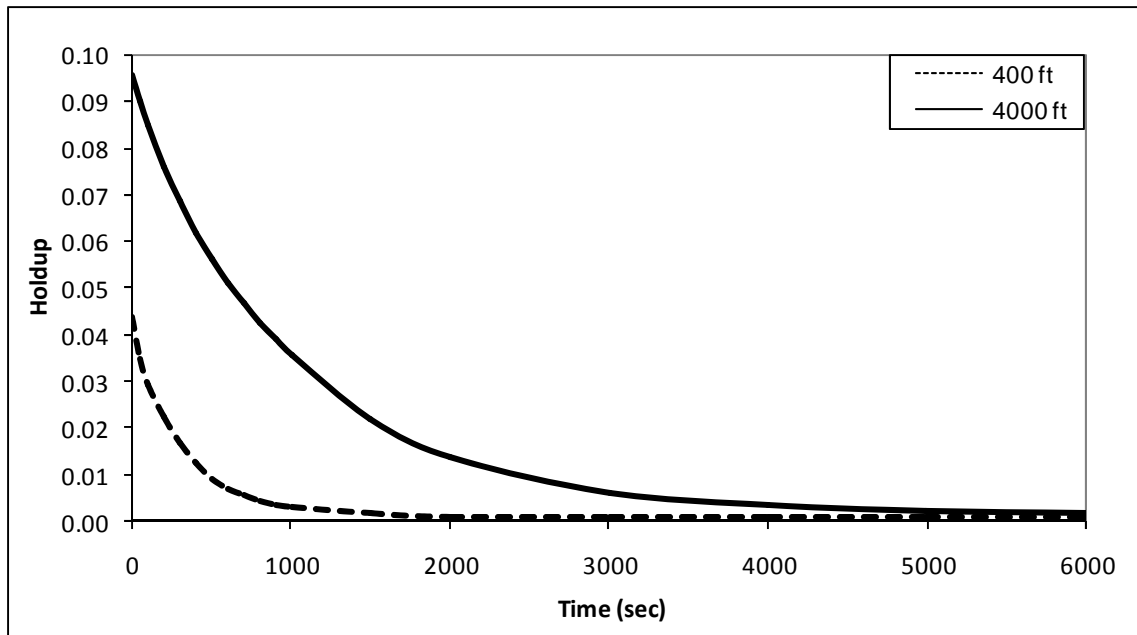


Figure 4.10 Simulated transient holdup profiles at the upper sections of the wellbore during shut in for a liquid loaded gas well (The well is completed with 2-7/8 tubing and was producing gas at an average rate of about 172 MSCF/D before shut in)

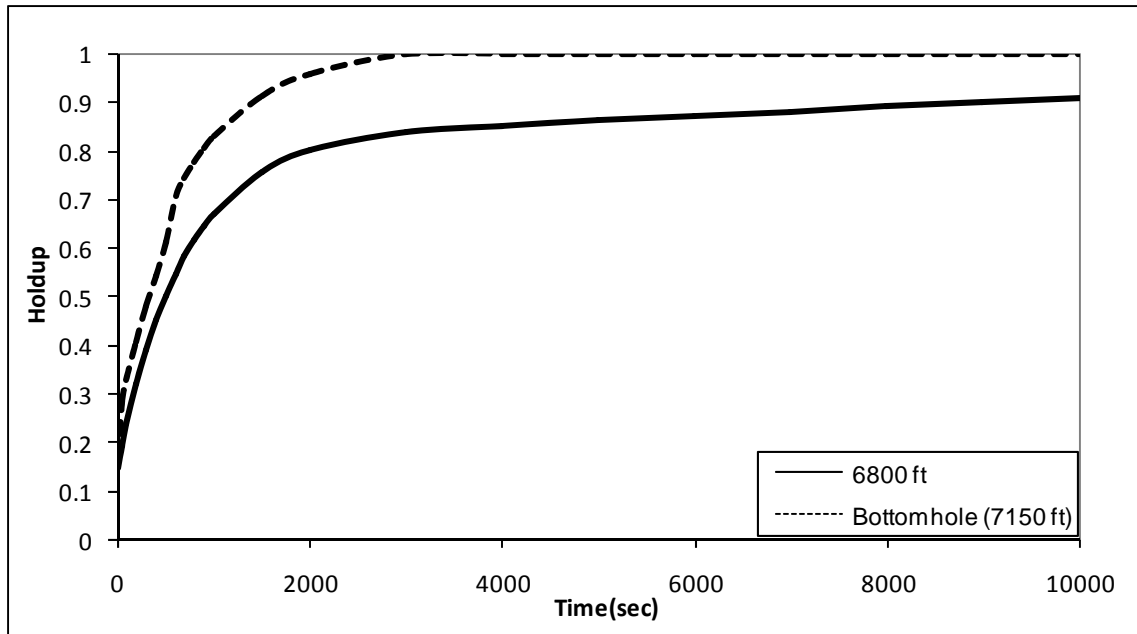


Figure 4.11 Simulated transient holdup profiles at the lower sections of the wellbore during shut in for a liquid loaded gas well (The well is completed with 2-7/8 tubing and was producing gas at an average rate of about 172 MSCF/D before shut in)

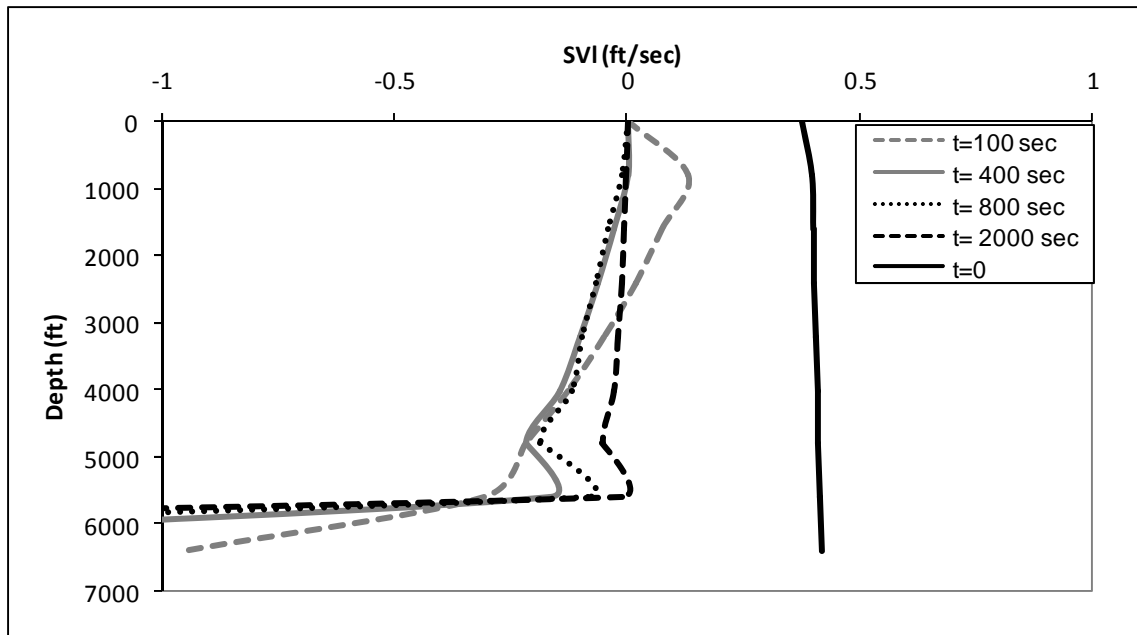


Figure 4.12 Simulated transient superficial velocity profiles in the wellbore during a shut in test for a liquid loaded gas well (The well is completed with 2-7/8 tubing and was producing gas at an average rate of about 172 MSCF/D before shut in)

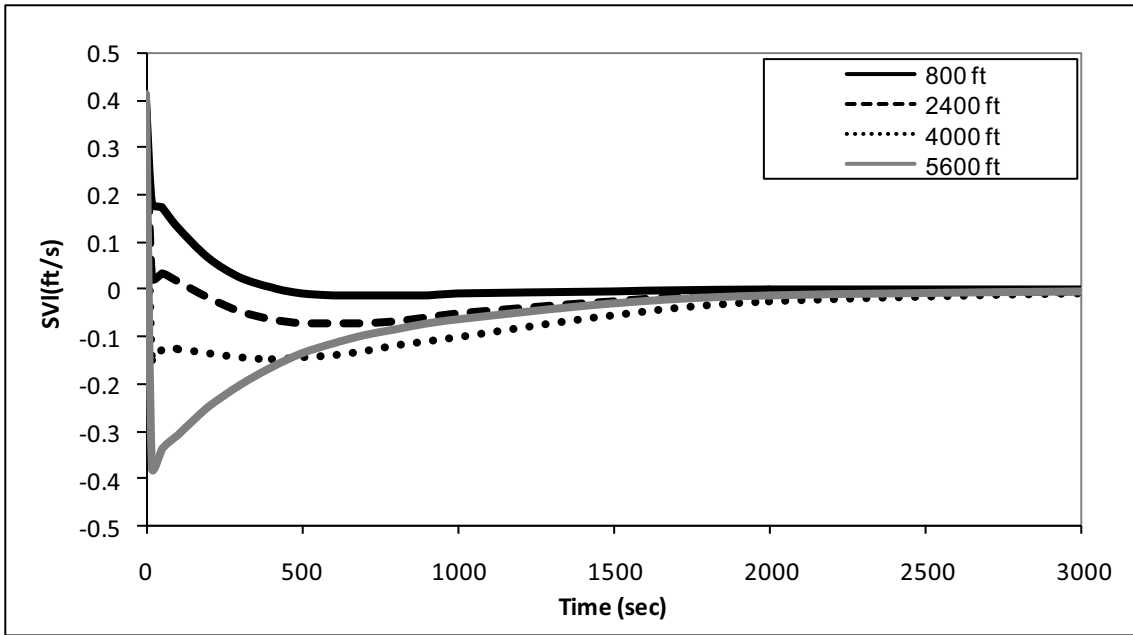


Figure 4.13 Simulated transient superficial velocity at different sections of the wellbore during shut in for a liquid loaded gas well (The well is completed with 2-7/8 tubing and was producing gas at an average rate of about 172 MSCF/D before shut in)

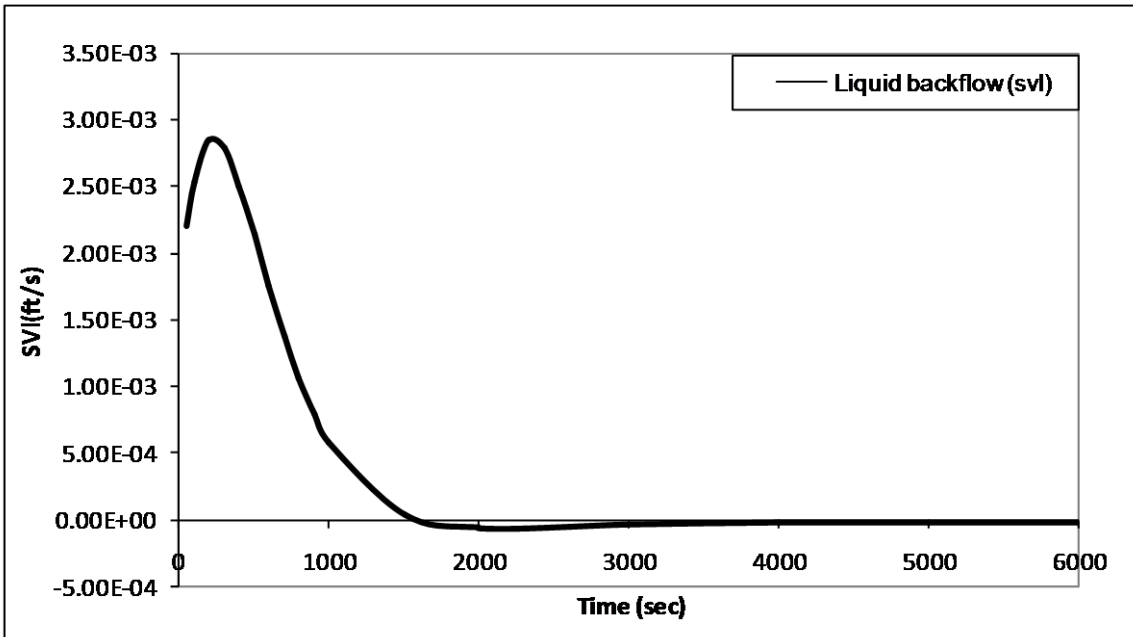


Figure 4.14 Simulated transient liquid backflow from the wellbore to reservoir during a shut in test for a liquid loaded gas well (The well is completed with 2-7/8 tubing and was producing gas at an average rate of about 172 MSCF/D before shut in)

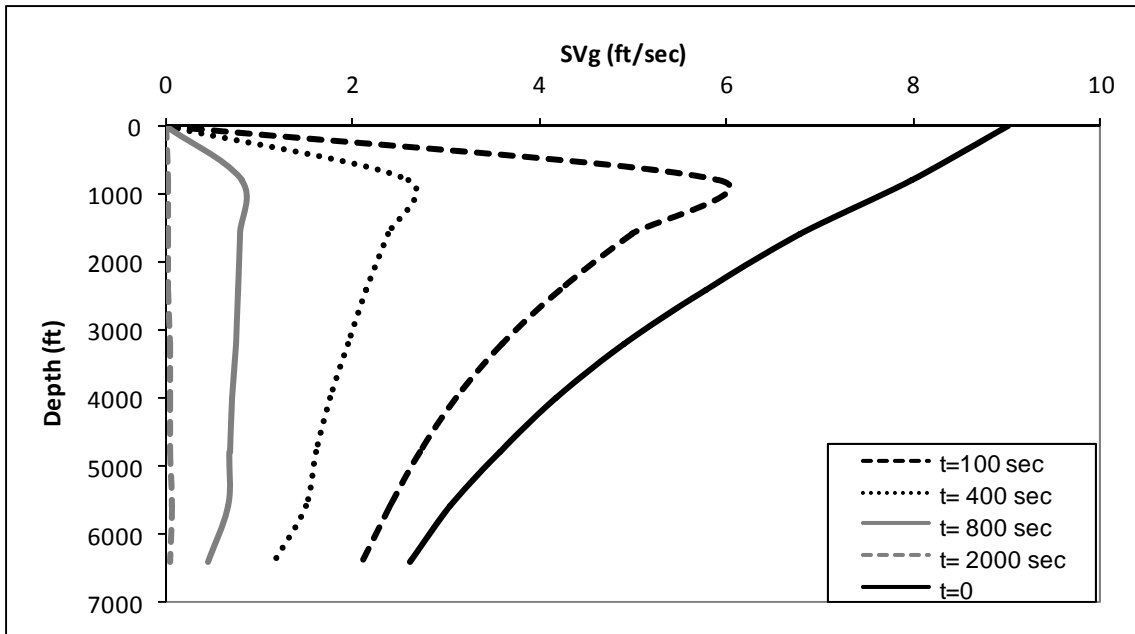


Figure 4.15 Simulated transient gas superficial velocity profiles in the wellbore during a shut in test for a liquid loaded gas well (The well is completed with 2-7/8 tubing and was producing gas at an average rate of about 172 MSCF/D before shut in)

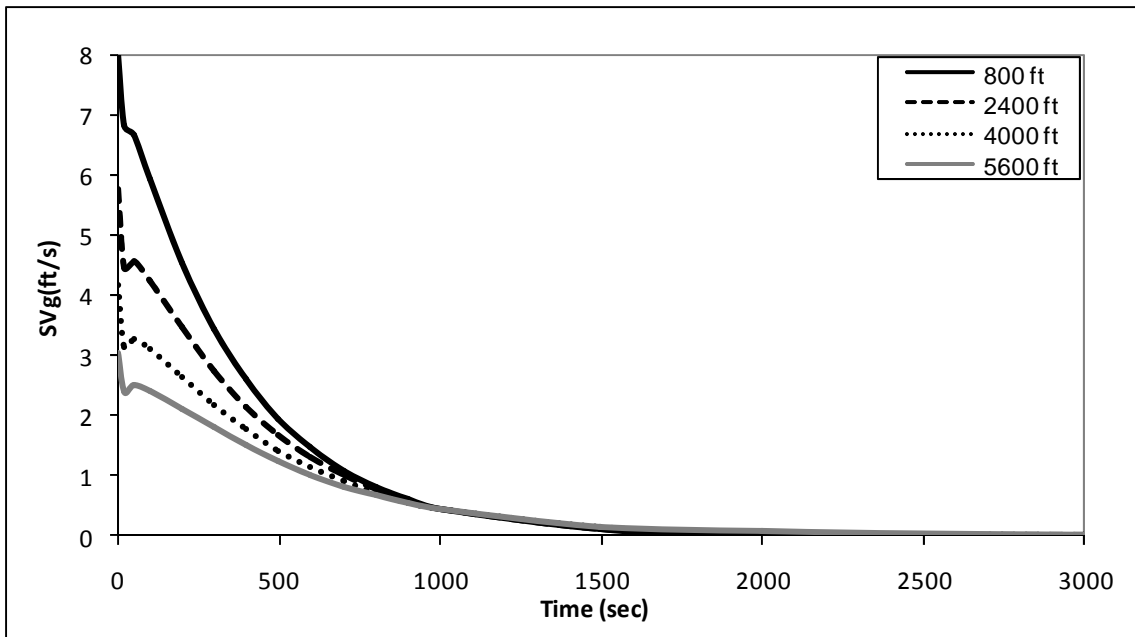


Figure 4.16 Transient gas superficial velocity at different sections of the well during shut in for a liquid loaded gas well (The well is completed with 2-7/8 tubing and was producing gas at an average rate of about 172 MSCF/D before shut in)

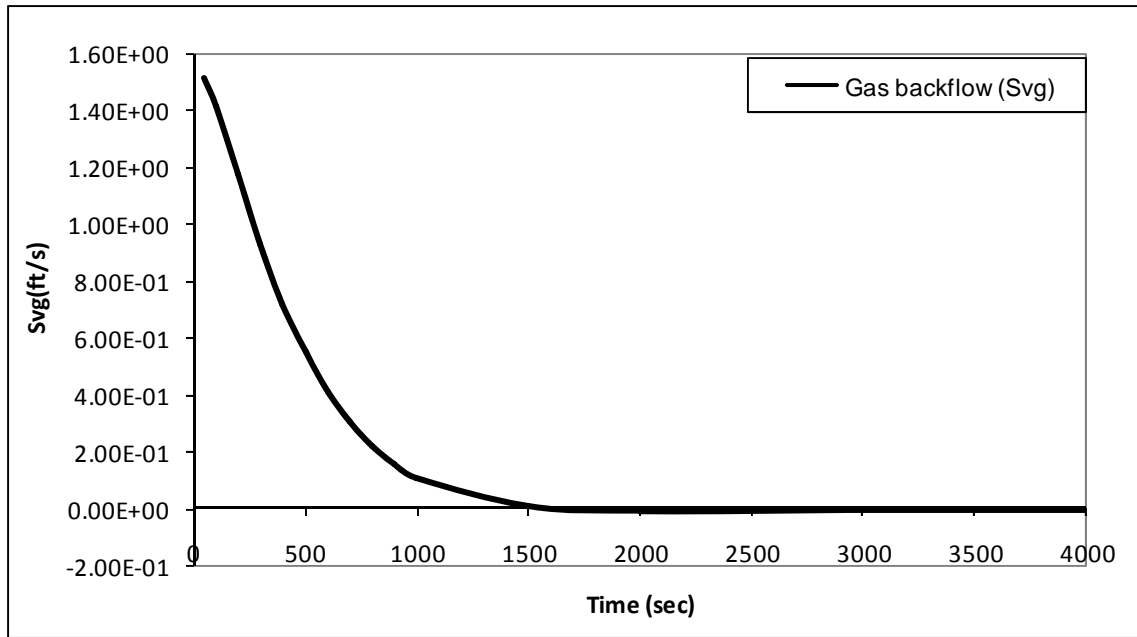


Figure 4.17 Simulated transient gas backflow during a shut in test for a liquid loaded gas well (The well is completed with 2-7/8 tubing and was producing gas at an average rate of about 172 MSCF/D before shut in)

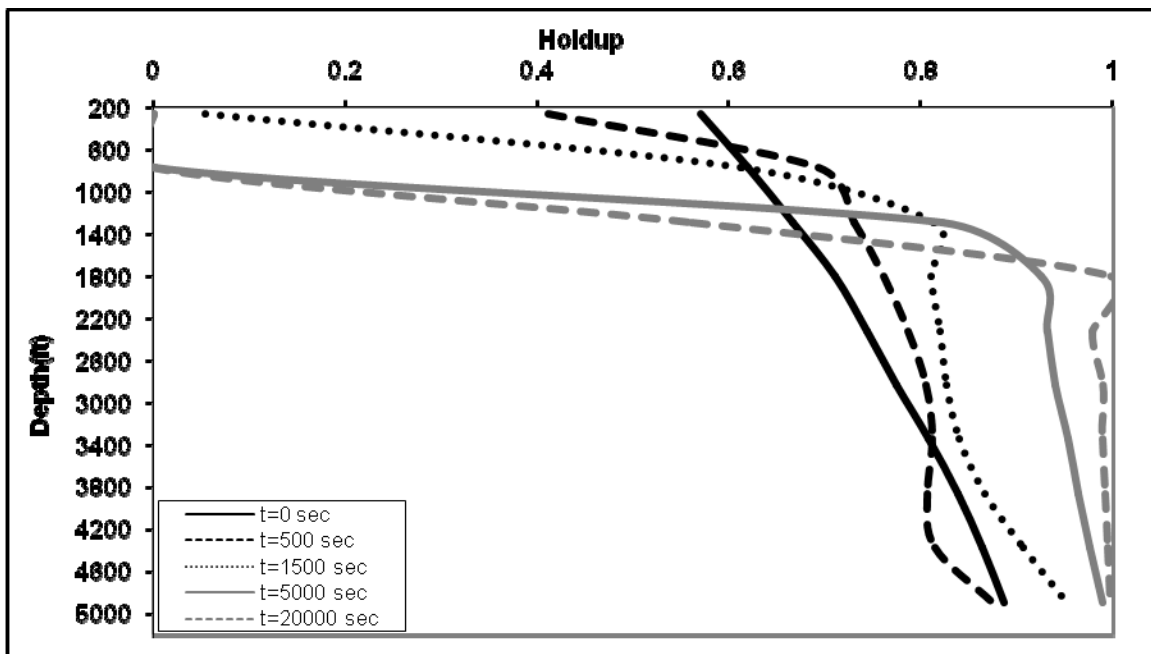


Figure 4.18 Simulated transient liquid holdup in the wellbore during a shut in test for a 5151 ft well with 0.125 ft tubing diameter which was producing 1140 STB/D oil and 513 Mscf/D gas before shut in

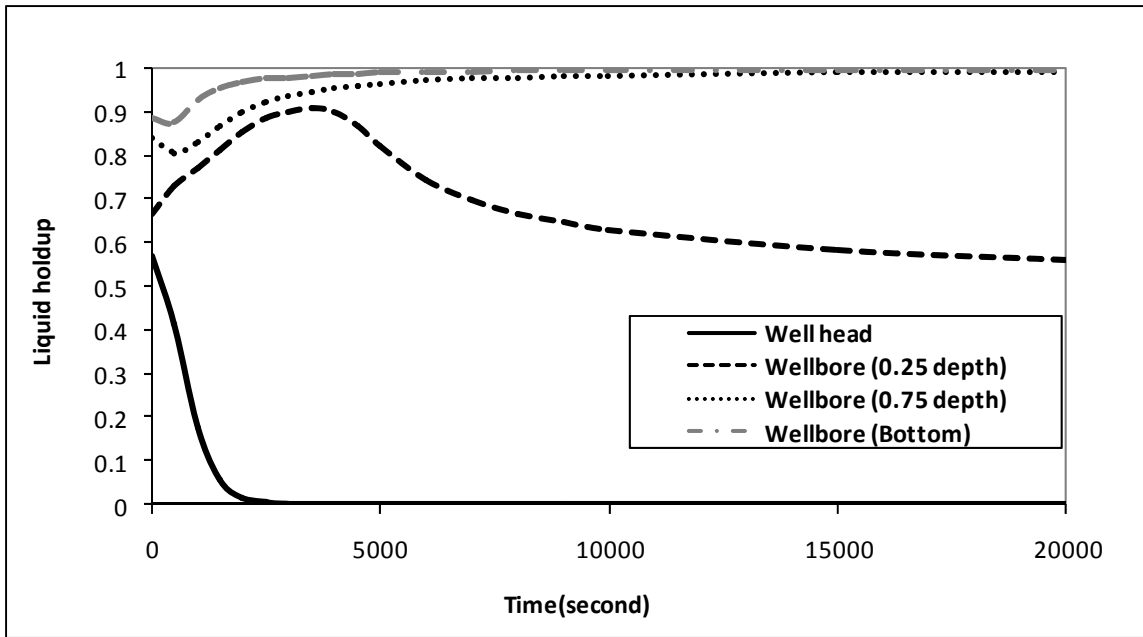


Figure 4.19 Simulated transient liquid holdup at different well depth during a shut in test for a 5151 ft well with 0.125 ft tubing diameter which was producing 1140 STB/D oil and 513 Mscf/D gas before shut in

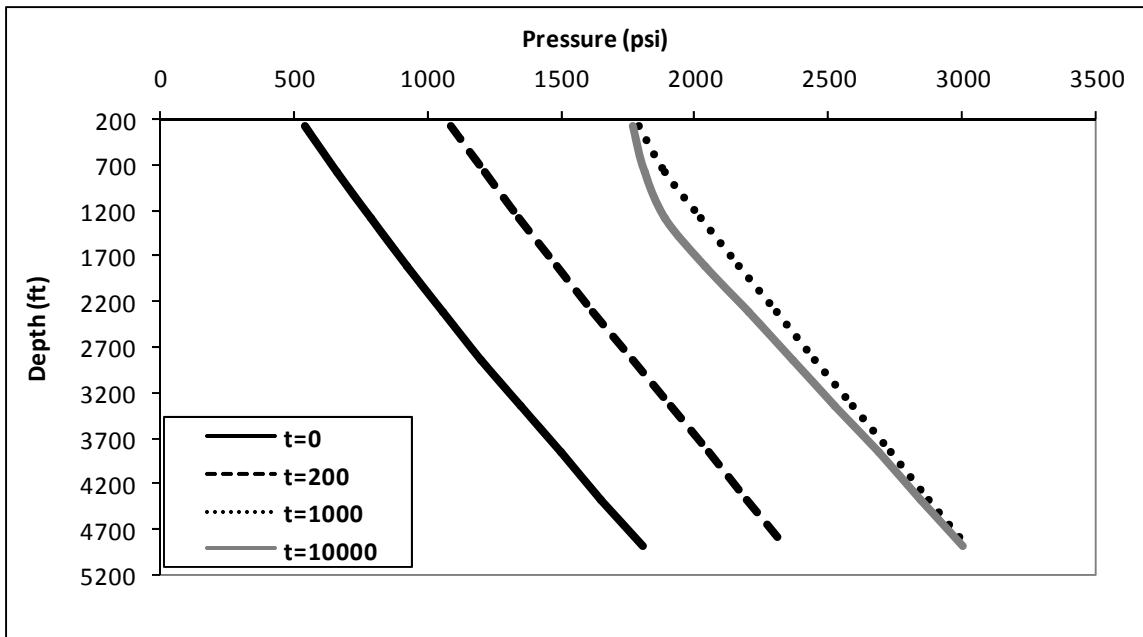


Figure 4.20 Simulated transient simulated pressure profiles during a shut in test for a 5151 ft well with 0.125 ft tubing diameter which was producing 1140 STB/D oil and 513 Mscf/D gas before shut in

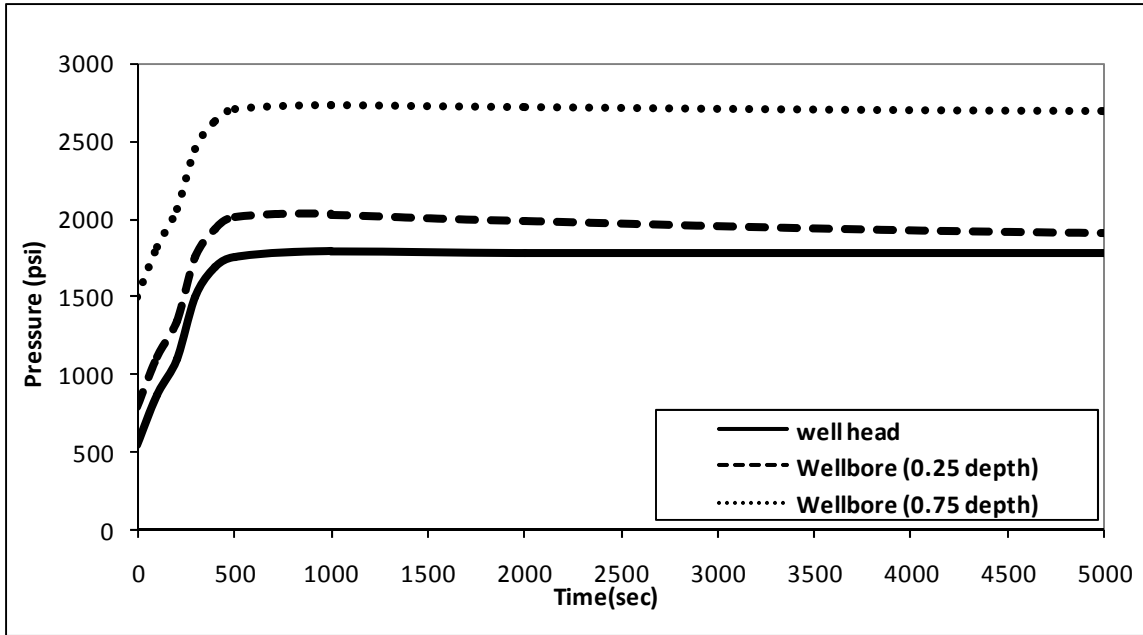


Figure 4.21 Simulated transient pressure history profiles in different well depth during a shut in test for a 5151 ft well with 0.125 ft tubing diameter which was producing 1140 STB/D oil and 513 Mscf/D gas before shut in

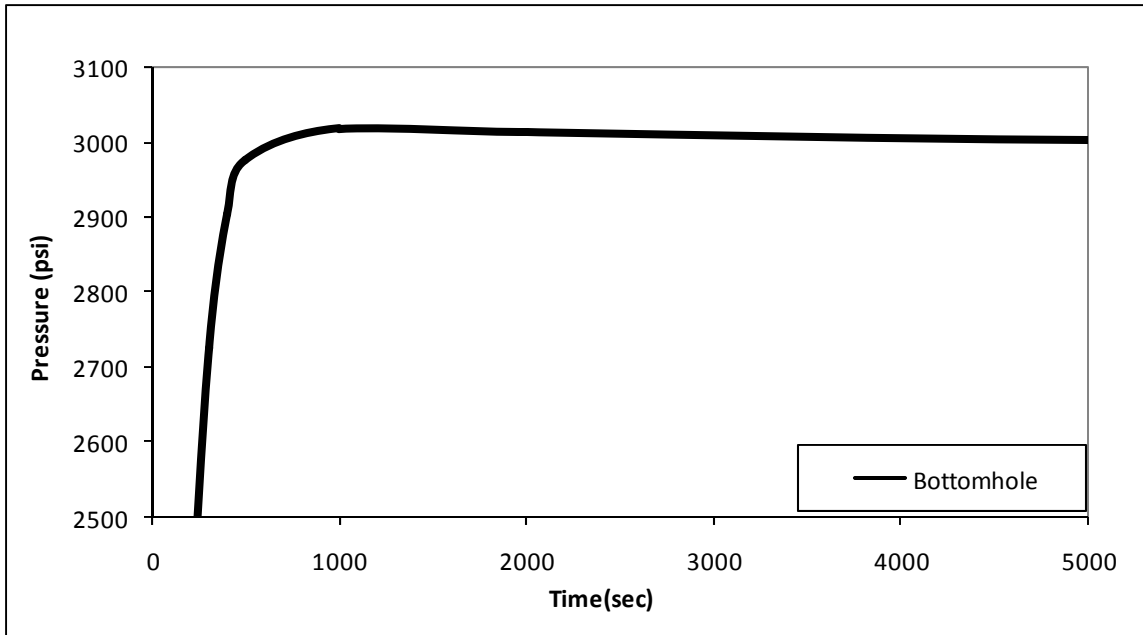


Figure 4.22 Simulated transient bottomhole pressure during a shut in test for a 5151 ft well with 0.125 ft tubing diameter which was producing 1140 STB/D oil and 513 Mscf/D gas before shut in

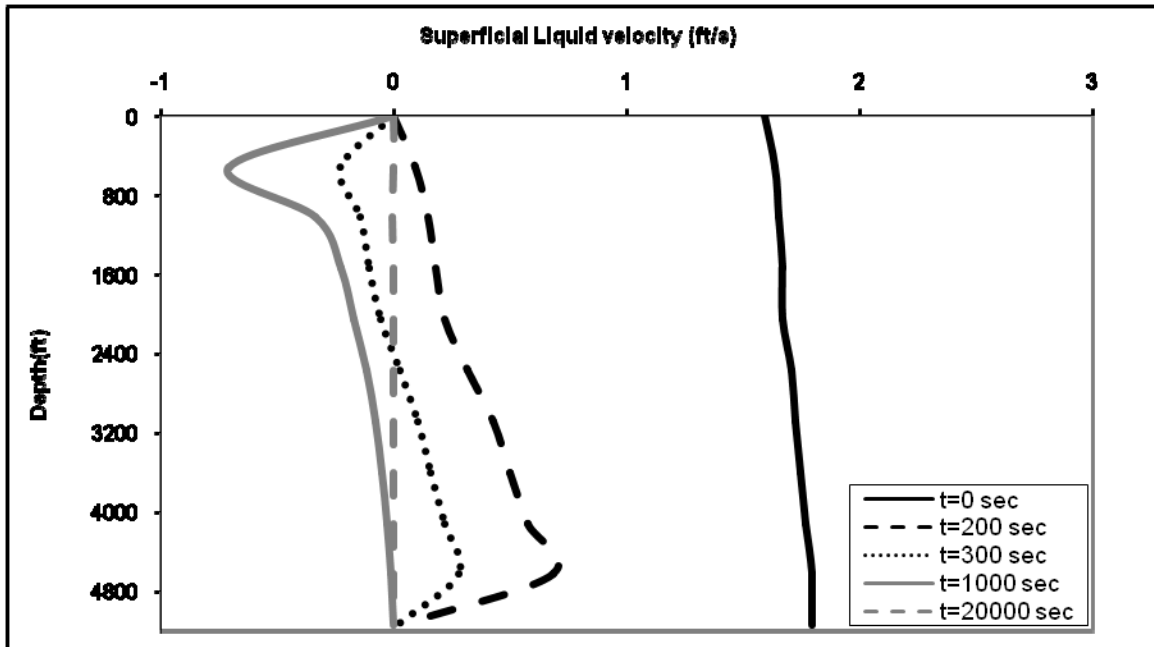


Figure 4.23 Simulated transient liquid superficial velocity profiles in wellbore during a shut in test for a 5151 ft well with 0.125 ft tubing diameter which was producing 1140 STB/D oil and 513 Mscf/D gas before shut in

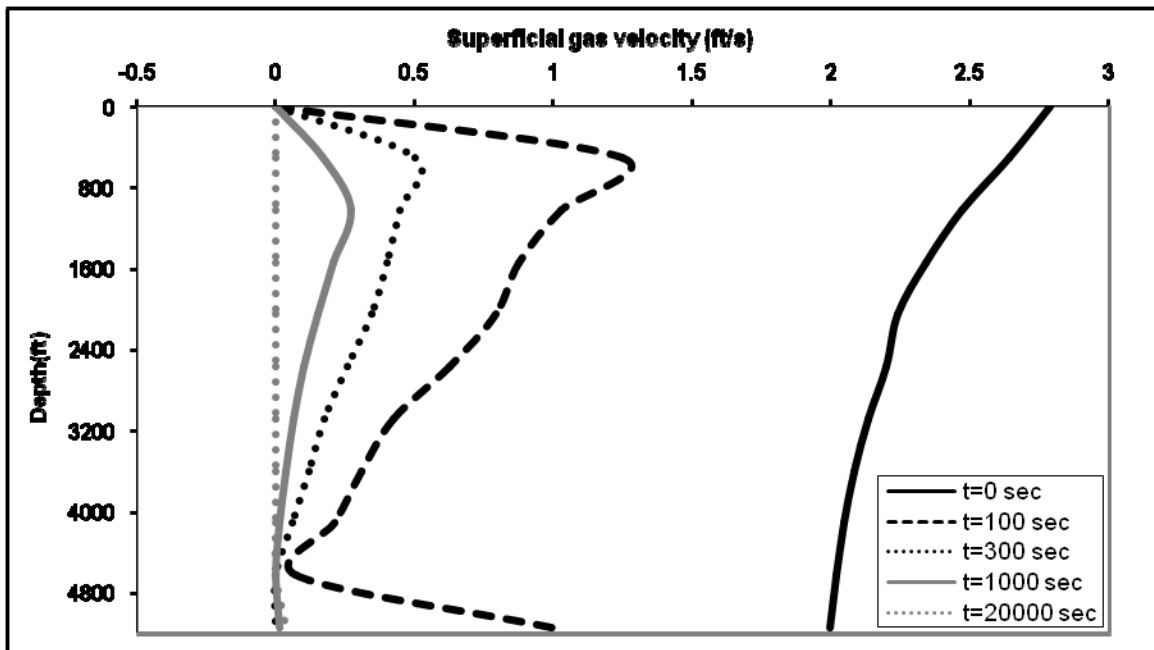


Figure 4.24 Simulated transient gas superficial velocity profiles in wellbore during a shut in test for a 5151 ft well with 0.125 ft tubing diameter which was producing 1140 STB/D oil and 513 Mscf/D gas before shut in

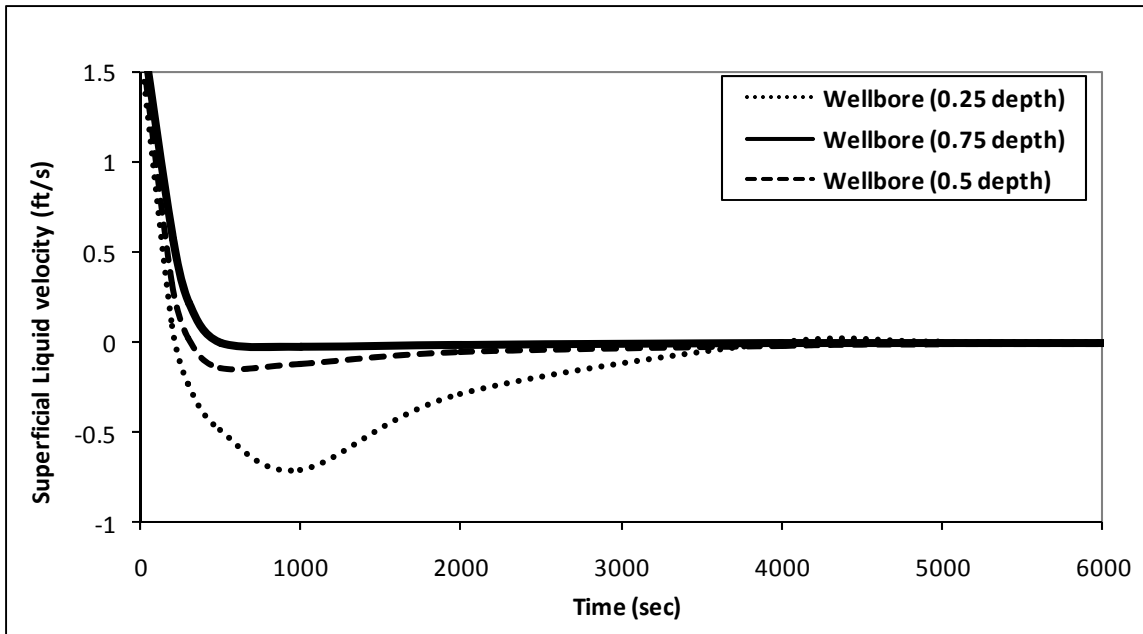


Figure 4.25 Simulated transient superficial liquid velocity history profiles in different well depth during a shut in test for a 5151 ft well with 0.125 ft tubing diameter which was producing 1140 STB/D oil and 513 Mscf/D gas before shut in

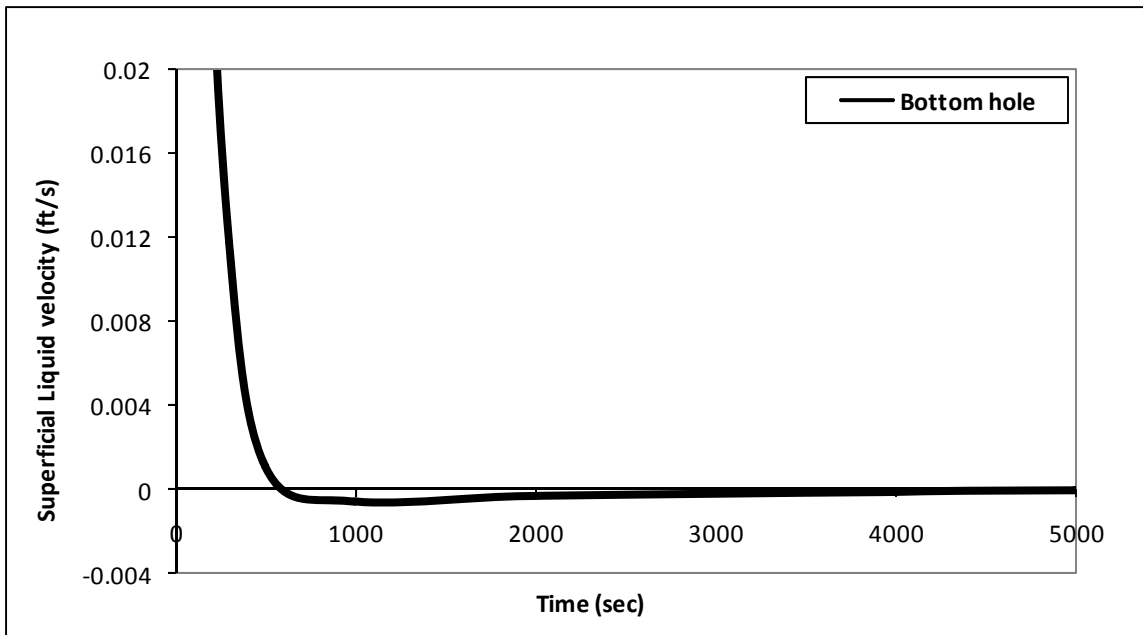


Figure 4.26 Simulated transient liquid afterflow history profile between reservoir and wellbore during a shut in test for a 5151 ft well with 0.125 ft tubing diameter which was producing 1140 STB/D oil and 513 Mscf/D gas before shut in

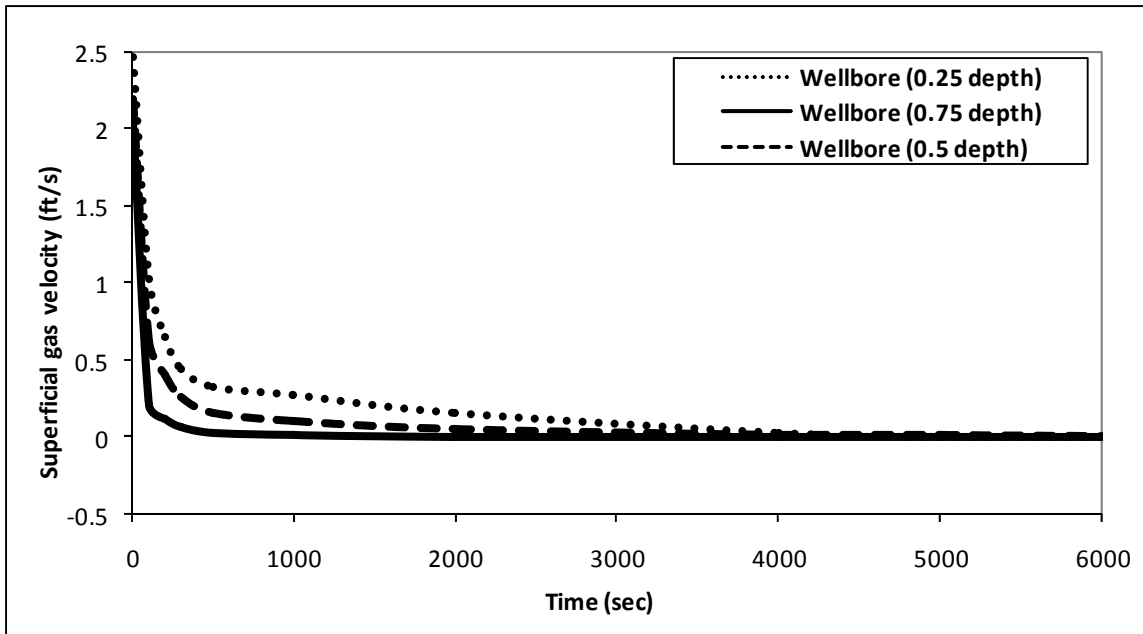


Figure 4.27 Simulated transient gas superficial velocity history profile at different well depth during a synthetic shut in test for a 5151 ft well with 0.125 ft tubing diameter which was producing 1140 STB/D oil and 513 Mscf/D gas before shut in

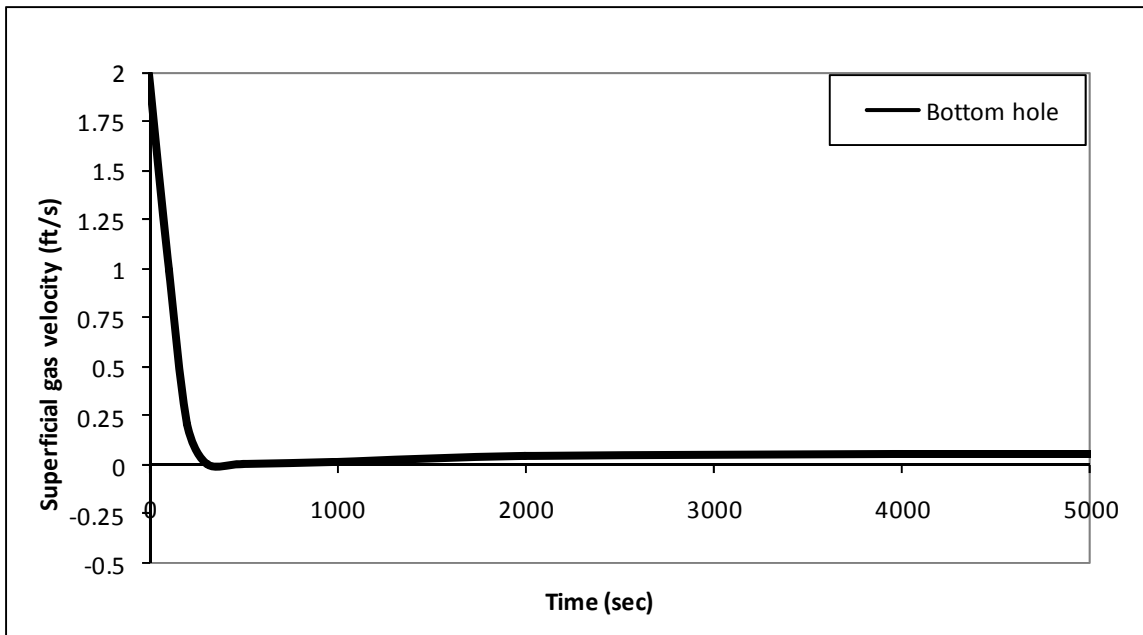


Figure 4.28 Simulated transient gas afterflow history profile between reservoir and wellbore during a shut in test for a 5151 ft well with 0.125 ft tubing diameter which was producing 1140 STB/D oil and 513 Mscf/D gas before shut in

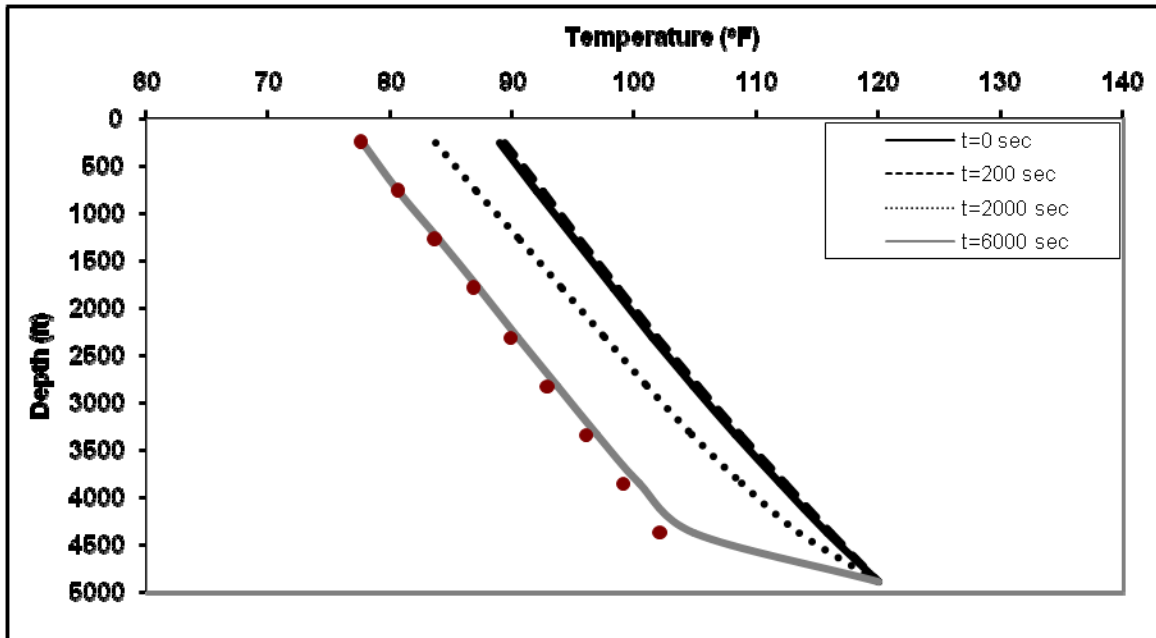


Figure 4.29 Simulated transient temperature distribution profiles during a shut in test for a 5151 ft well with 0.125 ft tubing diameter which was producing 1140 STB/D oil and 513 Mscf/D gas before shut in. The surface temperature is 76 °F and reservoir temperature is 120 °F

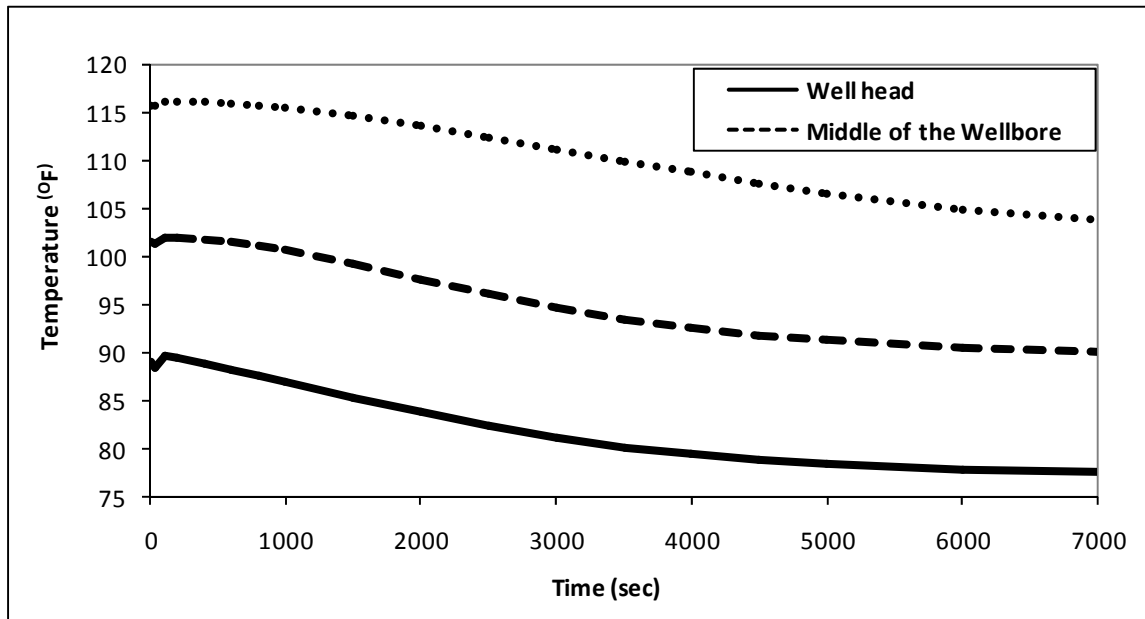


Figure 4.30 Simulated transient temperature distribution in different well depth during a shut in test for a 5151 ft well with 0.125 ft tubing diameter which was producing 1140 STB/D oil and 513 Mscf/D gas before shut in, the surface temperature is 76 °F and reservoir temperature is 120 °F

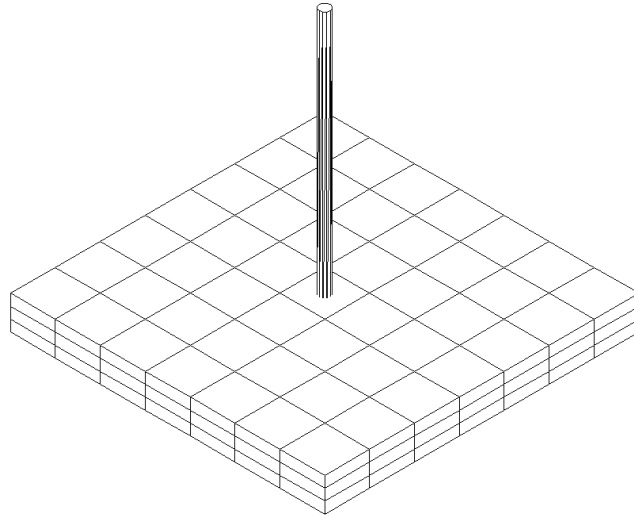


Figure 4.31 Schematic of a wellbore/reservoir system nodes, wellbore consists of 20 nodes in the vertical direction and $560 \times 560 \times 100$ hydrocarbon reservoir has 7 by 7 by 3 nodes

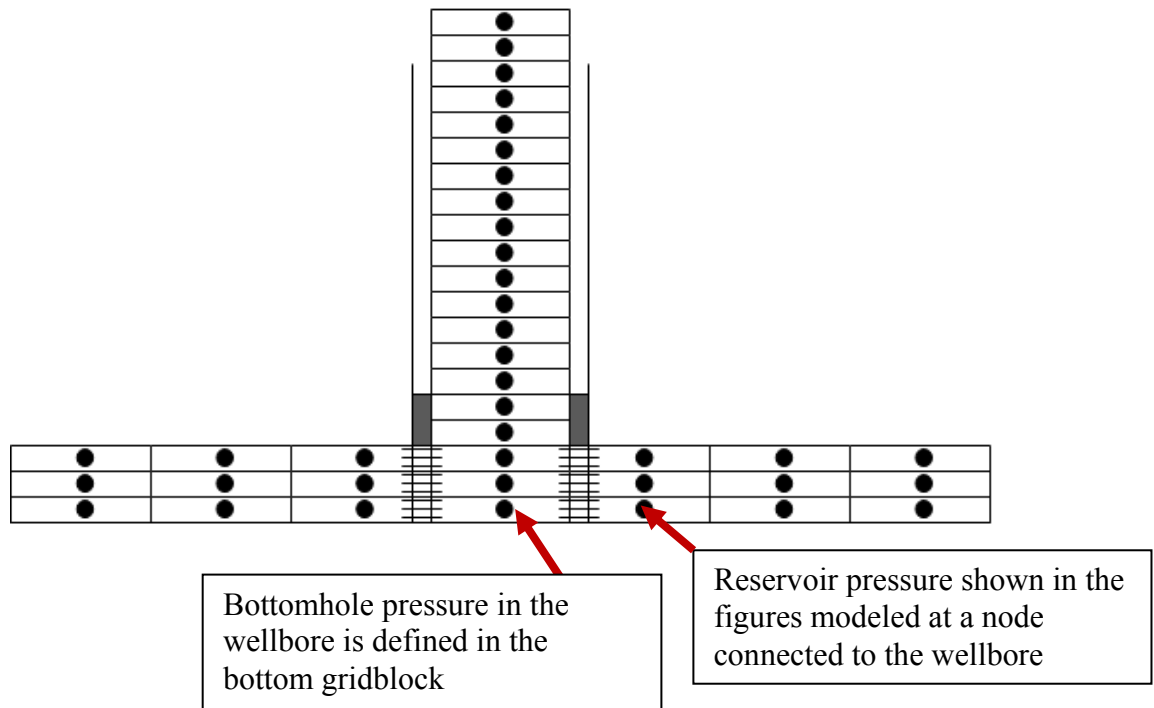


Figure 4.32 Schematic of pressure definition for wellbore and reservoir nodes to use in well model

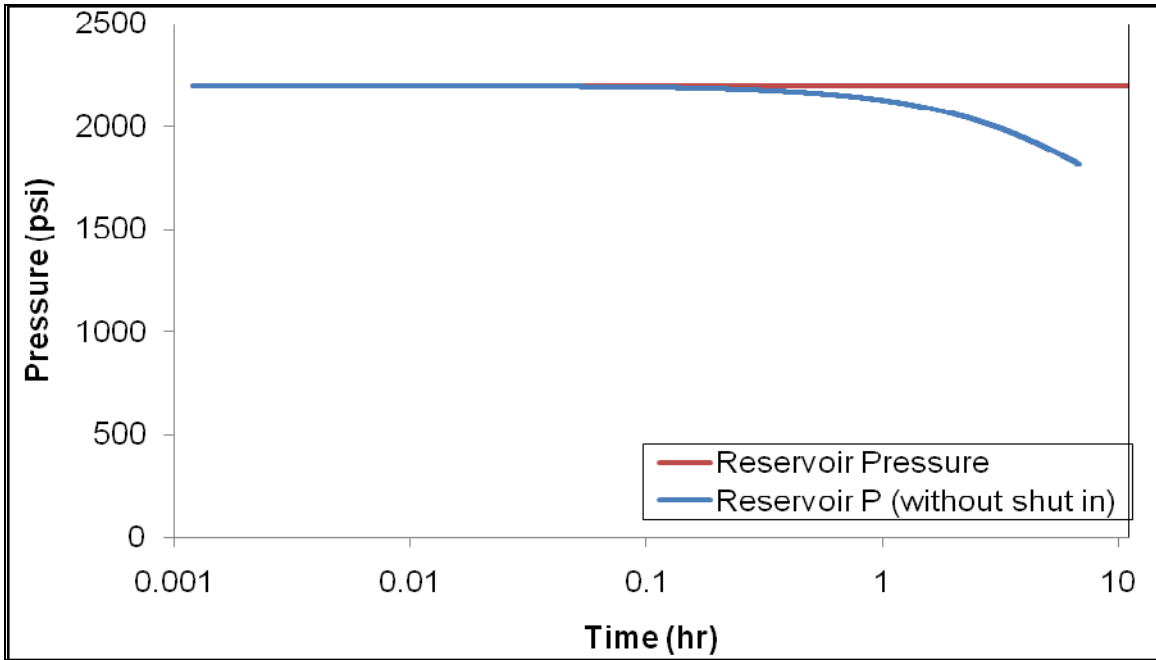


Figure 4.33 Simulation of the effect of shutting in the well at the top of the wellbore on reservoir pressure, the initial reservoir pressure is 2200 psi, and initial produced hydrocarbon composition is 0.57 C1, 0.09 C3, 0.01 C6, 0.01 C10, 0.21 C15 and 0.11 C20

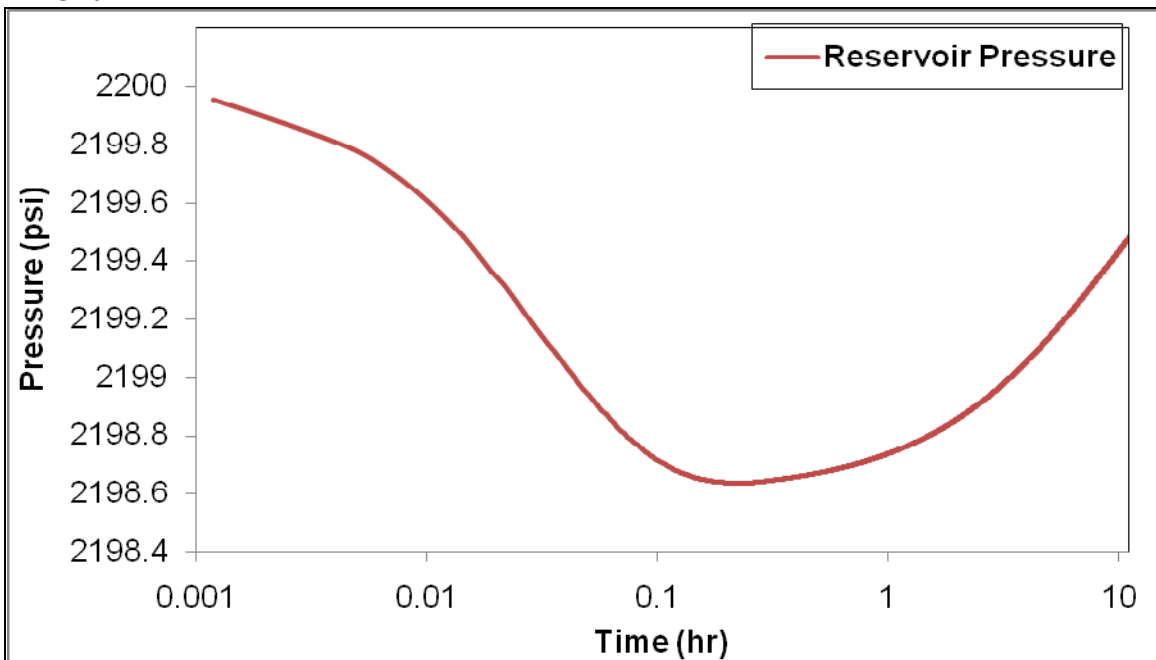


Figure 4.34 Simulated reservoir pressure near the wellbore during buildup test, the initial reservoir pressure is 2200 psi, and initial produced hydrocarbon composition before shut in consists of 0.57 C1, 0.09 C3, 0.01 C6, 0.01 C10, 0.21 C15 and 0.11 C20

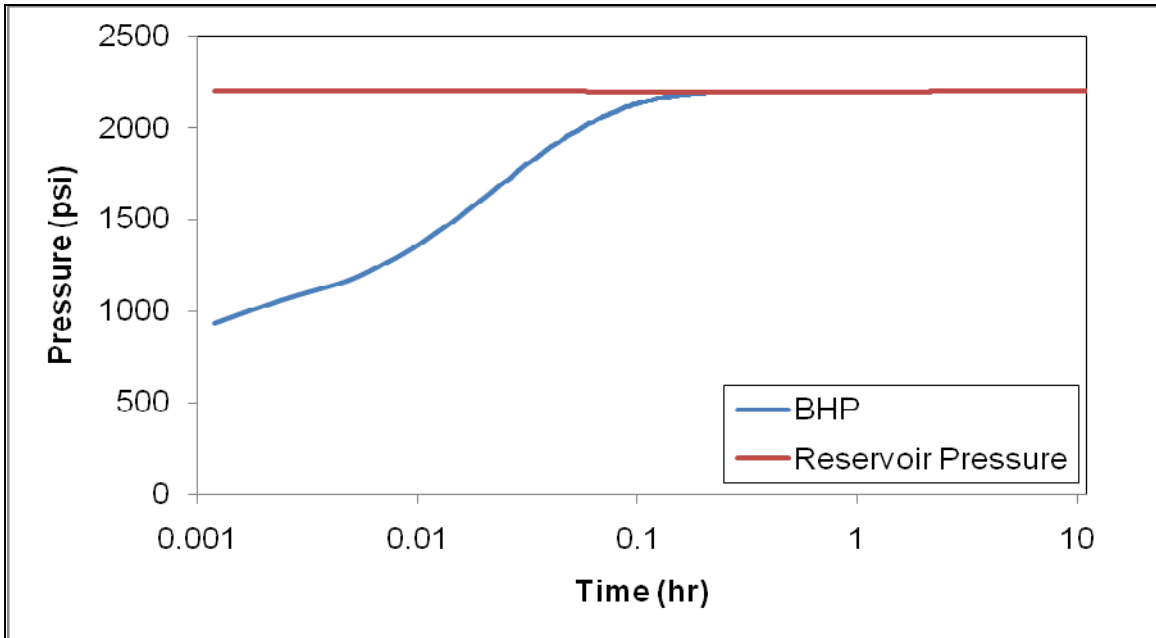


Figure 4.35 Simulated reservoir pressure and wellbore bottomhole pressure during buildup test for a 5300 ft wellbore with 0.165 ft tubing diameter, the initial reservoir pressure is 2200 psi, and initial produced hydrocarbon composition is 0.57 C1, 0.09 C3, 0.01 C6, 0.01 C10, 0.21 C15 and 0.11 C20

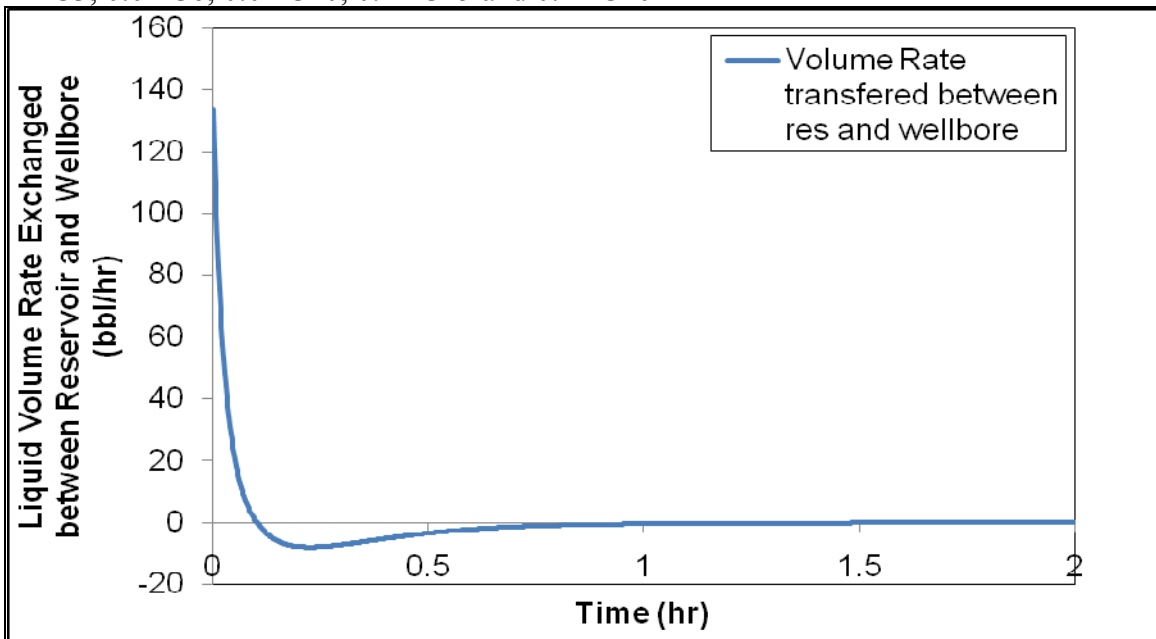


Figure 4.36 Simulated liquid volume rate exchanged between reservoir and wellbore after shut in for a 5300 ft wellbore with 0.165 ft tubing diameter, the initial reservoir pressure is 2200 psi, and initial produced hydrocarbon composition is 0.57 C1, 0.09 C3, 0.01 C6, 0.01 C10, 0.21 C15 and 0.11 C20

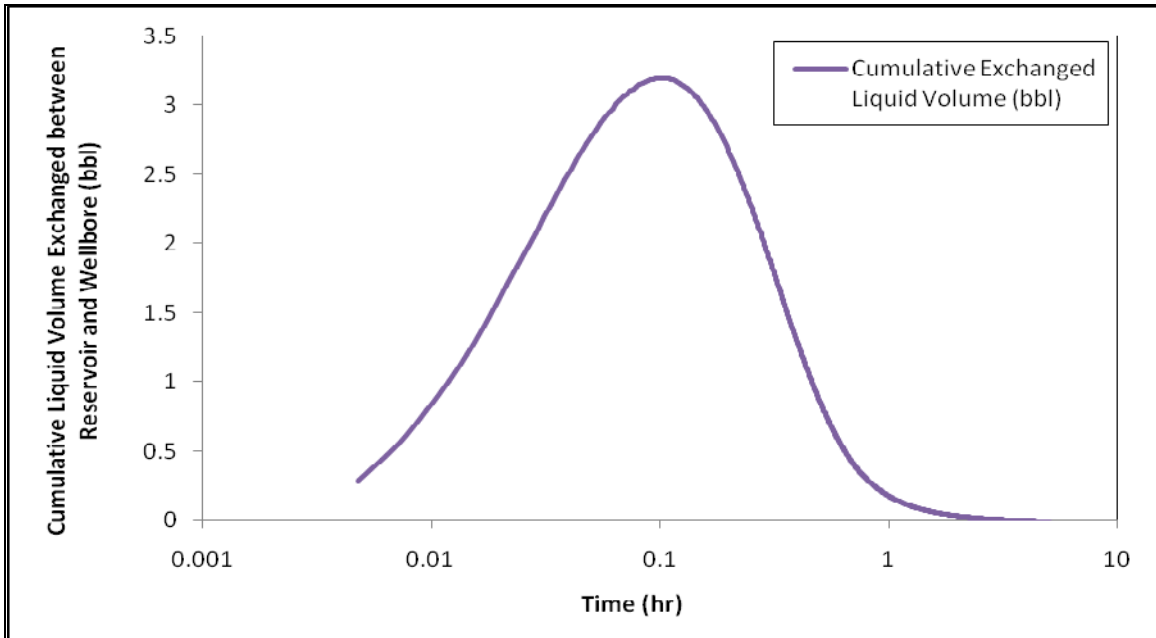


Figure 4.37 Simulated cumulative liquid volume exchanged between reservoir and wellbore after shut in for a 5300 ft wellbore with 0.165 ft tubing diameter, the initial reservoir pressure is 2200 psi, and initial produced hydrocarbon composition is 0.57 C1, 0.09 C3, 0.01 C6, 0.01 C10, 0.21 C15 and 0.11 C20

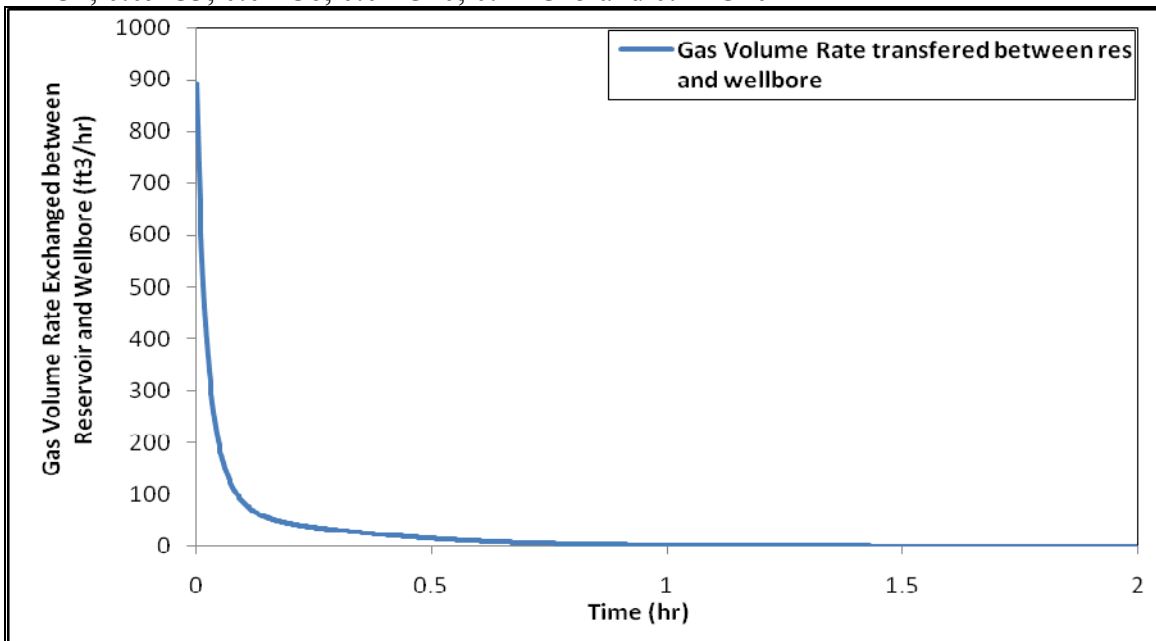


Figure 4.38 Simulated gas volume rate exchanged between reservoir and wellbore after shut in for a 5300 ft wellbore with 0.165 ft tubing diameter, the initial reservoir pressure is 2200 psi, and initial produced hydrocarbon composition is 0.57 C1, 0.09 C3, 0.01 C6, 0.01 C10, 0.21 C15 and 0.11 C20

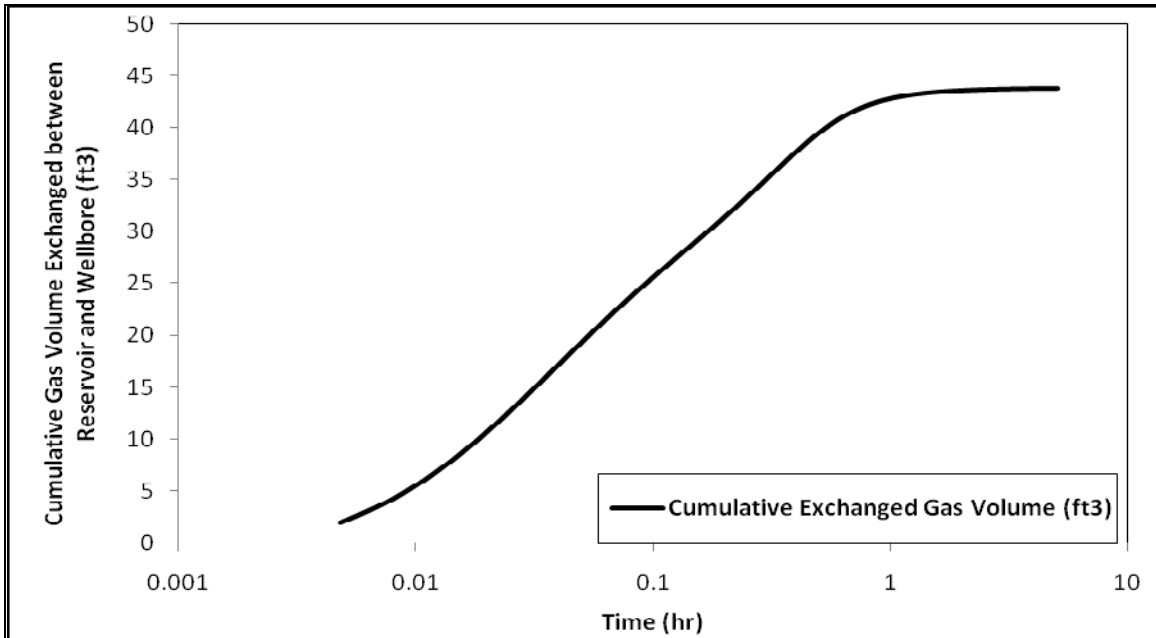


Figure 4.39 Simulated gas volume exchanged between reservoir and wellbore after shut in for a 5300 ft wellbore with 0.165 ft tubing diameter, the initial reservoir pressure is 2200 psi, and initial produced hydrocarbon composition is 0.57 C1, 0.09 C3, 0.01 C6, 0.01 C10, 0.21 C15 and 0.11 C20

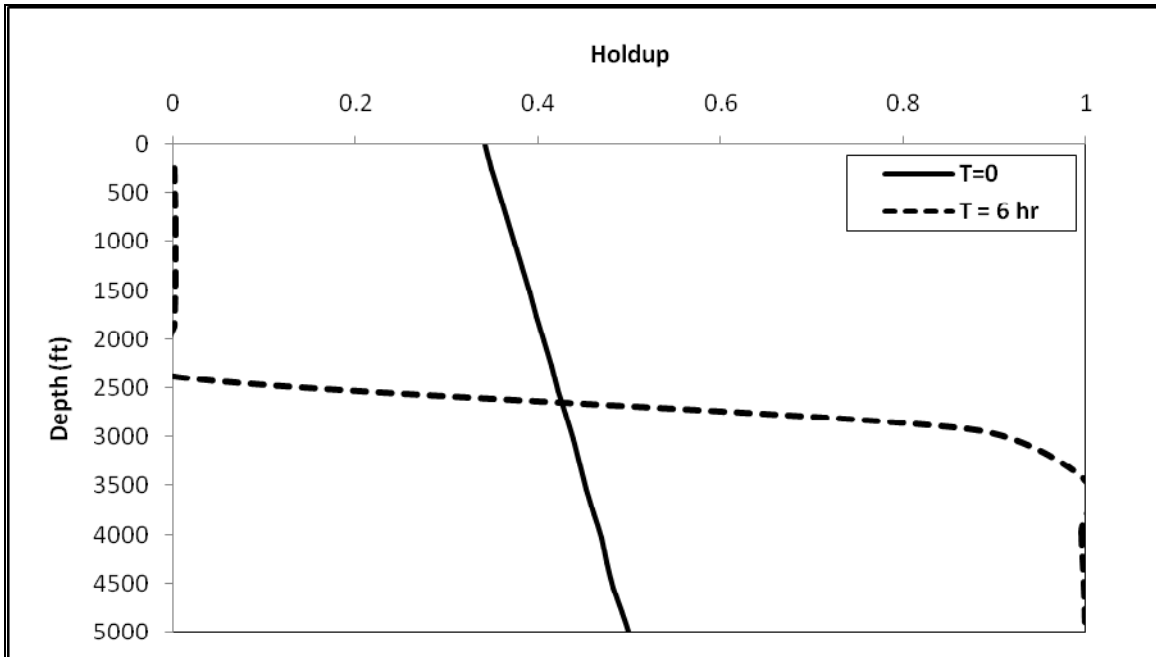


Figure 4.40 Simulated initial and final holdup profiles in the wellbore during shut in for a 5300 ft wellbore with 0.165 ft tubing diameter, initial produced hydrocarbon composition is 0.57 C1, 0.09 C3, 0.01 C6, 0.01 C10, 0.21 C15 and 0.11 C20

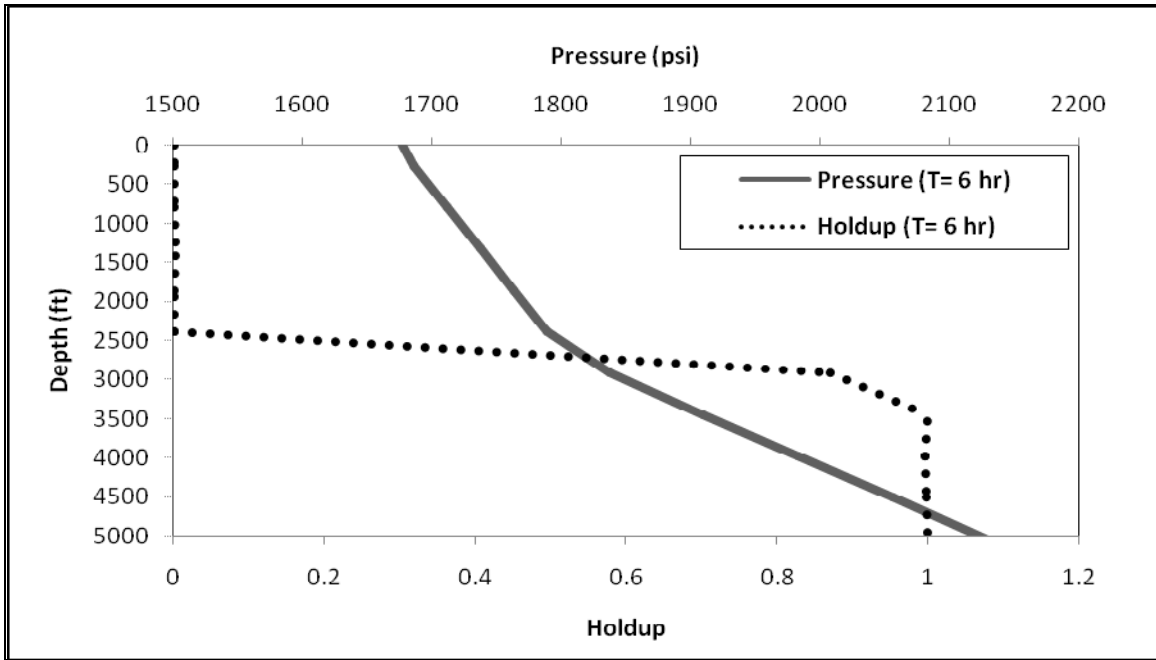


Figure 4.41 Simulated final pressure and holdup profiles in the wellbore during shut in for a 5300 ft wellbore with 0.165 ft tubing diameter, initial produced hydrocarbon composition is 0.57 C1, 0.09 C3, 0.01 C6, 0.01 C10, 0.21 C15 and 0.11 C20

Depth	7200 ft
Inner tubing radius	0.24 ft
Gas flow rate	172 Mscf/D
Oil API gravity	23
Gas gravity	0.6
Surface temperature	70 °F
Reservoir temperature	180 °F
Surface pressure	63 psi
Number of nodes	10
Dt	1 sec

Table 4.1. Wellbore parameters for transient Case 1

Depth	5151 ft
Inner tubing radius	0.125 ft
Wellbore radius	0.425 ft
Oil rate flow	1140 STB/D
Gas flow rate	513 Mscf/D
Oil API gravity	23
Gas gravity	0.8
Surface temperature	76 °F
Formation temperature gradient	0.006 °F /ft
Reservoir temperature	120 °F
Surface pressure	505 psi
Number of nodes	10
Dt	1 sec

Table 4.2. Wellbore parameters for transient Case 2

Dimensions	560 X 560 X 100
Grid Blocks	7X 7 X 3
Porosity	0.3
Permeability (md)	10
Initial P	2200 Psi
Initial Water Saturation	0.17
Initial Oil Saturation	0.512
Initial Gas Saturation	0.318
Initial Composition:C1,C3,C6,C10,C15,C20	0.57,0.09,0.01,0.01,0.21,0.11

Table 4.3. Reservoir input parameters for transient Case 3

Depth (ft)	5300
Inner tubing radius (ft)	0.165
Outer tubing radius (ft)	0.189
Wellbore radius (ft)	0.625
Inner casing radius (ft)	0.324
Outer casing radius (ft)	0.365
Tubing friction coefficient	0.0008
Surface formation temperature (°F)	84
Formation temperature gradient (°F /ft)	0.007
Formation heat conductivity (Btu/(hr-ft- °F))	1.3
Formation density (lbm/ft3)	132
Formation heat capacity (Btu/(lbm- °F))	0.21
Cementing heat conductivity (Btu/(hr-f- °F))	4.02
Annulus brine salinity (ppm)	35000
Bottomhole wellbore temperature (°F)	140
Time step (s)	4
Number of nodes	20
Number of phases	3
Number of components	6
Tolerance for pressure calculation	10 ⁻⁶

Table 4.4. Wellbore input parameters for transient Case 3

CHAPTER 5: APPLICATIONS

5.1 THE EFFECT OF PRESSURE SENSOR POSITION ON WELL TESTING ANALYSIS

5.1.1 Introduction

A transient pressure test is a fluid-flow test conducted on wells to obtain reservoir and well data. During the test, the well's flow rate is changed and the well's pressure response as a function of time is measured at the same well or at other neighboring wells. For example, a well is shut in and the pressure response of the reservoir is measured and analyzed. The pressure response is a function of reservoir rock properties, fluid properties and flow geometry. Hence, it is possible to calculate some of these parameters from analyzing the pressure response.

Several kinds of transient pressure tests have evolved depending on the well type. Based on the well type (injector or producer) and flow rate (producing or shut in) several kind of tests may be designed. One of the most common types is the pressure buildup test. This test is conducted on a well which has been producing at a constant rate, and is then shut in at the surface or sandface. A pressure recorder is lowered into the well to record the pressure in the wellbore for several hours depending on the anticipated formation permeability. The pressure may be measured opposite the producing zone near the formation or at other parts of the wellbore. If the recorder is located far from the perforation zones, the measured pressure should be converted to bottomhole pressure, which is then analyzed to estimate formation permeability, skin factor, average reservoir

pressure, distance to a fault if present, fracture length and fracture conductivity. The buildup test is perhaps the most widely performed transient test. It is easier to conduct and interpret than most of the other transient tests.

5.1.2 Analysis of a Buildup Test

All analysis of a buildup test begins with a log-log plot of ΔP versus Δt and the pressure derivative function versus Δt displaced on the same graph. Figure 5.1 shows an example for this log-log plot.

The pressure response during the buildup test can be divided into different periods. The log-log plot begins with a straight line at the unit slope. This unit slope straight line is an indication of the wellbore storage dominated period. Most wells shut in at the surface rather than at the bottomhole to minimize costs. Surface shut-in allows fluid influx from the reservoir for a long period after shut in. During this period, the sandface flow rate gradually fills the wellbore and causes the bottomhole pressure to increase. Hence, the pressure measured in this section is the wellbore response and not the reservoir response and cannot be analyzed to obtain reservoir parameters. As this period ends and the derivative curve reaches a constant value, data can be analyzed by different methods to obtain reservoir permeability, skin and size. Horner (1951) shows that after the wellbore storage period, a graph of the shut in bottomhole pressures versus $\log \{(t_P + \Delta t) / \Delta t\}$ will be linear with a negative slope, m , given by

$$m = -\frac{162.6q\mu B}{kh} \quad (5.1)$$

This semilog graph is known as a Horner plot. Figure 5.2 shows a typical semilog plot for an infinite acting reservoir. The dashed line shows how the pressure responds linearly after the wellbore storage period. Hence, correct estimation of shut in bottomhole pressure is essential for the Horner method analysis. Other methods such as Miller-Dyes-Hutchenson (MDH) (1950) and Muskat method (1937) can also be applied to calculate reservoir data from a buildup test. All of these methods are based on an accurate bottomhole pressure measurement and estimation.

It is important to be certain that the measured data are not affected by the wellbore dynamics. As discussed earlier, the main wellbore influence occurs due to wellbore storage, but an additional wellbore effect is caused when more than one phase is flowing simultaneously in the system. After shutting the well in at the surface, gas and liquid phases may segregate in the wellbore due to relative velocity, which is called phase segregation or phase redistribution. In such wells, the gravity effects cause the liquid to fall to the bottom and the gas to rise to the top of the tubing. Due to the relative incompressibility of the liquid phase and the inability of the gas to expand in a closed system, a net increase in the bottomhole pressure in the wellbore occurs by phase segregation. Stegemeier and Matthews (1958) observed the predominance of the phase redistribution phenomenon in wells with large positive skin and in reservoirs with moderate permeability. The pressure increase causes an anomalous hump on the pressure buildup analysis curves. Figure 5.3 is a typical plot of buildup data affected by phase redistribution. The pressure hump is obvious in this figure.

Phase segregation also changes the phase distribution in the wellbore. At the top sections of the wellbore gas stores, while liquid accumulates at the bottom. Hence, the pressure profile and pressure gradient change in the wellbore. We will show the effect of this phenomenon on bottomhole pressure measurement and pressure analysis later. It is important to distinguish phase redistribution in a buildup test. Different methods available for this purpose are as follows:

1) The simplest way to distinguish phase segregation is by identifying a hump in pressure response during buildup test. It should be noted that Thompson (1986) and Olarewaju et al. (1989) have shown that hump is not a necessary condition for phase redistribution.

2) Olarewaju and Lee (1989) stated that when phase redistribution effects exist in the wellbore, the pressure derivative type curve exhibits a V-shaped curvature. This method can sometimes be doubtful, because of the similarity of the V-shaped behavior to pressure derivative response in systems with dual-porosity.

3) Mattar and Zaoral (1992) proposed the use of the Primary Pressure Derivative (PPD) to differentiate between the wellbore dominated phenomena and the reservoir fluid flow responses. PPD is defined as the derivative of shut in bottomhole pressure with respect to time as

$$PPD = \frac{dP_{ws}}{d\Delta t} \quad (5.2)$$

They stated that if the wellbore dynamics affect the pressure buildup data, the PPD plot should exhibit an increasing trend, and then revert back to the normal decreasing trend at the end of the wellbore effects.

4) Qasem et al. (2001) showed that the derivative of $\log(PPD)$ with respect to $\log(\Delta t)$ is constant when the data are not affected by the wellbore effects. Hence, the deviation from this constant line is a sign of wellbore influences.

All wellbore related phenomena, such as phase redistribution, have a significant effect on the measured pressure during well testing and the obtained results. Hence it is important to study different concepts to deal with wellbore effects. In this section, we discuss the influences of some of these physical wellbore behaviors which are rarely seen in the literature.

5.1.3 Problem Statement

Fluid flow in the wellbore has influences on pressure response from the reservoir. As discussed, different physical behaviors, such as wellbore storage and phase redistribution, occur during a well test. Other important wellbore effects are related to the pressure gauge placement and data measurement. All the theories in well testing are based on analyzing the reservoir pressure and not the recorded pressure. Hence, the reservoir pressure should be measured at the producing zones. Downhole completion hardware or physical restrictions, such as plugs formed by hydrates, paraffins, or asphaltenes often prevent running a gauge all the way to the desired point in front of the perforation zones (Kabir et al., 1998). The problem that arises is the difference between

the recorded pressure and the reservoir true pressure due to the wellbore effects. Hence, the way we record the data and the method we use to convert them to the bottomhole pressure should be considered carefully. Very few papers have discussed issues related to pressure sensors' positions and their effect on well testing accuracy. Kabir et al. (1998) discussed the interpretation problems caused by wellbore thermal effects due to the sensor position. Mattar et al. (1992) also showed how the sensor position could make the well testing results invalid.

There are different methods of estimating bottomhole pressure in wellbores from measured data. For example:

- 1) Using a pressure recorder sensor: Pressure is measured in the wellbore with moving or stationary recording sensors and the value is then converted to the bottomhole pressure. The simplest way to convert recorded pressure to bottomhole pressure is by adding the hydrostatic head to the measured value. This method is not reliable, however, because it neglects pressure changes due to friction and acceleration; also, accurate prediction of fluid content and hydrostatic gradient in the wellbore is not possible. This problem is more severe when multi-phases are moving simultaneously in the wellbore. Due to slip velocity between phases and phase redistribution, the pressure gradient changes in the wellbore at different depths. Mattar et al. (1992) showed the effect of phase segregation on pressure conversion in more detail. They showed how inaccurate estimation of the pressure gradient in the wellbore can mask the precision of the well testing.

2) Using acoustic fluid level measurements: During phase segregation in a buildup test a liquid/gas interface appears in the wellbore. Another method to calculate bottomhole pressure from the measured surface pressure is to consider the presence of the liquid level. In this method at each time the surface pressure is recorded, an acoustic fluid level survey is also conducted to determine the depth of the fluid level in a well. By these data, it is possible to estimate pressure distribution in the wellbore. This method is based on the recording and analysis of an acoustic echo obtained from the shots done down to the well. Figure 5.4 shows one example of an acoustic recording during survey. The liquid level causes a distinct echo in response. It is possible to detect the gas/liquid interface moving by analyzing sequential responses during a buildup test. Each time, the fluid level is measured by acoustic shots. Figure 5.5 shows a schematic of liquid and gas distribution. Hence, h_l is detected in Figure 5.5 using the acoustic method.

Different methods and correlations can be used to estimate the gaseous column average gradient at the bottom (γ_l) and gas column gradient at the top (γ_g). Equation 5.3 is used to calculate BHP. In this equation L_w shows the well depth; P_B and P_{wh} are bottomhole pressure and wellhead pressure, respectively.

$$P_B = P_{wh} + \gamma_g h_l + \gamma_l (L_w - h_l) \quad (5.3)$$

3) Using a simulator to model bottomhole pressure in transient cases: We can model the transient problem with a coupled wellbore/reservoir simulator to obtain an accurate value for the pressure gradient as a function of time and depth in the wellbore. Using this method, it is possible to accurately convert recorded pressure at each depth to bottomhole pressure to analyze in well testing.

In this work, we use our developed wellbore/reservoir simulator to calculate correct values of the transient pressure gradient during a buildup test in wellbores. Our simulator is also able to model transient bottomhole pressure and phase fraction profiles in wellbores. We can compare the simulated results with results obtained from Method 1 (recorder sensor) and Method 2 (liquid level measurement) to answer questions about the validity of converting recorded data to sandface pressure.

5.1.4 Comparison with Method 1 (Pressure Recording at Different Depths)

To simulate the first method we run a buildup test with our coupled wellbore/reservoir simulator to model the bottomhole pressure profile. We assume different methods to record the pressure response during buildup with pressure sensors:

1) Recording the data at the perforation zone (Figure 5.6). The bottomhole pressure is measured directly, so the results calculated from the well test analysis are reliable.

2) Recording the data at the wellhead (Figure 5.7). We assume that the sensor is placed at the surface and pressure is recorded and then converted to the bottomhole pressure.

3) Recording the data at a point above the perforation zone (Figure 5.8). We assume that the recorder is stationary at a depth in the wellbore. Subsequently, the recorded pressure values change to the bottomhole pressure.

4) Recording the data by a moving sensor (Figure 5.9). In this case the sensor is lowered into the tubing from the surface to the sandface. During this lowering, pressure

data are measured, so each datum is a function of time and depth. Similar to the other cases, pressure at each depth is converted to the sandface pressure by adding the pressure gradient between that depth and bottomhole.

We ran a synthetic buildup test with our coupled wellbore/reservoir simulator to model the bottomhole pressure profile to compare with the results obtained from sensor measurements. A well is producing hydrocarbon in the middle of a reservoir. Figure 5.10 shows a schematic of this system. Reservoir parameters are presented in Table 5.1. Most of the components in the reservoir are light, so we expect production of gas and oil at the surface. Hence, multiphase flow moves in the wellbore before the shut in. Table 5.2 shows the wellbore description.

Because the well is shut in at the surface, the sandface flow rate does not stop immediately. Due to the gravity, the liquid phase tends to go down in the wellbore, and the gas phase moves upward. Hence, phases segregate from each other. This phenomenon is described in Chapter 4 in more detail. Figure 5.11 presents transient holdup profiles in the wellbore. It can be seen that the liquid fraction increases at the lower sections of the wellbore and the liquid interface moves upward. On the other hand, the gas fraction increases near the wellhead and the gas phase accumulates at upper sections of the well.

Figure 5.12 shows phase accumulation in more detail. At the deep sections of the wellbore, the liquid fraction increases with time; for example, there is no gas near the perforation zones after 2 hours. This graph shows how the gas phase travels upward. For instance, after about 1.5 hours from the shut in, no liquid exists at the wellhead and the upper sections of the wellbore are filled with the gas phase. Figure 5.12 shows that the

phase fractions change significantly in the wellbore during the buildup test and pressure gradient is no longer constant. Our simulator estimated the pressure gradient due to gravity, friction and acceleration in the wellbore. Hence, we are able to model the transient pressure distribution in the wellbore at different sections.

Case 1: We assume that the sensor is located exactly at the perforation zone, so it measures the bottomhole pressure directly. Figure 5.13 shows the transient bottomhole pressure in the wellbore. We can see how the pressure builds up during the test. Figure 5.14 is the log-log plot of bottomhole pressure response during buildup. The linear section of this graph represents the period in which the test is dominated by wellbore storage. One and one half cycles after the end of wellbore storage period the data can be used for semilog analysis. Semilog pressure curve at this period is shown in Figure 5.15. This graph can be analyzed to obtain reservoir properties. As we use the bottomhole pressure to plot this graph, the results are reliable.

Now we consider results obtained from recording the data at a location far from the perforation zones.

Case 2: We assume that the pressure data are recorded at the wellhead. The simplest way to convert pressure measured at the surface to bottomhole pressure is by using Equation 5.4.

$$P_B = P_1 + \gamma l \quad (5.4)$$

Where, P_1 is the measured data (here at wellhead), and l is the distance between the sensor position and the perforation zone. γ is the average hydrostatic gradient between the sensor location and the sandface. γ can be obtained from the steady state pressure

profile before shutting the well in. Figure 5.16 shows the pressure at the surface, bottomhole pressure converted by Equation 5.4, and the correct profile of sandface pressure.

The difference between converted pressure and accurate profiles is observed. Using converted pressure to obtain reservoir parameters leads us to the wrong conclusion. Figure 5.17 shows the semilog plot for these data. The parallel lines can be a diagnostic for a dual porosity system which is not correct in this case. Incorrect conversion of recorded data leads to misinterpretation of the information from the reservoir. As Mattar et al. (1992) explained, the change in the liquid fraction between the recorder and the midpoint of perforation causes this unusual behavior.

We can solve this problem using our simulator. Our transient wellbore/reservoir simulator models the pressure gradient in the wellbore. Figure 5.18 shows the pressure gradient at different times. Using these profiles, we can accurately convert the pressure at any point in the wellbore to the bottomhole pressure. For example, Figure 5.19 shows the gradient at $T=3$ hr. If the wellhead pressure is measured, we can calculate bottomhole pressure from Equation 5.5.

$$P_B = P_{wh} + S \quad (5.5)$$

where S is the integral of gradient curve shown in Figure 5.19.

Case 3: We assume that the pressure is recorded at a point higher than the perforation zones. A similar problem occurs when the sensor is left stationary at any other depths. For example, if the data are recorded at a depth equal to 5400 ft, the converted results do not match the bottomhole pressure, as shown in Figure 5.20. The semilog plot obtained

from the converted data presented in Figure 5.21 shows unusual behavior. Due to the accumulation of a denser phase between the sensor location and the bottomhole pressure, the gradient increases at this section. Hence, assuming constant gradient leads us to an anomalous error, as shown in Figure 5.21. The pressure is decreasing in this figure, which does not have any physical meaning in the buildup test. We can use our simulator to solve this problem, as in the previous case.

Case 4: In this case, we assume that the sensor is not stationary. The sensor is lowered into the wellbore and during movement data are recorded, so each datum depends on both time and location. We assume that the sensor is lowered at a constant speed. Figure 5.22 shows the depth of the sensor at any time. We can use Equation 5.6 to convert pressure at each time to bottomhole pressure.

$$P_B = P(h, t) + \gamma(L_w - vt) \quad (5.6)$$

where $P(h, t)$ is the pressure recorded at depth h and time t . L_w is the depth of the wellbore and v is the sensor velocity. Figure 5.23 shows the measured data, simulated bottomhole pressure and bottomhole pressure calculated by Equation 5.6. Analyzing the semilog plot obtained from this calculation, again, is doubtful. Figure 5.24 can mislead us into categorizing this reservoir as a dual porosity system, which is incorrect.

5.1.5 Comparison with Method 2 (Liquid Level Measurement)

We discussed liquid level measurement method in section 5.1.3. We now use it to calculate bottomhole pressure in a build up test. Before shutting the well, gas and liquid

are produced from the wellbore. The liquid fraction increases gradually from the wellhead to the sandface. Figure 5.25 shows the holdup profile before shut in.

After shutting in the flow at the surface, gravity causes liquid to fall back and accumulate in the lower sections of the wellbore so that a gas/liquid interface appears. When the after-flow stops, two sections can be distinguished in the wellbore: the liquid section and the gas section. This interface can be identified by acoustic measurements. Figure 5.26 presents the liquid level during the buildup test. In this case, at the end of the test a 2200 ft column of liquid accumulated at the bottom and the rest of the wellbore was full of gas. Knowing the surface pressure, we can use Equation 5.3 to calculate bottomhole pressure.

Figure 5.27 shows the bottomhole pressure calculated from this procedure. The actual bottomhole pressure modeled with our simulator is also shown in this figure. The solid line shows the semilog slope to calculate reservoir characteristics. It is obvious that the slope of this line is different from the semilog slope of actual data. It shows that this method also experiences errors in calculations. Hence, neglecting calculation and simulation of transient multiphase flow in wellbores during a buildup test causes noticeable errors in the analysis, which makes the well testing invalid. Our work shows the importance of preplanned simulations when downhole restrictions exist. Simulations will help us to convert the measured data to correct bottomhole pressure data for analysis.

5.2 ESTIMATION OF ACCUMULATED LIQUID PHASE IN A GAS WELL

5.2.1 Modeling Procedure

Thousands of natural gas wells are producing around the world. During their lives, reservoir pressure depletes, so that the production conditions change with time. Very few gas wells produce completely dry gas. When gas is produced, pressure and temperature decline from the sandface to the surface, so that part of the produced gas changes to condensate form. Interstitial water may also be produced with gas. Hence, we expect production of liquid besides gas in these wells. The formed liquid may be carried out of the well by the gas phase. At the early stage of the well life, due to the high velocity of the gas phase, liquid can be carried to the surface. In the later stages of the well, the gas phase does not have enough energy to carry the liquid phase. Hence, liquid accumulates in the bottom sections of the well. The inability of gas to remove the liquid phase causes production difficulties.

The accumulated liquid in the wellbore increases the back pressure on the formation. As the pressure difference between the reservoir and the wellbore is the reason for gas flow from the reservoir, larger back pressure reduces the gas flow rate. In some cases this problem may cease the flow. Accumulated liquid may also affect the data measured for well testing. Hence, it is important to determine if the flow rate of a well is sufficient to remove the liquid phase material. As Turner et al. (1969) showed, the minimum flow conditions necessary to remove the liquid from gas wells is a function of the largest liquid droplet size entrained in the gas phase. Coleman et al. (1991) studied

this problem for lower pressure gas wells in order to develop methods to define the well type.

The gas wells may be categorized into three groups:

- 1) High rate gas wells: the liquid is being produced with the gas phase. The gas velocity is sufficient to carry liquid in the shape of droplets and slugs to the surface. In this case, pressure distribution in the well is fairly uniform. This case occurs in the early period of a well's life. This kind of well is schematically presented in Figure 5.28 (Type 1).

- 2) Intermediate rate gas wells: due to the lower gas flow rate, some of the liquid cannot be carried to the surface. Hence, at the lower sections the percentage of liquid is higher. The flowing pressure gradient shows two behaviors; above the gas/liquid interface the gradient is low because of gas, and at the lower sections it is higher because of more liquid. This case, which is shown as Type 2 in Figure 5.28, occurs in the later stages of a gas well's life.

- 3) Low rate gas wells: At the late period of the well's life, gas velocity decreases more due to high reservoir depletion. The concentration of liquid at the bottom of the well grows to more than 90% due to low gas velocity. Potentially, there is no liquid flowing to the surface. This is similar to the behavior of the wells which are shut in for a long time. As discussed in Chapter 4, when a well is shut in the bottomhole pressure may temporarily exceed the reservoir pressure and causes backflow to the formation. This behavior is also shown in Figure 5.28 (Type 3).

Knowledge of the phase distribution and liquid accumulation in the wellbore is very important in determining the restrictions that may exist for the inflow from the formation. Excessive amounts of liquid near the perforation zones reduce the mobility of the gas phase. Hence, it is necessary to apply some technique to remove the accumulated liquid. For example, it is possible to install plungers, pumps or redesign the flow string size to increase the gas velocity. Hence, it is essential to know:

- 1) The gas flow rate at which liquid starts to accumulate.
- 2) How much liquid accumulates at the bottomhole if the gas flow rate declines?

What is the liquid fraction near the perforation zone at the lower gas flow rate?

Different methods are available to distinguish liquid levels in the wellbore. Rowlan et al. (2006) used acoustic fluid level tests to determine which flowing gradient conditions exist in a well and where the liquid level is located. They performed a series of fluid level and surface pressure measurements while the flow at the surface was stopped in order to identify the behavior and distribution of the fluids. The principle objective of the acoustic measurement in a flowing well is to determine the quantity of liquid in the tubing and also to define the liquid level, percentage of liquid in the liquid level and bottomhole pressure. The effect of the gas flow rate on the liquid level change is also considered. To identify the fluid level different fluid level shots were acquired. The main problem with this method is the uncertainty in determining acoustic velocity from the tubing collar's recess reflections. Hence, sometimes it is hard to see the echoes from the collar recesses. Sometimes noises caused by the high gas flow rate exceed the amplitude of the reflected signals from the collar recesses. Hence, the reflections are observed very

weak. It is also hard to identify the interface if low percentages of liquid are in the tubing. Several measurements should be taken to be sure about the gaseous column gradient. The other possible problem is liquid droplets. Liquid droplets or annular films on the tubing cover the tubing collar recesses and cause difficulties for reflections. In this section, we explain how we use our wellbore simulator to calculate the liquid level. Using the simulator gives us a fast estimation of the accumulated liquid at the bottom sections of the wellbore when the gas flow rate decreases.

During production, reservoir pressure decreases, so that the drawdown pressure declines causing lower gas velocity. We use our simulator to model this process. In practice, the variable that we can change at the surface of a well is not flow rate but pressure. The flow rate is a response of the wellbore and the formation to whatever pressure we have at the tubing head. As the formation depletes, the back pressure at the surface is reduced by the operator in order to maintain the flow rate at the level we want. We set up our model to change the pressure boundary condition at the surface and the reservoir pressure, in order to simulate the effect of depletion of the gas reservoir. The simulator should compute the resulting rates (gas and liquid) and the holdup in the wellbore. The procedure is as follows:

- 1) We reduce the pressure difference between the reservoir and wellbore. The new value of the wellbore pressure is like a new boundary condition for our model.

- 2) With this new boundary condition, we run the transient simulator to reach steady state again. The new fluid-flow conditions are the well response with the new

drawdown, this means that at that pressure difference we know the gas and liquid velocity profiles and holdup distribution.

3) To compute accumulated liquid we consider two extreme cases. Figure 5.29 (a) shows a schematic for a gridblock at the bottom section of the well. Two phases occupy this gridblock simultaneously. If all the liquid is carried out by the gas phase, both phases move with same velocity as shown in Figure 5.29 (a). Hence,

$$v_g = v_l \rightarrow \alpha_r = 0 \quad (5.7)$$

where α_r is the liquid fraction, which is accumulated at the grid block. In this case, there is no slip between the phases.

At the other extreme, we assume that liquid velocity is zero and all the liquid phase stores at the gridblock as shown in Figure 5.29 (b), so

$$v_l = 0 \rightarrow \alpha_r = H \quad (5.8)$$

where H is the mixture holdup. This means that the entire available liquid fraction accumulates at the bottom. When the gas flow rate declines, slip occurs between liquid and gas phases. We believe that this case stays between two extremes. As shown in Figure 5.29 (c), a portion of the liquid phase is carried out by the gas phase. This fraction moves with the same velocity as the gas phase. On the other hand, a portion of the liquid phase remains stationary in the block. Hence,

$$v_l H = v_g (H - \alpha_r) + 0(\alpha_r) \rightarrow \alpha_r = \frac{v_g - v_l}{v_g} H \quad (5.9)$$

Therefore,

$$\alpha_r = \frac{Hv_s}{v_g} \quad (5.10)$$

We can model the fluid flow in the wellbore, so that liquid holdup and slip velocity are known by any pressure boundary condition. Using Equation 5.10, we can calculate the fraction of the liquid which is accumulated at the bottom.

5.2.2 Results

Based on the above discussed procedure, we ran our simulator to calculate accumulated liquid at the bottom. A wellbore is coupled to the reservoir model. Wellbore and reservoir parameters are given in Tables 5.1 and 5.2. We ran the simulator for different boundary pressure conditions until reaching steady state. At the steady state the gas phase and the liquid phase produced with different velocity. As the pressure difference between reservoir and wellbore declines gas flow rate decreases. Hence, less liquid is hold up to the surface and the accumulation increases. Our simulations show this behavior in detail. Table 5.3 shows the drawdown pressure for each run. The lower the drawdown value in the table, the higher is the accumulation. Figure 5.30 and 5.31 present gas and liquid velocity versus drawdown pressure at each run. We can see that at higher drawdown, the mobility of phases is higher and they move faster. Figure 5.32 shows the slip velocity between phases. When there is 800 psi difference between reservoir pressure and bottomhole wellbore pressure, gas and liquid move with same speed so nothing remains near perforation zones. Figure 5.33 shows bottomhole holdup (H) and accumulated liquid fraction (α_r) versus gas velocity. The difference between two curves

is the fraction of liquid that is carried out to the surface. At high velocity this fraction is larger. Figure 5.34 shows the percentage of liquid that is accumulated. We can see that when gas velocity is about 7.5 ft/s all the liquid moves to the surface, but when gas velocity reduces from 7.5 to near 3 ft/s about 23% of the liquid stays at the bottomhole. This value becomes more than 85% when the velocity becomes 1.15 ft/s, which is a significant value. Figure 5.35 shows the accumulated fraction of the liquid phase versus pressure drawdown. This shows the ability of our simulator to estimate liquid at the bottomhole, which is important for gas mobility in gas wells.

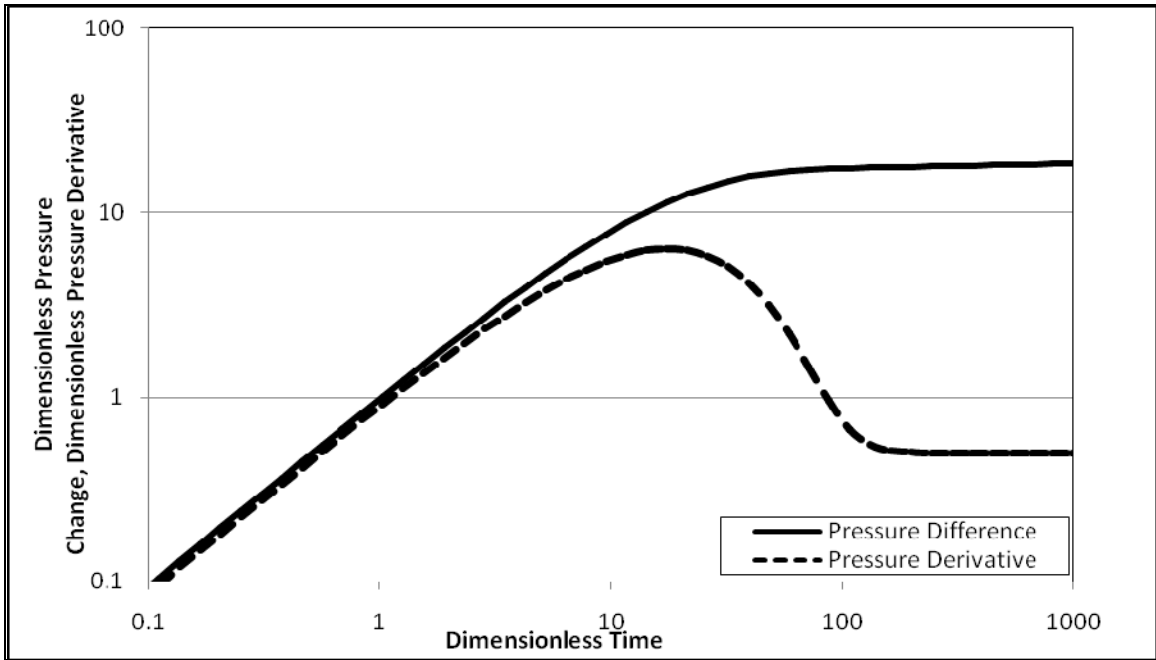


Figure 5.1 A typical log-log plot for a buildup test

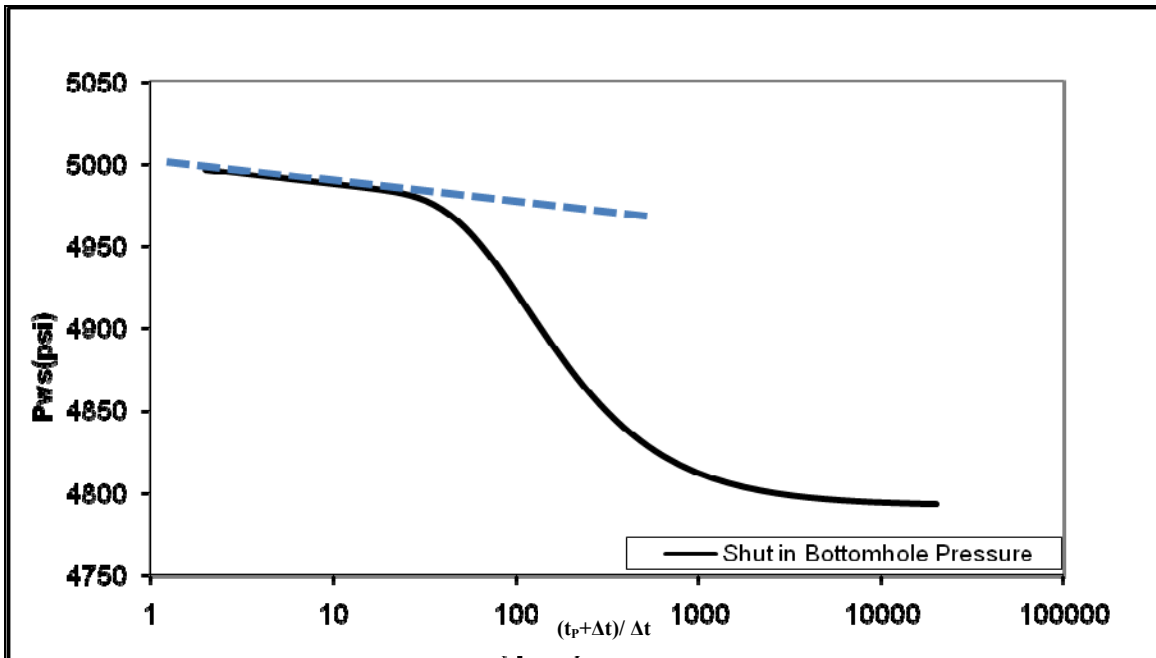


Figure 5.2 A typical semilog plot for buildup test

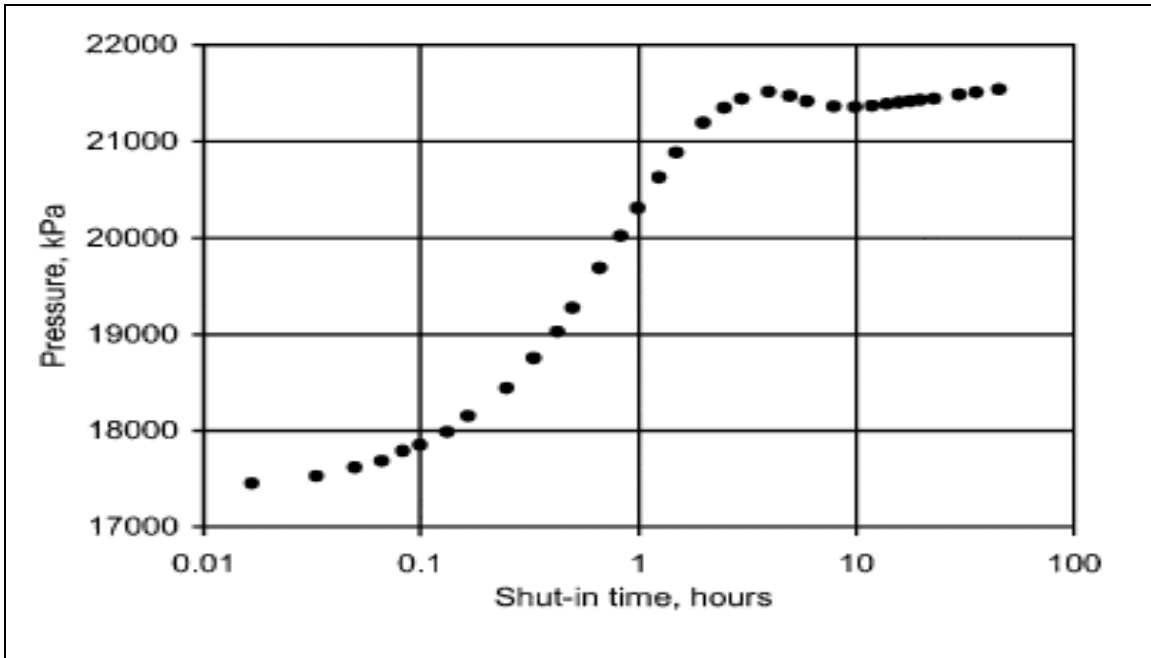


Figure 5.3 An example of bottomhole pressure response during a buildup test which is affected by phase redistribution between 1hr and 10 hr (Qasem et al., 2001)

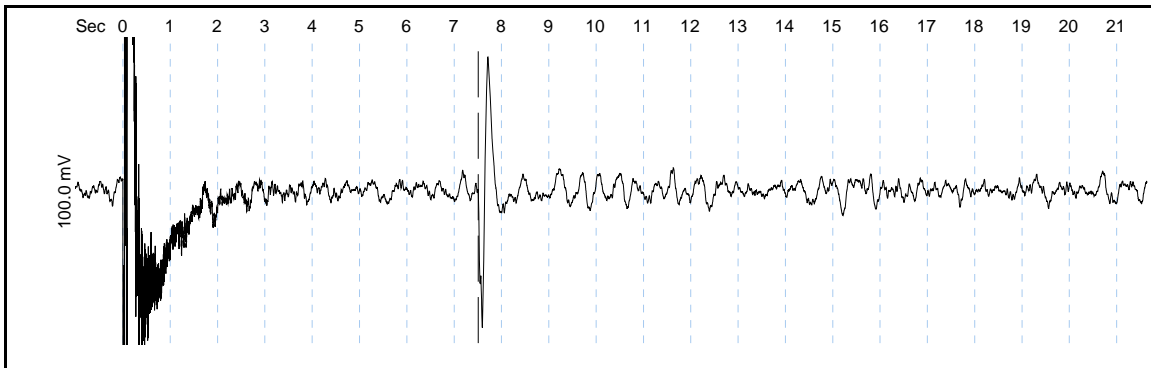


Figure 5.4 An example of an acoustic response of multiphase flow in a wellbore during a buildup test

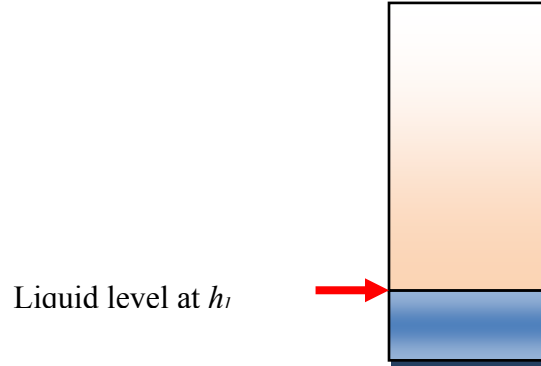


Figure 5.5 Schematic of liquid level in a wellbore containing more than one phase when the well is shut in at the surface (Liquid phase is accumulated at the lower section and gas fills the upper section of the wellbore.)

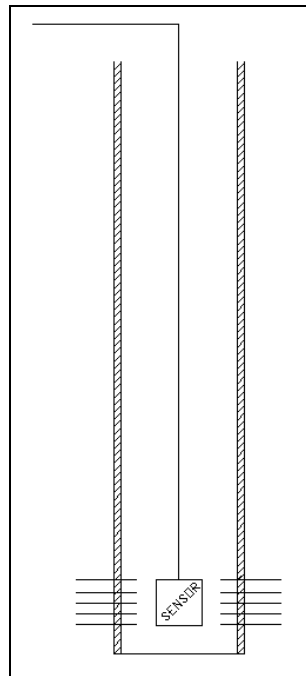


Figure 5.6 A schematic of pressure recording during a well test in a wellbore when pressure recorder sensor is located in front of the perforation zone (Case 1)

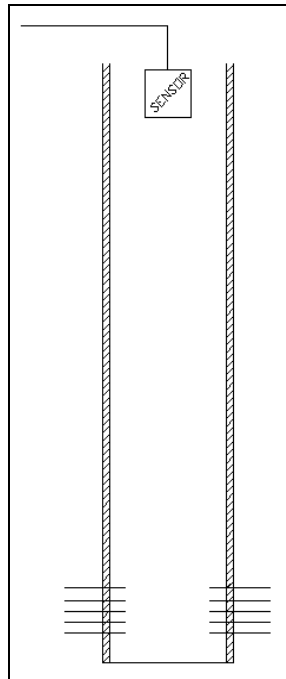


Figure 5.7 A schematic of pressure recording during a well test in a wellbore when pressure recorder sensor is located at the wellhead (Case 2)

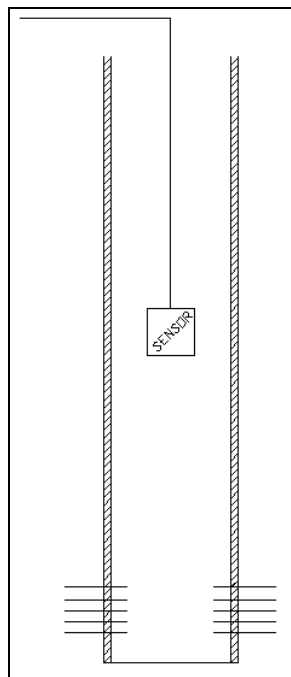


Figure 5.8 A schematic of pressure recording during a well test in a wellbore when pressure recorder sensor is located at a depth higher than the perforation zone (Case 3)

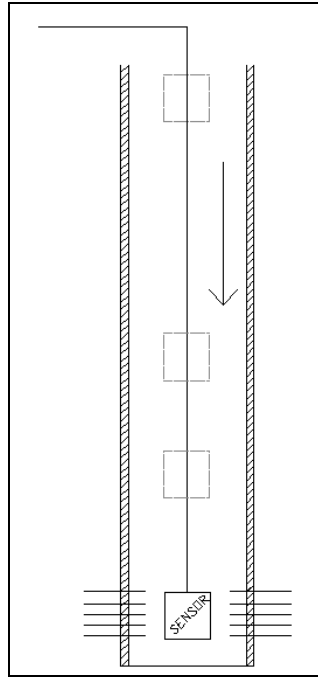


Figure 5.9 A schematic of pressure recording during a well test in a wellbore when pressure recorder sensor is lowering from the surface to the perforation zone (Case 4)

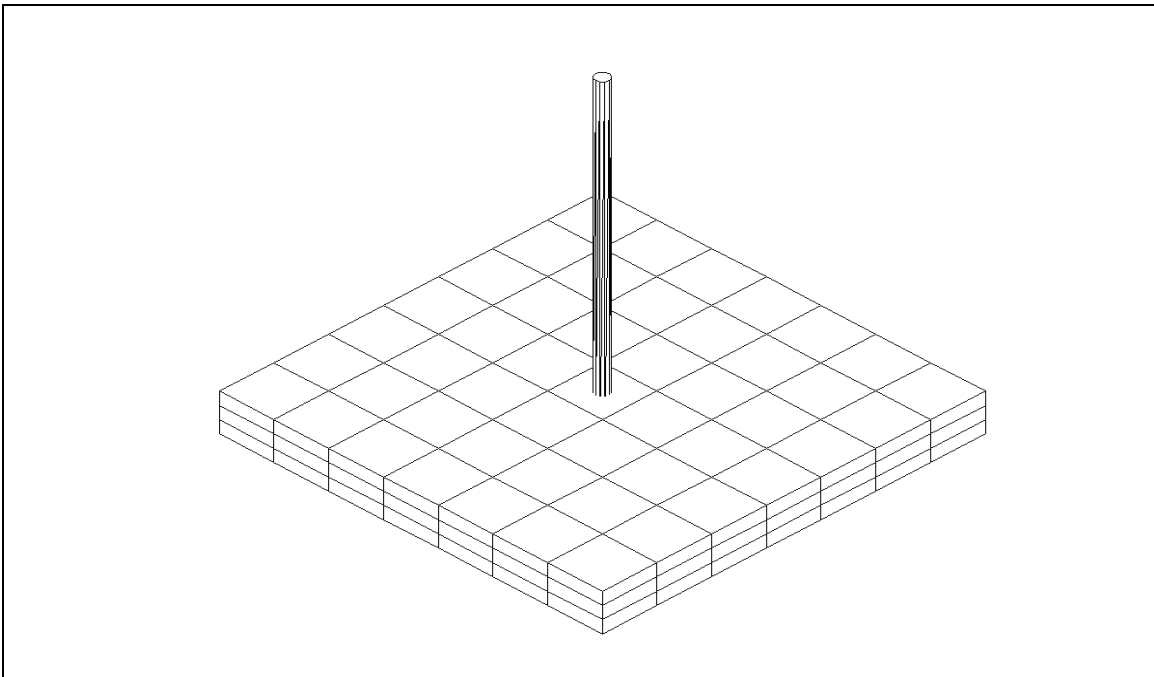


Figure 5.10 Schematic of wellbore/reservoir system used in buildup simulation (Reservoir size is $560 \times 560 \times 100$ ft which is divided to $7 \times 7 \times 3$ gridblocks and wellbore depth is 7200 ft which is divided to 20 vertical gridblocks)

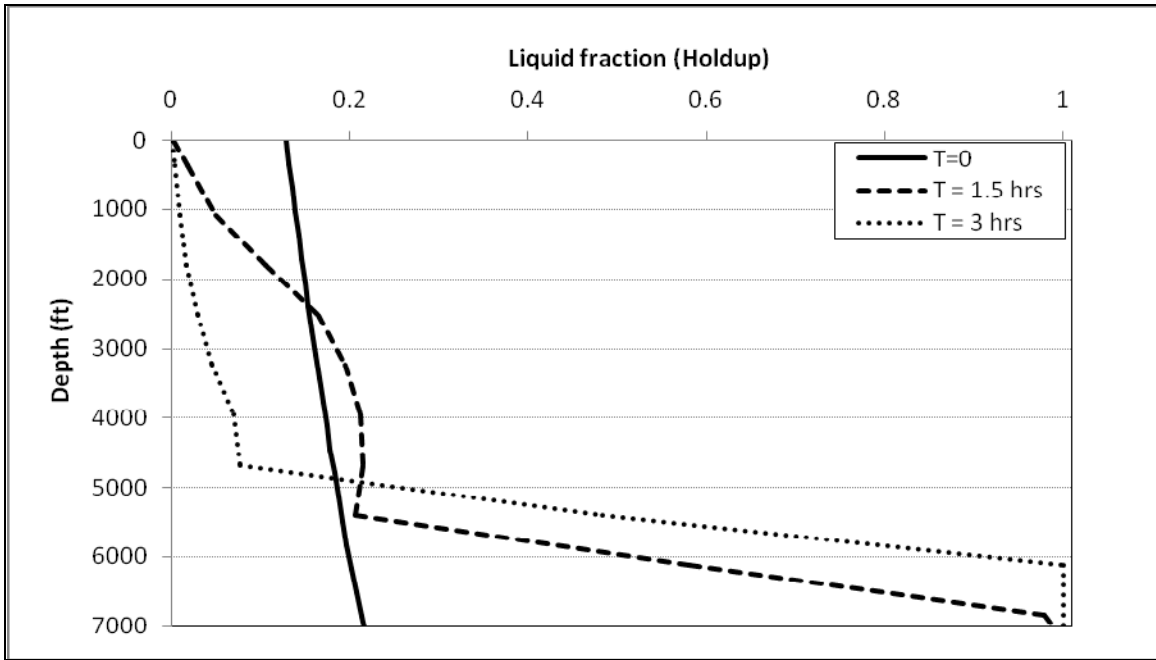


Figure 5.11 Simulated transient liquid fraction profiles during buildup test (Wellbore depth is 7200 ft and the tubing diameter is 0.125 ft. The well is shut in at the surface)

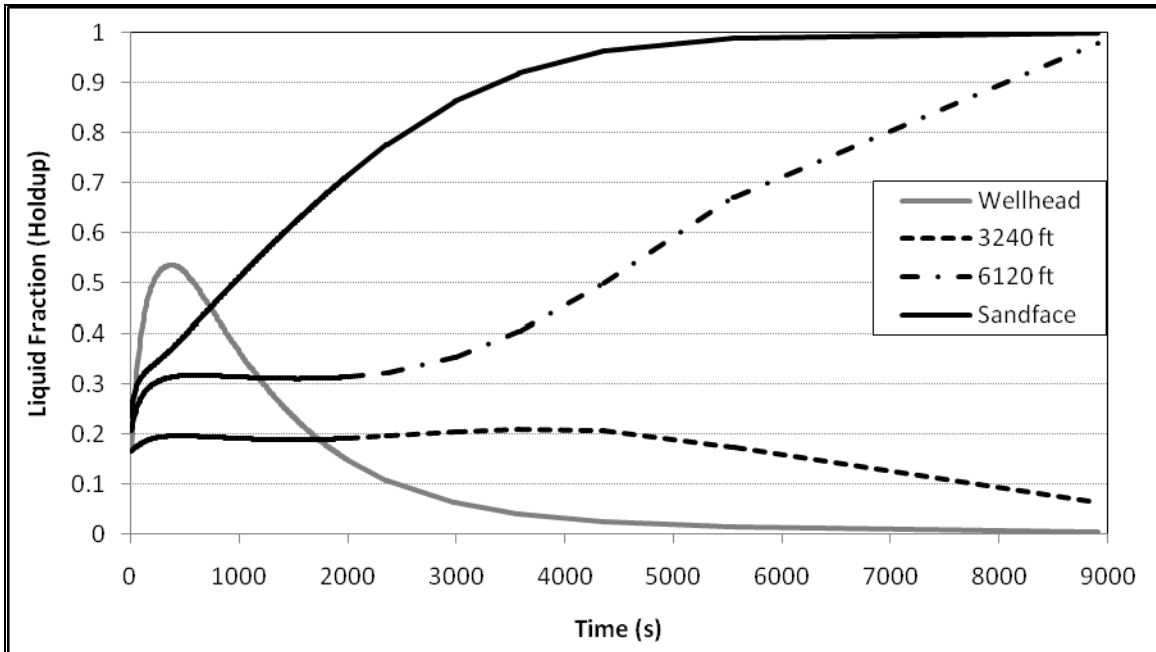


Figure 5.12 Simulated transient liquid fraction profiles at different sections of the wellbore during a buildup test (Wellbore depth is 7200 ft and the tubing diameter is 0.125 ft. The well is shut in at the surface)

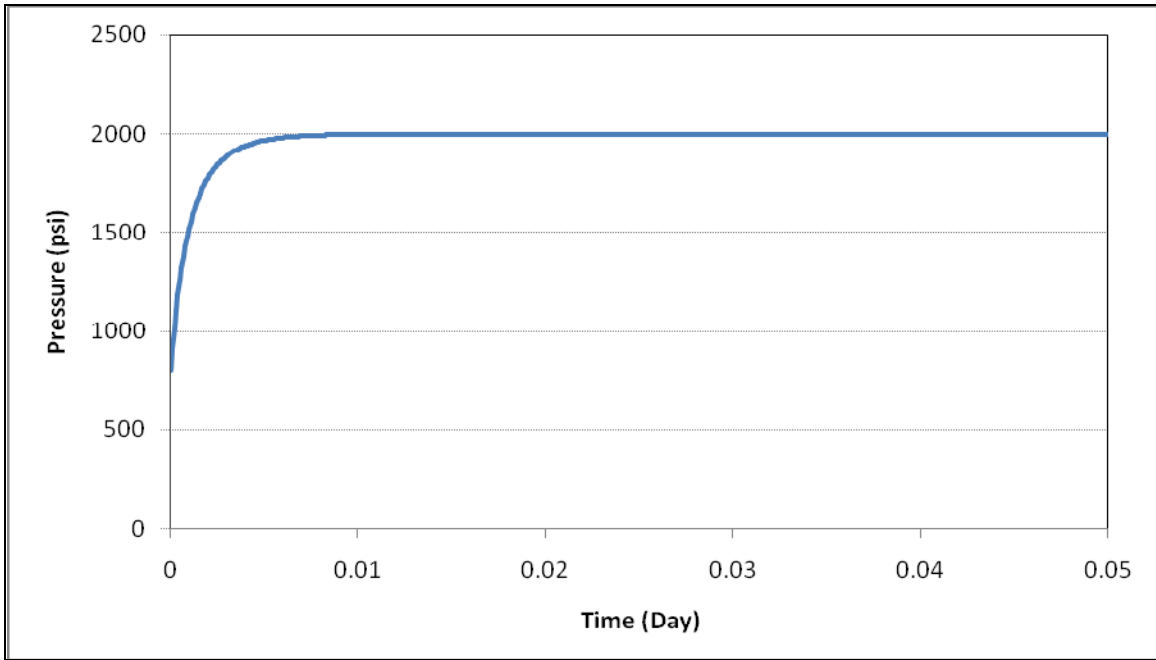


Figure 5.13 Simulated wellbore bottomhole Pressure history profile during buildup test (Wellbore depth is 7200 ft and the tubing diameter is 0.125 ft. The well is shut in at the surface)

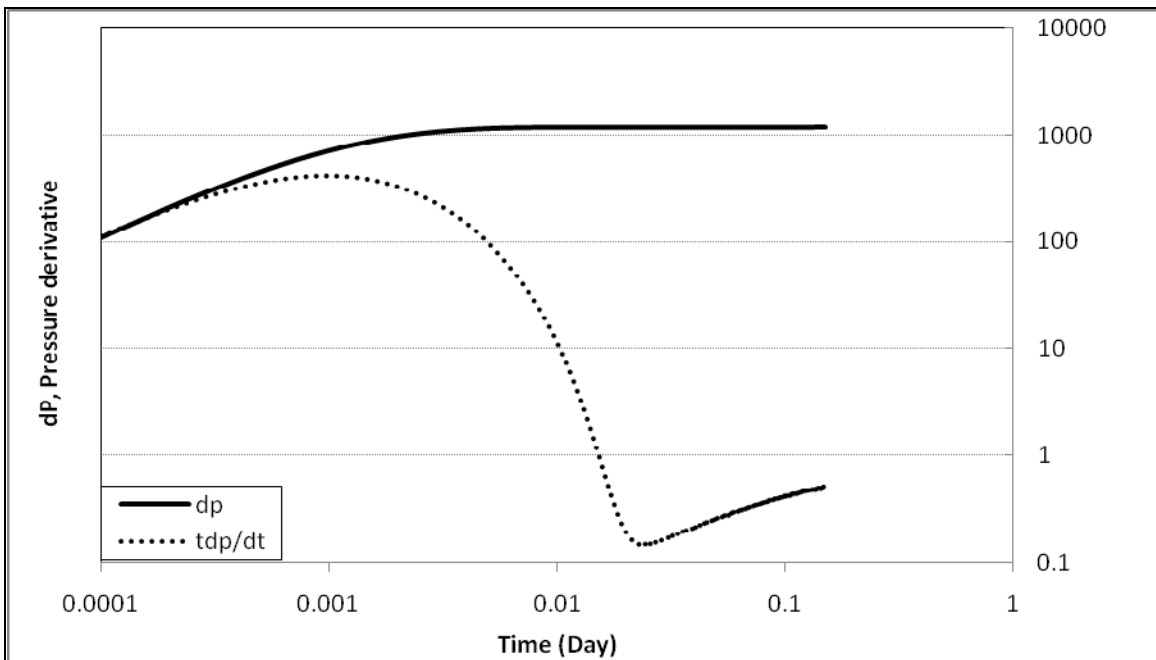


Figure 5.14 Simulated diagnostic pressure and pressure derivative plots during buildup test (Wellbore depth is 7200 ft and the tubing diameter is 0.125 ft. The well is shut in at the surface)

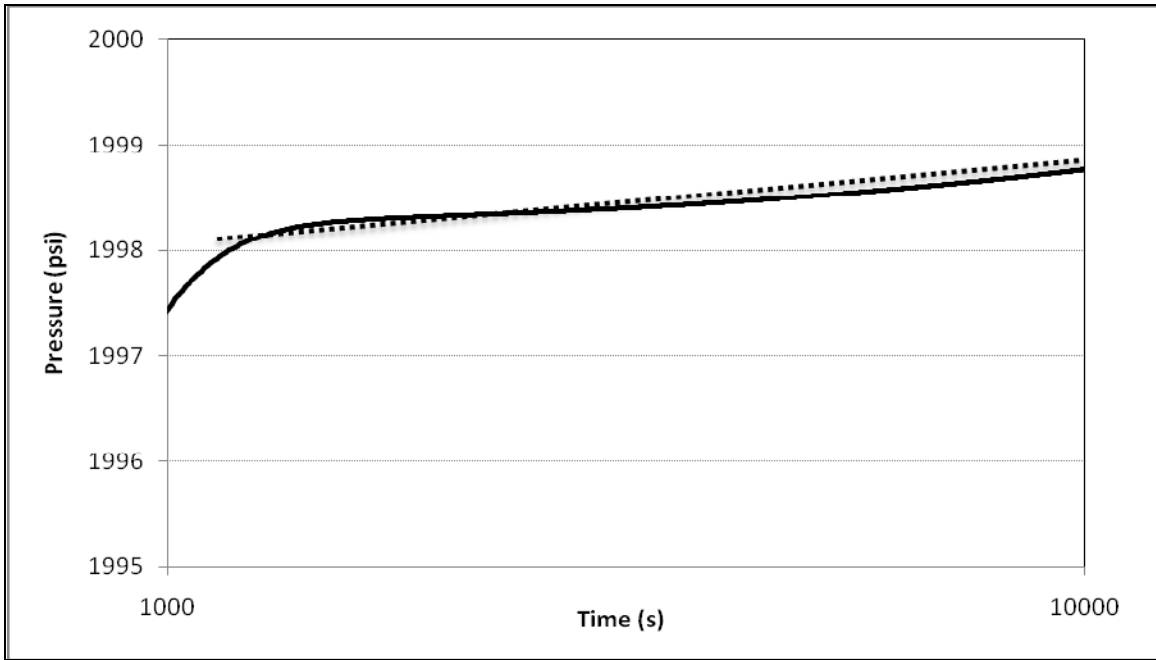


Figure 5.15 Semilog line used to analyze simulated buildup test and calculate reservoir properties

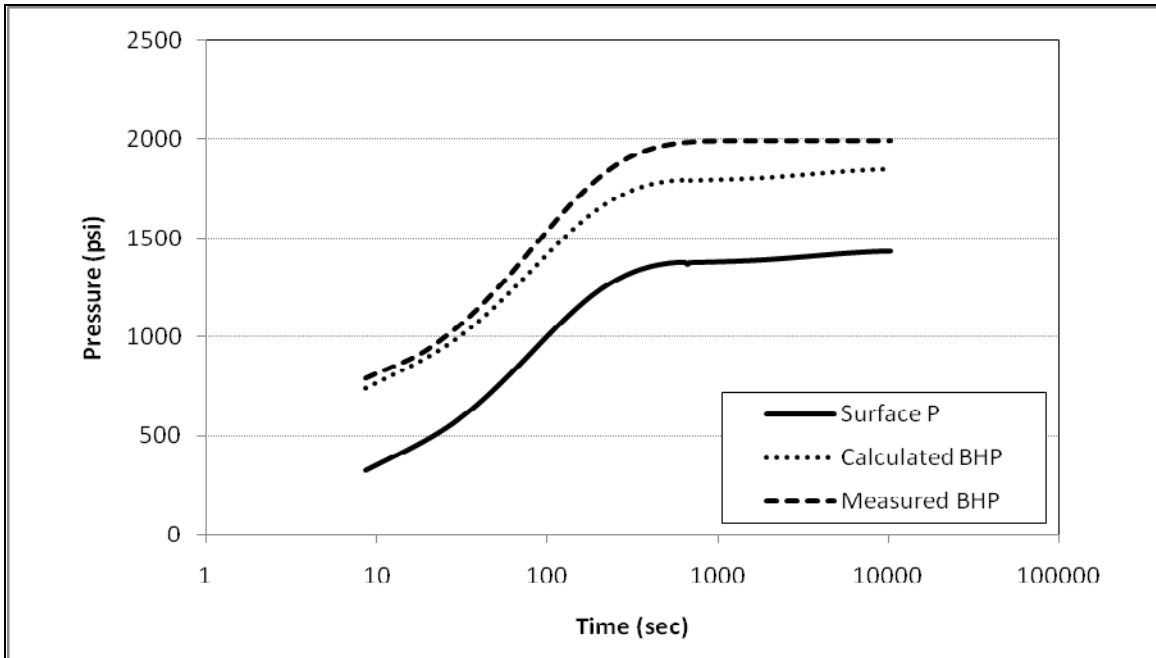


Figure 5.16 Calculated bottomhole pressure profile from measured pressure when recorder sensor is located at the wellhead

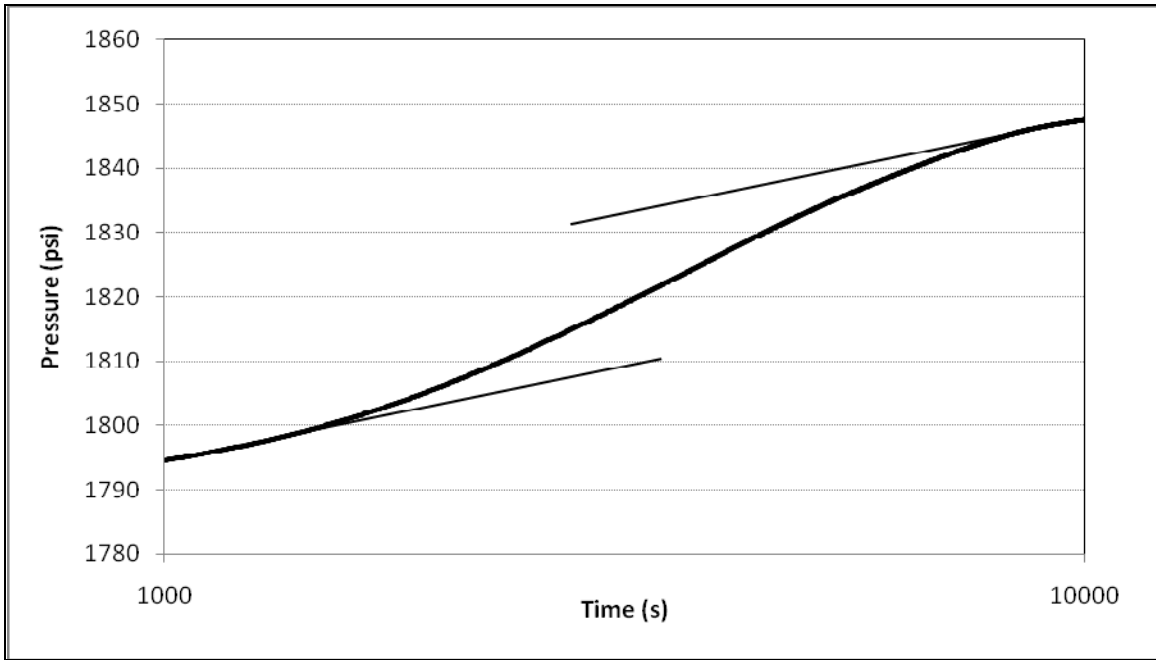


Figure 5.17 Semilog plot used to analyze buildup test when bottomhole pressure profile is calculated from recorded pressure at the wellhead

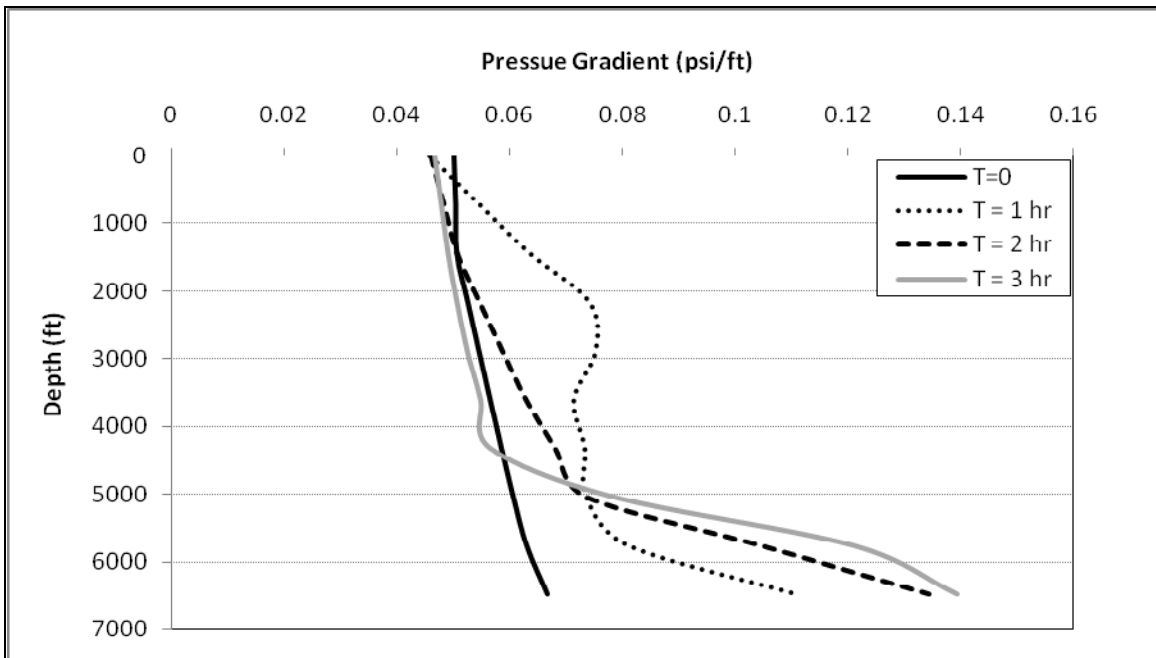


Figure 5.18 Simulated transient pressure gradient profiles in the wellbore during a buildup test (Wellbore depth is 7200 ft and the tubing diameter is 0.125 ft. The well is shut in at the surface)

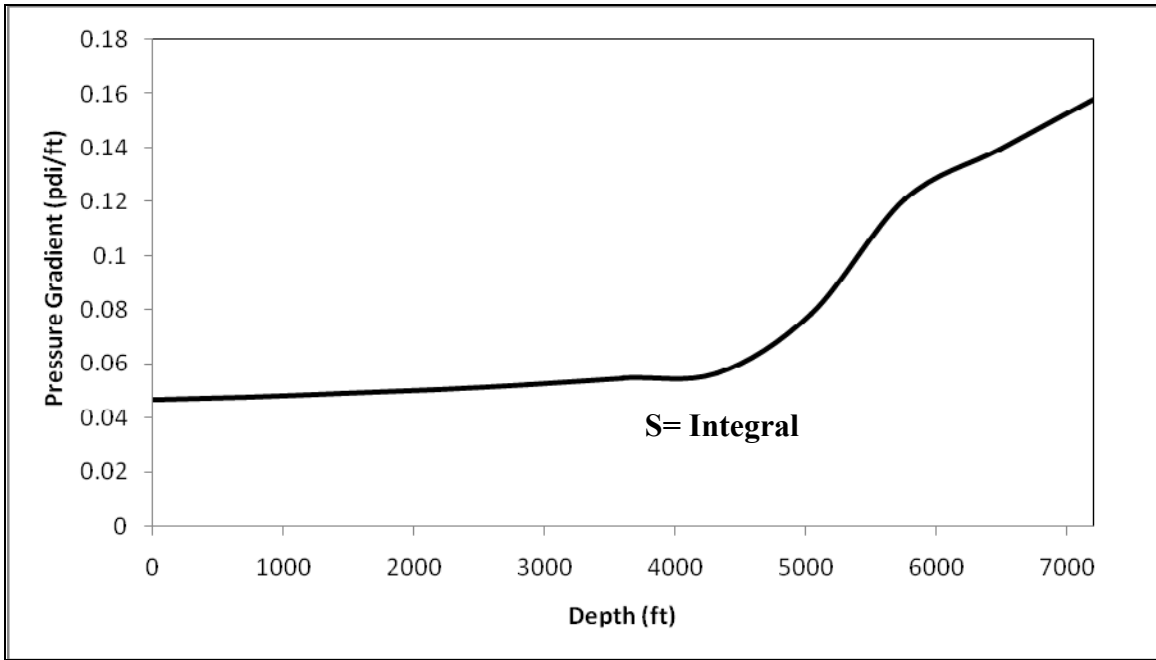


Figure 5.19 Simulated pressure gradient profile at T= 3 hr during a buildup test (The S area is used to calculate bottomhole pressure from the recorded surface pressure)

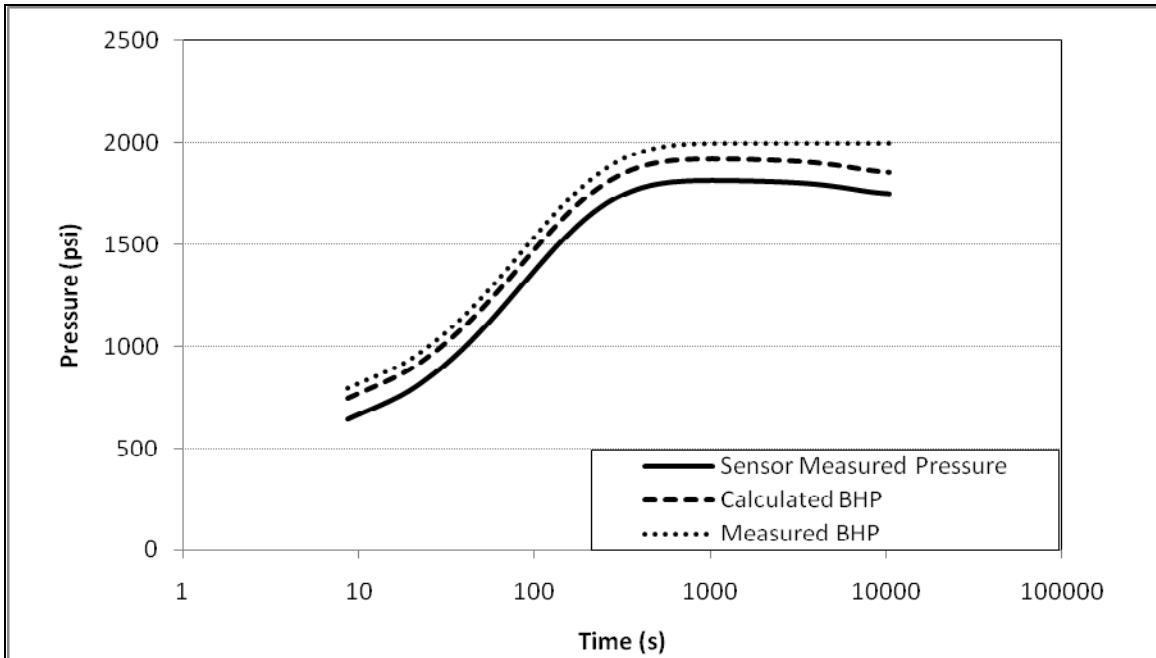


Figure 5.20 Calculated bottomhole pressure profile from measured pressure when recorder sensor is located at the depth equal to 5400 ft in the wellbore

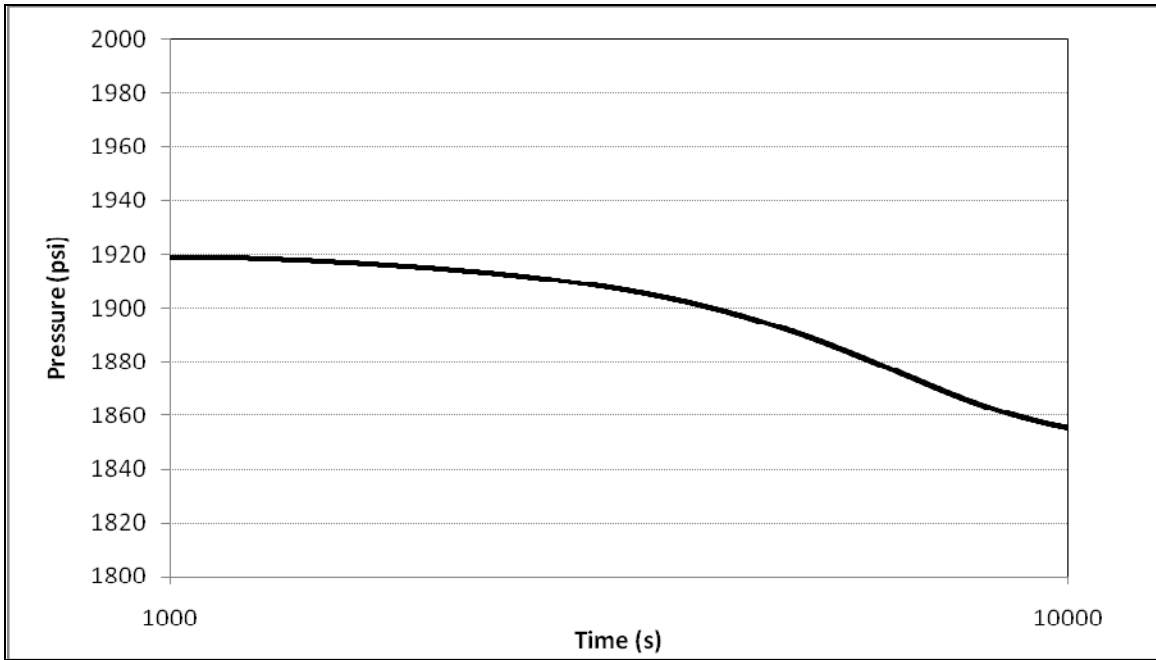


Figure 5.21 Semilog plot used to analyze buildup test when bottomhole pressure profile is calculated from recorded pressure at the depth equal to 5400 ft in the wellbore

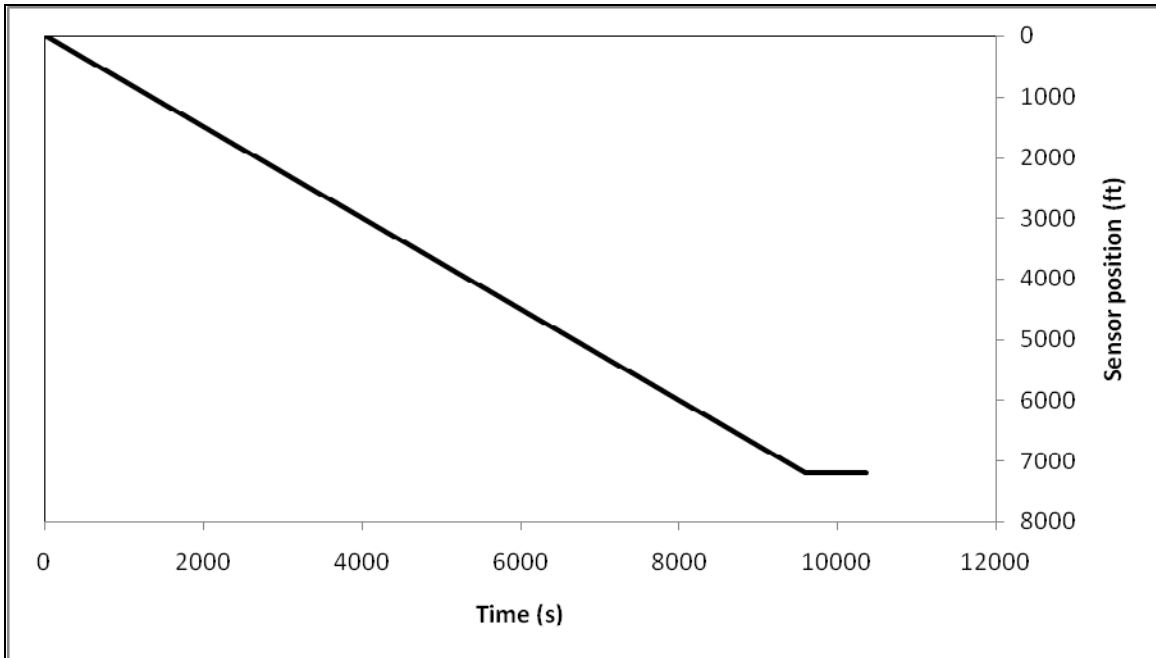


Figure 5.22 Transient pressure sensor position when pressure recorder is lowered into the wellbore from the surface to the sandface

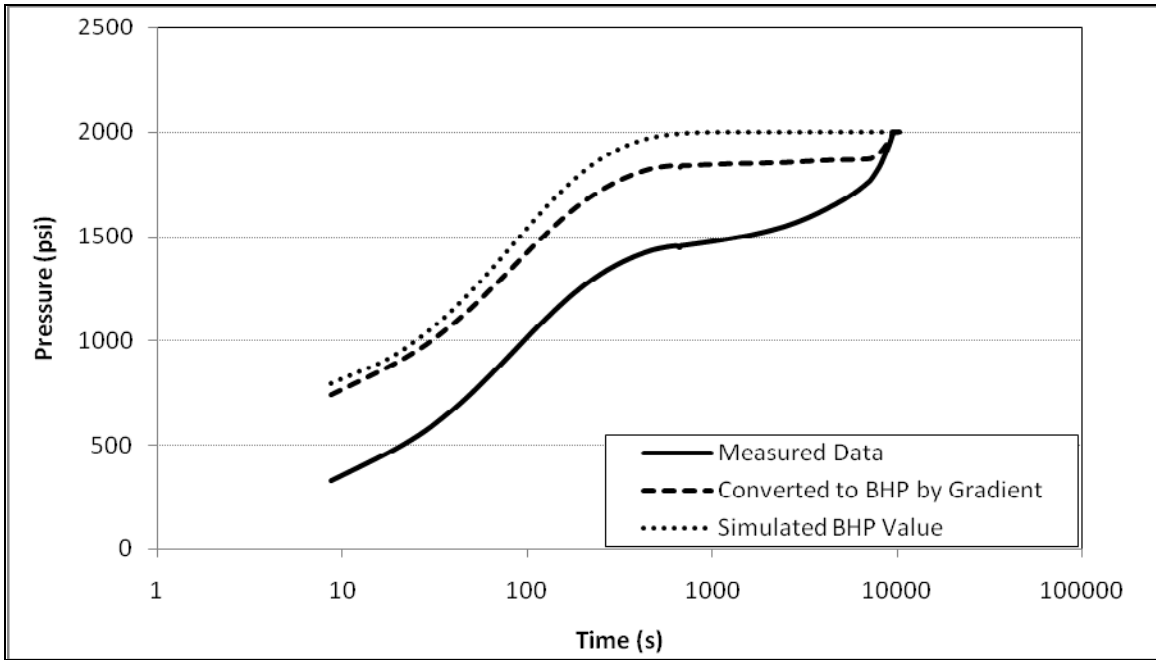


Figure 5.23 Calculated bottomhole pressure profile from measured pressure when recorder sensor is lowered from the wellbore surface to the perforation zone

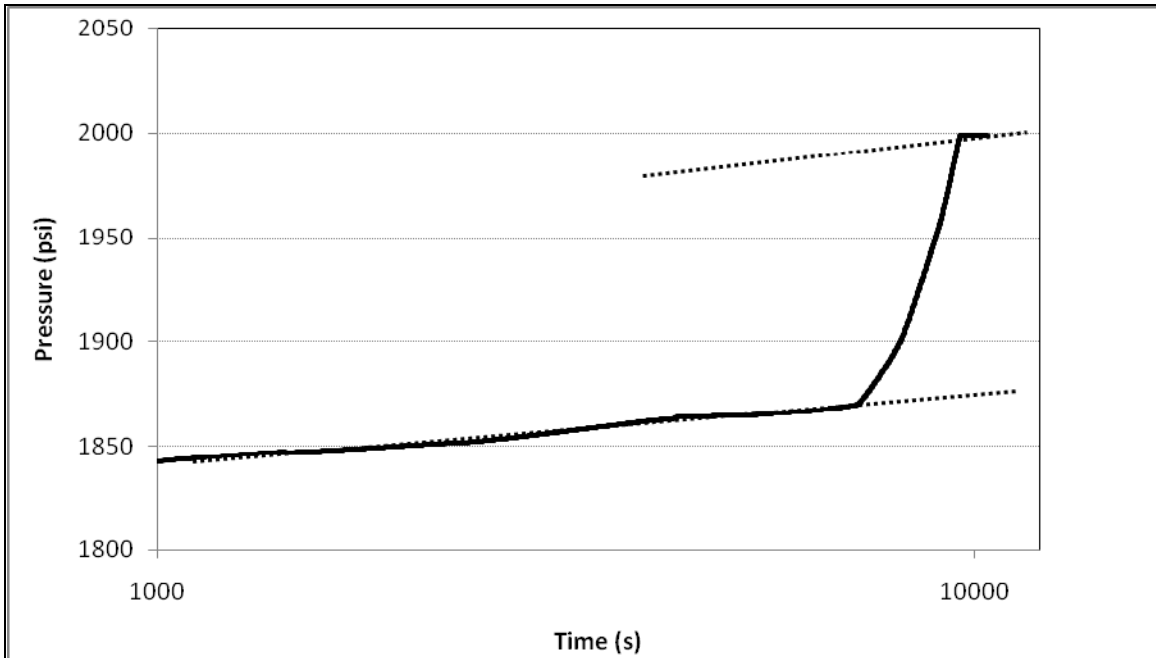


Figure 5.24 Semilog plot used to analyze buildup test when bottomhole pressure profile is calculated from recorded pressure by a moving sensor

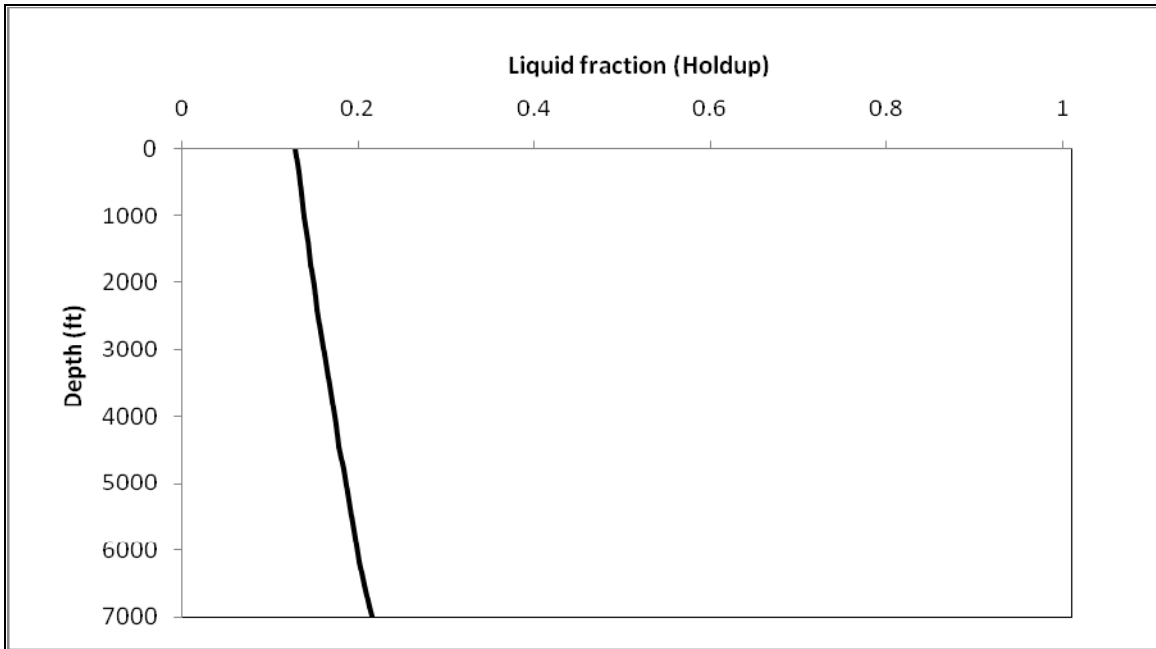


Figure 5.25 Simulated liquid fraction profile when well flows at steady rate before shut in (Wellbore depth is 7200 ft and the tubing diameter is 0.125 ft. Well produces 1500 lbm. mole/D hydrocarbon, the composition consists of 0.57 C1, 0.09 C3, 0.09 C6, 0.11 C10, 0.12 C15 and 0.02 C20)

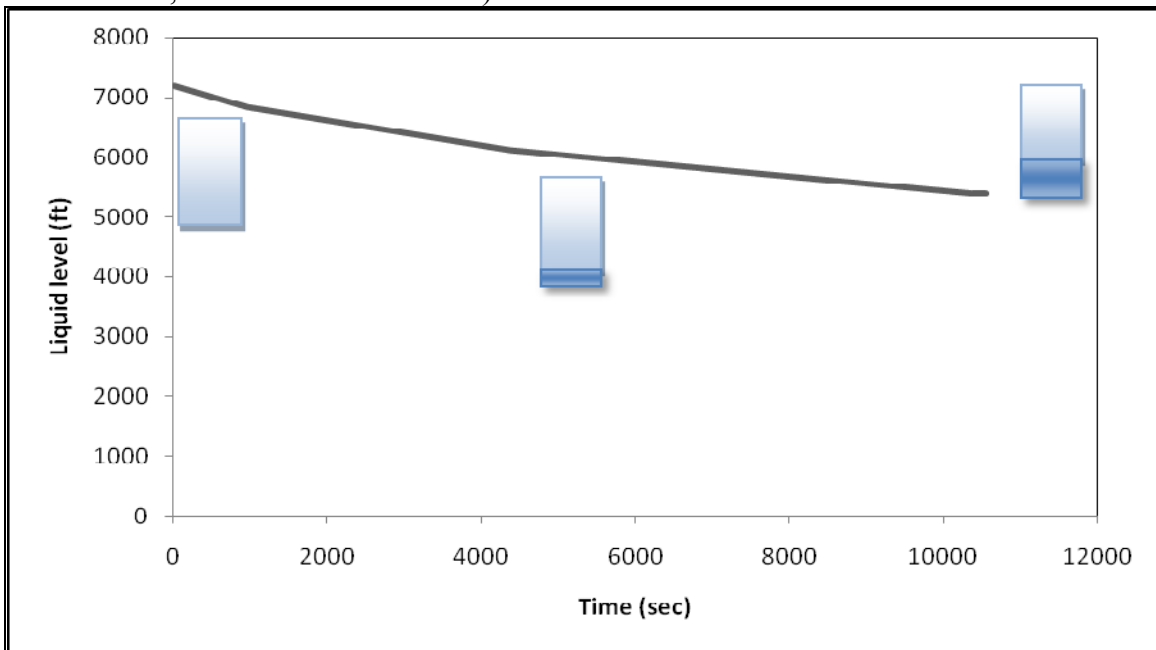


Figure 5.26 Simulated liquid level history profile in the wellbore during buildup test (Wellbore depth is 7200 ft and the tubing diameter is 0.125 ft. Well produces 1500 lbm.mole/D hydrocarbon before shut in, the composition consists of 0.57 C1, 0.09 C3, 0.09 C6, 0.11 C10, 0.12 C15 and 0.02 C20)

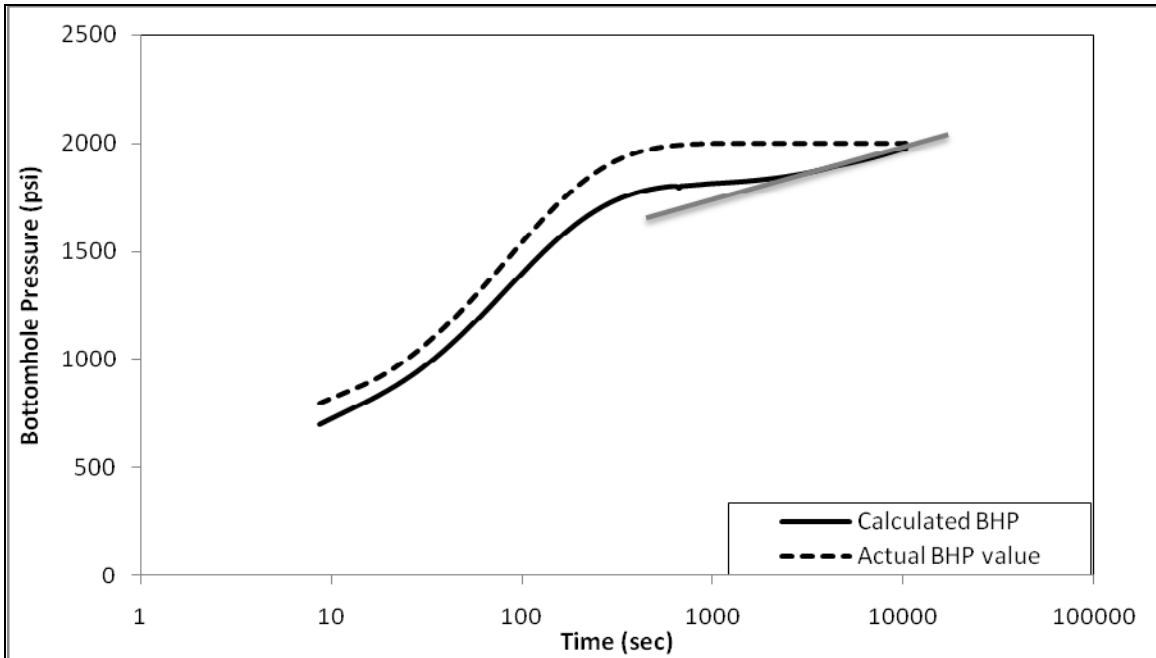


Figure 5.27 Simulated bottomhole pressure profile during a buildup test obtained from liquid level method

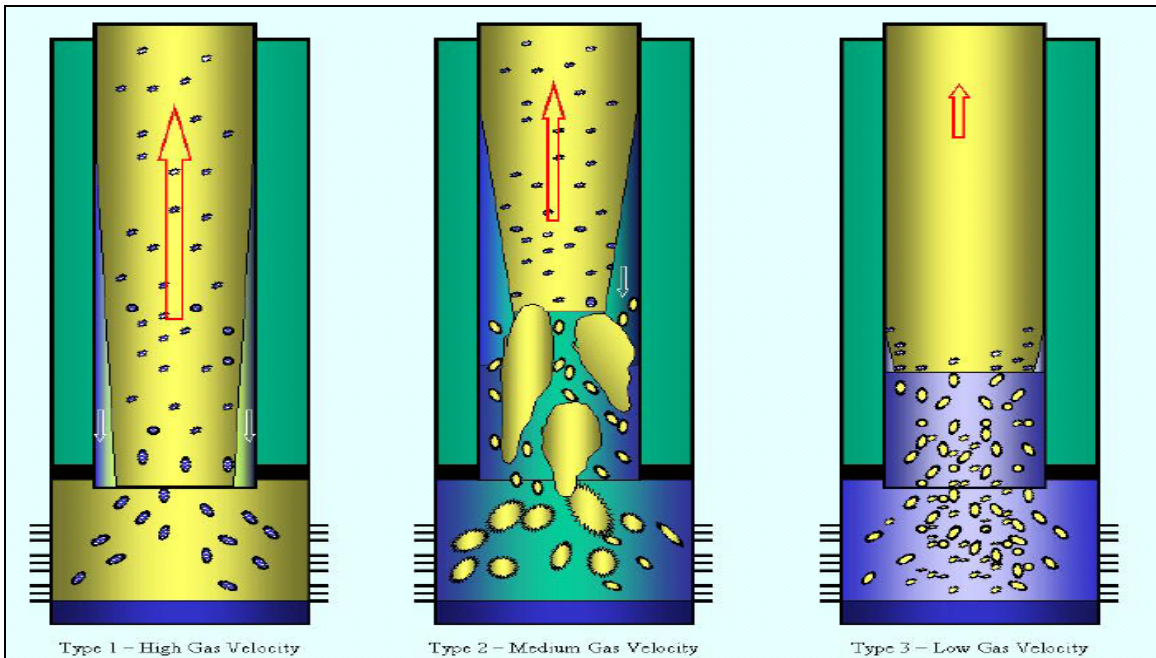


Figure 5.28 The schematic effect of gas velocity on liquid accumulation at the bottom section of a gas well (Type 1- left: High gas velocity, Type 2- middle: Medium gas velocity, Type 3- right: Low gas velocity) (Rowlan et al., 2006)

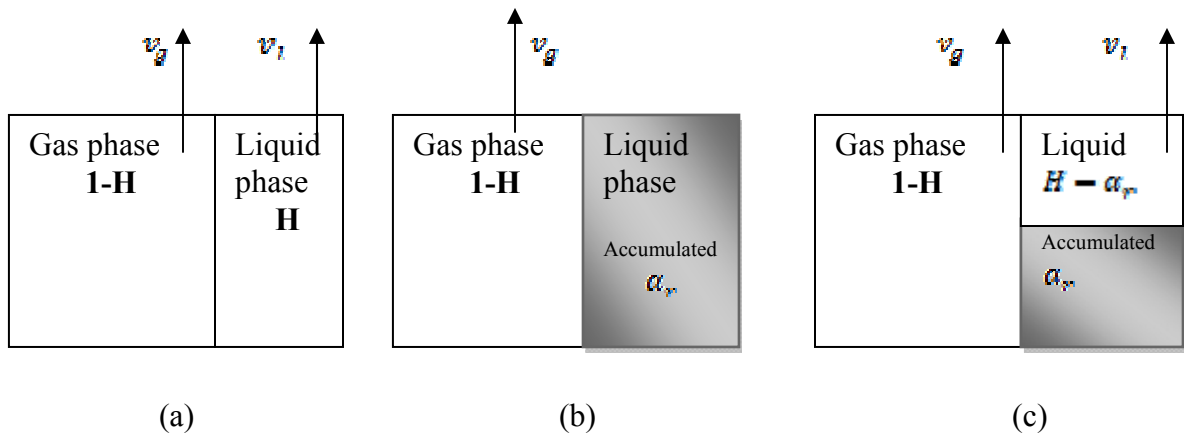


Figure 5.29 Schematic of liquid accumulation in a gridblock (a. Gas and liquid phases move with same velocity, b. Liquid phase velocity is zero, c. Gas moves faster than the liquid phase, the liquid velocity is not zero)

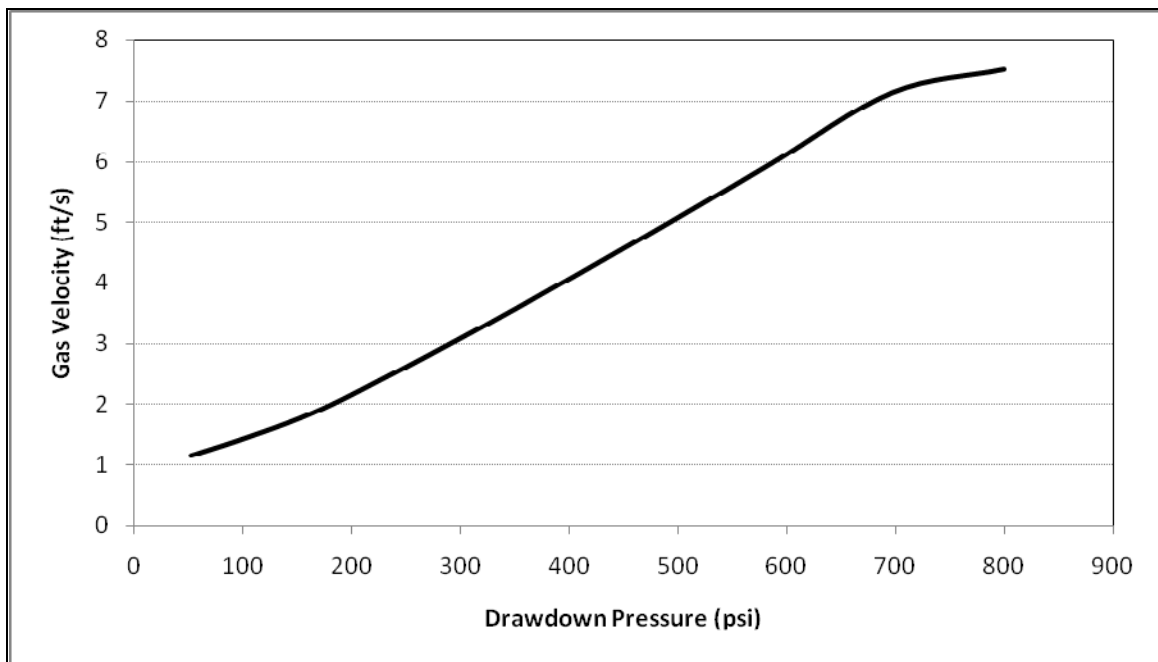


Figure 5.30 Simulated gas velocity at the surface versus pressure difference between reservoir and wellbore

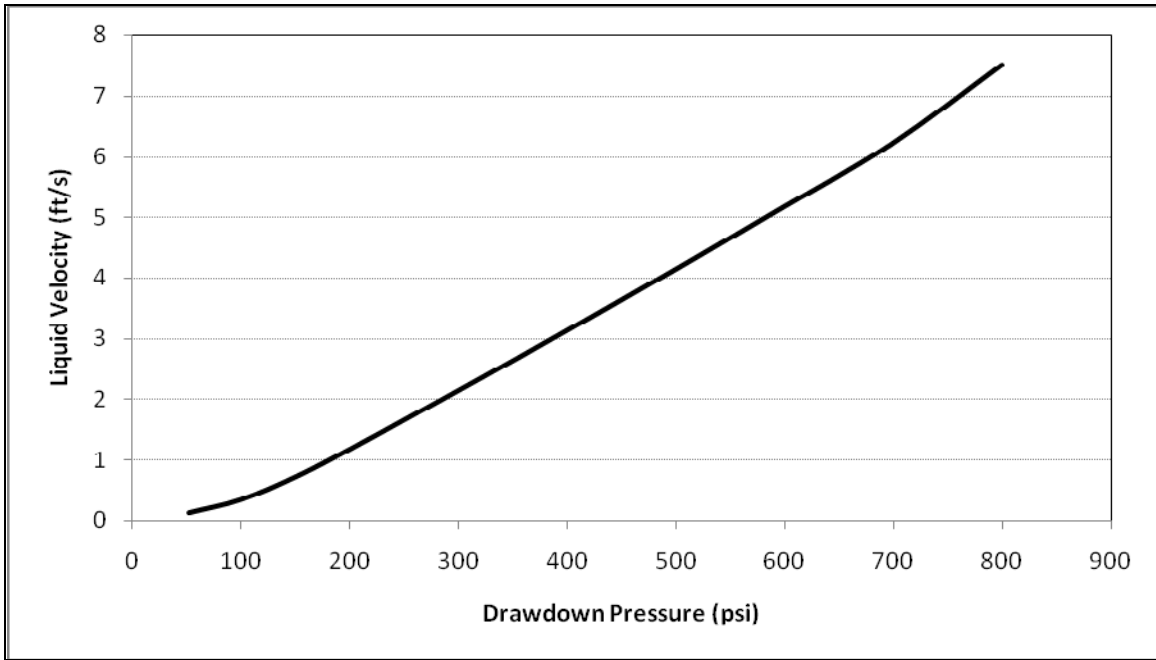


Figure 5.31 Simulated liquid velocity at the surface versus pressure difference between reservoir and wellbore

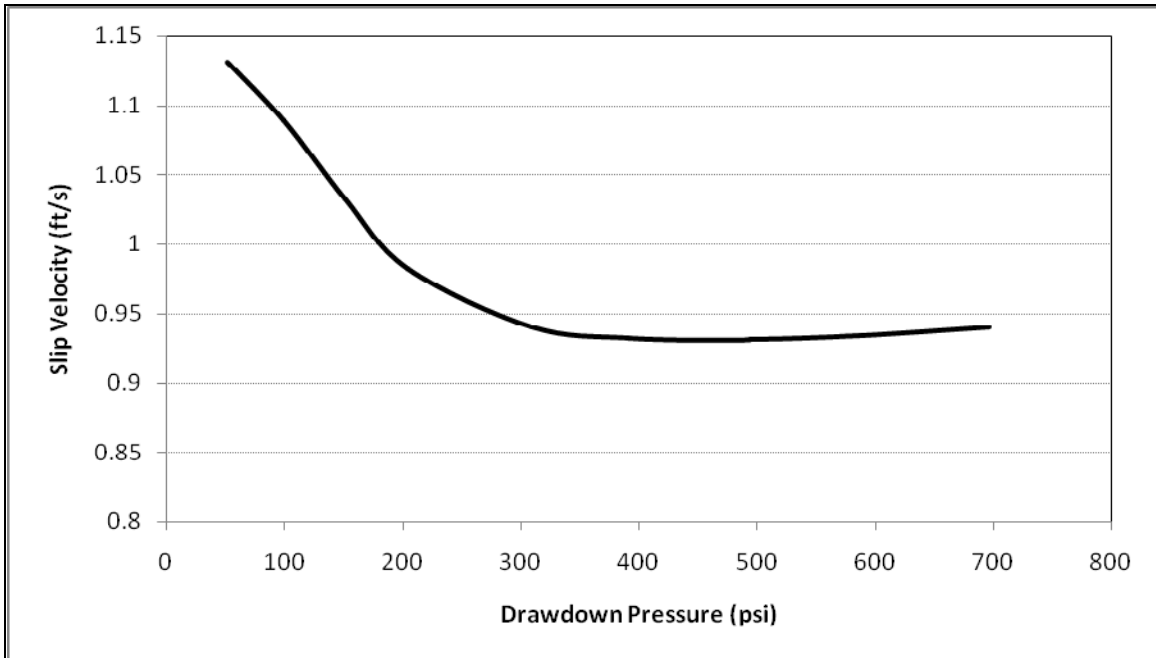


Figure 5.32 Simulated slip velocity at the surface versus pressure difference between reservoir and wellbore

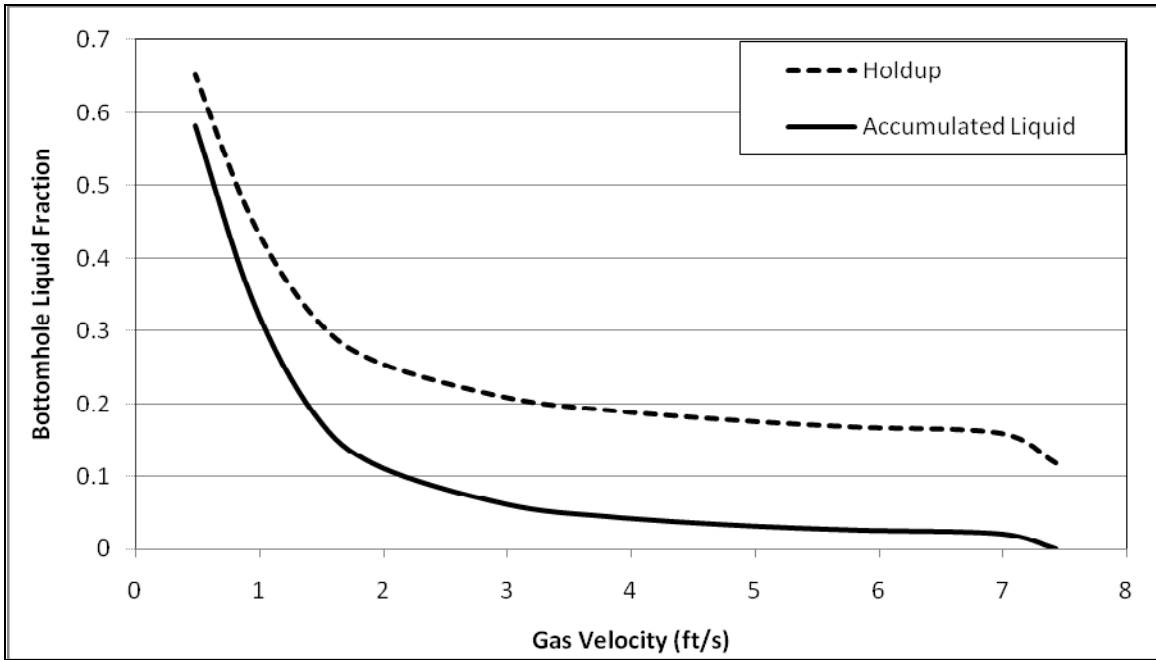


Figure 5.33 Simulated holdup and accumulated liquid fraction profiles versus surface gas velocity

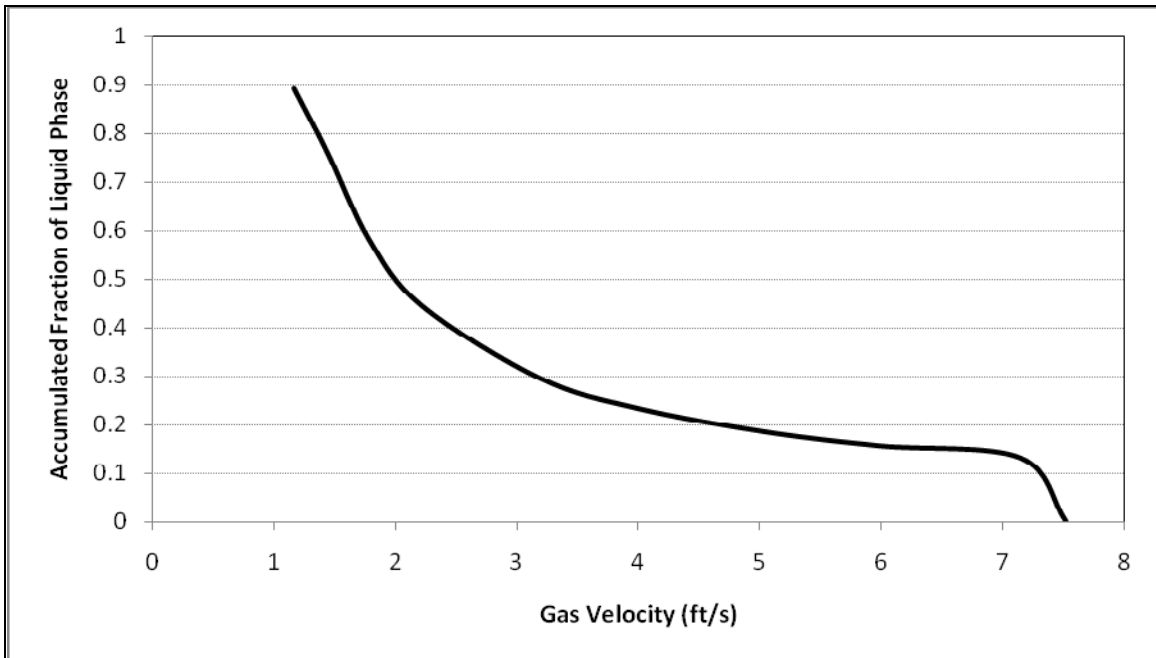


Figure 5.34 Accumulated fraction of liquid phase at the bottom of the wellbore versus surface gas velocity in a liquid loaded gas well

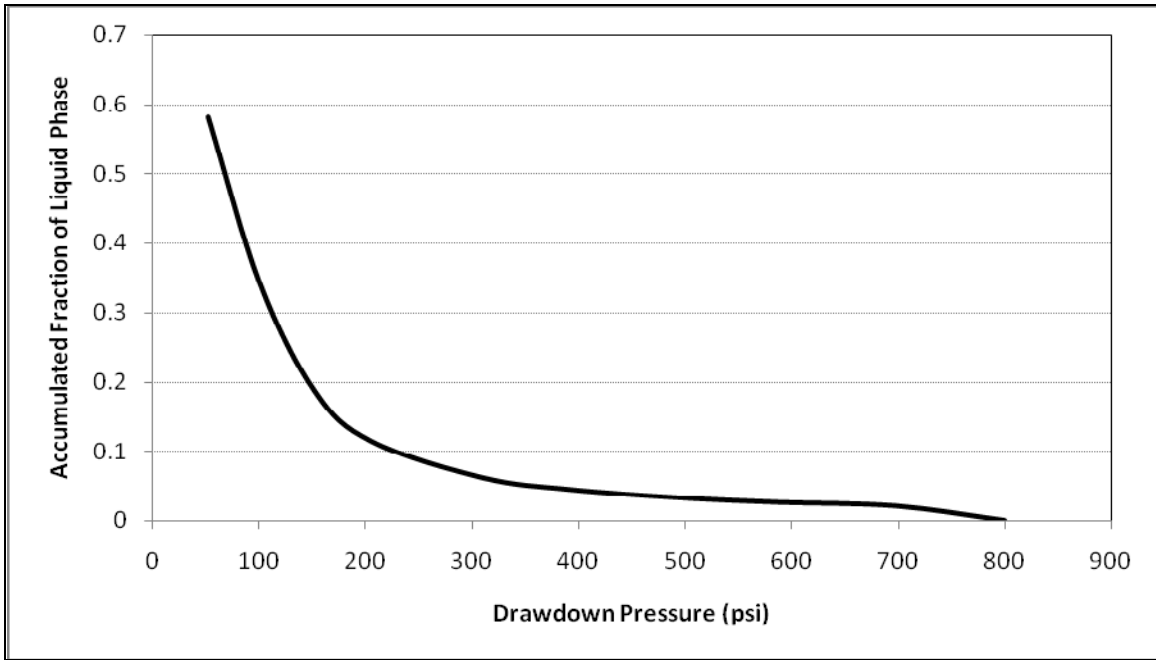


Figure 5.35 Accumulated fraction of liquid phase at the bottom of the wellbore versus pressure difference between wellbore and reservoir in a liquid loaded gas well

Dimensions	560 X 560 X 100
Grid Blocks	7X 7 X 3
Porosity	0.35
Permeability (md)	10
Initial P	2000 Psi
Initial Water Saturation	0.17
Initial Oil Saturation	0.512
Initial Gas Saturation	0.318
Initial Composition:C1,C3,C6,C10,C15,C20	0.57,0.09,0.09,0.11,0.12,0.02

Table 5.1. Reservoir initial parameters

Depth (ft)	7200
Inner tubing radius (ft)	0.125
Outer tubing radius (ft)	0.129
Wellbore radius (ft)	0.425
Inner casing radius (ft)	0.28
Outer casing radius (ft)	0.315
Tubing friction coefficient	0.0006
Surface formation temperature (°F)	76
Formation temperature gradient (°F/ft)	0.006
Formation heat conductivity (Btu/(hr-ft-°F))	1.4
Formation density (lbm/ft ³)	144
Formation heat capacity (Btu/(lbm-°F))	0.22
Cementing heat conductivity (Btu/(hr-ft-°F))	4.02
Annulus brine salinity (ppm)	35000
Bottomhole wellbore temperature (°F)	120
Time step (s)	4
Number of nodes	20
Number of phases	3
Number of components	6
Tolerance for pressure calculation	10 ⁻⁶

Table 5.2. Producer wellbore and solution parameters

Run number	Pressure difference between reservoir and wellbore (psi)	Accumulated fraction of liquid phase
1	800	0
2	697.2	0.021
3	587.1	0.026
4	494.1	0.032
5	391.5	0.044
6	309.6	0.061
7	204.5	0.114
8	151.8	0.186
9	99.7	0.342
10	51.4	0.581

Table 5.3. Accumulated fraction of liquid phase and drawdown pressure at different simulations

CHAPTER 6: SUMMARY, CONCLUSIONS AND RECOMMENDATIONS

6.1 SUMMARY AND CONCLUSIONS

- A new implicit wellbore simulator is developed to model multiphase fluid flow and temperature in a fully coupled wellbore/reservoir system. An equation-of-state, compositional, fully implicit simulator called GPAS is used as the reservoir simulator in this system. It is also possible to use the developed code as a stand-alone simulator for wellbores. This simulator can be applied to steady-state and transient problems.
- The simulator can be used to model steady-state oil and gas production from hydrocarbon reservoirs through wells to the surface. This multiphase flow simulator can model pressure profiles, temperature distributions, phase fractions, phase compositions, and phase velocities in the wellbore from the bottomhole to the surface.
- Whenever the flow in a section of the wellbore/reservoir system is perturbed, transient transfer of mass, momentum, and energy occurs in the wellbore. We can use our simulator to model these transient behaviors in wellbore/reservoir systems. Transient profiles of pressure, temperature, phase fractions, and phase velocities are simulated during any transient problems, such as well testing, using our coupled simulator.

- Two options are available to simulate wellbore fluid flow: using blackoil approximation or a compositional approach. The basic assumption in the blackoil approach is to consider three distinct phases: gas, oil, and water, where oil and gas specific gravity are assumed to be constant in the wellbore. On the other hand, the term “compositional” implies that the in-situ fluid composition may vary point by point in the wellbore as a function of pressure, temperature, and slip between phases. To the best of our knowledge, the compositional modeling of multi-phase/multi-component fluid flow in vertical wellbores has not been presented in literature.
- A mathematical description of multiphase flow in our coupled simulator involves coupling the wellbore flow equations with the reservoir fluid flow governing equations by using well models which is discussed in Appendix B. Wellbore governing equations consist of conservation of mass for each phase, conservation of momentum for liquid and gas and energy balance. These equations are coupled to reservoir equations, which consist of component-mass balance equations, phase equilibrium equations, equations constraining phase saturation and component concentrations, and energy balance equations.
- For a vertical case, the wellbore is divided into gridblocks in z direction. The fluids may communicate between reservoir and wellbore gridblocks through perforation zones. Governing equations are discretized using finite difference approximation and form a set of consistent equations where wellbore primary variables are phase velocities, phase fractions, pressure, and temperature. The

non-linear set of equations is solved by Newton's method using Petsc software available from Argonne National Laboratories.

- Steady state case studies were performed using this simulator; the simulated results were in good agreement with field data in different flow regimes such as bubble, slug, churn and annular flow.
- The transient simulation results of the new model were compared with the field data for pressure gradients and temperature distribution obtained from wireline conveyed pressure recorder and acoustic fluid level measurements for a gas/oil producer well during a buildup test. The transient pressure profiles were in good agreement with the field data. The computational results for transient temperature also matched the field data.
- During production or injection, temperature of the flowing fluid may vary along the wellbore due to heat exchange with surrounding formations, which adds complexity to the wellbore dynamics. We use our steady-state simulator to study the effects of production parameters such as flow rate, gas oil ratio, water oil ratio and wellbore parameters such as tubing geometry on the temperature profile in the wellbore. Our simulations show that some parameters such as well geometry and liquid flow rate, have the most noticeable effect on wellbore fluid temperature distribution.
- We used our simulator to answer questions about the validity of using blackoil approximation for wellbore fluid flow modeling. Comparisons were made between compositional and blackoil approaches to study the importance of

compositional modeling. Our simulations showed that during production of gas condensate and volatile oil, the difference between bottomhole pressure profiles estimated by compositional and blackoil approaches was noticeable; hence we recommend using the compositional approach for such cases. Results using blackoil approximation does not show significant difference from compositional approach results for temperature distribution in the different case studies.

- The presence of wellbore transients must be taken into consideration during a pressure transient analysis. The wellbore effects can mask the reservoir responses and make the well test results unreliable. Our transient coupled simulator can be used to model wellbore dynamics during transient problems such as well testing analysis. The simulations show phase segregation, counter-current flow and transient backflow during transient tests in a multiphase reservoir/wellbore system. Our model also shows how the temperature profiles change during a pressure transient test such as buildup test.
- Another important wellbore-related effect is pressure data measurements in wellbores. All of the well testing theories are based on the analysis of pressure at the producing zones. Due to downhole completion restrictions, pressure is recorded above the perforation zones and is then converted to bottomhole pressure. We investigated the effect of pressure gauge placement and pressure conversion methods on well testing analysis accuracy. We recommend using a transient wellbore simulator to correctly convert recorded pressure to bottomhole pressure when it is not possible to place the pressure gauge as close as possible to

the perforations. Neglecting transient effects for this conversion causes anomalies that can be easily misinterpreted as reservoir characteristics results.

- Liquid may accumulate at the bottom sections of gas wells during productions, which can reduce the gas flow rate. We used our simulator to predict this accumulation based on the drawdown pressure and gas velocity. This tool can be used to develop methods to remove the accumulated liquid and redesign the flow string size in wellbores.

6.2 RECOMMENDATIONS

- In this research, we developed transient and steady-state models for vertical or near vertical wells coupled to a reservoir system. There is a noticeable desire to drill and complete horizontal and deviated wells to improve reservoir productivity. We recommend extending the ability of the developed simulator to model fluid flow in horizontal and deviated wells. Hence, the coupled reservoir/wellbore can be used to model fluid exchange between reservoir layers and different types of wells. It can also be modified to model temperature distribution during hot or cold fluid injection into deviated or horizontal wells.
- In the current wellbore/reservoir simulator, we use the same size gridblocks in the wellbore as the gridblocks located next to the wellbore in the reservoir simulator. To make the results more accurate, we recommend modifying the gridding near the wellbore. Due to the complexity of multiphase flow near the wellbore, it is more accurate to use finer grids in this section. We recommend development of

unstructured grid for the reservoir simulator to overcome the above mentioned problem.

- We further recommend using radial gridblocks inside the wellbore. In our development, we have assumed that the fluids flow in only z direction in the wellbore, hence, the fluid velocity and temperature do not change in the radial direction inside the tubing. For future developments, we can add radial gridblocks inside the tubing to handle fluid flow and energy exchange from the reservoir more accurately.
- Hydrocarbon may be produced from different layers in the reservoir through wellbores. We can use our simulator as a tool to analyze the fluid flow from the different layers to estimate near wellbore reservoir properties such as permeability and porosity.

APPENDIX A: CORRELATIONS USED IN BLACKOIL MODELING

A.1 BLACKOIL FLUID CORRELATIONS

In a blackoil system, we use correlations to calculate fluid-flow properties such as density. In the proposed pressure change model, we used correlations for density, viscosity, solution of dissolved gas-oil ratio, and the formation factor, which are discussed below.

Solution of dissolved gas-oil ratio:

The Standing's correlation (Standing, 1947) is used to estimate the dissolved gas-oil ratio for saturated oils, as follows:

$$R_s = \gamma_g \left(\frac{P}{18 \times 10^{y_g}} \right)^{1.204} \quad (\text{A.1})$$

where

γ_g = Gas gravity (air =1)

y_g = Gas mole fraction = $0.00091T - 0.0125\gamma_{API}$

T = Reservoir temperature, °F

Formation volume factor:

For oil formation volume factor calculations, the Standing's correlation for saturated oil systems is used in our model, as follows:

$$B_o = 0.972 + 0.000147F^{1.175} \quad (\text{A.2})$$

where

$$F = \text{Correlating function} = R_s \left(\frac{\gamma_g}{\gamma_{osc}} \right) 0.5 + 1.25T$$

$$B_o = \text{Oil formation volume factor RB/STB}$$

The gas formation volume factor is defined by

$$B_g = \frac{\rho_{gsc}}{\rho_g y_g} \quad (\text{A.3})$$

where ρ_{gsc} and ρ_g are the gas-phase molar densities at standard and reservoir conditions, respectively, and y_g is the mole fraction of the gas at the surface.

Liquid and gas viscosities:

Correlations to estimate the oil viscosity are usually two-step procedures. First, the gas-free oil viscosity is estimated, and then the gas-saturated oil viscosity is computed. For the first step, we use Egbogah and Ng correlations (Egbogah et al., 1983) as

$$\log\{\log(\mu_{oD} + 1)\} = 1.8653 - 0.025086\gamma_{API} - 0.5644\log(T) \quad (\text{A.4})$$

where μ_{oD} is the gas-free oil viscosity at 14.7 psia. The Beggs and Robinson correlation (Beggs et al., 1975) can then be used as

$$\mu_o = A\mu_{oD}^B \quad (\text{A.5})$$

where

$$A = 10.715(R_s + 100)^{-0.515}$$

$$B = 5.44(R_s + 150)^{-0.338}$$

The water viscosity at atmospheric pressure can be estimated from McCain's equation (McCain, 1990). The gas viscosity can be also estimated using the method of Lee et al. (1966). The procedure for these two methods can be found in Walsh et al. (2003) in more detail.

A.2 THERMAL PARAMETERS CALCULATION

We need to calculate the flow thermal parameters, such as heat capacity, to use in the energy equation solution. We provide equations to compute values of specific heat capacities for fluids for ranges of pressure and temperature typically expected in the wellbore. We calculate the specific capacity of the mixture of fluids from the heat capacity of water, oil, and natural gas.

Water Heat Capacity:

The specific heat capacity of water is well known for a wide range of temperature and pressure based on the data measured by Holman (1958). For temperatures between 20°C and 290°C specific heat capacity is given by

$$c_{Pw(J/Kg.K)} = \frac{4245 - 1.841T}{\rho_w} \quad (A.6)$$

At temperatures higher than 290°C, Somerton (1992) proposed that

$$c_{Pw(J/Kg.K)} = \frac{3703}{\rho_w} e^{-\{0.00481(T-290)+0.000234(T-290)^2\}} \quad (A.7)$$

Oil Heat Capacity:

Gambill (1957) presented equations to calculate the oil-specific heat capacity as a function of temperature and oil-specific gravity. In our research, we used the following equation:

$$c_{p,oil(J/Kg.K)} = \frac{1684 + 3.389T}{\sqrt{\gamma_{oil}}} \quad (A.8)$$

Gas Heat Capacity:

The specific heat capacity of natural gas is considered based on the measurements done by Somerton (1992). The specific heat capacity of natural gas generally increases with both increasing temperature and increasing pressure. The temperature dependence of the specific heat capacity of natural gas can be described using a fourth-order polynomial (Walpes et al., 2004) as follows:

$$c_p = AT^4 + BT^3 + CT^2 + DT + E \quad (A.9)$$

In order to simplify inclusion of pressure in the heat capacity calculation, each of the coefficients in Equation A.9 was expressed as a third-order polynomial. In these equations, T is in °F, P is in psi, and heat capacity is in BTU/lbm.°F. For example, the following polynomials are used for methane:

$$A(P) = -2.52 \times 10^{-22} P^3 + 1.34 \times 10^{-18} P^2 + -9.15 \times 10^{-16} P + 1.62 \times 10^{-13} \quad (A.10)$$

$$B(P) = 5.37 \times 10^{-19} P^3 - 2.85 \times 10^{-15} P^2 + 1.37 \times 10^{-12} P - 4.67 \times 10^{-10} \quad (A.11)$$

$$C(P) = -3.47 \times 10^{-16} P^3 + 1.86 \times 10^{-12} P^2 + 2.01 \times 10^{-11} P + 3.95 \times 10^{-17} \quad (A.12)$$

$$D(P) = 7.70 \times 10^{-14} P^3 - 4.21 \times 10^{-10} P^2 - 5.96 \times 10^{-7} P + 3.70 \times 10^{-4} \quad (A.13)$$

$$E(P) = -1.03 \times 10^{-11} P^3 + 5.24 \times 10^{-8} P^2 + 1.55 \times 10^{-4} P + 4.88 \times 10^{-1} \quad (\text{A.14})$$

APPENDIX B: WELL MODEL

B.1 INTRODUCTION

As we previously discussed, our wellbore simulator is coupled to a compositional reservoir simulator by a well model. Well models are general equations that relate fluid flow and between the reservoir and the wellbore, and pressure. In general, a functional relation between the well rates and flowing bottomhole pressures is required to couple both reservoir and wellbore models. In our simulator, the well models based on Peaceman (1991) and Babu et al. (1991) are provided to relate the controlled variables for the reservoir to the wellbore. Different basic well conditions can be handled in our model, such as:

- Constant bottomhole flowing pressure injector
- Constant molar rate injector
- Constant volume rate injector
- Constant bottomhole flowing pressure producer
- Constant molar rate production wells
- Constant volume oil rate production wells

Generally, the relationship between volumetric flow rate, flowing bottomhole pressure, and gridblock pressure is expressed as

$$Q_j = PI_j (P_{wf} - P_j) \tag{B.1}$$

where PI_j is the phase productivity index for phase j . Chang (1990) showed that for a one-dimensional case simulation the productivity index can be expressed as a function of gridblock permeability, and size as follows:

$$PI_j = \frac{\sqrt{k_x k_y} \Delta z \lambda_{rj}}{25.15 \ln\left(\frac{r_o}{r_w}\right)} \quad j = 1, \dots, n_p \quad (\text{B.2})$$

This equation is valid for a well completed parallel to the z direction. The same productivity index is defined for a well completed parallel to the y direction. In this equation, permeabilities in the x and z directions (k_x and k_z) are used:

$$PI_j = \frac{\sqrt{k_x k_z} \Delta y \lambda_{rj}}{25.15 \ln\left(\frac{r_o}{r_w}\right)} \quad j = 1, \dots, n_p \quad (\text{B.3})$$

where $\Delta z, \Delta y$ are gridblock sizes (ft) in z and y directions, respectively. λ_{rj} is the relative mobility in cp^{-1} . For rectangular well blocks in anisotropic reservoirs, an equivalent radius is defined based on the well block dimensions. If the well is completed parallel to the z axis (vertical well), then

$$r_o = 0.28 \frac{\left[\left(\frac{k_y}{k_x} \right)^{\frac{1}{2}} \Delta x^2 + \left(\frac{k_x}{k_y} \right)^{\frac{1}{2}} \Delta y^2 \right]^{\frac{1}{2}}}{\left(\frac{k_y}{k_x} \right)^{\frac{1}{4}} + \left(\frac{k_x}{k_y} \right)^{\frac{1}{4}}} \quad (\text{B.4})$$

Then, same equation is used for a horizontal well parallel to the y axis

$$r_o = 0.28 \frac{\left[\left(\frac{k_z}{k_x} \right)^{\frac{1}{2}} \Delta x^2 + \left(\frac{k_x}{k_z} \right)^{\frac{1}{2}} \Delta z^2 \right]^{\frac{1}{2}}}{\left(\frac{k_z}{k_x} \right)^{\frac{1}{4}} + \left(\frac{k_x}{k_z} \right)^{\frac{1}{4}}} \quad (\text{B.5})$$

For equivalent radius equations, we assume that the grid spacing and permeability in different directions are uniform (i.e., constant Δx , Δz , k_x , and k_z).

B.2 CONSTANT FLOWING BOTTOMHOLE PRESSURE INJECTOR

With this criterion, the flowing bottomhole pressure for one reference point in the bottomhole is known. The objective is to compute pressure at different perforation zones in the wellbore and also component flow rate and phase flow rate into each layer of the reservoir. The following steps show the procedure of this calculation:

1) The flowing bottomhole pressure at each perforation layer is given based on the reference pressure. The method for calculation pressure change is discussed in Chapter 2. As a very simple assumption, we can neglect friction and acceleration terms in pressure change equations, and only consider pressure change with gravity. By this assumption, pressure at layer z , P_{wfs} is

$$P_{wfs} = P_{wf,ref} - \gamma_{inj}(z - z_{ref}) \quad (\text{B.6})$$

where $P_{wf,ref}$ is the known bottomhole pressure at location z_{ref} . γ_{inj} is the specific weight of the injected fluid at the well pressure.

2) The injected fluid consists of two parts: a water phase with fraction equal to f_1 , and a hydrocarbon phase. At layer z , the hydrocarbon component flow rates are calculated by

$$(q_i)_z = [1 - f_1]z_i(q_t)_z \quad \text{for } i=1, \dots, n_c \quad (\text{B.7})$$

and for water phase,

$$(q_{nc+1})_z = f_1(q_t)_z \quad (\text{B.8})$$

where $(q_t)_z$ is the total flow rate into layer z

$$(q_t)_z = \frac{(Q_t)_z}{(v_t)_{inj}} \quad (\text{B.9})$$

where $(Q_t)_z$ is the total volumetric flow rate into layer z

$$(Q_t)_z = \sum_{j=1}^{np} (PI_j)_z [(P_{wf})_z - (P_j)_z] \quad (\text{B.10})$$

and

$$(v_t)_{inj} = \left(\frac{f}{\xi_1} \right) + (1-f) \left[\left(\frac{L_2}{\xi_2} \right)_{inj} + \left(\frac{L_3}{\xi_3} \right)_{inj} \right] \quad (\text{B.11})$$

where $(\xi_j)_{inj}$ is the molar density of phase j . $j=1$ refers the molar density of water, and when j is 2 or 3, the molar density of oil and gas phases are considered, respectively.

$(L_j)_{inj}$ is a ratio of moles in hydrocarbon phase j to the total number of hydrocarbon moles in the injection fluid.

B.3 CONSTANT MOLAR RATE INJECTOR

In this case, the main criterion is the constant total molar rate q_t . Initially, we calculate the molar flow rate into each layer, and then calculate pressure distribution near the perforated zones in layers. We define molar flow rate for each component as

$$q_i = [1 - f_1](z_i)_{inj} q_t \quad \text{for } i=1, \dots, n_c \quad (\text{B.12})$$

for water phase, and

$$q_{n_c+1} = f_1 q_t \quad (\text{B.13})$$

Nolen and Berry (1972) showed that in simulating multiple layer reservoirs, the total injection rates can be allocated to the individual layers, according to a total mobility allocation scheme. This can be expressed as the productivity index ratio. Hence,

$$(q_i)_z = \frac{q_i (PI_t)_z}{\sum_{m=z_t}^{z_b} (PI_t)_m} \quad \text{for } i=1, \dots, n_c, n_c+1 \text{ and } z=z_t, \dots, z_b \quad (\text{B.14})$$

where z_t and z_b are the top and bottom layer numbers of a well, respectively. The total productivity index of a layer z is defined as a summation of the productivity index for all phases,

$$(PI_t)_z = \sum_{j=1}^{n_p} (PI_j)_z \quad (\text{B.15})$$

where $\sum_{m=z_t}^{z_b} (PI_t)_m$ is the summation of the total productivity index over all communicating layers for a well in a multi layer reservoir. By knowing each layer molar flow rate, it is possible to compute total volumetric flow rate,

$$(Q_t)_z = \sum_{j=1}^3 (Q_j)_z = (q_t)_z (v_t)_{inj} \quad (\text{B.16})$$

where $(v_t)_{inj}$ is defined as Equation B.11.

The bottomhole pressure is then calculated using the main definition of the productivity index.

$$(P_{wf})_z = P_z + \frac{(Q_t)_z}{(PI_t)_z} \quad (\text{B.17})$$

B.4 CONSTANT VOLUME RATE INJECTOR

The computational procedure for the constant volume rate injector well is very similar to that of a constant molar injection well. We already know that the gas injection rate, Q_g , (Mscf/D) and the water injection rate, Q_w , (STB/D). Also, the hydrocarbon composition of the injected fluid z_i is specified. First, we convert the known hydrocarbon volumetric rates to molar flow rates using the following equation:

$$q_i = 2.636 Q_g (z_i)_{inj} \quad \text{for } i=1, \dots, nc \quad (\text{B.18})$$

Then same equation is applied for water phase.

$$q_{nc+1} = 19.466 Q_w \quad (\text{B.19})$$

The method is exactly the same as constant molar injection model described in Section B.3.

B.5 CONSTANT MOLAR RATE PRODUCTION WELLS

The total molar production rate, q_t , is specified. The total production rate for each layer is calculated using

$$(q_t)_z = \frac{q_t \sum_{j=1}^{np} (\xi_j PI_j)_z}{\sum_{m=zt}^{zb} \sum_{j=1}^{np} (\xi_j PI_j)_m} \quad \text{for } z = z_t, \dots, z_b \quad (\text{B.20})$$

Again, we assume that the total production rates are allocated to the individual layers according to a total mobility allocation scheme.

At each layer, the component rate can be calculated by

$$(q_i)_z = \frac{(q_t)_z \sum_{j=2}^{np} (\xi_j x_{ij} PI_j)_z}{\sum_{j=1}^{np} (\xi_j PI_j)_z} \quad \text{for } i = 1, \dots, n_c \text{ and } z = z_t, \dots, z_b \quad (\text{B.21})$$

and for water phase by

$$(q_{nc+1})_z = \frac{(q_t)_z (\xi_1 PI_1)_z}{\sum_{j=1}^{np} (\xi_j PI_j)_z} \quad \text{for } z = z_t, \dots, z_b \quad (\text{B.22})$$

The volumetric rates and molar rates are related by

$$(Q_t)_z = \frac{(q_t)_z (PI_t)_z}{\sum_{j=1}^{np} (\xi_j PI_j)_z} \quad (\text{B.23})$$

Since we know the volumetric flow production from each layer, the productivity index definition can be used to obtain a pressure profile.

Hence,

$$(P_{wf})_z = P_z + \frac{(Q_t)_z}{(PI_t)_z} \quad (\text{B.24})$$

B.6 CONSTANT FLOWING BOTTOMHOLE PRESSURE PRODUCER

We already know the bottomhole production pressure at a given reference point in the bottom of the wellbore. Knowing this, we can compute a pressure profile at the perforation zones based on the method described in Chapter 2 for pressure change calculation. It is also possible to ignore friction and acceleration, and use Equation B.6 to calculate pressure distribution. The layer component flow rate is calculated by

$$(q_i)_z = \sum_{j=2}^{np} (\xi_j x_{ij} PI_j)_z (P_{wf} - P_j)_z \text{ for } i = 1, \dots, n_c \text{ and } z = z_t, \dots, z_b \quad (\text{B.25})$$

and

$$(q_{nc+1})_z = (\xi_1 PI_1)_z (P_{wf} - P_1)_z \text{ for } z = z_t, \dots, z_b \quad (\text{B.26})$$

B.7 CONSTANT VOLUME OIL RATE PRODUCER

In this case, the oil rate production, Q_o , is specified in STB/D. A flash calculation is performed at separator conditions to determine the molar fraction of oil phase in the produced hydrocarbon fluid using the overall hydrocarbon composition computed by

$$(z_i)_{prod} = \frac{\sum_{m=z_t}^{z_b} \sum_{j=2}^{np} (\xi_j x_{ij} PI_j)_m}{\sum_{m=z_t}^{z_b} \sum_{j=2}^{np} (\xi_j PI_j)_m} \text{ for } i=1, \dots, n_c \quad (\text{B.27})$$

The total molar flow rate is then calculated using

$$q_t = \frac{5.61Q_o}{(L_o)_{prod} (v_o)_{prod}} \frac{\sum_{m=zt}^{zb} \sum_{j=1}^{np} (\xi_j PI_j)_m}{\sum_{m=zt}^{zb} \sum_{j=2}^{np} (\xi_j PI_j)_m} \quad (\text{B.28})$$

The same allocation scheme for constant molar rate production wells is used to compute the layer component rates. The same procedure discussed in section B.5 is used to model pressure profile.

In GPAS, the main well model calculations are performed in the subroutine XWELL, which calls the subroutine WELLRATE and PRDWDEN. The WELLRATE subroutine calculates the molar flow rates and volumetric flow rates of each component, in each layer, and for each well. The productivity index is calculated in the subroutine IWELL. Subroutine WELLBORE is called in the XWELL to do wellbore calculations. With this new subroutine, it is possible to couple the reservoir calculations with the wellbore model. Subroutine WELLBORE calculates pressure profile, phase velocities, phase fractions, composition, and temperature distribution in wellbores.

APPENDIX C: DISCRETIZED GOVERNING EQUATIONS FOR BLACKOIL FLUID-FLOW IN THE WELLBORE

The discretized wellbore continuity equations for oil, water, and gas are given as

$$\frac{\rho^{n+1}{}_{o,i} H_i^{n+1} (1 - f_i^{n+1}) - \rho^n{}_{o,i} H_i^n (1 - f_i^n)}{\Delta t} + \frac{\rho^n{}_{o,i+1/2} v_{o,i+1/2}^{n+1} H_{i+1/2}^{n+1} (1 - f_{i+1/2}^{n+1}) - \rho^n{}_{o,i-1/2} v_{o,i-1/2}^{n+1} H_{i-1/2}^{n+1} (1 - f_{i-1/2}^{n+1})}{\Delta z} + \frac{m^n{}_{o,i}}{A(\Delta z)} = 0 \quad (C.1)$$

$$\frac{\rho^{n+1}{}_{w,i} H_i^{n+1} f_i^{n+1} - \rho^n{}_{w,i} H_i^n f_i^n}{\Delta t} + \frac{\rho^n{}_{w,i+1/2} v_{w,i+1/2}^{n+1} H_{i+1/2}^{n+1} f_{i+1/2}^{n+1} - \rho^n{}_{w,i-1/2} v_{w,i-1/2}^{n+1} H_{i-1/2}^{n+1} f_{i-1/2}^{n+1}}{\Delta z} + \frac{m^n{}_{w,i}}{A(\Delta z)} = 0 \quad (C.2)$$

$$\frac{\{\rho^{n+1}{}_{g,i} (1 - H_i^{n+1}) + \rho_{o,i}^{n+1} R_s^{n+1} H_i^{n+1} (1 - f_i^{n+1})\} - \{\rho^n{}_{g,i} (1 - H_i^n) + \rho_{o,i}^n R_s^n H_i^n (1 - f_i^n)\}}{\Delta t} + \frac{\{\rho_{g,i+1/2}^{n+1} v_{g,i+1/2}^{n+1} (1 - H_{i+1/2}^{n+1}) + \rho_{o,i+1/2}^{n+1} v_{o,i+1/2}^{n+1} R_s^{n+1} H_{i+1/2}^{n+1} (1 - f_{i+1/2}^{n+1})\} - \{\rho_{g,i-1/2}^{n+1} v_{g,i-1/2}^{n+1} (1 - H_{i-1/2}^{n+1}) + \rho_{o,i-1/2}^{n+1} v_{o,i-1/2}^{n+1} R_s^{n+1} H_{i-1/2}^{n+1} (1 - f_{i-1/2}^{n+1})\}}{\Delta z} + \frac{m^{n+1}{}_{g,i} + R_s^{n+1} m^{n+1}{}_{o,i}}{A(\Delta z)} = 0 \quad (C.3)$$

In the above equations,

f = Water fraction in liquid phase

H = Holdup

The finite difference form for the liquid and gas momentum equations becomes:

$$\frac{(\rho_{l,i}^{n+1} v_{l,i}^{n+1} H_i^{n+1} - \rho_{l,i}^n v_{l,i}^n H_i^n)}{\Delta t} + \frac{\rho_{l,i+1/2}^{n+1} (v_{l,i+1/2}^{n+1})^2 H_{i+1/2}^{n+1} - \rho_{l,i-1/2}^{n+1} (v_{l,i-1/2}^{n+1})^2 H_{i-1/2}^{n+1}}{\Delta z} + H_i^{n+1} \rho_l^{n+1} g \sin \theta + H_i^{n+1} \frac{P_{i+1}^{n+1} - P_i^{n+1}}{\Delta z} + \left(\frac{dP}{dz}\right)_{i,wall,friction} + \left(\frac{dP}{dz}\right)_{i,int\,erphase} = 0 \quad (C.4)$$

$$\begin{aligned}
& \frac{\{\rho_{g,i}^{n+1} v_{g,i}^{n+1} (1-H_i^{n+1}) - \rho_{g,i}^n v_{g,i}^n (1-H_i^n)\}}{\Delta t} + \frac{\rho_{g,i+1/2}^{n+1} (v_{g,i+1/2}^{n+1})^2 (1-H_{i+1/2}^{n+1})}{\Delta z} \\
& - \frac{\rho_{g,i-1/2}^{n+1} (v_{g,i-1/2}^{n+1})^2 (1-H_{i-1/2}^{n+1})}{\Delta z} + (1-H_i^{n+1}) \rho_g^{n+1} g \sin \theta \\
& + (1-H_i^{n+1}) \frac{P_{i+1}^{n+1} - P_i^{n+1}}{\Delta z} + \left(\frac{dP}{dz}\right)_{i,wall,friction} - \left(\frac{dP}{dz}\right)_{i,int\,erphase} = 0
\end{aligned} \tag{C.5}$$

The finite difference approximation of energy equation is expressed as:

$$\begin{aligned}
q_i^{n+1} &= \left(H_{m,i} - \frac{P_i}{\rho_{m,i}}\right)^{n+1} \frac{\rho_{m,i}^{n+1} - \rho_{m,i}^n}{\Delta t} \\
& + (\rho_{m,i} c_{Pm,i})^{n+1} \frac{T_i^{n+1} - T_i^n}{\Delta t} + (\rho_{icc,i} c_{Picc,i})^{n+1} \frac{T_i^{n+1} - T_i^n}{\Delta t} \\
& - (\rho_{m,i} \eta_{m,i} c_{Pm,i})^{n+1} \frac{P_i^{n+1} - P_i^n}{\Delta t} - \rho_{m,i}^{n+1} \frac{(P/\rho_m)_i^{n+1} - (P/\rho_m)_i^n}{\Delta t} \\
& + \rho_{m,i}^{n+1} v_{m,i}^{n+1} \left\{ \frac{H_{m,i+1/2}^{n+1} + \frac{(v_{m,i+1,2}^{n+1})^2}{2}}{\Delta z} - \frac{H_{m,i-1/2}^{n+1} + \frac{(v_{m,i-1,2}^{n+1})^2}{2}}{\Delta z} \right\} \\
& + \rho_{m,i}^{n+1} v_{m,i}^{n+1} g \sin \theta
\end{aligned} \tag{C.6}$$

APPENDIX D: BRIEF DESCRIPTION OF A GENERAL PURPOSE RESERVOIR SIMULATOR (GPAS)

D.1 GOVERNING EQUATIONS

We use a compositional reservoir simulator called GPAS (Wang et al., 1997; 1999; Han et al., 2006) in our coupled wellbore/reservoir model. A brief description of the simulator is presented below.

Multicomponent and multiphase flow in a porous medium can be described using four different types of equations:

1. Partial differential, component-mass balances describing component flow, in which Darcy's law is used to govern the transport of phases from one cell to another.
2. Phase equilibrium equations dealing with equilibrium component mass transfer between phases
3. Equations constraining phase saturation and component concentrations
4. Energy balance equations controlling energy flow

If we neglect mutual solubility between water and hydrocarbon phases for a system consisting of n_c hydrocarbon components and n_p fluid phases, and excluding the aqueous phase, the above four types of equations may be mathematically expressed for a control volume as follows:

Component material balance: The overall material balance for component i is written in terms of moles per unit time. N_i is the number of moles of component i per unit bulk volume.

$$\frac{\partial N_i}{\partial t} - \nabla \cdot \bar{N}_i - F_i = 0 \quad (\text{D.1})$$

\bar{N}_i is the flux vector of component i , and F_i is the molar rate of injection/production of component i . Each term of the equation can be written in more detail; for example, the accumulation term is a function of porosity, ϕ , the molar density of phase j , ξ_j , saturation of phase j , S_j , and the mole fraction of component i in phase j , x_{ij} as

$$N_i = \phi \sum_{j=1}^{n_p} \xi_j S_j x_{ij} \quad (\text{D.2})$$

The flux vector at each gridblock of the reservoir results from a combination of two mechanisms: convection and dispersion. The dispersion term is ignored in GPAS equations for simplicity. Hence, the flux vector in Equation D.1 can be expressed as

$$\bar{N}_i = \sum_{j=1}^{n_p} \xi_j x_{ij} \bar{v}_j \quad (\text{D.3})$$

Darcy's law is used to govern the transport of phases from one cell to another under the local pressure gradient, rock permeability, relative permeability, and viscosity. From Equations D.1 through D.3, the overall mass balance for each component is

$$\frac{\partial}{\partial t} \left(\phi \sum_{j=1}^{n_p} \xi_j S_j x_{ij} \right) - \nabla \cdot \left[\sum_{j=1}^{n_p} \xi_j x_{ij} \lambda_j (\nabla P_j - \gamma_j \nabla D) \right] - \frac{q_i}{V_b} = 0 \quad (\text{D.4})$$

In this molar equation, q_i is the molar flow rate for component i from the wellbore gridblocks. q_i is calculated by well model equations presented by Peaceman (1983).

Phase-equilibrium relationship: The component distribution among the various phases is determined by the phase-equilibrium calculation. This requires that the molar-balance constraint be preserved, the chemical potentials of each component be the same for all phases, and the Gibbs free energy at constant temperature and pressure be minimized. This can be described as

$$f_i^j - f_i^r = 0 \quad i = 1, 2, \dots, n_c \quad j = 1, 2, \dots, n_p - 1 \quad (\text{D.5})$$

where $f_i^j = \ln(x_{ij}\phi_{ij})$ and ϕ_{ij} is the fugacity coefficient of component i in phase j . Note that r superscript denotes a reference phase.

Volume constraints: The pore volume in each cell must be filled completely by the total fluid volume. This constraint gives rise to:

$$\sum_{i=1}^{n_c} N_i \sum_{j=1}^{n_p} L_j \bar{v}_j - \phi = 0 \quad (\text{D.6})$$

where L_j is the ratio of moles in phase j to the total number of moles in the mixture, and \bar{v}_j is the molar volume of phase j .

Molar energy balance: The molar energy balance for the control volume using internal energy as a primary variable can be expressed as

$$\frac{\partial u}{\partial t} + \bar{V} \cdot \sum_{j=1}^{n_p} \xi_j \lambda_j h_j (\nabla P_j - \gamma_j \nabla D) - \bar{V} \cdot (\lambda_T \nabla T) - q_H + q_L = 0 \quad (\text{D.7})$$

Equations D.4 through D.7 provide $(n_p n_c + 2)$ independent equations and unknowns for each cell. These equations are discretized on a rectangular grid, using finite differences, with one-point upstream weighting. In the fully implicit solution, this discretization results in a system of nonlinear equations that are solved using Newton's method. The independent variables used are P, h_T, N_i and $\ln K_i$, $i = 1, 2, \dots, n_c - 1$.

The equilibrium ratio, K_i is defined as

$$K_i = \frac{y_i}{x_i} \quad (\text{D.8})$$

where x_i and y_i are the mole fractions of component i in oil and gas phases, respectively.

D.2 ASSUMPTIONS USED IN GPAS

In the derivation of the above equations, the following assumptions are made:

- 1) Darcy's law describes the multiphase flow of the fluids through the porous media.
- 2) Impermeable zones represented by no-flow boundaries surround the reservoir.
- 3) The injection and production of fluids are treated as source or sink terms.
- 4) The rock is slightly compressible.
- 5) Each hydrocarbon phase is composed of n_c hydrocarbon components, which may include non-hydrocarbon components such as CO_2, N_2, H_2S .
- 6) Instantaneous local thermodynamic equilibrium occurs between hydrocarbon phases in the reservoir.

7) Negligible capillary pressure effects on hydrocarbon phase equilibrium can be assumed.

8) Water is slightly compressible and water viscosity is constant.

The linearization of the nonlinear equations requires solving large, sparse linear systems of size $(2nc)N$, where N is the number of gridblocks in the reservoir. The linear system is handled with solvers from PETSc (Described in Appendix E). Currently, we are using a general minimum residual solver with block Jacobi preconditioning with point block incomplete LU(0) on each block.

D.3 PHYSICAL PROPERTY MODELS

In this section, the physical models implemented in GPAS to calculate the viscosities, interfacial tension, relative permeability, and capillary pressure are discussed.

Viscosity: For gas and oil viscosity, Lohrenz et al.(1964) correlations are used.

Interfacial tension: The interfacial tension between two hydrocarbon phases is calculated from the Maclead-Sudgen correlation as reported in Reid-Prausnitz and Poling (1987).

Relative Permeability: The two-phase relative permeability in GPAS is given by user as a table. For three-phase flow, GPAS uses Stone's method I or II, where the two-phase data for oil/water and oil/gas are obtained from input tables.

Capillary Pressure: The gas/oil and water/oil capillary pressure data are inputted by the user in table format.

D.4 GPAS SOLUTION PROCEDURE

A fully-implicit solution method is used to solve the governing equations. The equations are nonlinear and must be solved iteratively. A Newton procedure is used to solve the nonlinear equations. The linearization is performed by using the Jacobian Matrix of the governing equations. The Jacobian matrix elements are the derivatives of the governing equations with respect to the independent variables. At each time step, the following sequences of steps are completed:

1. *Initialization in Each Gridblock:* The pressure, overall composition, and temperature of the fluids in each gridblock are specified.
2. *Phase identification and Physical Properties Calculation:* The flash calculations are performed in each gridblock to determine the phase saturations, compositions and densities. The phases are then identified as gas, oil or aqueous. More detail about the flash calculations and phase identification is discussed in Appendix F.
3. *Governing Equations Linearization:* All the governing equations are linearized in terms of the independent variables, and the elements of the Jacobian are calculated.
4. *Jacobian Factorization and Reduction of the Linear Systems:* A row elimination is performed to reduce the size of the linear system from $2n_c + 1$ to n_c for each gridblock. To achieve this, the linearized phase-equilibrium relations and the linearized volume constraint are used to eliminate both the secondary variables

- and one of the overall component moles from the linearized component mass balance equations.
5. *Solution of the Reduced System of the Linear Equations for the Primary Variables:* The reduced system of linear equations is simultaneously solved for pressure and the overall moles of $n_c - 1$ components per unit bulk volume for all cells.
 6. *Secondary Variables Calculation:* A back substitution method is employed to compute the secondary variables $\ln K_i$ and the overall moles of the component eliminated in Step 4 using the factorized Jacobian. The phase-stability analysis is then carried out for all the gridblocks using the newly updated pressure and overall component moles.
 7. *Updating Phase Densities and Viscosities, Determination of Single-Phase State, and Estimation of Phase Relative Permeability:* phase composition and the phase properties are updated.
 8. *Check for Convergence:* The residuals of the linear system obtained in Step 3 are used to determine convergence. If a tolerance is exceeded, the elements of the Jacobian and the residuals of the governing equations are then updated and another Newton iteration is performed by returning to Step 4. If the tolerance is met, a new time step is then started by returning back to Step 3.

APPENDIX E: PETSc LINEAR SOLVERS

The Portable Extensible Toolkit for Scientific computing (PETSc) is a large suite of parallel, general-purpose, object-oriented, timestepper, nonlinear and linear solvers for the scalable solution of partial-differential equations discretized using implicit and semi-implicit methods (Balay *et al.*, 1998; Wang *et al.*, 1999).

The goal of PETSc development is to diffuse the best and most practical aspects of both mathematics and computer science research in scientific computing into scientific and engineering application codes, with a particular emphasis on scalable parallel performance. PETSc is implemented in C, and can be used in conjunction with C, FORTRAN, and C++ codes. It uses MPI for communication across processors.

PETSc has been used for a wide variety of applications, including computational fluid dynamics, structural dynamics, materials modeling, and econometrics. Many of the solvers are appropriate for problems discretized using either structured grids or unstructured grids. The EOS compositional simulator uses the linear solver component of PETSc to solve the linearized Newton system of equations and uses the parallel data formats provided by PETSc to store the Jacobian and the vectors needed in the solution procedure. The simulator uses the linear solvers (SLES) component of PETSc. The solution of large-scale linear problems pervades many facets of computational science, and demands robust and flexible solution strategies. The SLES provides a powerful suite of data-structure-neutral numerical routines for such problems. Built on top of the data structures, SLES enables the user to easily customize the linear solvers according to the

application at hand. The SLES provides a flexible interface to Newton-based methods that use either line-search or trust-region approaches to control step size.

All the user needs to provide is a subroutine for the evaluation of the linear function whose zero value is to be determined. The linear solver components of PETSc provide a unified interface to various Krylov methods, such as conjugate gradient (CG), generalized minimal residual (GMRES), biconjugate gradient. Also PETSc provides various parallel preconditioners such as Jacobi, block preconditioners like block Jacobi, and domain decomposition preconditioners like additive Schwarz. GPAS uses the biconjugate gradient stabilized approach as the Krylov method and block Jacobi preconditioner, with point block incomplete factorization (ILU) on the subdomain blocks. The point block refers to treating all the variables associated with a single gridblock as a single unit. The number of subdomain blocks for block Jacobi is chosen to match the number of processors used, so that each processor gets a complete subdomain of the problem and does a single local incomplete factorization on the Jacobian corresponding to this subdomain. A discussion on the design of the SLES may be found in Gropp *et al.*, (1995).

APPENDIX F: PHASE BEHAVIOR AND EQUILIBRIUM CALCULATIONS

We use the phase equilibrium relationship in GPAS to determine the number, amounts, and compositions of all equilibrium phases.

The sequence of phase equilibrium calculations is as follows:

1. The number of phases in a gridblock is determined using the phase stability analysis.
2. After the number of phases is determined, the composition of each equilibrium phase is determined.
3. The phases in the gridblock are tracked for the next time step calculations.

F.1 PHASE STABILITY ANALYSIS

A stability analysis is used to find how many phases are in the mixture. The system is multiphase if the value of Gibbs' free energy is lower than a single-phase mixture of overall hydrocarbon composition, \bar{Z} (Michelsen, 1982). Hence, if we obtain less Gibbs Energy by assuming another phase, an additional phase must be added to the phase equilibrium calculation. This condition is expressed mathematically as

$$\Delta G = \sum_{i=1}^{n_c} y_i \left[\mu_i(\bar{Y}) - \mu_i(\bar{Z}) \right] \quad (\text{F.1})$$

where μ_i is the chemical potential of component i , and y_i is the mole fraction of component i in the trial phase. Thus, if for any set of mole fractions the value of ΔG at

constant temperature and pressure is greater than zero, then the phase will be stable. If a composition can be found such that $\Delta G < 0$, the phase will be unstable.

F.2 FLASH CALCULATION

Once a mixture has been shown to split into more than one phase by the stability calculation, the flash calculations are performed to compute the mole fraction and composition of each phase at a given temperature, pressure, and overall composition of the fluid. The governing flash equations require equality of component fugacities and mass balance. The equilibrium solution must satisfy three conditions:

- Mass conservation of each component in the mixture
- Chemical potentials for each component are equal in all phases
- Gibbs free energy at constant temperature and pressure is a minimum

Fugacity is calculated using the Peng-Robinson equation-of-state (Peng and Robinson, 1976). Both the phase composition constraint, which states that the sum of the mole fraction of all the components in a phase is equal to one, and the Rachford-Rice equation are used implicitly in the solution of the fugacity equation. The Rachford-Rice equation evaluates the amount and composition of each equilibrium phase in a classical flash calculation. This equation requires the values of the equilibrium ratios K_i , which are defined as the ratio of the mole fractions of component i in oil and gas phases, respectively. The K_i values are determined by the equality of component fugacities in each phase. The fugacity equality, the Rachford-Rice equation, and the Peng-Robinson equation of state are described in Section F.2.1 in detail.

F.2.1 Equality of the Component Fugacity

One of the criteria for phase equilibrium is the equality of the partial molar Gibbs free energies, or the chemical potentials, which can be expressed as fugacity (Sandler, 1999). Hence, in thermodynamic equilibrium between phases,

$$f_{ij} = f_{i\ell} \text{ for } i = 1, \dots, n_c \text{ and } j = 2, \dots, n_p (j \neq \ell) \quad (\text{F.2})$$

It should be noted that the fugacity of a component in a phase is taken as a function of pressure and phase composition. At a given temperature,

$$f_{ij} = f_{ij}(P, \bar{x}_j) \text{ for } i = 1, \dots, n_c \text{ and } j = 2, \dots, n_p (j \neq \ell) \quad (\text{F.3})$$

F.2.2 Composition Constraint

The phase composition constraint is

$$\sum_{i=1}^{n_c} x_{ij} - 1 = 0 \quad (\text{F.4})$$

where the mole fractions are defined as

$$x_{ij} = \frac{n_{ij}}{n_j} \text{ for } i = 1, \dots, n_c \text{ and } j = 2, \dots, n_p \quad (\text{F.5})$$

F.2.3 Rachford-Rice Equation

In a classical flash calculation, the amount and composition of each equilibrium phase is evaluated using a material-balance equation after each update of the K-value is derived from the equation-of-state:

$$r(v) = \sum_{i=1}^{n_c} \frac{(K_i - 1)Z_i}{1 + v(K_i - 1)} = 0 \quad (\text{F.6})$$

where v is the mole fraction of gas in the absence of water. K_i is the equilibrium ratio, Z_i is the overall mole fraction of component i in the feed and $r(v)$ is the residual of the Rachford-Rice equation.

After solving this equation, the component mole fractions in the liquid and gas phases are computed from:

$$x_i = \frac{Z_i}{1 + v(K_i - 1)} \quad (\text{F.7})$$

$$y_i = \frac{Z_i K_i}{1 + v(K_i - 1)} \quad (\text{F.8})$$

The range for v is defined by

$$v_l = \frac{1}{1 - K_{\max}} < 0$$

$$v_r = \frac{1}{1 - K_{\min}} > 0 \quad (\text{F.9})$$

Usually, a Newton iteration can efficiently solve equations F.6 through F.8. However, round-off errors could occur while solving the equations. To avoid any round-off errors, the original Rachford-Rice equation can be changed into a form that is more nearly linear with respect to v , as done by Leibovici and Neoschil (1992).

F.3 EQUATION OF STATE

The Peng-Robinson equation of state (Peng and Robinson, 1976) is

$$P = \frac{RT}{\underline{V} - b} - \frac{a(T)}{\underline{V}(\underline{V} + b) + b(\underline{V} - b)} \quad (\text{F.10})$$

The parameters a and b for a pure component are computed from

$$a(T) = 0.45724 \frac{R^2 T_c^2}{P_c} \alpha(T) \quad (\text{F.11})$$

$$\sqrt{\alpha} = 1 + \kappa \left(1 - \sqrt{\frac{T}{T_c}} \right) \quad (\text{F.12})$$

$$b = 0.07780 \frac{RT_c}{P_c} \quad (\text{F.13})$$

$$\kappa = 0.37464 + 1.54226\omega - 0.26992\omega^2 \quad \text{if } \omega < 0.49 \quad (\text{F.14})$$

$$\kappa = 0.379640 + 1.485030 \omega - 0.164423 \omega^2 + 0.016666 \omega^3 \quad \text{if } \omega \geq 0.49 \quad (\text{F.15})$$

For a multi-component mixture, the mixing rules for the two parameters are

$$a = \sum_{i=1}^{N_c} \sum_{j=1}^{N_c} x_i x_j \sqrt{a_i a_j} (1 - k_{ij}) \quad (\text{F.16})$$

$$b = \sum_{i=1}^{N_c} x_i b_i$$

where for component i, the a_i is computed from equation F.11, and b_i is computed from equation F.13. The constant, k_{ij} is called the binary interaction coefficient between components i and j.

The Peng-Robinson Equation of state can be written in the form

$$Z^3 + \alpha Z^2 + \beta Z + \gamma = 0 \quad (\text{F.17})$$

where $Z = \frac{PV}{RT}$ is the compressibility factor, and the parameters are expressed as

$$\alpha = -1 + B \quad (\text{F.18})$$

$$\beta = A - 3B^2 - 2B \quad (\text{F.19})$$

$$\gamma = -AB + B^2 + B^3 \quad (\text{F.20})$$

$$A = \frac{aP}{(RT)^2} \quad (\text{F.21})$$

$$B = \frac{bP}{RT} \quad (\text{F.22})$$

In GPAS, the equation-of-state parameters for each pure component are calculated and then mixture values are determined. The fugacity coefficient is computed from the equation-of-state calculations. Then, the Peng-Robinson cubic equation-of-state is solved, and the compressibility factor and its derivative are calculated. To calculate the equation of state parameters, the pure component critical temperature, critical pressure, critical volume, acentric factors, molecular weights, and binary interaction coefficients are needed. In GPAS, the flash calculation is done at a given initial composition, temperature, and pressure. The number of components, binary interaction coefficients, and the equilibrium ratio values are given to the flash calculation subroutine. An initial values for the equilibrium values are estimated and passed to the flash calculations. The flash subroutine calculates the liquid and vapor phase mole fractions, liquid and vapor compressibility factors, and the negative residual of component i in cell k .

F.4 PHASE IDENTIFICATION AND TRACKING

Phase identification deals with the labeling of a phase as oil, gas, or aqueous based on the initial conditions, or when a new phase appears. After a phase has been identified, phase tracking executes the labeling of a phase during the simulation. Labeling phases consistently is important because of the need to assign a consistent relative permeability to each phase during a numerical simulation. Perschke (1988) developed a method for phase identification and tracking in which both phase mass density and phase composition are used which is the procedure followed in GPAS. Once a phase has been identified, it is tracked during simulation by comparing the mole fraction value of a selected or key component in the equilibrium phases at the new time step, with the values at the old time step. The phases at the new time step are labeled such that the mole fraction values are closest to the values of the old time step.

APPENDIX G: INPUT DATA DESCRIPTION AND EXAMPLES

G.1 WELLBORE/RESERVOIR INPUT DATA DESCRIPTION

Wellbore and reservoir data are input to the computation stage of the simulator by using a free-form keyword input format. The order of data input is free-form in the sense that the order in which the simulator reads input data is independent of the order of data in the input file. Hence, the user simply enters the name of the flags or variables, which follows the data the user wants to assign to the variable. Note that an equal sign between the variable names and the data is optional. The simulator does not read any line that begins with a \$ symbol, so it is possible to disable any keyword by adding this symbol before it. The following tables show the input parameters for reservoir and wellbore in GPAS.

G.1.1 GPAS General Input Flags

TITLE ()	Case title
DESCRIPTION ()	Case description: parameters such as reservoir/wellbore geometry and gridblocks may be described in this section
COMPOSITIONAL_MODEL	EOS compositional model flag
DEBUGS	Single processor debug output key
DEBUGM	Multiple processor debug output key
OUTPUT_PRE	Print the fracture gridblock pressure
OUTPUT_NPH	Print the presence of the particular phase

OUTPUT_SAT	Print the fracture gridblock phase saturations
OUTPUT_OIL	Print the gridblock oil phase compositions
OUTPUT_GAS	Print the gridblock gas phase compositions
OUTPUT_WEL	Print the well output
OUTPUT_HIS	Print the history file
OUTPUT_DEN	Print the gridblock phase molar densities
OUTPUT_VIS	Print the phase viscosity
PROCOUT	Print the grid element distribution on multiprocessor machines
TDPVOPT	Change the values of output time from days to pore volume
TIME_ENLARGE	Time-enlarge on/off option
NO_CRASH	Proceed to run even if the solution is not fully converged
IOILVIS	Specify constant oil viscosity as the input parameter

G.1.2 GPAS General Data Variables

TIMEEND	Reservoir time at which simulation stops (in days)
OUTLEVEL	Normal print level, from 1 (Minimum) to 3 (Maximum)
OUTPUT_TIME	The time at which the output is obtained
DOWN ()	Normalized gravity vector (Use 0 0 1)
NX(), NY(), NZ()	Number of gridblocks in X, Y, and Z directions
DX(), DY(), DZ()	Interval lengths of gridblocks in X, Y, and Z directions, ft
ISTEP (), JSTEP (), KSTEP ()	Print indexes for grid elements arrays

COMPOUND ()	Component name
CRIT ()	Nonaqueous component critical temperatures
CRIP ()	Nonaqueous component critical pressures
CRIV ()	Nonaqueous component critical volumes
ACEN ()	Nonaqueous component acentric factors
PARA ()	Nonaqueous component Parachor values
VSP ()	Nonaqueous component VSP values
BINC ()	Nonaqueous binary interaction coefficients
MOLW ()	Nonaqueous component molecular weights
NPHASE	Maximum number of phases
OILVIS	Oil viscosity input, cp
ROCKZ	Rock compressibility at a reference pressure, 1/psi
ROCKP	Reference pressure for rock compressibility, psi
H2OZ	Water compressibility at a reference pressure, 1/psi
H2OP	Reference pressure for water compressibility, psi
H2OD	Water molar density, lbm.mole/ft ³
SURFT	Surface temperature, °F
SURFP	Surface pressure, psi
RESTF	Reservoir temperature (if isothermal reservoir assumes), °F
CVGOPT	Convergence option (1 for relative changes; 2 for absolute residuals)
METHOD	Method of allocating grid elements to processors
TOL_FLASH	Convergence tolerance for fugacity equations
TOL_VOLUME	Convergence tolerance for volume equations
TOL_MASS	Convergence tolerance for hydrocarbon mass equations
TOL_WATER	Convergence tolerance for water mass equations

MAXNEWT	Maximum number of Newtonian iterations
POROSITY1 ()	Gridblocks porosities array
XPERM1 ()	Permeabilities array in X direction, md
YPERM1 ()	Permeabilities array in Y direction, md
ZPERM1 ()	Permeabilities array in Z direction, md
SWINI1 ()	Initial gridblocks water saturations array
PINI1 ()	Initial gridblocks pressures array, psi
VIS1 ()	Gridblocks viscosities array
OILVIS	Constant oil viscosity if IOILVIS flag is on
ZXY1 ()	Gridblocks initial compositions array
MODREL ()	Three-phase oil relative permeability model
ENDPT ()	Relative permeability endpoints
NRELFUN	Use Corey function relative permeability if the value is 1
SR ()	Residual saturation for each phase
RELP	Relative permeability option (1 for table lookup; 2 for function-based)
EXPN ()	Relative permeability function exponents

G.1.3 GPAS General Input Flags for Well Description

WELLBOREMODEL	Wellbore modeling is on if this flag is set to 1
TRANSIENTFLAG	For wellbore transient fluid flow modeling, this flag is set to 1

G.1.4 GPAS General Data Variables for Well Description

NUMWEL	Total number of wells, including any that may be activated at some advanced reservoir time
WELLNAME ()	Well names

KINDWELL	Well type 1 for a injector when bottomhole pressure is specified 2 for an injector when volume rate is specified 3 for a producer when bottomhole pressure is specified 4 for a producer when oil volume rate is specified 5 for a producer when liquid volume rate is specified
WELLTOP	X,Y,Z locations of the well tops, ft
WELLBOTTOM	X,Y,Z locations of the well bottom, ft
DEPTH	Wellbore depth, ft
TETA	Wellbore inclination degree, Radian
RTI	Inner tubing radius, ft
RTO	Outer tubing radius, ft
RWB	Wellbore radius, ft
RCI	Inner casing radius, ft
RCO	Outer casing radius, ft
EW	Tubing friction coefficient
IFT	Interfacial tension
TP	Producing time before shut-in (for shut-in modeling), hr
TEARTH_REF	Formation surface temperature, °F
GE	Formation temperature gradient, °F/ft
KEARTH	Formation heat conductivity, Btu/hr-ft-°F
DENEARTH	Formation density, lbm/ ft ³
CEARTH	Formation heat capacity, Btu/lbm-°F
KCEM	Cementing heat conductivity, Btu/hr-ft-°F
SALINITY	Annulus brine salinity, ppm
BHT	Reservoir fluid temperature, °F
W_SEGMENT	Number of gridblocks in wellbore

WELLPQ ()	Input of either rate or bottomhole pressure vs. time for each well based on the KINDWELL
-----------	--

G.2 SAMPLE INPUT FILES

In this section, the GPAS input files used in the wellbore/reservoir simulator or stand-alone wellbore simulator, as discussed in Chapters 3 and 4, are given. The input file in Section G.2.1 is for a transient case where a producing well is shut in at the surface. The well was producing gas and oil (with 6 components) before shut-in. Section G.2.2 is a wellbore/reservoir modeling input file for a gas injection case. An input file used for a stand-alone steady-state blackoil wellbore simulator is presented in Section G.2.3. The Makefile that compiles and links the different parts of a coupled wellbore/reservoir simulator on the PETROS server presented in Section G.2.4.

G.2.1 Transient Wellbore/Reservoir Case

```
TITLE(2)="3-D SIX COMPONENT GAS/OIL PRODUCTION"

DESCRIPTION( )=
"THICKNESS (FT) : 100"
"LENGTH (FT) : 560"
"WIDTH (FT) : 560"
"GRID BLOCKS : 7x7x1"

COMPOSITIONAL_MODEL
$DEBUGS

TIMEEND = 0.3

$ I/O OPTIONS

OUTLEVEL = 1
$SPLINEOUT
$GEOMOUT
```

```

PROCOUT
OUTPUT_PRE
$OUTPUT_NPH
OUTPUT_SAT
OUTPUT_OIL
OUTPUT_GAS
$OUTPUT_DEN
OUTPUT_WEL
OUTPUT_HIS
WELLFILE = "6COMP.WEL"

HISDATA_NUM = 100
OUTPUT_TIME() = 100 1000 2000 3000 3650
$NO_CRASH

$OUTPUT FREQUENCY
ISTEP(,,)=1
JSTEP(,,)=1
KSTEP(,,)=1

$ FAULT BLOCK AND MESH DATA
METHOD = 2
DOWN() = 0 0 1
NX(1) = 7  NY(1) = 7  NZ(1) = 1
MES = "cart"
DX() = 80  DY() = 80  DZ() = 100

$ COMPOUND NAMES
COMPOUND(1) = "C1"      COMPOUND(2) = "C3"
COMPOUND(3) = "C6"      COMPOUND(4) = "C10"
COMPOUND(5) = "C15"     COMPOUND(6) = "C20"

$ COMPOUND CRITICAL TEMPERATURES
CRIT() 343.0 665.7 913.4 1111.8 1270.0 1380.0

$ COMPOUND CRITICAL PRESSURES
CRIP() 667.8 616.3 436.9 304.0 200.0 162.0

$ COMPOUND CRITICAL VOLUMES
CRIV() 1.599 3.211 5.923 10.087 16.696 21.484

$ COMPOUND ACEN
ACEN() 0.013 0.152 0.301 0.488 0.650 0.850

$ COMPOUND MOL WEIGHTS
MOLW() 16.0 44.1 86.2 142.3 206.0 282.0

$ COMPOUND PARA
PARA() 71.00 151.0 271.0 431.0 631.0 831.0

$ VSP
VSP() -0.1538 -0.0733 -0.00499 0.0754 0.1451 0.1436

```

```

$ BINARY INTERACTION COEFFICIENTS
BINC(,) = 0.0  0.0  0.0  0.0  0.0  0.0
          0.0  0.0  0.0  0.0  0.00 0.0
          0.0  0.0  0.0  0.0  0.0  0.0
          0.0  0.0  0.0  0.0  0.0  0.0
          0.0  0.00 0.0  0.0  0.0  0.0
          0.0  0.00 0.0  0.0  0.0  0.0

$ MAX NUMBER OF PHASES
NPHASE = 3

$ MAXNEWT MAX NUMBER OF NEWTON ITERATION
MAXNEWT = 20

$ Initial rock & water properties
ROCKZ = 0.000001  ROCKP = 1500
H2OZ = 0.000003  H2OP = 14.696  H2OD = 3.468
SURTF = 60.0  SURPS = 14.696
RESTF = 160.0

$ TOLERANCE
CVGOPT = 2
TOL_FLASH = 0.0001
TOL_VOLUME = 0.0001
TOL_MASS = 0.0001
TOL_WATER = 0.0001

$ POROSITY
POROSITY1() = 0.3

$ PERMEABILITIES
XPERM1() = 3.6
YPERM1() = 3.6
ZPERM1() = 3.6
XYPERM1() = 0
XZPERM1() = 0
YZPERM1() = 0

$ INITIAL WATER SATURATION
SWINI1() = 0.17

$ INITIAL WATER CELL PRESSURE
PINI1() = 1350.0

$ INITIAL PHASE VISCOSITIES AT EACH CELL
VIS1() = 1.0

$ INITIAL COMPOSITIONS
ZXY1(,,,1) = .45
ZXY1(,,,2) = .15
ZXY1(,,,3) = .02
ZXY1(,,,4) = .11
ZXY1(,,,5) = .12

```

```

ZXY1(,,6) = .15

$ RELPERM DATA
$ RELP 1 for table lookup, 2 for function based

RELP 2
$MODREL(1) = 3

$ NRELFUN 1 for corey, more to be added later
NRELFUN 1
$ data for each phase : water, phase 2 and phase 3
ENDPT() = 0.4 0.9 0.9
SR() = 0.3 0.1 0.0
EXPN() = 3.0 2.0 2.0

$ ===== WELL SPECIFICATIONS =====

NUMWELL = 1

$ --- The first well ---

WELLNAME(1) = "PRODUCER 1"
KINDWELL(1) = 3
WELLBOREMODEL = 1
TRANSIENTFLAG = 1

$ --- Wellbore Paramers ---
DEPTH = 5700.
TETA = 1.5707
RTI = 0.098
RTO = 0.189
RWB = 0.425
RCI = 0.3243
RCO = 0.3654
EW = 0.0008
QWATER = 0.
GW = 1.
IFT = 31.6
TP = 158
TEARTH_REF = 84.
GE = 0.006976
KEARTH = 1.3
DENEARTH = 132
CEARTH = 0.21
KCEM = 4.021
SALINITY = 35000
BHT = 140
WP_FLAG = -1
W_SEGMENT = 10
$ --- End Wellbore Parameters ----

WELLTOP(1 TO 3,1,1) = 280 280 0
WELLBOTTOM(1 TO 3,1,1) = 280 280 100

```

```

DIAMETER(1,1) = 0.2
WELLPQ(1) Block
  Interpolation Linear
  Extrapolation Constant
  Data 0. 900.
EndBlock

EndInitial

$ TRANSIENT DATA INPUT BLOCKS
BeginTime 0.0
TIME_CONTROL = 1
DELTIM = 0.0001 DTIMMUL = 1.0 DTIMMAX = 30 DTIMMIN = 0.0001
TUNE = 0.5 DCMAX = 0.5 DAQCMAX = 0.5 DPMAX = 0.5 DSMAX = 0.5
$MAXMOL = 1 MAXP = 10000 ERRLIMIT = 0.2
$ WZ() 0.77 0.20 0.01 0.01 0.005 0.005 0.0
EndTime

```

G.2.2 Gas Injection Case

Gas injection in a one-injector/one-producer system is modeled by using our coupled wellbore/reservoir simulator. At each time step multiphase fluid flow is modeled in the reservoir and producer by the following input file.

```

TITLE(2)="3-D SIX COMPONENT GAS INJECTION"

DESCRIPTION( )=
"THICKNESS (FT) : 100"
"LENGTH (FT) : 560"
"WIDTH (FT) : 560"
"GRID BLOCKS : 7x7x3"

COMPOSITIONAL_MODEL
$DEBUGS

TIMEEND = 3650

$ I/O OPTIONS

OUTLEVEL = 1
$SPLINEOUT
$GEOMOUT
PROCOU

```



```

OUTPUT_PRE
$OUTPUT_NPH
OUTPUT_SAT
OUTPUT_OIL
OUTPUT_GAS
$OUTPUT_DEN
OUTPUT_WEL
OUTPUT_HIS
WELLFILE = "6COMP.WEL"

HISDATA_NUM = 100
OUTPUT_TIME() = 100 1000 2000 3000 3650
$NO_CRASH

$OUTPUT FREQUENCY
ISTEP(,,)=1
JSTEP(,,)=1
KSTEP(,,)=1

$ FAULT BLOCK AND MESH DATA
METHOD = 2
DOWN() = 0 0 1
NX(1) = 7  NY(1) = 7  NZ(1) = 3
MES = "cart"
DX() = 80  DY() = 80  DZ() = 20 30 50

$ COMPOUND NAMES
COMPOUND(1) = "C1"      COMPOUND(2) = "C3"
COMPOUND(3) = "C6"      COMPOUND(4) = "C10"
COMPOUND(5) = "C15"     COMPOUND(6) = "C20"

$ COMPOUND CRITICAL TEMPERATURES
CRIT() 343.0 665.7 913.4 1111.8 1270.0 1380.0

$ COMPOUND CRITICAL PRESSURES
CRIP() 667.8 616.3 436.9 304.0 200.0 162.0

$ COMPOUND CRITICAL VOLUMES
CRIV() 1.599 3.211 5.923 10.087 16.696 21.484

$ COMPOUND ACEN
ACEN() 0.013 0.152 0.301 0.488 0.650 0.850

$ COMPOUND MOL WEIGHTS
MOLW() 16.0 44.1 86.2 142.3 206.0 282.0

$ COMPOUND PARA
PARA() 71.00 151.0 271.0 431.0 631.0 831.0

$ VSP
VSP() -0.1538 -0.0733 -0.00499 0.0754 0.1451 0.1436
$ BINARY INTERACTION COEFFICIENTS

```

```
BINC(,) = 0.0  0.0  0.0  0.0  0.0  0.0
          0.0  0.0  0.0  0.0  0.00 0.0
          0.0  0.0  0.0  0.0  0.0  0.0
          0.0  0.0  0.0  0.0  0.0  0.0
          0.0  0.00 0.0  0.0  0.0  0.0
          0.0  0.00 0.0  0.0  0.0  0.0
```

```
$ MAX NUMBER OF PHASES
NPHASE = 3
```

```
$ MAXNEWT MAX NUMBER OF NEWTON ITERATION
MAXNEWT = 20
```

```
$ Initial rock & water properties
ROCKZ = 0.000001  ROCKP = 1500
H2OZ = 0.000003  H2OP = 14.696  H2OD = 3.468
SURTF = 60.0  SURPS = 14.696
RESTF = 160.0
```

```
$ TOLERANCE
CVGOPT = 2
TOL_FLASH = 0.0001
TOL_VOLUME = 0.0001
TOL_MASS = 0.0001
TOL_WATER = 0.0001
```

```
$ POROSITY
POROSITY1() = 0.35
```

```
$ PERMEABILITIES
XPERM1() = 10
YPERM1() = 10
ZPERM1() = 10
XYPERM1() = 0
XZPERM1() = 0
YZPERM1() = 0
```

```
$ INITIAL WATER SATURATION
SWINI1() = 0.17
```

```
$ INITIAL WATER CELL PRESSURE
PINI1() = 1500.0
```

```
$ INITIAL PHASE VISCOSITIES AT EACH CELL
VIS1() = 1.0
```

```
$ INITIAL COMPOSITIONS
ZXY1(,,,1) = .5
ZXY1(,,,2) = .03
ZXY1(,,,3) = .07
ZXY1(,,,4) = .2
ZXY1(,,,5) = .15
ZXY1(,,,6) = .05
```

```

$ RELPERM DATA
$ RELP 1 for table lookup, 2 for function based

RELP 2
$MODREL(1) = 3

$ NRELFUN 1 for corey, more to be added later
NRELFUN 1
$ data for each phase : water, phase 2 and phase 3
ENDPT() = 0.4 0.9 0.9
SR() = 0.3 0.1 0.0
EXPN() = 3.0 2.0 2.0

$ ===== WELL SPECIFICATIONS =====

NUMWELL = 2

$ --- The first well ---
WELLNAME(1) = "INJECTOR 1"
KINDWELL(1) = 2
WELLTOP(1 TO 3,1,1) = 40 40 0
WELLBOTTOM(1 TO 3,1,1) = 40 40 100
DIAMETER(1,1) = 1.0
PRLIMIT(1) = 14695
WELLPQ(1) Block
    Interpolation Linear
    Extrapolation Constant
    Data 0.      1000.
EndBlock

$ --- The 2nd well ---
WELLNAME(2) = "PRODUCER 1"
KINDWELL(2) = 3
WELLBOREMODEL = 1
TRANSIENTFLAG = 0
$ --- Wellbore Paramers ---
DEPTH = 10000.
TETA = 1.5707
RTI = 0.128
RTO = 0.219
RWB = 0.532
RCI = 0.356
RCO = 0.392
EW = 0.0007
QWATER = 500.
GW = 1.
IFT = 31.6
TP = 158
TEARTH_REF = 70.
GE = 0.008
KEARTH = 1.3
DENEARTH = 132

```

```

CEARTH = 0.21
KCEM = 4.02
SALINITY = 35000
BHT = 140
WP_FLAG = -1
W_SEGMENT = 20
$ --- End Wellbore Parameters ----
WELLTOP(1 TO 3,1,2) = 520 520 0
WELLBOTTOM(1 TO 3,1,2) = 520 520 100
DIAMETER(1,2) = 1.0
WELLPQ(2) Block
    Interpolation Linear
    Extrapolation Constant
    Data 0. 1300.
EndBlock

EndInitial

$ TRANSIENT DATA INPUT BLOCKS
BeginTime 0.0
TIME_CONTROL = 2
DELTIM = 1 DTIMMUL = 1.0 DTIMMAX = 30 DTIMMIN = 0.1
TUNE = 0.5 DCMAX = 0.5 DAQCMAX = 0.5 DPMAX = 0.5 DSMAX = 0.5
$MAXMOL = 1 MAXP = 10000 ERRLIMIT = 0.2
WZ() 0.77 0.20 0.01 0.01 0.005 0.005 0.0
EndTime

```

G.2.3 Stand-alone Steady-State Wellbore Simulation

We can use the blackoil wellbore simulator or the compositional wellbore simulator as a stand-alone simulator to model fluid flow and temperature in the wellbore.

The following input file is a sample to enter well data for the calculations.

```

* Input file
* Sagar Example
* Steady state Temperature/Flow parameters
*****
***** Well Geometry
*   depth (depth) (ft)
5355
*   inner tubing radius (rti) (ft)
0.1198
*   outer tubing radius (rto) (ft)
0.125

```

```

*   wellbore radius (rwb) (ft)
0.375
*   inner casing radius (rci) (ft)
0.269
*   outer casing radius (rco) (ft)
0.292
*   tubing friction coefficient (ewellbore) (-)
0.0006

***** Production/Injection data
*   Oil flow rate (qoil) (STB/D)
59
*   Water flow rate (qwater) (STB/D)
542
*   Gas flow rate (qgas) (Mscf/D)
41
*   Oil API gravity (api) (-)
34.3
*   Water gravity (gw) (-)
1.01
*   Gas gravity (gammag) (-)
1.04
*   Interfacial liquid/gas tension (tension) (dyne/cm)
31.6
*   Procuction/injection time (tp) (hr)
158

***** Formation temperature data
*   Surface formation temperature (Tearthref) (F)
76
*   Formation temperature gradient (ge) (F/ft)
0.005976
*   Formation heat conductivity (ke) (Btu/(hr-ft-F))
1.4
*   Formation density (dene) (lbm/ft3)
144
*   Formation heat capacity (ce) (Btu/(lbm-F))
0.22

***** Wellbore parameters
*   Cementing heat conductivity (Kcem) (Btu/(hr-ft-F))
4.021
*   Annulus brine salinity (salinity) (ppm)
35000
***** Solver parameters
*   Bottomhole wellbore temperature (bht) (F)
108
*   Reference pressure (refp) (psig)
113
*   Reference pressure flag (ref_flag) (1/-1)
1
*   Number of nodes (segment) (-)
20

```

G.2.4 Makefile

```
#PGI Linux.mak - Makefile Executive for GPAS on Linux

# make                Builds production program
# make clean          Deletes work files

##### Linux/Dos Controls #####
# Define the slash for file names
S=/
# Define the target file name
EXENAM=gpasv3_6
# Define the object file extension
O=.o
# Define the copy instruction
COPY=cp
##### Misc #####

default:$(EXENAM)
SIZE=.$(S)size
SIZDAT=..$(S)size$(S)ipars.siz
SETSIZE=echo $(SIZDAT) $@ > ech
SETSIZE1=echo $(SIZDAT) $< $@ > ech
SIZEIT=$(SIZE) < ech
MAKDIR=..$(S)make$(S)modular$(S)
WORK=.
COPYIT=$(COPY) $? $(WORK)
COPYIT1=$(COPY) $< $(WORK)
.SUFFIXES:
.SUFFIXES: .o .f .F .c .C .cpp .h .df .dc .dh .dC .dcpp .in .obj

##### Framework include files #####
# frame_t.mak - Framework (TICAM version) make include file

##### Object files #####

FOBJA=ipars$(O) read1$(O) read2$(O) units$(O) comp$(O) table$(O)
idata$(O)
FOBJB=extvar$(O) memman1$(O) memman2$(O) divide$(O) timer$(O)
prtout$(O)
FOBJC=tdata$(O) stdout$(O) initial$(O) iwll$(O) owll$(O) prop$(O)
restart$(O)
FOBJD=cputime$(O) meminfo$(O) memman3$(O) ccallc$(O)
FRAMEOBJ=$(FOBJA) $(FOBJB) $(FOBJC) $(FOBJD)

##### Source files #####
msjunk.h: ..$(S)framework$(S)drive$(S)msjunk.h
```

```

$(COPYIT)

control.h: ..$(S)framework$(S)drive$(S)control.h mcontrol.h
$(SETSIZE1)
$(SIZEIT)

mcontrol.h: ..$(S)framework$(S)drive$(S)mcontrol.dh
$(SETSIZE1)
$(SIZEIT)

scrat1.h: ..$(S)framework$(S)input$(S)scrat1.dh
$(SETSIZE1)
$(SIZEIT)

scrat2.h: ..$(S)framework$(S)input$(S)scrat2.dh
$(SETSIZE1)
$(SIZEIT)

readdat.h: ..$(S)framework$(S)input$(S)readdat.dh
$(SETSIZE1)
$(SIZEIT)

blkary.h: ..$(S)framework$(S)input$(S)blkary.h
$(SETSIZE1)
$(SIZEIT)

rock.h: ..$(S)framework$(S)input$(S)rock.dh
$(SETSIZE1)
$(SIZEIT)

output.h: ..$(S)framework$(S)print$(S)output.dh
$(SETSIZE1)
$(SIZEIT)

compc.h: ..$(S)framework$(S)util$(S)compc.h
$(COPYIT)

unitsex.h: ..$(S)framework$(S)input$(S)unitsex.h
$(COPYIT)

restc.h: ..$(S)framework$(S)print$(S)restc.h
$(COPYIT)

utltdat.h: ..$(S)framework$(S)util$(S)utltdat.dh
$(SETSIZE1)
$(SIZEIT)

memory.h: ..$(S)framework$(S)memman$(S)memory.dh
$(SETSIZE1)
$(SIZEIT)

layout.h: ..$(S)framework$(S)memman$(S)layout.dh
$(SETSIZE1)

```

```

$(SIZEIT)

times.h: ..$(S)framework$(S)util$(S)times.dh
$(SETSIZE1)
$(SIZEIT)

wells.h: ..$(S)framework$(S)wells$(S)wells.dh
$(SETSIZE1)
$(SIZEIT)

ipars.F: ..$(S)framework$(S)drive$(S)ipars.df layout.h control.h
scrat1.h blkary.h wells.h msjunk.h output.h restc.h xarydat.h rock.h
$(SETSIZE1)
$(SIZEIT)
#VE mpif.h

idata.F: ..$(S)framework$(S)input$(S)idata.df layout.h control.h rock.h
blkary.h output.h unitsex.h utldat.h msjunk.h rock.h
$(SETSIZE1)
$(SIZEIT)

tdata.F: ..$(S)framework$(S)input$(S)tdata.df control.h layout.h
output.h unitsex.h restc.h
$(SETSIZE1)
$(SIZEIT)

read1.F: ..$(S)framework$(S)input$(S)read1.df scrat1.h control.h
readdat.h msjunk.h
$(SETSIZE1)
$(SIZEIT)

read2.F: ..$(S)framework$(S)input$(S)read2.df scrat1.h control.h
layout.h readdat.h
$(SETSIZE1)
$(SIZEIT)

units.F: ..$(S)framework$(S)input$(S)units.f
$(SETSIZE1)
$(SIZEIT)

divide.F: ..$(S)framework$(S)memman$(S)divide.df layout.h control.h
msjunk.h
$(SETSIZE1)
$(SIZEIT)

comp.F: ..$(S)framework$(S)util$(S)comp.df control.h output.h compc.h
msjunk.h
$(SETSIZE1)
$(SIZEIT)

table.F: ..$(S)framework$(S)util$(S)table.df utldat.h output.h
control.h scrat2.h msjunk.h
$(SETSIZE1)

```



```

$(SIZEIT)

prtout.F: ..$(S)framework$(S)print$(S)prtout.df control.h layout.h
msjunk.h
$(SETSIZE1)
$(SIZEIT)

stdout.F: ..$(S)framework$(S)print$(S)stdout.df control.h layout.h
output.h unitsex.h
$(SETSIZE1)
$(SIZEIT)

timer.F: ..$(S)framework$(S)util$(S)timer.df times.h
$(SETSIZE1)
$(SIZEIT)

cputime.c: ..$(S)framework$(S)util$(S)cputime.dc
$(SETSIZE1)
$(SIZEIT)

initial.F: ..$(S)framework$(S)util$(S)initial.df control.h layout.h
blkary.h msjunk.h
$(SETSIZE1)
$(SIZEIT)

iwell.F: ..$(S)framework$(S)wells$(S)iwell.df control.h wells.h
blkary.h layout.h msjunk.h unitsex.h compwel.h
$(SETSIZE1)
$(SIZEIT)

owell.F: ..$(S)framework$(S)wells$(S)owell.df control.h wells.h
$(SETSIZE1)
$(SIZEIT)

prop.F: ..$(S)framework$(S)util$(S)prop.df control.h utldat.h rock.h
wells.h
$(SETSIZE1)
$(SIZEIT)

restart.F: ..$(S)framework$(S)print$(S)restart.df layout.h control.h
blkary.h output.h msjunk.h restc.h
$(SETSIZE1)
$(SIZEIT)

extvar.c: ..$(S)framework$(S)util$(S)extvar.dc compc.h
$(SETSIZE1)
$(SIZEIT)

memman3.c : ..$(S)framework/memman/memman3.dc
$(SETSIZE1)
$(SIZEIT)

memman1.c: ..$(S)framework$(S)memman$(S)memman1.dc memory.h

```

```

$(SETSIZE1)
$(SIZEIT)

memman2.c: ..$(S)framework$(S)memman$(S)memman2.dc memory.h
$(SETSIZE1)
$(SIZEIT)

cfsimple.h: ..$(S)framework$(S)util$(S)cfsimple.h
$(COPYIT1)

meminfo.c: ..$(S)framework$(S)memman$(S)meminfo.c cfsimple.h
$(SETSIZE1)
$(SIZEIT)

meminfo.$(O): cfsimple.h

ccallc.F: ..$(S)framework$(S)util$(S)ccallc.df
$(SETSIZE1)
$(SIZEIT)

# parall_c.mak - Parallel framework make include file using C routines

##### Object files #####
PARALOBJ= putil$(O) \
    manyc$(O) manyf$(O) parbuf$(O)
##### Source files #####

SORC=..$(S)framework$(S)parall$(S)

putil.F: $(SORC)putil.df control.h restc.h wells.h
$(SETSIZE1)
$(SIZEIT)

parbuf.F: $(SORC)parbuf.df control.h layout.h scrat1.h output.h
$(SETSIZE1)
$(SIZEIT)

manyf.F: $(SORC)manyf.df control.h layout.h
$(SETSIZE1)
$(SIZEIT)

manyc.c: $(SORC)manyc.c cfsimple.h
$(SETSIZE1)
$(SIZEIT)

##### PETSC Linear Solver #####

PETSC_DIR=/share/apps/petsc
include $(PETSC_DIR)/bmake/common/variables

SOLVELIB = $(PETSC_LIB)

```

```

##### Compositional Model files #####

# Object files #####

XOBJ1=xarray$(0) xtdata$(0) xisdat$(0) xiadat$(0) xstep$(0) xivdat$(0)
xprop$(0) xsurface$(0) estep$(0) xsurfacee$(0) xprope$(0)

XOBJ2=xwdata$(0) xstdout$(0) xupdate$(0) xflash$(0) aqueous$(0)
xeos$(0) xupdatee$(0) xflashe$(0)

XOBJ3=influid0$(0) eos_lph$(0) rowpw$(0) jmass$(0) vis$(0)
influid0e$(0) vise$(0) jmasse$(0) rowpwe$(0)

XOBJ4=jaccum$(0) eos_jaco$(0) relderiv$(0) zderiv$(0) rrderiv$(0)
ift$(0) jaccume$(0) zderieve$(0) relderive$(0) eos_jacoe$(0)

XOBJ5=mresipw$(0) roderiv$(0) eosxi2ni$(0) xeosbas$(0) jaco2pw$(0)
jsource$(0) jsourcee$(0) mresipwe$(0) jaco2pwe$(0) roderive$(0)

XOBJ6=jprint$(0) xprint$(0) xquit$(0) xsolver$(0) xwell$(0) xtimmul$(0)
xwelle$(0) xsolvere$(0)

# akjohn 4/16/2003 added xrelperm.o here

XOBJ7=xtrans$(0) jacobian$(0) xsolve$(0) xdelta$(0) xaqcomp$(0)
xrelperm$(0) xtrapn$(0) xsurf$(0) jacobiane$(0) xsolvee$(0) xdeltae$(0)
xtranse$(0)

# chan 10/28/03: added files for fully implicit automatic time stepping
(FIATS)

XOBJ8=fiats$(0) fiatsol1$(0) fiatsol2$(0) jimpsurf$(0)

# for phase

XOBJ9= aibi$(0) flash3$(0) flash3e$(0) lines$(0) phadis$(0) phdlnf$(0)
plnfx$(0) thrphs$(0) chodec$(0) flash$(0) phadrp$(0) phest$(0)
sastp$(0) track$(0) dirneg$(0) parlnf$(0) phafla$(0) plfc$(0) stmin$(0)
train$(0)

# for wellbore

XOBJ10= mainssCom$(0) vis2$(0) ssmaker$(0) properties$(0)
comproperties$(0) zmaker$(0) tssmaker$(0) newP$(0)

XOBJ11= maintransient$(0) readdata$(0) jr$(0) solver$(0) transientt$(0)
propertiesb$(0) openresult$(0)

# chan

MODELOBJ=$(XOBJ1) $(XOBJ2) $(XOBJ3) $(XOBJ4) $(XOBJ5) $(XOBJ6) $(XOBJ7)
$(XOBJ8) $(XOBJ9) $(XOBJ10) $(XOBJ11)

```

```

# Source files #####
SORC=..$(S)eoscomp$(S)

xarydat.h: $(SORC)include$(S)xarydat.h
           $(SETSIZE1)
           $(SIZEIT)

xgendat.h: $(SORC)include$(S)xgendat.dh
           $(SETSIZE1)
           $(SIZEIT)

tcpcom.h: $(SORC)include$(S)tcpcom.dh
           $(SETSIZE1)
           $(SIZEIT)

simple.in: $(SORC)include$(S)simple.in
           $(COPYIT)

compini.in: $(SORC)include$(S)compini.in
            $(COPYIT)

const.in: $(SORC)include$(S)const.in
           $(SETSIZE1)
           $(SIZEIT)

model.in: $(SORC)include$(S)model.in
           $(COPYIT)

para.in: $(SORC)include$(S)para.in
          $(COPYIT)

nc.in: $(SORC)include$(S)nc.in
        $(COPYIT)

ooip.in: $(SORC)include$(S)ooip.in
          $(COPYIT)

cotrans.in: $(SORC)include$(S)cotrans.in
             $(COPYIT)

lookup.in: $(SORC)include$(S)lookup.in
            $(SETSIZE1)
            $(SIZEIT)

compwel.h: $(SORC)include$(S)compwel.dh
            $(SETSIZE1)
            $(SIZEIT)

#VE  Petsc.h

wellden.h: $(SORC)include$(S)wellden.dh
            $(SETSIZE1)

```

```

$(SIZEIT)

#VE  petsc.h

xbal.dat.h: $(SORC)include$(S)xbal.dat.h
$(COPYIT1)

#VE  petsc.h

xchem.dat.h: $(SORC)include$(S)xchem.dat.dh
$(SETSIZE1)
$(SIZEIT)

xtdata.F: $(SORC)init$(S)xtdata.df control.h xgendat.h xchem.dat.h
$(SETSIZE1)
$(SIZEIT)

xarray.F: $(SORC)init$(S)xarray.df xgendat.h xarydat.h xchem.dat.h
$(SETSIZE1)
$(SIZEIT)

xisdat.F: $(SORC)init$(S)xisdat.df control.h xgendat.h compwel.h
compini.in model.in const.in para.in nc.in wellden.h xchem.dat.h
tcpcom.h
$(SETSIZE1)
$(SIZEIT)

xiadat.F: $(SORC)init$(S)xiadat.df control.h xgendat.h compini.in
model.in const.in para.in nc.in xchem.dat.h compwel.h
$(SETSIZE1)
$(SIZEIT)

xwdata.F: $(SORC)well$(S)xwdata.df nc.in para.in wells.h control.h
compwel.h xchem.dat.h
$(SETSIZE1)
$(SIZEIT)

xstdout.F: $(SORC)output$(S)xstdout.df control.h xgendat.h xarydat.h
xchem.dat.h
$(SETSIZE1)
$(SIZEIT)

xstep.F: $(SORC)drive$(S)xstep.df control.h xgendat.h xarydat.h
blkary.h compwel.h blkary.h xbal.dat.h nc.in para.in const.in model.in
compini.in wellden.h ooip.in xchem.dat.h wells.h rock.h layout.h
$(SETSIZE1)
$(SIZEIT)

xtimmul.F: $(SORC)drive$(S)xtimmul.df control.h model.in xgendat.h
xchem.dat.h
$(SETSIZE1)
$(SIZEIT)

```

```

xprop.F: $(SORC)prop$(S)xprop.df blkary.h control.h wells.h rock.h
nc.in para.in const.in model.in xgendat.h xchemdat.h xarydat.h
compini.in compwel.h
$(SETSIZE1)
$(SIZEIT)

xprope.F: $(SORC)prop$(S)xprope.df blkary.h control.h wells.h rock.h
nc.in para.in const.in model.in xgendat.h xchemdat.h xarydat.h
compini.in compwel.h
$(SETSIZE1)
$(SIZEIT)

xsurface.F: $(SORC)well$(S)xsurface.df control.h xgendat.h xarydat.h
blkary.h compwel.h blkary.h xbaldat.h nc.in para.in const.in model.in
compini.in wellden.h ooip.in xchemdat.h
$(SETSIZE1)
$(SIZEIT)

xsurfacee.F: $(SORC)well$(S)xsurfacee.df control.h xgendat.h xarydat.h
blkary.h compwel.h blkary.h xbaldat.h nc.in para.in const.in model.in
compini.in wellden.h ooip.in xchemdat.h rock.h
$(SETSIZE1)
$(SIZEIT)

xtrans.F: $(SORC)residual$(S)xtrans.df control.h xgendat.h xarydat.h
blkary.h compwel.h blkary.h nc.in para.in const.in model.in compini.in
wellden.h ooip.in xbaldat.h xchemdat.h
$(SETSIZE1)
$(SIZEIT)

xtranse.F: $(SORC)residual$(S)xtranse.df control.h xgendat.h xarydat.h
blkary.h compwel.h blkary.h nc.in para.in const.in model.in compini.in
wellden.h ooip.in xbaldat.h xchemdat.h
$(SETSIZE1)
$(SIZEIT)

jacobian.F: $(SORC)jacobian$(S)jacobian.df control.h xgendat.h
xarydat.h blkary.h compwel.h blkary.h nc.in para.in const.in model.in
compini.in wellden.h ooip.in xchemdat.h
$(SETSIZE1)
$(SIZEIT)

jacobiane.F: $(SORC)jacobian$(S)jacobiane.df control.h xgendat.h
xarydat.h blkary.h compwel.h blkary.h nc.in para.in const.in model.in
compini.in wellden.h ooip.in xchemdat.h
$(SETSIZE1)
$(SIZEIT)

xsolve.F: $(SORC)solver$(S)xsolve.df control.h xgendat.h xarydat.h
blkary.h compwel.h blkary.h nc.in para.in const.in model.in compini.in
wellden.h ooip.in xchemdat.h
$(SETSIZE1)
$(SIZEIT)

```

```

xsolvee.F: $(SORC)solver$(S)xsolvee.df control.h xgendat.h xarydat.h
blkary.h compwel.h blkary.h nc.in para.in const.in model.in compini.in
wellden.h ooip.in xchemdat.h
    $(SETSIZE1)
    $(SIZEIT)

# chan 10/28/03: added FIATS
fiats.F: $(SORC)solver$(S)fiats.df control.h xgendat.h xarydat.h
blkary.h compwel.h blkary.h nc.in para.in const.in model.in compini.in
wellden.h ooip.in xchemdat.h
    $(SETSIZE1)
    $(SIZEIT)

# chan

xaqcomp.F: $(SORC)aqcomp$(S)xaqcomp.df layout.h control.h blkary.h
wells.h para.in model.in compwel.h nc.in xgendat.h xarydat.h xchemdat.h
    $(SETSIZE1)
    $(SIZEIT)

xsurf.F: $(SORC)aqcomp$(S)xsurf.df layout.h control.h blkary.h wells.h
para.in model.in compwel.h nc.in xgendat.h xarydat.h xchemdat.h
control.h model.in
    $(SETSIZE1)
    $(SIZEIT)

xprint.F: $(SORC)output$(S)xprint.df control.h xgendat.h xarydat.h
blkary.h compwel.h blkary.h nc.in para.in const.in model.in compini.in
wellden.h xchemdat.h
    $(SETSIZE1)
    $(SIZEIT)

xdelta.F: $(SORC)jacobian$(S)xdelta.df control.h xgendat.h xarydat.h
blkary.h compwel.h blkary.h nc.in para.in const.in model.in compini.in
wellden.h ooip.in xchemdat.h
    $(SETSIZE1)
    $(SIZEIT)

xdeltae.F: $(SORC)jacobian$(S)xdeltae.df control.h xgendat.h xarydat.h
blkary.h compwel.h blkary.h nc.in para.in const.in model.in compini.in
wellden.h ooip.in xchemdat.h
    $(SETSIZE1)
    $(SIZEIT)

xwell.F: $(SORC)well$(S)xwell.df control.h wells.h compwel.h wellden.h
cotrans.in xchemdat.h blkary.h rock.h nc.in para.in const.in model.in
xgendat.h xarydat.h compini.in
    $(SETSIZE1)
    $(SIZEIT)

xwelle.F: $(SORC)well$(S)xwelle.df control.h wells.h compwel.h
wellden.h cotrans.in xchemdat.h blkary.h rock.h nc.in para.in const.in
model.in xgendat.h xarydat.h compini.in

```

```

$(SETSIZE1)
$(SIZEIT)

xivdat.F: $(SORC)init$(S)xivdat.df control.h times.h xchemdat.h
$(SETSIZE1)
$(SIZEIT)

xupdate.F: $(SORC)jacobian$(S)xupdate.f control.h nc.in para.in
const.in model.in xchemdat.h compwel.h
$(SETSIZE1)
$(SIZEIT)

xupdatee.F: $(SORC)jacobian$(S)xupdatee.f control.h nc.in para.in
const.in model.in xchemdat.h compwel.h rock.h
$(SETSIZE1)
$(SIZEIT)

xquit.F: $(SORC)drive$(S)xquit.df control.h
$(SETSIZE1)
$(SIZEIT)

xsolver.F: $(SORC)solver$(S)xsolver.df para.in nc.in model.in const.in
xchemdat.h rock.h
$(SETSIZE1)
$(SIZEIT)

xsolvere.F: $(SORC)solver$(S)xsolvere.df para.in nc.in model.in
const.in xchemdat.h rock.h
$(SETSIZE1)
$(SIZEIT)

# chan 10/28/03 added fiatsol1 and fiatsol2
fiatsol1.F: $(SORC)solver$(S)fiatsol1.df para.in nc.in model.in
const.in xchemdat.h
$(SETSIZE1)
$(SIZEIT)

fiatsol2.F: $(SORC)solver$(S)fiatsol2.df para.in nc.in model.in
const.in xchemdat.h
$(SETSIZE1)
$(SIZEIT)

jimpsurf.F: $(SORC)jacobian$(S)jimpsurf.f para.in xchemdat.h compini.in
control.h model.in rock.h xgendat.h
$(SETSIZE1)
$(SIZEIT)

xflash.F: $(SORC)eos$(S)xflash.f model.in para.in
$(SETSIZE1)
$(SIZEIT)

xflashe.F: $(SORC)eos$(S)xflashe.f model.in para.in

```



```

$(SETSIZE1)
$(SIZEIT)

aqueous.F: $(SORC)prop$(S)aqueous.f para.in
$(SETSIZE1)
$(SIZEIT)

influid0.F: $(SORC)init$(S)influid0.df control.h blkary.h xarydat.h
xgendat.h compini.in model.in ooip.in para.in nc.in const.in xchemdat.h
$(SETSIZE1)
$(SIZEIT)

eos_lph.F: $(SORC)eos$(S)eos_lph.f const.in
$(SETSIZE1)
$(SIZEIT)

xeos.F: $(SORC)eos$(S)xeos.f para.in nc.in const.in rock.h tcpcom.h
$(SETSIZE1)
$(SIZEIT)

rowpw.F: $(SORC)jacobian$(S)rowpw.df control.h nc.in para.in simple.in
xchemdat.h xarydat.h
$(SETSIZE1)
$(SIZEIT)

rowpwe.F: $(SORC)jacobian$(S)rowpwe.df control.h nc.in para.in
simple.in xchemdat.h xarydat.h
$(SETSIZE1)
$(SIZEIT)

vis.F: $(SORC)prop$(S)vis.f control.h nc.in para.in const.in model.in
xchemdat.h
$(SETSIZE1)
$(SIZEIT)

jaccum.F: $(SORC)jacobian$(S)jaccum.f control.h para.in nc.in const.in
model.in compini.in xchemdat.h
$(SETSIZE1)
$(SIZEIT)

jaccume.F: $(SORC)jacobian$(S)jaccume.f control.h para.in nc.in
const.in model.in compini.in xchemdat.h rock.h
$(SETSIZE1)
$(SIZEIT)

jmass.F: $(SORC)jacobian$(S)jmass.f control.h para.in nc.in const.in
model.in compini.in xchemdat.h
$(SETSIZE1)
$(SIZEIT)

jmasse.F: $(SORC)jacobian$(S)jmasse.f control.h para.in nc.in const.in
model.in compini.in xchemdat.h rock.h
$(SETSIZE1)

```

```

$(SIZEIT)

eos_jaco.F: $(SORC)jacobian$(S)eos_jaco.f control.h para.in nc.in
xchemdat.h
$(SETSIZE1)
$(SIZEIT)

eos_jacoe.F: $(SORC)jacobian$(S)eos_jacoe.f control.h para.in nc.in
xchemdat.h
$(SETSIZE1)
$(SIZEIT)

relderiv.F: $(SORC)jacobian$(S)relderiv.f control.h nc.in para.in
const.in compini.in rock.h xchemdat.h
$(SETSIZE1)
$(SIZEIT)

relderive.F: $(SORC)jacobian$(S)relderive.f control.h nc.in para.in
const.in compini.in rock.h xchemdat.h
$(SETSIZE1)
$(SIZEIT)

zderiv.F: $(SORC)jacobian$(S)zderiv.f control.h nc.in para.in
$(SETSIZE1)
$(SIZEIT)

zderive.F: $(SORC)jacobian$(S)zderive.f control.h nc.in para.in
$(SETSIZE1)
$(SIZEIT)

rrderiv.F: $(SORC)jacobian$(S)rrderiv.f control.h nc.in para.in
$(SETSIZE1)
$(SIZEIT)

ift.F: $(SORC)prop$(S)ift.f control.h nc.in para.in
$(SETSIZE1)
$(SIZEIT)

ifte.F: $(SORC)prop$(S)ifte.f control.h nc.in para.in
$(SETSIZE1)
$(SIZEIT)

roderiv.F: $(SORC)jacobian$(S)roderiv.f control.h nc.in para.in
xchemdat.h
$(SETSIZE1)
$(SIZEIT)

roderive.F: $(SORC)jacobian$(S)roderive.f control.h nc.in para.in
xchemdat.h
$(SETSIZE1)
$(SIZEIT)

eosxi2ni.F: $(SORC)eos$(S)eosxi2ni.f control.h nc.in para.in xchemdat.h

```

```

$(SETSIZE1)
$(SIZEIT)

xeosbas.F: $(SORC)eos$(S)xeosbas.f control.h nc.in para.in const.in
$(SETSIZE1)
$(SIZEIT)

##
mainssCom.F: $(SORC)wellbore$(S)mainssCom.f
$(SETSIZE1)
$(SIZEIT)

vis2.F: $(SORC)wellbore$(S)vis2.f para.in
$(SETSIZE1)
$(SIZEIT)

ssmaker.F: $(SORC)wellbore$(S)ssmaker.f
$(SETSIZE1)
$(SIZEIT)

properties.F: $(SORC)wellbore$(S)properties.f
$(SETSIZE1)
$(SIZEIT)

comproperties.F: $(SORC)wellbore$(S)comproperties.f
$(SETSIZE1)
$(SIZEIT)

zmaker.F: $(SORC)wellbore$(S)zmaker.f
$(SETSIZE1)
$(SIZEIT)

tssmaker.F: $(SORC)wellbore$(S)tssmaker.f
$(SETSIZE1)
$(SIZEIT)

newP.F: $(SORC)wellbore$(S)newP.f
$(SETSIZE1)
$(SIZEIT)

#updatex.F: $(SORC)wellbore$(S)updatex.f
# $(SETSIZE1)
# $(SIZEIT)
##
# Transient
maintransient.F: $(SORC)transient$(S)maintransient.f
$(SETSIZE1)
$(SIZEIT)

readdata.F: $(SORC)transient$(S)readdata.f
$(SETSIZE1)
$(SIZEIT)

openresult.F: $(SORC)transient$(S)openresult.f

```

```

$(SETSIZE1)
$(SIZEIT)

jr.F: $(SORC)transient$(S)jr.f
$(SETSIZE1)
$(SIZEIT)

solver.F: $(SORC)transient$(S)solver.f
$(SETSIZE1)
$(SIZEIT)

transientt.F: $(SORC)transient$(S)transientt.f
$(SETSIZE1)
$(SIZEIT)

propertiesb.F: $(SORC)transient$(S)propertiesb.f
$(SETSIZE1)
$(SIZEIT)

#c for phase
aibi.F: $(SORC)phase$(S)aibi.f
$(SETSIZE1)
$(SIZEIT)

lines.F: $(SORC)phase$(S)lines.f
$(SETSIZE1)
$(SIZEIT)

phafla.F: $(SORC)phase$(S)phafla.f
$(SETSIZE1)
$(SIZEIT)

sastp.F: $(SORC)phase$(S)sastp.f
$(SETSIZE1)
$(SIZEIT)

track.F: $(SORC)phase$(S)track.f
$(SETSIZE1)
$(SIZEIT)

chodec.F: $(SORC)phase$(S)chodec.f
$(SETSIZE1)
$(SIZEIT)

phdlnf.F: $(SORC)phase$(S)phdlnf.f
$(SETSIZE1)
$(SIZEIT)

train.F: $(SORC)phase$(S)train.f
$(SETSIZE1)
$(SIZEIT)

dirneg.F: $(SORC)phase$(S)dirneg.f

```

```

$(SETSIZE1)
$(SIZEIT)

parlnf.F: $(SORC)phase$(S)parlnf.f
$(SETSIZE1)
$(SIZEIT)

phest.F: $(SORC)phase$(S)phest.f
$(SETSIZE1)
$(SIZEIT)

flash3.F: $(SORC)phase$(S)flash3.f tcpcom.h
$(SETSIZE1)
$(SIZEIT)

flash3e.F: $(SORC)phase$(S)flash3e.f tcpcom.h
$(SETSIZE1)
$(SIZEIT)

flash.F: $(SORC)phase$(S)flash.f
$(SETSIZE1)
$(SIZEIT)

phadis.F: $(SORC)phase$(S)phadis.f
$(SETSIZE1)
$(SIZEIT)

plfc.F: $(SORC)phase$(S)plfc.f
$(SETSIZE1)
$(SIZEIT)

stmin.F: $(SORC)phase$(S)stmin.f
$(SETSIZE1)
$(SIZEIT)

phadrp.F: $(SORC)phase$(S)phadrp.f
$(SETSIZE1)
$(SIZEIT)

plnfx.F: $(SORC)phase$(S)plnfx.f
$(SETSIZE1)
$(SIZEIT)

thrphs.F: $(SORC)phase$(S)thrphs.f
$(SETSIZE1)
$(SIZEIT)

#c for phase ~ end

jaco2pw.F: $(SORC)jacobian$(S)jaco2pw.f control.h para.in control.h
xchemdat.h
$(SETSIZE1)
$(SIZEIT)

```

```

jaco2pwe.F: $(SORC)jacobian$(S)jaco2pwe.f control.h para.in control.h
xchemdat.h
    $(SETSIZE1)
    $(SIZEIT)

jprint.F: $(SORC)jacobian$(S)jprint.f control.h para.in nc.in const.in
model.in compini.in xgendat.h xchemdat.h
    $(SETSIZE1)
    $(SIZEIT)

jsource.F: $(SORC)jacobian$(S)jsource.df layout.h control.h para.in
nc.in const.in model.in wellden.h wells.h rock.h cotrans.in compwel.h
compini.in xchemdat.h
    $(SETSIZE1)
    $(SIZEIT)

jsourcee.F: $(SORC)jacobian$(S)jsourcee.df layout.h control.h para.in
nc.in const.in model.in wellden.h wells.h rock.h cotrans.in compwel.h
compini.in xchemdat.h
    $(SETSIZE1)
    $(SIZEIT)

mresipw.F: $(SORC)residual$(S)mresipw.df layout.h control.h nc.in
para.in model.in xchemdat.h
    $(SETSIZE1)
    $(SIZEIT)

mresipwe.F: $(SORC)residual$(S)mresipwe.df layout.h control.h nc.in
para.in model.in xchemdat.h rock.h compwel.h
    $(SETSIZE1)
    $(SIZEIT)

xrelperm.F: $(SORC)prop$(S)xrelperm.f rock.h nc.in xchemdat.h
    $(SETSIZE1)
    $(SIZEIT)

xtrapn.F: $(SORC)prop$(S)xtrapn.f blkary.h xgendat.h xarydat.h layout.h
    $(SETSIZE1)
    $(SIZEIT)

influid0e.F: $(SORC)init$(S)influid0e.df control.h blkary.h xarydat.h
xgendat.h compini.in model.in ooip.in para.in nc.in const.in xchemdat.h
rock.h
    $(SETSIZE1)
    $(SIZEIT)

estep.F: $(SORC)drive$(S)estep.df control.h xgendat.h xarydat.h
blkary.h compwel.h blkary.h xbal.dat.nc.in para.in const.in model.in
compini.in wellden.h ooip.in xchemdat.h wells.h rock.h layout.h
    $(SETSIZE1)
    $(SIZEIT)

```

```

vise.F: $(SORC)prop$(S)vise.f control.h nc.in para.in const.in model.in
xchemdat.h
    $(SETSIZE1)
    $(SIZEIT)

##### Combine object/lib files #####

#### (mpesz) the original sequence $(MODELOBJ) $(MORTAROBJ) was
modified
####         because the code for mortars was not modular (keyword
MORTAR
####         is used on include statements)
####         For exmaple, hstep uses mb_f.h from /mblk
####
#OBS = $(FRAMEOBJ) $(MORTAROBJ) $(MODELOBJ) $(SOLVEOBJ) $(GRAPHOBJ)
$(PARALOBJ)
#LIBS = $(FRAMELIB) $(MORTARLIB) $(MODELLIB) $(SOLVELIB) $(GRAPHLIB)
$(PARALLIB)
OBS = $(FRAMEOBJ) $(MODELOBJ) $(SOLVEOBJ) $(PARALOBJ)
LIBS = $(FRAMELIB) $(MODELLIB) $(SOLVELIB) $(PARALLIB)
##### Machine and Compiler include file (one only) #####
# Machine and compiler make include file

CC      = mpicc
CPP     = mpiCC
FORT    = ifort
LINK    = ifort
FFLAGS  = -c -g -w $(PETSC_INCLUDE)
CFLAGS  = -g -c
CPPFLAGS = $(MACE_CPPFLAGS) $(DAGHMB_CPPFLAGS)
#####
# arch and mbsysflag used only by mortar.mak

ARCH     = Linux
MBSYSFLAG = -DLINUX -DDAGH_NO_MPI
# system used by mortar.mak and mace.mak, macesysflag by mace.mak
SYSTEM   = linux
MACSYSFLAG = -DLINUX -DWant_c_files -DDEBUG_PRINT -DDICE -DACE_NO_MPI

#####

.f.o:
    $(FORT) $(FFLAGS) $*.f

.F.o:
    $(FORT) $(FFLAGS) $*.F

.c.o:
    $(CC) $(CFLAGS) $*.c

.C.o:
    $(CPP) $(CPPFLAGS) $*.C

```

```
.cpp.o:
    $(CPP) $(CPPFLAGS) $*.cpp

$(EXENAM): $(OBJS) $(LIBS_TO_STAMP)
    $(LINK) $(OBJS) -o $(EXENAM) $(LFLAGS) $(LIBS) $(PETSC_LIB)

clean:
    rm -f $(WORK)/*.f
    rm -f $(WORK)/*.F
    rm -f $(WORK)/*.stb
    rm -f $(WORK)/*.c
    rm -f $(WORK)/*.C
    rm -f $(WORK)/*.cpp
    rm -f $(WORK)/*.h
    rm -f $(WORK)/*.o
    rm -f $(WORK)/*.i
    rm -f $(WORK)/*.lst
    rm -f $(WORK)/ech
    rm -f $(WORK)/*.in
    rm -f $(EXENAM)
```


Glossary

The following list of nomenclature includes only the generalized symbols used in the text. Symbols which have been used to represent different quantities have been defined as they were used in the text.

A	Tubing cross sectional area, ft ²
B	Phase volume formation factor
c_p	Heat capacity, Btu/(lbm- °F)
C_{lg}	Drag coefficient between the gas phase and the liquid phase
d	Tubing diameter, ft
E	Absolute surface roughness, ft
E	Internal energy, Btu/lbm
F	Friction factor, dimensionless
g	Acceleration owing to gravity, ft/sec ²
g_T	Geothermal gradient (°F/psi)
G	Gas phase fraction in equilibrium
Gr	Grashof number, dimensionless
h	Fluid enthalpy, Btu/lbm
h_c	Convective heat transfer coefficient, Btu/(hr-ft- °F)
h_r	Radiative heat transfer coefficient, Btu/(hr-ft- °F)
H	Liquid holdup, dimensionless
k	Fluid thermal conductivity, Btu/(hr-ft- °F)
K	Permeability, md

L_e	Liquid phase fraction in equilibrium
L_{ne}	Liquid phase fraction not in equilibrium
L_w	Wellbore depth, ft
M	Molecular weight, lbm mole/lbm
m'_i	Molar flow rate for ith component between wellbore and reservoir, lbm mole/Day
n_c	Number of components
n_p	Number of phases
N	Overall concentration of component i
\bar{N}_i	Molar flux vector, lbm mole/ft
P	Pressure, psi
Pr	Prandtl number, dimensionless
q	Phase flow rate, ft ³ /hr
q_H	Enthalpy injection rate per unit rock volume, Btu/lbm.sec
q_L	Heat loss to the over- and underburdens per unit rock volume, Btu/lbm.sec
Q	Heat transfer rate, Btu/(hr-ft)
r	Radius, Ft
R	Gas constant
Re	Reynolds number, dimensionless
S	Saturation
t_D	Dimensionless time, $k_e t / \rho_e c_{pe} r_{wb}^2$
T	Temperature, °F
T_D	Dimensionless temperature, $2\pi k_e (T_{wb} - T_{sf}) / Q$
u	Sum of internal energies per unit rock and the fluid contained in the unit rock, Btu/lbm
U_{to}	Overall heat transfer coefficient between wellbore fluid and wellbore outer surface, Btu/(hr-ft ² - °F)
U	Overall heat transfer coefficient, Btu/(hr-ft ² - °F)
v	Fluid velocity, ft/sec

\bar{v}_j	Molar volume of phase j
V	Volume, ft ³
w	Phase mass flow rate, lbm/hr
W	Overall concentration, lbm mole/ft ³
x_i	Molar fraction of i th component in liquid phase
y_i	Molar fraction of i th component in gas phase
z	Overall hydrocarbon composition
Z	Phase compressibility

Greek Symbols

ρ	Density, lbm/ft ³
Θ	Wellbore angle, radian
ϕ	Porosity
ζ	Molar density, lbm mole/ft ³
λ	Mobility ratio, Darcy/cp
γ_j	Gravity term for phase j , defined as ρ_j/g
η	Joule-Thomson coefficient, 1/psi
σ	Surface interfacial tension, lbm/sec ²
μ	Viscosity, cp

Subscripts

<i>a</i>	Annulus
<i>B</i>	Bottomhole
<i>ce</i>	Cement
<i>m</i>	
<i>ci</i>	Casing inside
<i>co</i>	Casing outside
<i>e</i>	Earth
<i>Ins</i>	Insulation
<i>f</i>	Flowing fluid
<i>g</i>	Gas
<i>i</i>	Component
<i>j</i>	Phase
<i>l</i>	Liquid
<i>m</i>	Mixture
<i>s</i>	Slip
<i>ti</i>	Tubing inside
<i>to</i>	Tubing outside
<i>wb</i>	Wellbore
<i>wh</i>	Wellhead

References

- Agarwal, R. G., Al-Hussainy, R., and Ramey, H. J. Jr.: "An Investigation of Well Bore Storage and Skin Effect in Unsteady Liquid Flow: I. Analytical Treatment," *Journal of Society of Petroleum Engineering*, Sep 1970, 279-290.
- Almehaideb, R. A., Aziz, K. A., and Pedrosa, O. J. Jr.: "A Reservoir/Wellbore Model for Multiphase Injection and Pressure Transient Analysis," Paper SPE 17941 presented at 6th Middle East Oil Technical Conference and Exhibition, Manama, Bahrain, 11-14 March 1989.
- Alves, I. N., Alhanati, F. J. S., and Shoham, O.: "A Unified Model for Predicting Flowing Temperature Distribution in Wellbores and Pipelines," *SPE Production Engineering Journal*, Nov 1992, 4, 363-367.
- Ansari, A. M., Sylvester, N. D., Sarica, C., Shoham, O., and Brill, J. P.: "A Comprehensive Mechanistic Model for Upward Two-Phase Flow in Wellbores," *SPE Production & Facilities Journal*, 1994, 143-151.
- Anis, M. and Buthod, P.: "How Flashing Fluids Change Phase in Pipelines," *Oil and Gas Journal*, 1974, 24, 150-155.
- Aziz, K., Govier, G. W., and Fogarasi, M.: "Pressure Drop in Wells Producing Oil and Gas," *Journal of Canadian Petroleum Technology*, 1972, 11, 38-46.
- Balay, S., Gropp, W., McInnes, L.C. and Smith, B.: "PETSc 2.0 User Manual," Argonne National Laboratory, ANL-95/11 – Revision 2.0.22, April 1998.
- Barnea, D.: "A Unified Model for Predicting Flow-Pattern Transition for the Whole Range of Pipe Inclinations," *International Journal of Multiphase Flow*, 1987, 13, 1-12.
- Beggs, H. D. and Brill, J. P.: "A Study of Two-Phase Flow in Inclined Pipes," *Journal of Petroleum Technology*, May 1973, 607-617.
- Beggs, H. D., and Robinson, J. R.: "Estimating the Viscosity of Crude Oil Systems," *Journal of Petroleum Technology*, September 1975, 27, 1140-1141.

- Chang, Y. B.: "Development and Application of an Equation of State Compositional Simulator," PhD Dissertation, The University of Texas at Austin, 1990.
- Chen, Y.: "Modeling Gas- Liquid Flow in Pipes: Flow Pattern and Transitions and Drift-Flux Modeling," Master of Science Report, Stanford University, 2001.
- Coleman, S. B., Clay, H.B., McCurdy, D.G. and Norris III, H. L.: "A New Look at Predicting Gas Well Load-up," Journal of Petroleum Technology, March 1991, 329-333.
- Dake, L.P.: *Fundamentals of Reservoir Engineering*, Elsevier Science, 1978.
- Dropkin, D., Somerscales, S.: "Heat Transfer by Natural Convection in Liquids Confined by Two Parallel Plates Which are Inclined at Various Angles with Respect to the Horizontal," Journal of Heat Transfer; Trans., ASME, February 1965, 87, 77-78.
- Duns, H. Jr. and Ros, N. C. J.: "Vertical Flow of Gas and Liquid Mixtures in Wells," Proceeding of the Sixth World Petroleum Congress, Frankfurt, June 1963, Section II, Paper 22-PD6.
- Egbogah, E. O. and Ng, J. T. H.: "An Improved Temperature-Viscosity Correlation for Crude Oil Systems," Paper No. 83-34-32 presented at the 34th Annual Technical Meeting of the Petroleum Society of CIM un Banff, May 11-13, 1983.
- Fair, W. B.: "Pressure Buildup Analysis with Phase Redistribution," Society of Petroleum Engineering Journal, April 1981, 259-270.
- Fairuzov, Y. V., Gonzalez Guevara, J., Lobato Barradas, G., Camacho Velazquez, R., and Fuentes Nucamendi, F.: "A Lumped-Parameter Model for Transient Two-Phase Gas-Liquid Flow in a Wellbore," SPE Production and Facilities Journal, 2002, 17, 1, 36-41.
- Fan, L., Lee, W. J., and Spivey, J. P.: "Semi-Analytical Model for Thermal Effect on Gas Well Pressure Buildup Tests," Paper SPE 56612 presented at the SPE ATCE, Houston, Texas, 3-6 October, 2000.
- Furukawa, H., Shoham, O., and Brill, J. P.: "Predicting Compositional Two-Phase Flow Behavior in Pipelines," ASME Journal of Energy Resource Technology, 1986, 108, 207-210.

- Gregory, G. A., and Aziz, K.: "Calculation of Pressure and Temperature Profiles in Multiphase Pipeline and Simple Pipeline Networks," *Journal of Petroleum Technology*, March 1973, 373-384.
- Gringarten, A. C., Bourdet, D. P., Landel, P. A., and Kniazeff, V. J.: "A Comparison between Different Skin and Wellbore Storage Type-Curves for Early-Time Transient Analysis," Paper SPE 8205 Presented in SPE-AIME 54th Annual Technical Conference and Exhibition, Las Vegas, Nevada, 1979.
- Gambill, W. R.: "You Can Predict Heat Capacities," *Chemical Engineering Journal*, June 1957, 243-248.
- Gould, T. L.: "Compositional Two-Phase Flow in Pipelines," 1975. Paper SPE 5685 presented in the 50th Annual Fall Meeting of the Society of Petroleum Engineers of AIME, Dallas, TX, USA, 28 September 1975.
- Gropp, W. D., McInnes, L. C., Smith, B. F.: "Scalable Libraries for Solving Systems of Nonlinear Equations and Unconstrained Minimization Problems," Paper Presented at the Scalable Parallel Libraries Conference, Mississippi State U, 1995.
- Hagedorn, A. R. and Brown, K. E.: "Experimental Study of Pressure Gradients Occurring During Continuous Two-Phase Flow in Small Diameter Vertical Conduits," *Journal of Petroleum Technology*, April 1965, 475-484.
- Hegeman, P. S., Hallford, D. L., and Joseph, J. A.: "Well-Test Analysis with Changing Wellbore Storage," Paper SPE 21829 presented at the SPE Rocky Mountain Regional/Low Permeability Reservoirs Symposium, Denver, Colorado, April 15-17, 1991
- Han, C., Delshad, M., Sepehrmoori, K., and Pope, G. A.: "A Fully Implicit, Parallel, Compositional Chemical Flooding Simulator," *Society of Petroleum Engineering Journal*, 2007, 12, 3, 322-338.
- Harmathy, T. Z.: "Velocity of Large Drops and Bubbles in Media of Infinite or Restricted Extent," *AIChE Journal*, 1960, 6, 281-286.
- Hasan, A. R., and Kabir, C. S.: "A Study of Multiphase Flow Behavior in Vertical Wells," *SPE Production Engineering Journal*, May 1988, 263-272.
- Hasan, A. R. and Kabir, C. S.: "Modeling Changing Storage During a Shut-in Test," Paper SPE 24717 Presented at the SPE Annual Technical Conference and Exhibition, Washington DC, October 4-7 1992.

- Hasan, A. R., and Kabir, C. S.: "Aspects of Wellbore Heat Transfer During Two-Phase Flow," SPE Production & Facilities Journal, August 1994, 3, 211-216.
- Hasan, A. R., and Kabir, C. S.: "A Wellbore/Reservoir Simulator for Testing Gas Wells in High-Temperature Reservoirs," SPE Formation Evaluation Journal, June 1996, 128-135.
- Hasan, A. R., Kabir, C. S., and Wang, X.: "Development and Application of a Wellbore/Reservoir Simulator for Testing Oil Wells," SPE Formation Evaluation Journal, September 1997, 182-188.
- Hasan, A. R., Kabir, C. S., and Wang, X.: "Wellbore Two-Phase Flow and Heat Transfer during Transient Testing," Society of Petroleum Engineering Journal, June 1998, 3, 2, 174-180.
- Hasan, A. R., and Kabir, C. S.: *Fluid flow and heat transfer in wellbores*, Society of Petroleum Engineers, Richardson, TX, 2002.
- Hasan, A. R., and Kabir, C. S.: "A Simple Model for Annular Two-Phase Flow in Wellbores," Paper SPE 95523 Presented in SPE Annual Technical Conference and Exhibition, Dallas, Texas, 9-12 October 2005.
- Hasan, A. R., Kabir, C. S., and Lin, D.: "Analytic Wellbore Temperature Model for Transient Gas-Well Testing," SPE Reservoir Evaluation and Engineering Journal, 2005, 8, 3, 240-247.
- Holman, J. P.: *Heat transfer (4th edition)*, McGraw-Hill Book Co, New York, 1958.
- Horner, D. R.: "Pressure Build-up in Wells," Proceeding of the Third World Petroleum Congress, The Hague, 1951, Sec. II. 503-523.
- Gomez, L. F., Shoham, O., Schmidt, Z., Chokshi, R. N, Brown, A., and Northug, T.: "Unified Mechanistic Model for Steady-State Two-Phase Flow: Horizontal to Vertical Upward Flow," Society of Petroleum Engineering Journal, September 2000, 5, 3, 339-350.
- Gringarten, A. C., Bourdet, D. P., Landel, P. A., and Kniazeff, V. J.: "A Comparison Between Different Skin and Wellbore Storage Type Curves for Early- Time Transient Analysis," Paper SPE 8205 Presented at the 54th SPE Annual Technical Conference and Exhibition, Las Vegas, Nevada, 23-26 September 1979.

- Izgec, B., Kabir, C. S., Zhu, D., and Hasan, A. R.: "Transient Fluid and Heat Flow Modeling in Coupled Wellbore/Reservoir Systems," Paper SPE 102070 Presented at SPE Annual Technical Conference and Exhibition, San Antonio, Texas, 24-27 Sep 2006.
- Kabir, C. S., and Hasan, A. R.: "Does Gauge Placement Matter in Downhole Transient Data Acquisition?," Paper SPE 36527 Presented in SPE Annual Technical Conference and Exhibition, Denver, CO, 6-9 October 1996.
- Kaya, A. S., Sarica, C., and Brill, J. P.: "Mechanistic Modeling of Two-Phase Flow in Deviated Wells," Society of Petroleum Engineering Production and Facilities Journal, August 2001, 156-165.
- Lee, A. L., Gonzalez, M. H., Eakin, B. E.: "The Viscosity of Natural Gases," Trans. AIME, 1966, 237, 997-1000.
- Leibovici, C. F. and Neoschil, J.: "A New Look at the Rachford-Rice Equation for Flash Calculations," Fluid Phase Equilibria, 1992, 74, 303-308.
- Lin, D.: "Transient Fluid Flow and Heat Transfer in Petroleum Production Systems," Ph.D. dissertation, The University of North Dakota, 2001.
- Lohrenz, J., Bray, B. G. and Clark, C. R.: "Calculating Viscosity of Reservoir Fluids from Their Compositions," Trans., AIME, 1964, 231, 1171-1176.
- Mattar, L., and Santo, M.: "How Wellbore Dynamics Affect Pressure Transient Analysis," Journal of Canadian Petroleum Technology, April 1992, 9, 63-70.
- Mattar, L., and Zaoral, K.: "The Primary Pressure Derivative (PPD)- A New diagnostic Tool in Well Test Interpretation," Journal of Canadian Petroleum Technology, 1992, 4, 63-70.
- McCain, W. D.: *The properties of petroleum fluids*, Tulsa: Petroleum Publication Co, 1973.
- Michelsen, J. L.: "The Isothermal Flash Problem. Part I. Stability," Fluid Phase Equilibria, 1982, 9, 1-19.
- Miller, C. W.: "Wellbore Storage Effect in Geothermal Wells," Society of Petroleum Engineering Journal, Dec 1980, 555-566.

- Miller, C. C., Dyes, A. B., and Hutchinson, C. A. Jr.: "The Estimation of Permeability and Reservoir Pressure from Bottomhole Pressure Buildup Characteristics," Trans., AIME, 1950, 189, 91-104.
- Mukherjee, H., and Brill, J. P.: "Liquid Holdup Correlations for Inclined Two-Phase Flow," Journal of Petroleum Technology, May 1983, 1003-1008.
- Muskat, B.: "Use of Data on the Buildup of Bottomhole Pressures," Trans. AIME, 1937, 123, 44-48.
- Naimi-Tajdar, R.: "Development and Implementation of Naturally Fractured Reservoir Model into a Fully Implicit, Equation-of-State Compositional, Parallel Simulator," Ph.D. dissertation, The University of Texas at Austin, 2005.
- Nolen, J. S., and Berry, D. W.: "Test of the Stability and Time-Step Sensitivity of Semi-Implicit Reservoir Simulation Techniques," Society of Petroleum Engineering Journal, June 1972, 12, 3, 253-266.
- Olarewaju, L. S., and Lee, W. J.: "Effects of Phase Segregation on buildup Test data from Gas Wells," Paper SPE 19100 Presented in SPE Gas Technology Symposium, Dallas, Texas, 7-9 June 1989.
- Olarewaju, L. S.: "Detection and Interpretation of Well Test Data Distorted by Phase Segregation," Journal of Petroleum Science and Engineering, 1990, 5, 201-212.
- Orkiszewski, J.: "Predicting Two-Phase Pressure Drops in Vertical Pipe," Journal of Petroleum Technology, June 1967, 829-838.
- Ozon, P. M., Ferschneider, G., and Chwetzoff, A.: "A New Multiphase Flow Model Predicts Pressure and Temperature Profile," Paper SPE 16535 Presented at the SPE Offshore Europe Conference, Aberdeen, 8-11 September 1987.
- Peaceman, D. W.: "Interpretation of Well-Block Pressures in Numerical Reservoir Simulation with Nonsquare Grid Blocks and Anisotropic Permeability," Society of Petroleum Engineering Journal, June 1983, 531-543.
- Peng, D. Y., and Robinson, D. B. : "A New Two-Constant Equation of State," Industrial and Engineering Chemistry: Fundamentals, 1976, 15, 59-64.
- Perschke, D. R.: "Equation of State Phase Behavior Modeling for Compositional Simulator," Ph.D. dissertation, The University of Texas, Austin, 1988.

- Petalas, N., and Aziz, K.: "A Mechanistic Model for Multiphase Flow in Pipes," Journal of Canadian Petroleum Technology, June 2000, 39, 43-55.
- Pitzer, S. C., Rice, J. D., and Thomas, C. E.: "A Comparison of Theoretical Pressure Buildup Curves with Field Curves Obtained from Bottomhole Shut-in Tests," Trans. AIME, 1959, 216, 416-419.
- Qasem, F. H., Nashawi, I. S. and Mir, M. I.: "A New Method for the Detection of Wellbore Phase Redistribution Effects During Pressure Transient Analysis," Paper SPE 67239 Presented at the SPE Production and Operation Symposium, Oklahoma City, Oklahoma, 24-27 March 2001.
- Qasem, F. H, Nashavi, I. S., Mir, M. I.: "Detection of Pressure Buildup Data Dominated by Wellbore Phase Redistribution Effects," Journal of Petroleum Science and Engineering, 2002, 34, 109-122.
- Ramey, H.: "Wellbore Heat Transmission," Journal of Petroleum Technology, April 1962, 427-435.
- Reid, R. C., Prausnitz, J. M. and Poling, B. E.: *The Properties of Gases and Liquids*, Fourth Edition, McGraw-Hill, Inc., NY, 1987.
- Rowlan, O. L., McCoy, J. N. and Podio, A. L.: "Acoustic Liquid-Level Determination of Liquid Loading in Gas Wells," Paper SPE 100663 Presented in SPE Western Regional/AAPG Pacific Section/GSA Cordilleran Section Joint Meeting, Anchorage, Alaska, USA, 8-10 May 2006.
- Sagar, R. K., Doty, D. R., Schmidt, Z.: "Predicting Temperature Profiles in a Flowing Well," SPE Production Engineering Journal, Nov 1991, 6, 441-448.
- Sandler, S. I.: *Models for thermodynamic and phase equilibrium calculations.*, Chemical industries, v. 52. New York, Dekker, 1999.
- Satter, A., "Heat Losses during Flow of Stream Down a Wellbore," Journal of Petroleum Technology, July 1965, 845-851.
- Shi, H., Holmes, J. A., Diaz, L. R., Durlofsky, L. J., and Aziz, K.: "Drift-Flux Parameters for Three-Phase Steady-State Flow in Wellbores," Society of Petroleum Journal, June 2005, 130-137.
- Shoham, O.: "Flow Pattern Transition and Characterization in Gas-Liquid Two-Phase Flow in Inclined Pipes," Ph.D. dissertation, University of Tel Aviv, 1982.

- Standing, M. B.: "A Pressure-Volume-Temperature Correlation for Mixtures of California Oils and Gases," *Drill. and Prod. Prac.*, API, 1947.
- Stegemeier, G. L., and Matthews, C. S.: "A Study of Anomalous Pressure Build-Up Behavior," *Trans.*, AIME, 1958, 213, 44-50.
- Stone, T. W., Edmund, N. R., and Kristoff, B. J.: "A Comprehensive Wellbore/Reservoir Simulator," Paper SPE 18419 presented at the SPE Reservoir Simulation Symposium, Houston, Texas, 6-8 February 1989.
- Somerton, W. H.: *Thermal Properties and Temperature-related Behavior of Rock/Fluid Systems*, Elsevier, 1992.
- Taitel, Y., and Dukler, A. E.: "A Model for Predicting Flow Regime Transitions in Horizontal and Near Horizontal Gas-Liquid Flow," *AIChE Journal*, 1976, 22, 47-57.
- Taitel, Y., Barnea, D., and Duker, A.E.: "Modeling Multi Pattern Transitions for Steady Upward Gas-Liquid Flow in Vertical Tubes," *AIChE Journal*, 1980, 26, 345-354.
- Thompson, L. G., Jones, J. R., and Reynolds, A. C.: "Analysis of Pressure Buildup Data. Influenced by Wellbore Phase Redistribution Effects," *SPE Formation Evaluation Journal*, October 1986, 435-452.
- Turner, R. G., Hubbard, M. G., and Dukler, A. E.: "Analysis and Prediction of Minimum Flow Rate for the Continuous Removal of Liquids from Gas Wells," *Journal of Petroleum Technology*, November 1969, 1475-1482.
- Van Everdingen, A. F. and Hurst, W.: "The Application of the Laplace Transformation to Flow Problems in Reservoirs," *Trans. AIME*, 1949, 186, 305-324.
- Walpes, D. W. and Waples, J. S.: "A review and Evaluation of Specific Heat Capacities of Rocks, Minerals, and Subsurface Fluids. Part 2: Fluids and Porous Rocks", *Natural resources research*, June 2004, 131, 2, 123-130.
- Walsh, M. P., and Lake, L.W: *A Generalized Approach to Primary Hydrocarbon Recovery. Handbook of petroleum exploration and production, 4*. Amsterdam, Elsevier, 2003.
- Wang, P., Yotov, I., Wheeler, M., Arbogast, T., Dawson, C., Parashar, M., and Sepehrnoori, K.: "A New Generation EOS Compositional Reservoir Simulator: Part I – Formulation and Discretization," Paper SPE 37979 Presented in SPE Reservoir Simulation Symposium, Dallas, TX, 8-11 June 1997.

- Wang, P., Balay, S., Sepehrnoori, K., Wheeler, J., Abate, J., Smith, B., and Pope, G.A.: "A Fully Implicit Parallel EOS Compositional Simulator for Large Scale Reservoir Simulation," Paper SPE 51885 Presented at the SPE Reservoir Simulation Symposium, Houston, TX, 14-17 February 1999.
- Wang, X.: "Modeling Coupled Transient Transport of Mass, Momentum and Energy in Wellbore/Reservoir Systems" Ph.D. dissertation, The University of North Dakota, 1996.
- Winterfeld, P. H.: "Simulation of Pressure Buildup in a Multiphase Wellbore Reservoir System," SPE Formation Evaluation Journal, June 1989, 4, 2, 247-252.
- Xiao, J. J., Shoham, O., and Brill, J. P.: "A Comprehensive Mechanistic Model for Two-Phase Flow in Pipelines," Paper SPE 26031 presented at 65th ATC&E of SPE, New Orleans, 23-26 September 1990.
- Xiao, J. J., Fuentes-N, F. A., Alhanati, F., and Reynolds, A. C.: "Modeling and Analyzing Pressure Buildup Data Affected by Phase Redistribution in the Wellbore," SPE Advanced Technology Series, 1996, 4, 1, 28-37.

Vita

Peyman Pourafshary was born on April 15, 1979, the son of Majid Pourafshary and Masoomeh Iraniha, in Tehran, Iran. He received his B.Sc. and M.Sc. degrees in Mechanical engineering (Solid Mechanics) and Mechanical Engineering (Thermo-Fluid Mechanics), respectively, from Sharif University of Technology in Iran in 2000 and 2002, respectively. He received a scholarship from University of Tehran to study petroleum engineering. In 2003, he started his PhD program in petroleum engineering at The University of Texas at Austin (USA). For his dissertation, he developed a coupled wellbore/reservoir simulator to model multiphase flow and temperature distribution in wellbores.

Peyman is married to Bahar Hassani Dorabadi.

Permanent address: No 9, Behrooz Ave, Vali-asr Street, Tehran, Iran, 19656

This dissertation was typed by the author.